THEORETICAL STUDIES OF NONLINEAR PLANAR OPTICAL WAVEGUIDES

by

Hai-Tan Tran

A thesis submitted for the degree of
Doctor of Philosophy
of the Australian National University.

Canberra
February, 1993.

DECLARATION

This is an account of research undertaken in the Optical Sciences Centre within the Research School of Physical Sciences and Engineering at The Australian National University between January 1990 and January 1993, while I was enrolled for the degree of Doctor of Philosophy.

Dr. A.Ankiewicz and Prof. A.W.Snyder supervised the work, but unless specifically disowned, the material presented therein is my own.

None of the work reported here has ever been submitted for any other degree at this or any other institution of learning.

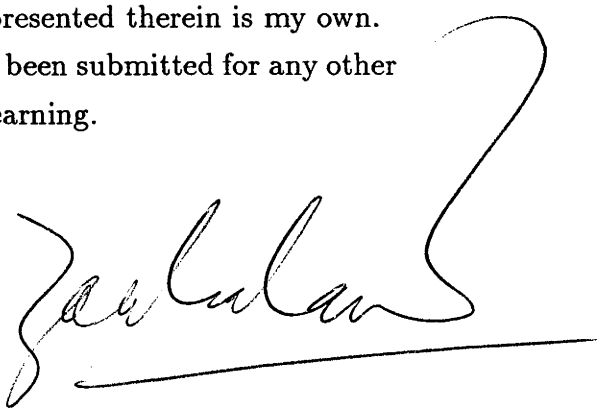

HAI-TAN TRAN

1 February, 1993.

My parents.

To my parents,

brothers and sisters,

and friends.

ACKNOWLEDGEMENTS

Now that three years (and two weeks) have gone by since I came to this pleasant place, the Optical Sciences Centre, to start my Ph.D. studies. That first day at the Centre still seems to me like yesterday. And between then and now, there have been a lot of events and enjoyments that will certainly always be in my mind and heart.

There are special people to whom I would like to express my sincere gratitude. Firstly I would like to thank Dr. Adrian Ankiewicz, my supervisor, for his unfailing support, guidance and encouragement. His readiness and friendliness to explain in many hours of helpful, enjoyable discussion during the three years are sincerely appreciated.

I owe much gratitude to Prof. Allan W. Snyder for his help, encouragement, enthusiasm, and very special character without which this Centre would probably be very different. Thanks are also due to John Mitchell and Leon Poladian for the valuable discussions on stability problems, to Nail Akhmediev for his almost instant solutions to my mathematical balls-ups, to Simon Hewlett and David Rowland for the enjoyable bush-walks and for helpfully proof-reading parts of the manuscript, to Javid Atai for some help with a numerical calculation in the earlier days of my stay, to Andrea Robins for her liveliness, friendly character and administrative help, and to all friends (Trevor, Cathryn, Erica, Tim, John and Yang) that I have met, both in the Optical Sciences Centre and the next-door Department of Applied Mathematics.

And of course, I have to thank the Australian National University and the Australian Government for giving me this precious opportunity to pursue my studies. Without their financial support (the Australian Postgraduate Research Award), this thesis would have never come into existence.

Last but not least, I owe deep, deep gratitude to God who creates and governs this wonderful universe for us brothers and sisters to live in and to learn.

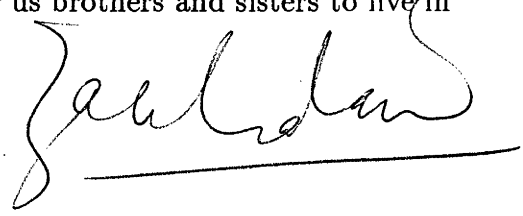

ABSTRACT

This thesis is concerned with the transverse-electric propagation of light in nonlinear planar optical waveguides which, at the present time, hold a great promise for the field of integrated optics. The thesis is centred around two primary questions:

(a) - What transverse electric (TE) modes can be supported by a nonlinear planar waveguide ?, and

(b) - Are the supported modes stable to small perturbations ?

These are some of the most important questions that must be answered before any applications can be made of the nonlinear guided waves.

Question (a) symbolizes what we call modal characteristics. In this thesis, the full complexity of the TE_0, TE_1, and TE_2 modal structures in asymmetric nonlinear waveguides is analytically described. We explain how the so-called power-dispersion curves reduce to the symmetric and extreme asymmetric limits. For waveguides involving self-defocusing nonlinearities, the modal characteristics are calculated both analytically and numerically. We also find that a whole range of 'dark' TE modes exists in planar interface and slab waveguide structures which involve self-defocusing nonlinearities in the bounding media and which are fortunately amenable to analytical calculations.

Question (b) is the important question of stability because if a mode (or stationary wave) turns out to be unstable, then it can never be used in practice. In this thesis, the main tool used to study stability is linear stability analysis. We discover that, for any types of nonlinearity, the growth rates in linear stability analysis is either real or purely imaginary for fundamental modes but can be complex for non-fundamental modes - This is a quite significant contribution. We also review, clarify, and discuss the methods and approaches currently available for solving the stability problems of nonlinear guided waves.

Analytical stability results for various types of guided waves, both 'bright' and 'dark', are reported. These results are confirmed using numerical (BPM) simulations.

Related experiments carried out by other researchers on nonlinear guided and self-guided waves are discussed and shown to be in consistence with the theoretical calculations presented here.

Finally, the investigation is extended to strutures involving power-law nonlinearities where it is found that surface and slab-guided wave properties are similar to those found in the Kerr-law case, unless the nonlinear exponent q becomes greater than 2. Other issues related to real nonlinear materials (such as absorption, nonlinear saturation, mode excitation) and experimental realization of these guided waves are briefly discussed.

PUBLICATIONS

Papers published:

[1] A. Ankiewicz and H. T. Tran, *'A new class of nonlinear guided waves'*, Journal of Modern Optics, **38**, 1093-1106, (1991)

[2] H. T. Tran and A. Ankiewicz, *'Instability Regions of Nonlinear Planar Guided Waves'*, IEEE Journal of Quantum Electronics, **QE-28**, 488-492, (1992),

[3] Y. Chen and H. T. Tran, *'Gray and Dark Spatial Solitary Waves'*, Optics Letters, **17**, 530-2, (1992)

[4] H. T. Tran, *'Stability of TE_0 Modes in Selfdefocusing-Core Nonlinear Planar Waveguides'*, Optics Communications, **93**, 202, (1992)

[5] H. T. Tran, J. D. Mitchell, N. N. Akhmediev, and A. Ankiewicz. *Complex Eigenvalues in Stability Analysis of Nonlinear Planar Guided Waves'*, Optics Communications, **93**, 227, (1992)

[6] H.T. Tran, *'Stability of TE bright waves in slab waveguides with a self-defocusing bounding medium'*, Optics Letters, **17**, 1767-9 (1992)

[7] H. T. Tran, *'Stability of Dark Solitons: Linear Analysis'*, Physical Review A, **46**, 7319-21 (1992)

[8] N. N. Akhmediev, A. Ankiewicz, and H. T. Tran, *'Stability Analysis of Even and Odd Waves of Symmetric Nonlinear Planar Optical Waveguides'*, Journal of The Optical Society of America B

[9] H.T. Tran and A.W. Snyder, *'Surface Modes of Power-Law Nonlinearities'*, Optics Communications, **98**, 309-312 (1993)

Papers submitted:

[10] H. T. Tran, *'Stability of Stationary Dark Waves Guided by Nonlinear Surfaces and Waveguides'*, Journal of The Optical Society of America B

[11] A.W. Snyder and H.T. Tran, *'Power-Law Nonlinear Waveguides'*, IEEE Journal of Quantum Electronics

Conference presentations:

1. H. T. Tran and A. Ankiewicz, *'New States in Nonlinear Planar Guides'*, 15 th Australian Conference on Optical Fibre Technology (ACOFT), Dec. 1990, Sydney, New South Wales.

2. H. T. Tran and A. Ankiewicz, *' A Novel Self- Induced Coupler'*, 16th ACOFT, Dec. 1991, Adelaide, South Australia.

3. H. T. Tran, *'Stability of Nonlinear Surface and Guided Waves'*, 17th ACOFT, Dec. 1992, Hobart, Tasmania.

4. H.T. Tran, *Stability of dark guided waves'*, Workshop on Guided Waves Optics, organized by The Optical Fibre Technology Centre, University of Sydney, Nov. 1992.

Notes on the text:

(1) All references are numbered consecutively and listed at the end of the thesis.

(2) The equations are numered consecutively within each chapter. In the notation (n, m), n is the chapter number and m is the equation number.

The figures are numbered in a similar fashion.

(3) - Acronyms: Where appropriate, the following acronyms are used:

SF : self-foucusing

SDF : self-defocusing

L : linear

Contents

1 Introduction **1**

1.1 What is an Optical Waveguide ? 1

1.2 Propagation in waveguides 3

1.3 On the background of nonlinear optics 5

1.4 Applications 8

1.5 Nonlinear Materials 9

1.6 Summary of Presentation 12

2 Solutions of the Wave Equation **15**

2.1 Wave Equation 16

2.1.1 Planar Geometry 17

2.1.2 Types of Nonlinearity 17

2.2 Exact Solutions for a Homogeneous Medium 19

2.2.1 Linear medium 20

2.2.2 Kerr-law Medium 20

2.2.3 Power-law Medium 23

2.2.4 Quartic Model 24

2.3 Mechanical Interpretation and Phase Diagrams 25

2.4 Layered Structures 28

2.5 Numerical Solutions 33

2.5.1 Iterative Finite Element Method (IFEM) 34

2.5.2 Slowly-Varying Waves 34

2.6 Conversion of Parameters 36

3 Stability Analysis **39**

3.1 Linear Analysis 40

3.1.1 Linearization 40

3.1.2 The form of perturbation functions 41

3.1.3 The eigenvalue Ω . . . 42
3.1.4 Exact forms of the perturbation functions . . . 43
3.1.5 Bright Solitons . . . 46
3.1.6 Dark Solitons . . . 47
3.1.7 Numerical Linear Analysis . . . 49
3.1.8 Kolokolov's Work . . . 50
3.1.9 Jones and Moloney's Work . . . 53
3.1.10 Mitchell and Snyder's Work . . . 55
3.2 Lyapunov Theory . . . 56
3.2.1 Background . . . 56
3.2.2 Application to guided waves . . . 58
3.2.3 Discussion . . . 59
3.3 Numerical Beam Propagation . . . 61
3.4 Transverse Stability . . . 61

4 Waveguides with Kerr SF Bounding Media 65
4.1 Waveguide Geometry and Parameters . . . 65
4.2 Dispersion Relations . . . 67
4.2.1 Boundary Conditions . . . 68
4.2.2 The First Approach . . . 68
4.2.3 The Second Approach . . . 69
4.3 Fundamental (TE_0) modes . . . 72
4.3.1 Modal characteristics . . . 72
4.3.2 Stability . . . 78
4.4 First-order (TE_1) modes . . . 80
4.4.1 Modal characteristics . . . 80
4.4.2 Stability . . . 85
4.5 In Terms of Surface Wave Stability . . . 92
4.5.1 Stability of a Surface Mode . . . 93
4.5.2 Lateral Field Shift in Nonlinear Medium . . . 93
4.5.3 Particle Analogy . . . 95
4.6 Second-order (TE_2) modes . . . 97
4.6.1 Modal Characteristics . . . 97
4.6.2 Stability . . . 98
4.7 Experimental Relevance . . . 100

5 Waveguides involving SDF Nonlinearities **103**
5.1 Waveguides with SDF bounding media 104
5.1.1 Modal Characteristics 104
5.1.2 Stability 108
5.1.3 Potential Applications 112
5.2 Waveguides with a Self-defocusing Core 112
5.2.1 Calculation of Modes 113
5.2.2 Modal Stability 115

6 Dark Guided Waves **119**
6.1 Surface Waves 120
6.1.1 Linear-SDF Interface 121
6.1.2 SDF-SDF Interface 123
6.1.3 SF-SDF Interface 126
6.2 Guided Waves 129
6.2.1 Symmetric Modes 130
6.2.2 Anti-symmetric Modes 133
6.2.3 Asymmetric Modes 142
6.2.4 Asymmetric Waveguides 142
6.3 Experimental Relevance 143

7 Generalization, Discussions, and Conclusion **145**
7.1 Guided Waves in Power-law Media 145
7.1.1 Surface Waves 146
7.1.2 Guided Waves 151
7.1.3 Stability 157
7.2 Discussions 158
7.2.1 Nonlinear films 159
7.2.2 Nonlinear saturation 159
7.2.3 Lossy media 160
7.2.4 Mode excitation 160
7.3 Conclusion 162

Chapter 1

Introduction

We begin with an elementary introduction to optical waveguides, in the humble expectation that it will be readily understandable to most people in the scientific and technological community including those not directly involved in this field.

Firstly, some basics about optical waveguides are briefly described, and the fundamental difference between linear and nonlinear waveguides is explained. Then the two approaches for describing light propagation in waveguides are briefly mentioned. It will be explained how the contributions to the field made by the work in this thesis fit into the general picture of nonlinear optics. The fascinating applications of waveguides are reviewed. A brief survey of currently available nonlinear materials are presented. And finally, a summary of the thesis is given.

1.1 What is an Optical Waveguide ?

As the name suggests, an optical waveguide is a dielectric structure that guides electromagnetic waves at optical or near optical frequencies.

Basically, an optical waveguide consists of two parts: a central region, typically a few microns in size, called the *core*, and a surrounding medium of different refractive index. For cylindrical waveguides, this bounding medium is called the *cladding*, whereas for planar and channel waveguides, the term 'cladding' often refers to the bounding medium on one side of the core, while on the other side, it is called the *substrate*. These are illustrated in fig.1.1. The terminology reflects the use of the latter type of waveguide in integrated optics. Steady guidance of light by the structure is possible only when the refractive index of the core is *higher* than that of the bounding medium. Underlying the guidance is the basic principle of total internal reflection, which is well-known from the nineteenth century [1].

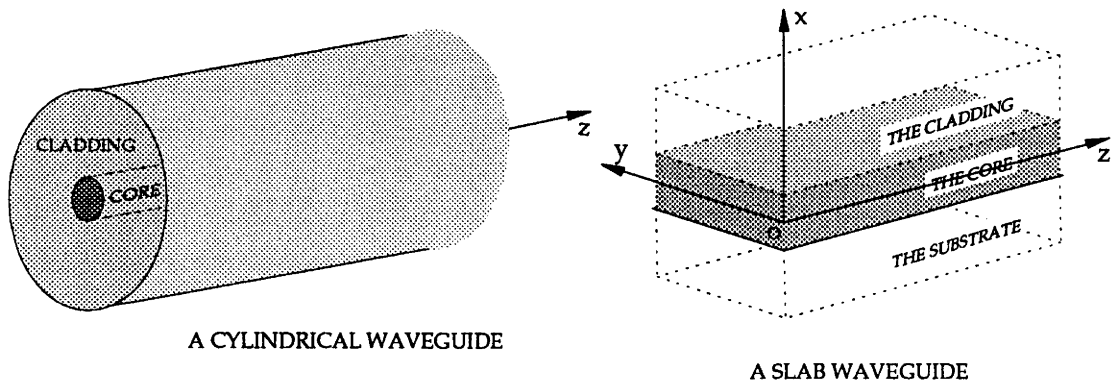

Figure 1.1: Sketches of a cylindrical waveguide and a slab waveguide.

Optical waveguides may be classified into two categories: *linear* waveguides and *nonlinear* waveguides, with the following fundamental difference:

LINEAR WAVEGUIDES are characterised by the fact that the form of light propagation in the waveguides is independent of the light intensity. In mathematical terms, the equations governing the propagation (i.e. Maxwell's equations) are all linear.

In NONLINEAR WAVEGUIDES, light propagation depends on the local light intensity. This dependence manifests itself through the variation of the refractive index n on local light intensity I. There are two possible cases: n may increase or decrease with increasing I. In the first case, the waveguide medium is called *self-focusing*, while in the latter case, it is called *self-defocusing*. In mathematical terms, the equations governing the propagation are all nonlinear. Compared with linear waveguides, nonlinear waveguides possess a much richer variety of interesting phenomena [2,3].

Here are a few more terms that are often encountered in waveguide optics: If a waveguide can support only one bound mode (explained in the next section), it is called a *single-moded* waveguide. In practical fibers, this occurs when the fiber radius is not more than about 5 microns. If a waveguide can support many bound modes, then it is called a *multimoded* waveguide. Somewhere in between, it can be called a *few-mode* waveguide. This thesis is concerned primarily with the first and last types.

1.2 Propagation in waveguides

To describe light propagation in waveguides, two different approaches are available, namely *ray* or *geometrical optics* and *electromagnetic wave theory.* The former approach is suitable in cases where the dimension of the waveguide is very large compared with an optical waveglength, and propagation characteristics can then be studied using ray tracing techniques well-known in geometrical optics.

When the waveguide dimension is comparable with an optical wavelength, the wave nature of light cannot be neglected, and use of the wave theory of light is absolutely necessary. In this approach, the concept of a *mode* is fundamentally important. As usual in physics, a mode (or normal mode) of a system is a state of that system which vibrates at a single frequency. In optical waveguide terminology, that frequency is a spatial frequency called the *propagation constant* β which appear in the following context:

$$\mathbf{E}(x, y, z) = \mathbf{e}(x, y) \exp(i\beta z - i\omega t). \tag{1.1}$$

This is the mathematical representation of a optical mode which propagates along the z-direction. In (1.1), x, y, z are Cartesian coordinates (with z being longitudinal), ω is the optical frequency, and $\mathbf{E}$ is the total optical electric field. The magnetic component of the optical field can be expressed in a similar form

$$\mathbf{H}(x, y, z) = \mathbf{h}(x, y) \exp(i\beta z - i\omega t).$$

However, in calculations with optical fields, especially those for TE waves, it is more convenient to work exclusively with the electric component, while the magnetic component serves in deriving boundary conditions at interfaces between different dielectric media, if there are any. (See section c4boundary).

A mode is called a *bound mode* if $\mathbf{e}(x, y)$ vanishes at infinity (i.e. at large distances from the center of the waveguide). Otherwise, it is called an *unbound or radiation mode.* In fact, in any waveguide, there is an infinite number of radiation modes which form a continuous spectrum. The optical power carried by a bound mode is called *modal power.* However, when the number of bound modes is large, a modal description becomes complicated and a ray description is preferred.

In linear waveguides, the *principle of linear superposition* holds. This means any waveform propagating in a linear waveguide can be expressed as a linear sum of the bound and radiation modes of the waveguide. This nicety no longer exists in nonlinear waveguides. Nevertheless, once a nonlinear mode propagates in a nonlinear

waveguide, it can be regarded as a linear mode of the waveguide it induces or modifies from the existing (zero-power) waveguide. This is called the *equivalence principle* [4]. It is useful in interpreting a nonlinear mode in terms of its linear counterpart, and in some very special cases [5,6,7], in calculating it. However, it has some major limitations:

1. The principle applies only to fundamental modes, i.e. modes with no nodes in their shapes (or profiles).

2. It does not help in determining all the modes that can be supported by an arbitrary nonlinear waveguide, nor does it predict the course of evolution that a non-stationary nonlinear wave may take along the waveguide.

Two regimes of nonlinearity

These are the weak and strong nonlinearities. In the *weak regime*, the nonlinearity changes the refractive index by a very small amount, and thus changes the propagation constant β slightly but does not change the modal field $\mathbf{e}(x,y)$ to any noticable extent. This leads to an analysis which often involves the so-called coupled-mode theory (see, e.g., [8,9,10,11,12]. The result is an accumulated phase shift after a certain distance of propagation, which forms the basis of many device applications, such as power-dependent couplers [13].

In the *strong nonlinearity regime*, with which the present thesis is concerned, both the modal field and the propagation constant β can vary significantly with modal power. In this regime, it is necessary to obtain solutions (either analytical or numerical) for the nonlinear wave equations involved. And since β is a very large number, the word 'vary significantly' used here for β should be given a clear interpretation. In fact, highly nonlinear phenomena [14] have been shown to be possible with β changing by a factor of about one or a few parts in a thousand ! (Instead of using β in a description, the effective refractive index n_{eff}, defined by $n_{eff} = \beta/k$, has also been widely used.) On a more fundamental basis, this regime arises from the fact that the nonlinear polarizations are strong enough to compete with the linear waveguiding mechanism.

In practice, light propagating in waveguides, e.g. single-mode optical fibers, is often in the form of pulses, although there are also lasers which can maintain continuous wave (cw) light propagation. The transverse profile of these pulses may be described in terms of modes as discussed above, while the longitudinal shape is very much affected by the nonlinearity of the medium. In linear optical fibers,

it is well-known that pulses spread out as they propagate along a fiber due to dispersion, causing one of the major problems in telecommunication systems using optical fibers. In nonlinear single-mode optical fibers, the self-focusing effect can change the situation drastically. It has been shown that dispersion and self-focusing effects can cancel each other, with the result that pulses retain their shape, in the form of *solitons*, during propagation [15].

Of course, solitons exist only in the strong nonlinearity regime. This is not to say that the existence of solitons requires a high nonlinear coefficient of the dielectric medium. For example, common silica fibers, which possesses one of the weakest nonlinearities, are well-known to be capable of supporting soliton pulses. Rather, it is meant that the soliton shape very much depends on its power. Soliton pulses are also called temporal solitons. Another type of soliton is the spatial soliton. This is a longitudinally invariant beam with a soliton cross-section in either one or two transverse dimensions [16,17]. Part of this thesis (section 3.1) is devoted to the stability of these solitons. The mathematical descriptions of spatial and temporal solitons are identical, with the time t in the temporal case being mathematically equivalent to the longitudinal dimension z in the spatial case. Likewise, pulse dispersion (or spreading) in the temporal case is equivalent to diffraction in the spatial case.

1.3 On the background of nonlinear optics

Needless to say, the topic of nonlinear guided waves is only part of the much broader field of nonlinear optics. It is therefore important to be aware of the circumstances in which other possible nonlinear phenomena can interfere with the propagation of guided waves. The attempt here is only to give a brief account of some nonlinear effects and related problems. For a more throrough, rigorous and comprehensive treatment, the reader is referred to standard texts [18,19,20].

Broadly speaking, optical nonlinearity arises from the interaction of light waves with matter. Let us now consider in a simple way how this interaction occurs.

Dielectric materials which concern us in optics can be thought of as a collection of charged particles (electrons and positive ion cores) which are bound together with some 'elasticity'. When an electric field is applied to a dielectric material, the electron clouds of the atoms are distorted, resulting in an induced polarization. If the applied field is the oscillating electric field

$$E = E_o \cos(\omega t)$$

of a passing light wave with optical angular frequency ω, the induced polarization is also oscillatory and has the form

$$P = \epsilon_o \chi^{(1)} E \tag{1.2}$$

where $\chi^{(1)}$ denotes linear susceptibility.

However, the harmonic response (1.2) of the polarization is valid only for low light intensities, and then the motion of the charged particles may be regarded as being governed by an harmonic potential well (see, e.g. [20]). For high enough intensities, (1.2) must be replaced by a more general form

$$P = \epsilon_o \left(\chi^{(1)} E + \chi^{(2)} E^2 + \chi^{(3)} E^3 + \cdots\right) \tag{1.3}$$

where $\chi^{(2)}$, $\chi^{(3)}$,... are called the nonlinear susceptibilities of the medium. The nonlinear terms in (1.3) arise basically from the nonlinear response of charged particles in an anharmonic potential well. Intensity levels above which it becomes necessary to include these nonlinear terms depend on the particular phenomenon and material under investigation. For example, for nonlinear switching in erbium-doped glass fibers requires intensities of the order of kW/cm^2 [21] (or equivalent of powers of less than 1 W in a 3 μm diameter fiber) ; while for second harmonic generation in fibers required intensities corresponding to about 1 mW input powers in a fiber waveguide [22]

In generally anisotropic media in which material propertities are directionally dependent, the polarization P and electric field E, and susceptibilities $\chi^{(i)}$ must be replaced by vectors $\mathbf{P}$ and $\mathbf{E}$, and tensors $\chi^{(i)}$. And more sophisticated treatment are necessary [18,19,20].

Quadratic Polarization $P^{(2)} = \epsilon_o \chi^{(2)} E^2$

This component of polarization gives rise to effects which are basically all mixing phenomena, involving the generation of sum and difference frequencies (see e.g. [20]). However, of interest here is the fact that, in isotropic materials which have inversion symmetry, $\chi^{(2)}$ vanishes identically. This is because in these materials, opposite directions are completely equivalent, and so the polarization must change sign when the optical field is reversed. Consequently, there can be no even powers of the field in the expansion (1.3) of the polarization.

Cubic Polarization $P^{(3)} = \epsilon_o \chi^{(3)} E^3$

This gives rise to third-order processes such as third-harmonic generation and the intensity-dependent refractive index, of which the latter is the most important. Let

us assume that the dielectric medium is isotropic. If we can restrict the investigation to the cubic term in the polarization expansion (1.3), then

$$P = \epsilon_o (\chi^{(1)} E + \chi^{(3)} E^3) \tag{1.4}$$

Since the dielectric displacement is $D = \epsilon_o E + P$, the refractive index n satisfies

$$n^2 = 1 + \chi^{(1)} + \chi^{(3)} E^2 \tag{1.5}$$

with the assumption that the material is lossless. This gives rise to the well-studied *Kerr-law* nonlinearity

$$n = n_0 + n_2 |E|^2, \tag{1.6}$$

in which the refractive index n is a linear function of light intensity. Here n_0 is the linear refractive index, and n_2 is called the nonlinear coefficient. (n_2 is proportional to the familiar Kerr coefficient which is in units of m^2/W. It should be noted that $|E|^2$ is not the light intensity but a quantity proportional to it.) The Kerr nonlinearity is used extensively in later chapters of this thesis.

The Kerr effect and third-harmonic generation mentioned above belong to a broader category called 'non-resonant' or 'non-dissipative' phenomena, in which the optical frequencies are far from the resonance frequencies of the medium. In a second category are those phenomena which are 'resosonant' or 'dissipative'. Some examples of this category are stimulated Raman scattering (SRS), two-photon absorption, and the nonlinear refractive index arising from saturated absorption [20]; these can significantly interfere with nonlinear guided-wave phenomena.

SRS [23,24] occurs when a probe beam at frequency ω_s, which is coincident with a pump beam at frequency ω_p, is amplified, provided that $\omega_p - \omega_s$ lies in the Raman gain spectrum. In guided-wave applications there is often only the pump, and the weak probe waves are provided by spontaneous Raman scattering. However, this interference is significant only when the guided wave is above some threshold power. Unlike SRS, two-photon absorption [25] can occur when $\omega_p + \omega_s$ is in some appropriate range resulting in the absorption of the pump wave.

Another effect is stimulated Brillouin scattering (SBS) [23,26] which can cause severe interference with guided waves. SBS manifests itself through the generation of a backward propagating wave once the Brillouin threshold is reached.

A practical distinction between these two categories is in the widely differing speed of response. Non-resonant phenomena involve electronic transitions and hence can be very fast, of the order of 1 fs (10^{-15} s), while the speed of resonant phenomena

depends on relaxation times: typical response times are in the picosecond range or longer.

The studies in this thesis exploit only the intensity-dependent refractive index within some idealizations in which the above effects, whether detrimental or beneficial, are not present. This is permissible when guided-wave powers are not too high. Furthermore, we assume instantaneous nonlinear response in the dielectric medium, and hence all possible phenomena related to non-local or thermal effects, which can occur in real media, are beyond the scope of these studies.

1.4 Applications

Linear waveguides have already brought about fascinating applications, such as those in telecommunications and integrated optics.

In telecommunication systems, optical fibers are currently the most efficient means for signal transmission due to the following factors:

1. high optical frequencies, and hence huge bit rates, available.

2. low loss over a relative wide range of wavelengths (especially $\sim 1.5\mu$m).

3. small size and low cost.

4. no electromagnetic interference.

Some large-scaled fiber optic systems for telecommunication have already come inot existence. For example, TAT-8, the first Trans-Atlantic fiber optic system, operational in June of 1988, is comprised of a total of about 3,500 nautical miles of cable laid on the ocean floor connecting Tuckerton (New Jersey), Widemouth (England) and Penmarch (France) (see e.g. Ref.[27]). There have also been two other similar systems, the Hawaii/Transpac3 (or TPC-3) and Tasman 2 (by the Australian Overseas Telecommunications Commission) already in service, which spanned many thoudsands of nautical miles on the sea bed. For more detailed information, the serious reader is referred to better documented reviews and standard texts [28]-[33].

Among numerous applications in integrated optics, waveguides are attractive in implementing efficient nonlinear interactions, due to two factors: 1) high power densities are possible with moderately low total power, due to beam confinement in the small cross-section of a waveguide; and 2) the diffractionless propagation along

a waveguide allows for long interaction lengths, and thus optimizes interaction efficiency [2]. Devices such as directional couplers, Y-junction splitters, loop resonators have already been widely used in optoelectronics.

Adding to the existing advantages of linear waveguides, nonlinear waveguides promise to be the choice for the near future. In telecommunication, soliton transmission systems, which have even much higher bandwidths due to the possibility of eliminating pulse spreading, are now the subject of great interest with nonlinear fibers. Direct light pulse amplification, using a laser for example, is another possibility with nonlinear optics that would help eliminate the need for intervening, slow electronics.

In integrated optics, the nonlinear directional coupler has been proposed [13,34] for power-dependent switching and has been extensively studied [35,36]. Numerous others applications are: nonlinear grating devices, nonlinear Mach-Zehnder interferometer, nonlinear mode sorters, and devices based on optical bistability [2]. By 1985, several proposals for applications of nonlinear guided waves had been reported [3]. These include: optical limiters (or upper threshold devices), an example of which is studied in chapter 5; lower threshold devices, i.e., those that pass optical devices above a threshold power; and optical switches. These are discussed in more detail in later chapters. More recently, dark waves have been suggested as means of writing stable waveguide structures [37].

However, these potential device applications depend very much on the availability of suitable nonlinear materials, and this is the subject of the next section. Nevertheless, we can confidently say that the rapid developments in this area, both experimental and theoretical, herald a new revolution in all-optical information processing.

1.5 Nonlinear Materials

This section contains a very brief survey of the existing nonlinear materials and trends of current developements in this area of research.

To be suitable for used in a real integrated circuit or communication system, a dielectric material must generally satisfy the following conditions: low loss, easy processing, accurate waveguide definition, stability (to physical, chemical, mechanical, electrical and thermal conditions), compatibility with other materials used in the circuit, high electro-optic coefficients, high damage threshold, and low cost. In view of the present theoretical studies, however, the most important and relevant

parameter is the Kerr coefficient which characterises the strength of nonlinearity of a particular material. On the practical side, the important parameters are the so-called 'figures of merit' (FOM) T and W, and the absorption coefficient α. These are explained in the following.

In general, α linearly depends on local light intensity I,

$$\alpha = \alpha_0 + \beta_2 I$$

where α_0 and $\beta_2 I$ are the one and two photon absorption coefficients. High intensities, in practice, can be maintained typically over one attenuation length $L \leq \alpha^{-1}$.

The figures of merits T and W arise from factors limiting the maximum nonlinear effects, and are defined as

$$T = 2\lambda\beta_2/n_2$$

$$W = \Delta_{sat}/\lambda_0\lambda$$

where λ is the free-space wavelength used, and Δ_{sat} is the maximum nonlinear index change when saturation is reached. The general aim of materials research efforts is to reduce T and increase W. The exact requirements on these FOM's depend on the particular application under investigation. For example, for switching in nonlinear directional couplers, we need $T < 1$ and $W > 2$ [38].

There are basically three types of nonlinear materials: semiconductors, organics, and glasses, each of which is associated with a different mechanism giving rise nonlinearity (see e.g. [38] and references there in). The properties of some currently

available materials are summarised in Table 1 (see [38,39]).

Material	n_2 cm^2/W	α cm^{-1}	W	T	λ microns
SEMICONDUCTORS					
GaAs	$< -3 \times 10^{-13}$	1.0	< 2.8	> 17	1.06
AlGaAs	2×10^{-13}	0.1	8	< 0.3	1.56
AlGaAs	-4×10^{-12}	18	2.5	0.9	0.81
ORGANICS					
PTS (crystal)	-4×10^{-12}	0.8	40	4	1.06
poly-4BCMU	5×10^{-14}	< 0.2	> 2.5	< 1.0	1.3
DANS	8×10^{-14}	< 0.2	> 4.0	≈ 1	1.06
(polymer)	8×10^{-14}	< 0.2	> 5.0	≈ 0.2	1.31
DEANST (20%)	6×10^{-14}	$< 10^{-2}$	> 40	< 1	1.06
DAN (crystal)	5×10^{-12}	3	26		0.63
	$\times 10^{-13}$	3	0.5		0.63
DAN2(polymer)	2×10^{-13}	< 1	> 2	< 1	1.06
GLASS					
SiO_2	2×10^{-16}	10^{-6}	$> 10^3$	$<< 1$	> 1.06
RN (Corning)	1.3×10^{-14}	0.01	13	< 0.1	1.06

Table 1: Parameters of some nonlinear materials. Here $I = 1\text{GW/cm}^2$ has been assumed for $\Delta n_{sat} = n_2 I$. Other nonlinear self-defocussing materials, such as chlorophyll [37], have been used to demonstrate dark waves but not listed here due to lack of sufficient details.

Although various types glass have some of the smallest nonlinearities known, they are probably the most successful in demonstrating both temporal and spatial solitons (in one transverse dimension) [40]. Currently, there is a strong interest in organic materials which are already recognized as exhibiting the largest non-resonant nonlinearities [41], although loss is currently relative high. (For more details, the serious reader is referred to Refs.[38] and [42]. The main feature we would like to point out here is that there are already some materials with a $|n_2| \geq 10^{-12}$ cm^2/W which can allow the realization of nonlinear guided waves studied in this thesis, except for some unwanted properties.

1.6 Summary of Presentation

The rest of this thesis can be summarized as follows.

Chapter 2 sets up the background needed in later chapters. This includes the form of the scalar wave equation for TE modes and the available exact solutions, including the new solutions for power-law nonlinearities. It discusses the usefulness of phase diagrams and the mechanical interpretation of differential equations. It also briefly describes some of the numerical methods used for solving the wave equation in cases where this cannot be solved analytically. And lastly, the conversions between actual parameters and the scaled, dimensionless parameters used throughout this thesis are explained.

Chapter 3 describes and discusses various methods for determining the stability characteristics of stationary waves (i.e. modes). These methods include: linear stability analysis and Lyapunov theory. In the linear analysis section, it is discovered that growth rates can be complex, contrary to the traditional assumption that they can only be real or purely imaginary. Furthermore, some new exact solutions are reported which lead to a straightforward determination of stability of several classes of nonlinear modes. Earlier works by several other authors are also reviewed and discussed. In the next section, the background of Lyapunov's theory is given. It is then shown how this can be applied to the study of nonlinear guided waves. The chapter ends with a brief section discussing problems associated with transverse stability.

Chapter 4 studies nonlinear planar waveguides with a linear core and Kerr self-focusing bounding media. It describes two different analytical approaches for calculating the dispersion characteristics. The main subject of the chapter is the investigation of TE_0, TE_1 and TE_2 modes and their stability. Of significant importance is the fact that the pattern of stability regimes for the TE_1 and TE_2 modes are quite complicated due to the existence of complex 'growth rates' in linear stability analysis. An attempt is made to explain physically, in terms of surface modes, the difference between the stability characteristics of the symmetric TE_0 and anti-symmetric TE_1 modes in the region of high β. Lastly, some related experimental works done by other researchers are discussed.

Chapter 5 examines two types of symmetric waveguides which involve Kerr self-defocusing nonlinearities. The first type consists of a linear core and self-

defocusing bounding media. By linear analysis, all modes supported by this type of waveguides are stable. In the second type, the core is self-defocusing and the bounding media are self-focusing, and in which the characteristics of the TE_0 modes are somewhat similar to that of the waveguide with linear core and self-focusing bounding media.

Chapter 6. Here, various types of dark and bright-dark modes are calculated analytically in interface and slab waveguide structures. Again, linear analysis is used to study stability characteristics. These are then tested numerically using beam propagation methods. A discussion on related experiments is given.

Chapter 7. The first section of this last chapter is an extension of the preceeding three chapters to include power-law nonlinearities. Power-law interfaces have similar characteristics to Kerr-law interfaces, except that when the medium on either side of the interface possesses a nonlinear exponent $q > 2$, the surface modes are all unstable. The consideration for waveguides is restricted to TE_0 modes in symmmetric structures. The results are similar to the Kerr-law counterparts, except that if the bounding media have $q > 2$, then all TE_0 modes are unstable beyond the bifurcation point.

The second section of the chapter briefly discusses related problems such as nonlinear films, effects due to properties of realistic materials such as absorption and nonlinear saturation that were not taken into account in the present considerations. Provided that these effects are small, it is expected that the treatments presented here still give a good description of the phenomena. Some comments on mode excitation are also included.

Chapter 2

Solutions of the Wave Equation

This chapter contains background material needed for developments in later chapters. The material includes a discussion of the TE scalar wave equation and its solutions; these govern the existence and characteristics of possible guided (or self-guided) modes. In the 1960's when interests in third-order nonlinear effects started out, the direction of research efforts was to search for exact analytical solutions for stationary waves [43,44], which are important in studying guided-wave phenomena. Up until the present time, analytical solutions are available for only a few types of nonlinearity. These include Kerr type, power-law type, and a quartic model.

A contribution to the field made in this chapter is the exact solution for the power-law nonlinearity, which may prove important in studying waveguides involving materials such as semiconductors [45]-[48]. The present analysis is greatly simplified by using a scaling law by which the scalar wave equation and its solutions are written such that the system can be described with a minimal number of parameters.

The structure of this chapter is as follows. Section 2.1 starts from Maxwell's equations in a medium with no current sources and shows how these are reduced to simple but exact equations for TE waves, and the types of nonlinearities which have received considerable attention in the literature. Section 2.2 contains the available exact solutions for several types of nonlinearities. Among the useful tools, which nowaday do not seem so popular, are the method of phase diagrams and the mechanical interpretation of a differential equation. These are especially useful when the nonlinearity is such that exact solutions are not readily available, or when only qualitative behaviour of a nonlinear solution is required. Section 2.3 is devoted to these methods. Section 2.4 further demonstrates the usefulness of the phase diagram method when it is applied to layered structures. Finally, section 2.5 discusses numerical methods available that are for calculating stationary solutions and for

non-stationary but slowly-varying solutions when they propagate along a structure.

2.1 Wave Equation

As for all electromagnetic phenomena, Maxwell's equations (see, for example [49, chp.30]) are the basis and govern the propagation of electromagnetic waves in dielectric optical waveguides. When there are no current sources, Maxwell's equations reduce to simpler forms in which the spatial dependences of the electric $\mathbf{E}(x,y,z)$ and magnetic $\mathbf{H}(x,y,z)$ vector fields are given by

$$\begin{aligned} \{\nabla^2 + n^2k^2\}\mathbf{E} &= -\nabla(\mathbf{E}_t \cdot \nabla_t \ln n^2) \\ \{\nabla^2 + n^2k^2\}\mathbf{H} &= (\nabla \times \mathbf{H}) \times \nabla_t \ln n^2 \end{aligned} \tag{2.1}$$

where $k = 2\pi/\lambda$ is the free-space wavenumber, λ is the wavelength of light in free space, $n(x,y,z)$ is the refractive index, x and y are cartesian transverse coordinates, z is the longitudinal coordinate, and the subscript t denotes the transverse component. A full description of the phenomena would involve both the electric field $\mathbf{E}$ and the magnetic field $\mathbf{H}$. However, for the non-magnetic materials which normally constitute optical waveguiding structures, the magnetic permeability μ is very nearly equal to the free-space value μ_o. Consequently, only the electric field $\mathbf{E}$ in Eqn.(2.1) is studied in this thesis. The magnetic field $\mathbf{H}$ has only an insignificant interaction with dielectric materials, and is invoked only in calculations leading to optical power of a mode (section 2.6) and in setting boundary conditions (section 4.2.1).

Translationally invariant guiding structures, which are the subjects of this thesis, have $n = n(x,y)$, and can support modes of the form

$$\mathbf{E}(x,y,z) = \mathbf{e}(x,y)e^{i\beta z} \tag{2.2}$$

where β is called the propagation constant. With this, the first equation of (2.1) becomes

$$\{\nabla_t^2 + n^2k^2 - \beta^2\}\mathbf{e} = -(\nabla_t + i\beta z)\mathbf{e}_t \cdot \nabla_t \ln n^2. \tag{2.3}$$

If n is independent of $\mathbf{e}$, then Eqn.(2.3) is a linear equation which defines a complete set of orthogonal normal modes the spectrum of which usually consists of both a discrete part (bound modes) and a continuous part (radiation modes) that were briefly mentioned in section 1.2. All forms of light propagation down a dielectric struture can then be expresssed by this spectrum. When n depends also on $\mathbf{e}$, interesting new phenomena can arise which can be described by the solutions

to the nonlinear equation (2.3). However, finding these solutions is not always a trivial process. In any case, a necessary condition for light guidance is that $n(x,y)$ be a bound (i.e. localized) function, because light has a tendency to be attracted to higher index regions.

2.1.1 Planar Geometry

Planar geometry reduces the number of transverse dimensions to one, i.e. the refractive index distribution n and the modal fields are functions only of x:

$$n = n(x), \quad \mathbf{e}(x,y) = \mathbf{e}(x).$$

Strictly speaking, this is an idealisation because the structure is allowed to be infinite in the y-dimension. Nevertheless, in realistic planar structures where the y-dimension is very long compared with the x-dimension, edge effects can be ignored, and planar geometry often provides a satisfactory description. In cartesian planar coordinates, $\mathbf{e} = (e_x, e_y, e_z)$, and Eqn.(2.3) has components [49]

$$\frac{d^2e_x}{dx^2} + \frac{d}{dx}\left\{e_x \frac{d\ln n^2}{dx}\right\} + (n^2k^2 - \beta^2)e_x = 0, \tag{2.4}$$

$$\frac{d^2e_y}{dx^2} + (n^2k^2 - \beta^2)e_y = 0, \tag{2.5}$$

$$\frac{d^2e_z}{dx^2} + i\beta\frac{d\ln n^2}{dx}e_x + (n^2k^2 - \beta^2)e_z = 0. \tag{2.6}$$

Of interest are the transverse electric (TE_m) modes which have $e_x = e_z = 0$, while e_y is governed by equation (2.5), which is an ordinary second-order differential equation. (From here on, e_y is rewritten as E.) It should be emphasized that this simple scalar form of the resulting wave equation (2.5) does not involve any approximation such as weak guidance [49], which is often assumed in many waveguide geometries. Thus later, when we allow n to vary with $\mathbf{e}$, we can allow an index change which is large compared with linear-index profile heights.

2.1.2 Types of Nonlinearity

As has been mentioned in the Introduction, the Kerr nonlinearity is the type of nonlinearity that receives the most attention. Other types of nonlinearities have also been considered in the past few years.

Due to various mechanisms such as two-photon absorption, the refractive index of most practical materials saturate at high intensities. This is described by the

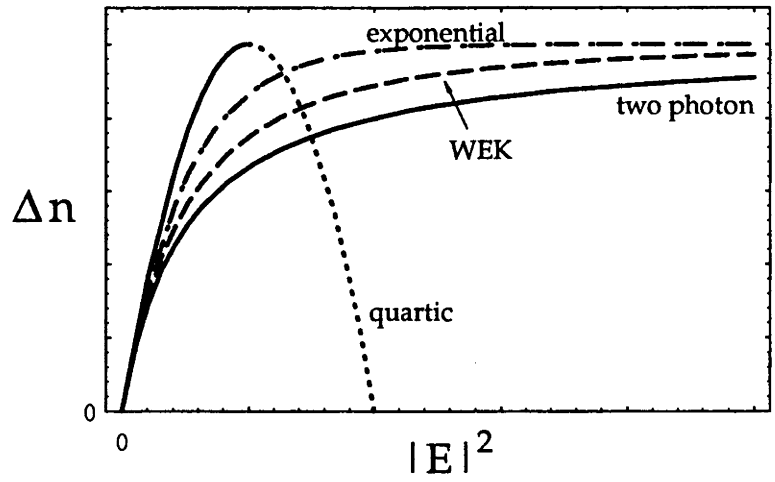

Figure 2.1: Comparison of the four different types of saturable nonlinearity. The vertical axis shows the nonlinear contribution Δn to the the refractive index n.

saturable two-level model [50]

$$n = n_0 + n_2 \frac{|E|^2}{1 + \gamma |E|^2}, \tag{2.7}$$

where γ is a constant. (However, real materials whose refractive index can be approximated by this model often has loss built in; this is discussed further in chapter 7.)

For mathematical convenience, other models for saturation effects have also been used in the literature, such as the *exponential model* [51]

$$n = n_0 + n_2(1 - e^{-\gamma |E|^2}), \tag{2.8}$$

the *quartic model* [52]

$$n = n_0 + n_2 |E|^2 - n_4 |E|^4, \tag{2.9}$$

where $n_4 > 0$ may be called the 'quartic coefficient', and the *Wood-Evans-Kenan (WEK) model* [53]

$$n = n_0 + n_2 \frac{t(2+t)}{(1+t)^2}, \tag{2.10}$$

where $t = |E|^2/2$. A comparison of these models is made in fig.2.1.

Of special interest are the quartic and WEK models for which calculations can be carried out analytically. This is important in determining the range of validity of numerical calculations of guided-wave properties and for estimation of the step

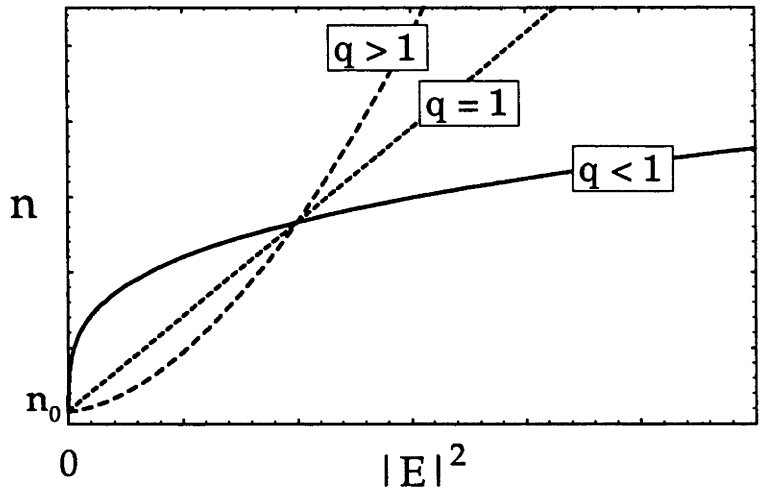

Figure 2.2: Schematic behaviour of some power-law nonlinearities $n = n_0 + |E|^{2q}$.

sizes required to achieve a desired level of accuracy. These models also often provide a more qualitative understanding of the significance of the model parameters than can be obtained from numerical work.

In special materials, including semiconductors [45]-[48], power-law nonlinearities of the form

$$n = n_0 + n_2 |E|^{2q} \tag{2.11}$$

where q is a positive constant, are also possible. These will be studied in some detail in chapter 7. The schematic variation of n with $|E|^2$ in these cases is shown in fig.2.2 for several values of q.

2.2 Exact Solutions for a Homogeneous Medium

At the present time, exact solutions to the wave equation exist only for TE modes, which are given by solutions of equation (2.5), for some particular types of nonlinearity in planar geometry. These nonlinearities include the Kerr type, the quartic type, and the power-law type expressed by (1.6), (2.9), and (2.11) respectively.

To present a description of modal characteristics in a simple and consistent way throughout the thesis, the wave equation governing the TE modes is written as

$$\frac{d^2\psi}{dX^2} - B\psi + hF(|\psi|^2)\psi = 0, \tag{2.12}$$

where X is the transverse coordinate scaled by a length ρ (a conveniently-chosen scaling length, of the order of a wavelength, i.e. $x = X\rho$), $B = \rho^2(\beta^2 - k^2 n_0^2)$ is called the modal parameter, n_0 is the linear index of the nonlinear medium. $F(|\psi|^2)$ is a function characterizing the nonlinearity, and ψ is a field quantity defined, in the case of Kerr law, by

$$\psi = |\alpha|^{1/2} E. \tag{2.13}$$

Here α is the scaled nonlinear coefficient defined by $\alpha = 2n_0 n_2 k^2 \rho^2$, and h is equal to 1, 0, or -1 if the medium is self-focusing, linear, or self-defocusing respectively.

Once ψ is known, the other components of the electromagnetic field can be derived [49]. All quantities in Eqn.(2.12) are now dimensionless. The major advantage of this notation will become clearer when it comes to studying waveguide structures in later chapters. Solutions for some particular types of nonlinearity are now discussed.

2.2.1 Linear medium

This is certainly the simplest possible type of dielectric medium. The wave equation reduces from (2.12) to

$$\frac{d^2\psi}{dX^2} - B\psi = 0. \tag{2.14}$$

The most general solution of (2.14) is

$$\psi(X) = a_1 \sinh(\sqrt{B}\,X) + a_2 \cosh(\sqrt{B}\,X). \tag{2.15}$$

in which a_1, a_2 are arbitrary constants. In cases where $B < 0$, this solution may be written in terms of trigonometric sine and cosine functions.

If ψ is required to decay to zero as $X \to \infty$, then (2.15) is replaced by

$$\psi(X) = a \exp(-\sqrt{B}\,X). \tag{2.16}$$

(a is an arbitrary constant) whereas if the decay is as $X \to -\infty$ then X is replaced by $-X$ in (2.16).

Solution (2.15) is used in later chapters for linear regions which are finite, while (2.16) is used for linear, semi-infinite bounding media.

2.2.2 Kerr-law Medium

When the nonlinear coefficient n_2 in (1.6) is small (which is really the case in most currently available materials), the nonlinear law can be written in the more convenient form

$$n^2 = n_0^2 + 2n_0 n_2 |E|^2. \tag{2.17}$$

Since ψ is real, Eqn.(2.12) becomes

$$\frac{d^2\psi}{dX^2} - B\psi + h\psi^3 = 0. \tag{2.18}$$

In a homogeneous medium, Eqn.(2.18) has a general solution in the form of a sn elliptic function [54]

$$\psi = \vartheta^{\frac{1}{2}} \,\mathrm{sn}\,(\varrho X, \kappa) \tag{2.19}$$

where

$$\begin{aligned} \vartheta &= \frac{1}{h}\left[B \pm \sqrt{B^2 + 2hC}\right], \\ \varrho &= \sqrt{\frac{C}{\vartheta}}, \\ \kappa &= -\frac{h}{2}\frac{\vartheta}{\varrho^2}, \end{aligned} \tag{2.20}$$

C is an arbitrary real constant, and in the plus or minus sign is chosen such that $\vartheta > 0$. One can readily verify that, when $h = 1$ (i.e. self-focusing), there are two possible classes of solutions in the form of (2.19). One class has nodes, the other does not. In the case $h = -1$ (self-defocusing) there is only one class of solutions with nodes. These will be verified using another approach later in this chapter.

Of great interest are the limits when these sn solutions approach a constant at large distances from the coordinate origin. These are soliton solutions discussed below.

Bright solitons

This is the limit when $C \to 0$ in the self-focusing case. The solution is a bright soliton given [54] by

$$\psi(X) = \sqrt{2}\, W \,\mathrm{sech}[W(X - X_0)], \tag{2.21}$$

where $W = \sqrt{B}$, and X_0 is an arbitrary real constant. The soliton shape is illustrated graphically in fig.2.3. The condition for existence is $B > 0$. In physical terms, this condition means that the effective refractive index $n_{eff} = \beta/k$ must be greater than the linear index n_0 of the medium. One may regard this as a trivial and obvious condition because the effect of the nonlinearity is to increase the refractive index in the self-focusing case! Sometimes, it helps to note that this nonlinear mode is a mode of the linear waveguide it induces [4], which has a sech index profile.

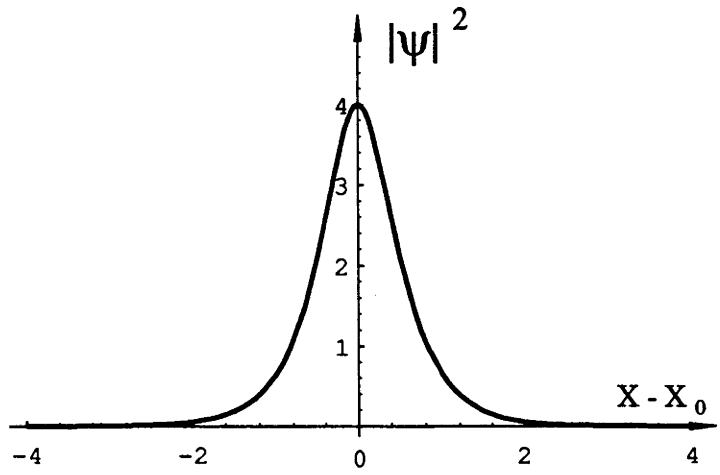

Figure 2.3: The shape of a bright soliton.

Dark solitons

In a self-defocusing medium ($h = -1$), the elliptic function (2.19) can have two different limits, depending on the sign of B.

If $B > 0$, the limit is a dark soliton (fig 2.4) given by [15,43]

$$\psi(X) = W \tanh\left[\frac{W}{\sqrt{2}}(X - X_0)\right], \tag{2.22}$$

which looks like a planar wave with a gradual π twist of phase in the 'dark' region around the coordinate origin.

To interpret the dark soliton solution physically, it is noted that the induced index profile is also a sech profile. With a bit of thought, it can be seen that a dark soliton can be regarded as a reflectionless plane wave of the waveguide it induces [55]. When there are reflections, the interference between the incident and reflected plane waves corresponds to the periodic sn solution given by (2.19). The stability of the dark soliton is discussed in chapter 3.

On the other hand, if $B = -W^2 < 0$ then the solution is [56]

$$\psi(X) = \sqrt{2}\, W \,\mathrm{cosech}[W(X - X_0)], \tag{2.23}$$

which is clearly not physical in a homogeneous medium, but is completely valid in layered structures, such as the self-defocusing waveguides and interfaces considered in chapters 5 and 6.

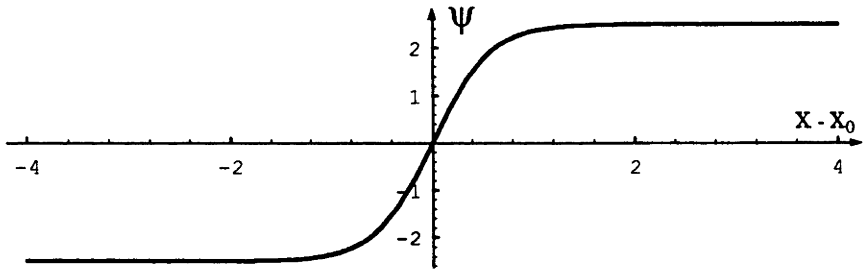

Figure 2.4: The shape of a dark soliton.

2.2.3 Power-law Medium

This is a generalization of the Kerr law discussed above, and may be written as

$$n^2 = n_0^2 + 2n_0 n_2 |E|^{2q}, \tag{2.24}$$

with q being an arbitrary positive real number. The wave equation is then

$$\frac{d^2\psi}{dX^2} - B\psi + h\psi^{2q+1} = 0, \tag{2.25}$$

where

$$\psi = |\alpha|^{1/2q} E,$$

and other quantities involved are defined in the same way as in (2.18). While power-law solutions in the self-focusing case (i.e. $h = 1$) are readily obtainable and are presented below, solutions in the self-defocusing case ($h = -1$) are not known, although they are expected to have a shape similar to the tanh function in the Kerr-law case.

There are two different approaches for solving the power-law self-focusing problem. The first approach is purely mathematical and involves integrating Eqn.(2.25) directly, and hence may be called the *direct approach.* The second approach bears more physical insight and involves first solving a linear planar waveguide with some index profile $n^2(X)$, and then inverting the problem to determine what nonlinearity an homogeneous self-focusing medium must have to give rise to the index profile and the associated modal field [5]; this may be called the *linear inversion approach.* It turns out that when $n^2(X)$ is a sech^2 profile, the linear solution is expressible in terms of sech function, and hence a power-law nonlinearity follows. While examples of the linear inversion approach can be found in references [6], [7], the direct approach is described in more detail in the following.

For a bright guided wave solution of Eqn.(2.25) to exist, it is necessary that $B > 0$. Let $B = W^2$, then the first integral of Eqn.(2.25) is

$$(\psi')^2 - W^2\psi^2 + \frac{1}{q+1}\psi^{2q+2} = C,$$

where the constant C is readily seen to be zero from the asymptotically vanishing condition on $\psi(X)$ at infinity. On rearranging,

$$\psi' = \pm W\psi\left[1 - \frac{\psi^{2q}}{W^2(q+1)}\right]^{1/2}$$

and hence

$$X = \int_{-\infty}^{\infty} \frac{d\psi}{\pm W\psi\left[1 - \frac{\psi^{2q}}{W^2(q+1)}\right]^{1/2}}. \tag{2.26}$$

With the substitution $\frac{1}{W}\left(\frac{1}{q+1}\right)^{1/2}\psi^q = \mathrm{sech}\theta$, the above integral becomes

$$q\,W\,X = \pm\theta = \mathrm{sech}^{-1}\left[\frac{1}{W}\left(\frac{1}{q+1}\right)^{1/2}\psi^q\right]$$

or

$$\psi(X) = W^{\frac{1}{q}}(q+1)^{\frac{1}{2q}}\,\mathrm{sech}^{\frac{1}{q}}(qWX) \tag{2.27}$$

with a trivial and arbitrary translational constant X_0 being implicitly assumed. When $q = 1$, this solution reduces to solution (2.21) for the Kerr-law case.

Similarly, the power-law counterpart of (2.23) is

$$\psi(X) = W^{\frac{1}{q}}(q+1)^{\frac{1}{2q}}\,\mathrm{cosech}^{\frac{1}{q}}(qWX) \tag{2.28}$$

Solutions (2.27) and (2.28) are used in studying power-law waveguides and interfaces in chapter 7.

2.2.4 Quartic Model

Although this model is not investigated in this thesis, it is shown here in the simplest possible form[1] for the sake of completeness. The exact solution of the TE wave equation with this model of nonlinearity was first obtained by Mihalache *et al.* [52]. In the present notation, the wave equation has the concise form

$$\psi'' - W^2\psi + \psi^3 + \kappa\psi^5 = 0, \tag{2.29}$$

where ψ and W are defined as for the Kerr-law case, and $\kappa = -n_4/2n_0n_2^2k^2\rho^2$.

[1]Instead of the complicated appearance when it was first reported in Ref.[52].

The solution of (2.29) is

$$\psi = 2W\left[\sqrt{\nu}\cosh(2WX)+1\right]^{-\frac{1}{2}}, \tag{2.30}$$

where $\nu = 1+\frac{16}{3}W^2\kappa$. It can be easily verified that when $\kappa = 0$ this solution reduces to the Kerr solution (2.21).

2.3 Mechanical Interpretation and Phase Diagrams

To demonstrate the usefulness of mechanical interpretation and phase diagrams, we choose to discuss possible solutions to the wave equation (2.18), which assumes Kerr-law nonlinearity. This choice is only representative and allows a convenient comparison with what already well-known. The first step is to obtain an equation which involves only ψ and its first derivative ψ'.

Multiplying Eqn.(2.18) by $2\psi'$ (where the dash denotes d/dX) and integrating gives

$$(\psi')^2 - B\psi^2 + \frac{h}{2}\psi^4 = C, \tag{2.31}$$

where C is an arbitrary constant. This is called the first integral of the wave equation (2.18).

Mechanical Interpretation

In Eqn.(2.31), if $(\psi')^2$ is interpreted as the kinetic energy of a particle, and $h\psi^4/2 - B\psi^2$ as its potential energy [57], then C is the total conserved 'energy'. It should be noted that C need not always be positive, as the potential energy is arbitrary up to an additive constant.

Let us first discuss the case of stationary solutions in a self-focusing medium, which correspond to $h = 1$, $B > 0$. The potential well is shown in fig.2.5. Suppose the particle is released from rest at some point A; the subsequent motion of the paricle can be one of three types, depending on position of the point A on the potential curve. If A is above the local maximum at the origin (i.e. above the dashed line), then the particle rolls back and forth passing the extremum points M and D and stopping again at A' to reverse. This corresponds to periodic solutions which have nodes (or zero-crossings). If A is right on the dashed line then the particle would roll down passing M and stop at the local maximum D. This corresponds to the bright soliton solution (2.21). If A is below the dashed line, the particle just

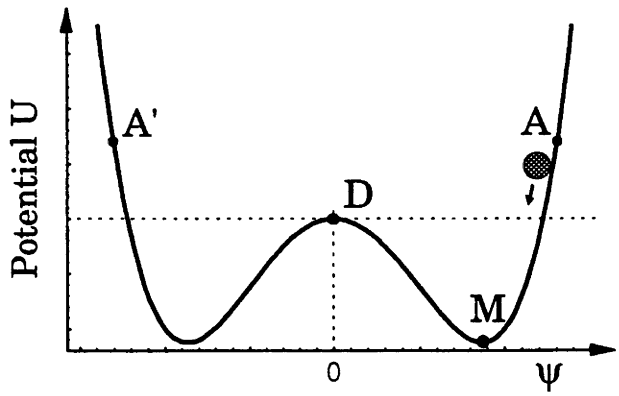

Figure 2.5: Schematic behaviour of the potential $U = \frac{1}{2}\psi^4 - B\psi^2$ of a self-focusing medium.

oscillates about M, giving a periodic solution with no nodes. It is obvious that, in this self-focusing medium, if $B < 0$ then the potential curve in fig.2.5 only has one minimum at D and no other turning points, and hence only supports periodic solutions with nodes.

If the medium is self-defocusing, the potential is similar to that of fig.2.5 but upside down. If $B < 0$, there is a local minimum, as shown in fig.2.6. Dark solitons of the form (2.22) corresponds to the motion of a particle from one maximum M' to another maximum M, while the cosech solution (2.23) corresponds to the motion of a particle outside the maxima, e.g. from a point A in the fig.2.6. Oscillations between the maxima corresponds to periodic solutions with nodes. When $B > 0$, no local minimum exists, and only modes of the cosech type exist.

Phase Diagrams

Phase diagrams [58] display the relationship between ψ and ψ', and constitute a method equivalent to the mechanical interpretation discussed above. To obtain phase diagrams, Eqn.(2.31) is rewritten in the form

$$\psi' = \pm\left[C + B\psi^2 - \frac{h}{2}\psi^4\right]^{1/2}. \tag{2.32}$$

Let us first take the simple example of stationary solutions in a self-focusing medium, for which the phase equation (2.32) is illustrated in fig 2.7 for several values of C. The three different types of solutions correspond to the different signs of C. The

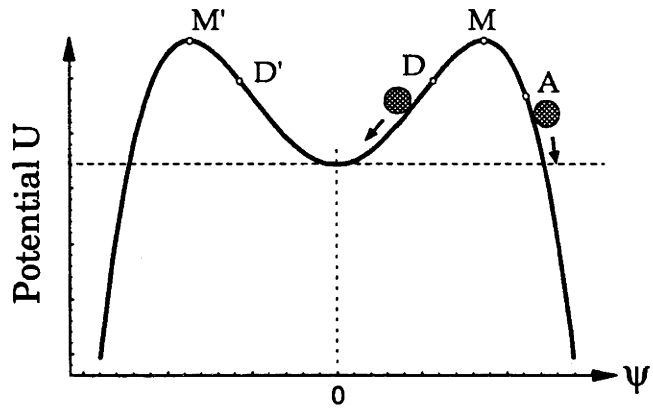

Figure 2.6: Schematic behaviour of the potential $U = -\frac{1}{2}\psi^4 - B\psi^2$ of a self-defocusing medium.

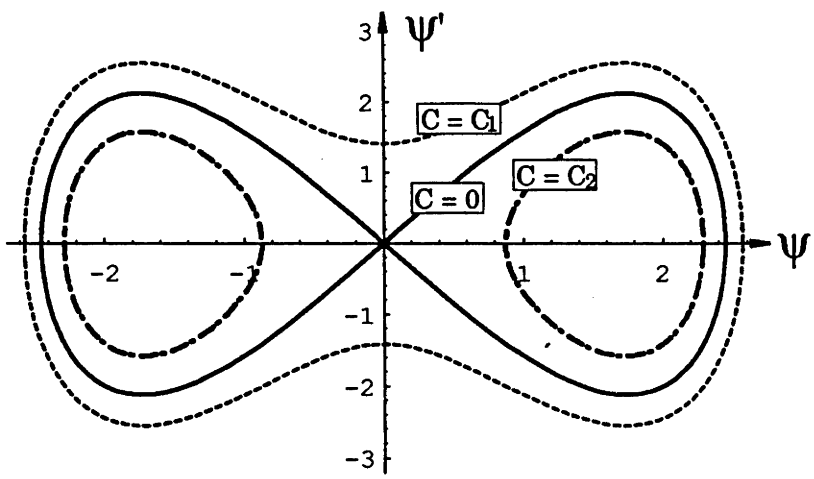

Figure 2.7: Typical phase diagrams of solutions in a self-focusing medium. In relation to Eqn.2.32, $C = 0, C_1, C_2$ where $C_2 < 0 < C_1$.

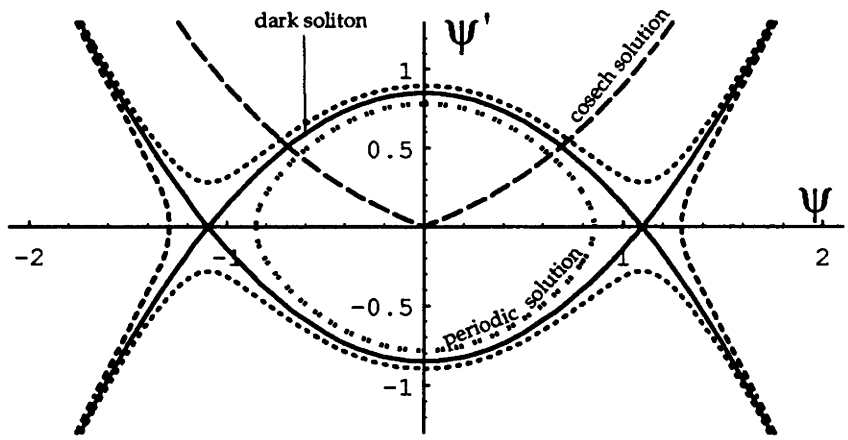

Figure 2.8: Typical phase diagrams of solutions in a self-defocusing medium.

trajectories with $C > 0$ are closed loops enclosing the origin, and thus correspond to periodic solutions with nodes. The trajectory with $C = 0$ intersects at the origin and corresponds to bright soliton solutions which decay at infinity, while $C < 0$ leads to the appearance of two separate mirror image loops, which correspond to periodic solutions with no nodes.

In a self-defocusing medium, phase diagrams have typical shapes shown in fig.2.8 for both $B < 0$ and $B > 0$. It is easy to recognize that the part of the solid curves between the nodes in fig.2.8 corresponds to the dark soliton solution (2.22), the loop around the origin corresponds to the periodic solutions, and the long-dashed curves correspond the cosech solution (2.23). These are the same types of solution discussed in the mechanical interpretation above.

One of the advantages of phase diagrams, or the mechanical interpretation, is that one can see qualitatively what types of solutions are possible without explicitly solving for them. This is particularly useful when the nonlinearity is such that obtaining exact solutions is a difficult procedure.

2.4 Layered Structures

The preceeding section discusses the existence problem of modes in a homogeneous medium, for which the wave equation (2.18) is autonomous, i.e. not explicitly involving X. In inhomogeneous media, B and h are no longer constants (at a fixed value of β) but are functions of X. In most cases, exact analytical solutions for modal fields are not available, and obtaining phase diagrams for these cases also

becomes more difficult. It is noted that phase diagrams were also used earlier by Jones and Moloney in Ref.[59].

However, if $n(X)$ and $\alpha(X)$ are only single-step functions with the step occurring at $X = 0$, then phase diagrams can be constructed without too much trouble. This situation corresponds to single-interface problems considered in examples 1 and 2 below.

Example 1: SF-SF Interface

This particular structure was first studied using exact solutions in Ref.[60]. Here from the point of view of phase diagrams, it is shown how these solutions arise.

In terms of $B(X)$:

$$B(X) = \begin{cases} B_l, & X < 0 \\ B_r, & X > 0 \end{cases} \qquad h(X) = \begin{cases} h_l, & X < 0 \\ h_r, & X > 0 \end{cases}$$

where B_r, B_l are constants characterizing the planar interface at $X = 0$ between two homogeneous nonlinear media.

Both sides of the interface being Kerr self-focusing media means that $h_i = 1$, $B_i > 0\,(i = r, l)$, and definition (2.13) has to be replaced by

$$\psi = |\alpha_r|^{1/2} E. \tag{2.33}$$

(This definition for ψ is used whenever a structure under investigation involves one or more interfaces between Kerr media.) Here $\alpha_i = 2n_i n_{2i} \rho^2 k^2$ is the *scaled* nonlinear coefficient of the left $(i = l)$ and right $(i = r)$ medium.

As a convention, the right-hand bounding medium will always be assumed nonlinear and self-focusing throughout this thesis, implying that α_r is always positive and finite. The phase equation (2.32) for a homogeneous medium is now replaced by

$$\psi' = \begin{cases} \pm\left[C_l + B_l\psi^2 - \dfrac{1}{2\eta}\psi^4\right]^{1/2}, & X < 0 \\ \pm\left[C_r + B_r\psi^2 - \dfrac{1}{2}\psi^4\right]^{1/2}, & X > 0 \end{cases} \tag{2.34}$$

where $\eta = \alpha_l/\alpha_r$ is called the asymmetry parameter of the nonlinear structure. This type of interface supports bright surface waves, with constants C_l, C_r in (2.34) being equal to zero. The procedure consists of two steps:

Step 1: Drawing two individual trajectories described by (2.32) with $B = B_l$ and $B = B_r$ as if they are for a homogeneous medium (see e.g.[59]). Each trajectory

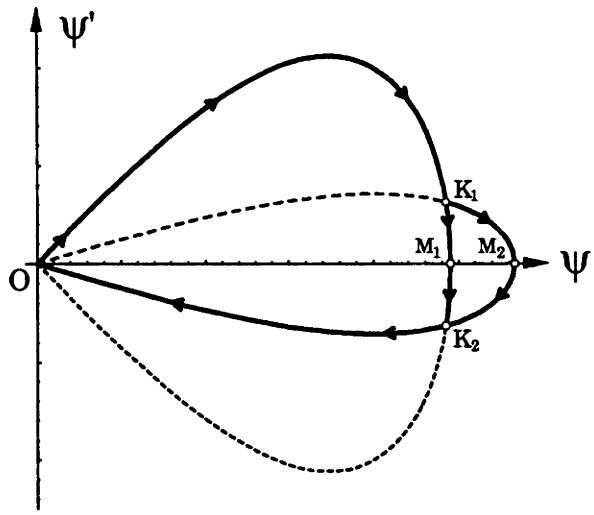

Figure 2.9: Phase diagram a surface wave. Trajectories $OK_1M_1K_2O$ and $OK_1M_2K_2O$ correspond modes with the peak in the left and right media respectively.

is a loop symmetrical about the horizontal axis (fig.2.9) and has a common point at the origin O. In a homogeneous medium, the node O would correspond to the field at infinite X, while M_1 or M_2 would correspond to the peak of a bright soliton. Depending on the parameters B_r, B_l and η, the two loops either have no common points other than O, or they intersect at two points (indicated by K_1 and K_2) which correspond to the interface. The former case means that no bright surface mode exists for those parameters, while the latter case means two bright surface modes exist for the same set of parameters.

Step 2: Forming composite trajectories by matching the individual trajectories appropriately. There are two possible composite trajectories, indicated by the solid lines, corresponding to two bright surface modes, one with the peak on each side of the interface. Trajectory $OK_1M_1K_2O$ corresponds to the mode with the peak (point M_1) in the left medium and the interface at K_2, while trajectory $OK_1M_2K_2O$ corresponds to the mode with the peak (point M_2) in the right medium and the interface at K_1. The origin corresponds to a point in the infinite left (or right) tail of a surface mode.

Existence condition

A pair of bright surface modes exists if the two individual trajectories described by (2.34) intersect, at some ψ_a, say. This leads to

$$\frac{1}{2}\psi_a^2 = (B_l - B_r)/\left(\frac{1}{\eta} - 1\right) \geq 0.$$

Hence the existence condition is: *If* $n_l > n_r$, *i.e.* $B_l < B_r$, *then* $\eta > 1$. In other words, if the left medium has a higher linear index, then it must be less nonlinear.

In addition to elegantly giving the existence condition, these phase trajectories in fig.2.9 should also prove useful in numerically calculating the surface mode using a 'shooting' method. For example, starting at the interface $X = 0$, one can use the initial condition ψ_o, ψ_o' corresponding to point K_1 and integrate back to the origin O through $K_1M_2K_2O$ to obtain the part of the mode in the right-hand medium, and through K_1O (along the solid curve) for the remaining part in the left medium. This is especially convenient when exact analytical eigenmodes are not available for the respective media but the first integrals of the wave equations can be written in a simple form.

Example 2: SDF-SF Interface

The phase equation for this type of interface is

$$\psi' = \begin{cases} \left[B_l\psi^2 + \frac{1}{2\eta}\psi^4\right]^{1/2}, & X < 0 \\ \pm\left[B_r\psi^2 - \frac{1}{2}\psi^4\right]^{1/2}, & X > 0 \end{cases} \tag{2.35}$$

where $\eta = |\alpha_l|/\alpha_r$. A typical composite trajectory is shown by the solid curve in fig.2.10. Since the point of intersection K can only be in the upper-half plane, there can only be one possible mode for a particular set of parameters, with the peak (corresponding to point M) in the right (self-focusing) medium.

As before, the existence condition can be derived from the requirement that the two individual trajectories (of the left and right media) intersect at more than the point O. This leads to

$$B_r - B_l = \frac{1}{2}\psi_o^2\left(\frac{1}{\eta} + 1\right) > 0.$$

In other words, the condition is simply

$$n_l > n_r. \tag{2.36}$$

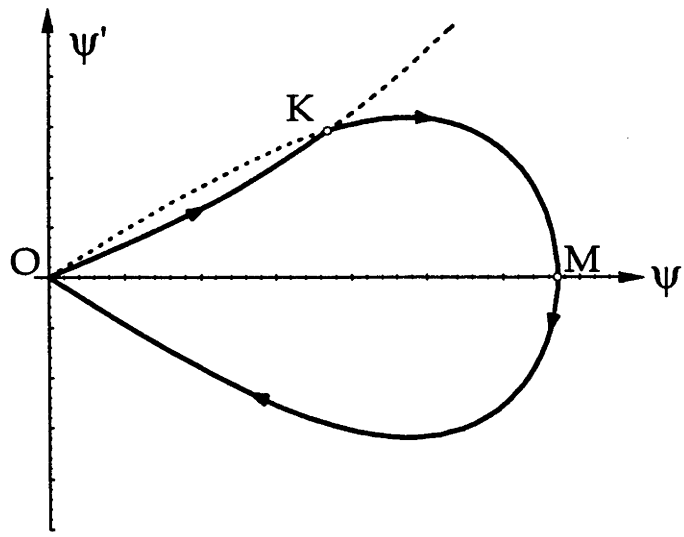

Figure 2.10: Phase diagram a surface mode at a SDF-SF interface.

The relative ease of constructing composite phase trajectories in the above examples comes from the fact that the constants C_i in the first integrals of of the two media vanish, and the individual trajectories pass through the origin O. However, when there are more than one interface, this is no longer true for the intermediate layers, and this complicates the construction of phase diagrams enormously. Let us consider the simplest example of a symmetric slab waveguide with linear core and a Kerr self-focusing bounding medium.

Example 3: Slab Waveguide

The structure has two interfaces and well-known modal solutions [61]. The phase equation is

$$\psi' = \begin{cases} \pm\left[B_l\psi^2 - \frac{1}{2}\psi^4\right]^{1/2}, & |X| > 1 \\ \pm\left[C_{co} + B_{co}\psi^2\right]^{1/2}, & |X| < 1 \end{cases} \tag{2.37}$$

where $C_{co} \neq 0$, and $B_{co} = \rho^2(\beta^2 - k^2 n_{co}^2)$ is the modal parameter for the core. The trajectory for the linear core is either an ellipse (fig.2.11a) or a hyperbola (fig.2.11b) centered at the origin. For a bounding medium, this is a loop as seen in the previous examples. The complication is that C_{co} must be chosen such that, as one goes from K_1 (e.g. in fig.2.11) corresponding to the first interface, to K_2 (second interface) through M, the distance 'travelled' in X is exactly 2, the thickness of the core. A symmetric mode at low powers may correspond to the composite trajectory OK_1MK_2O in fig.2.11(a) with the peak residing in the core, while at high powers,

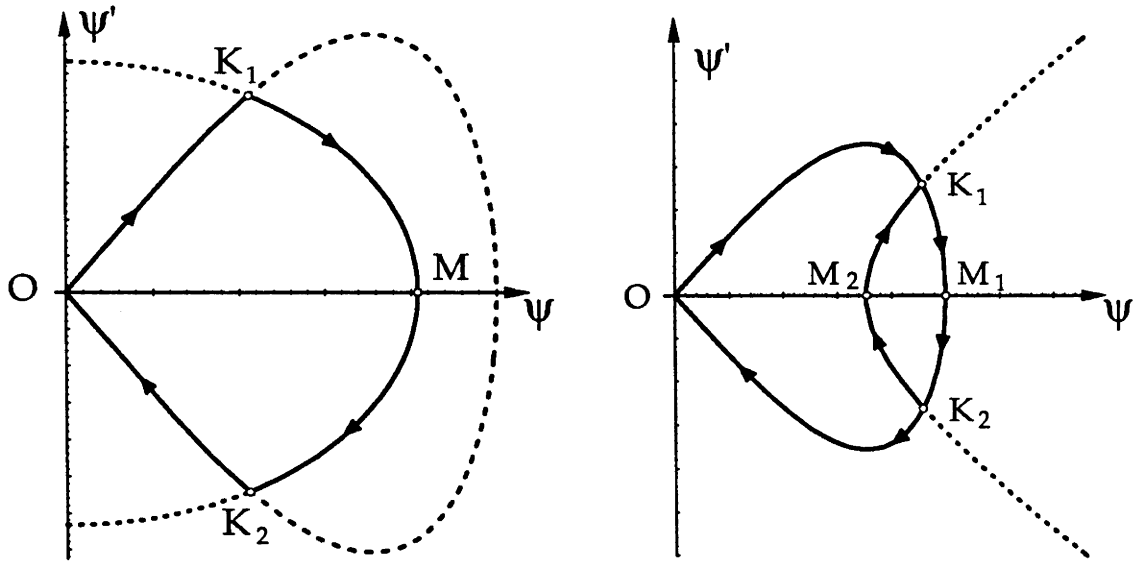

Figure 2.11: Composite phase trajectories for TE_0 even modes. (a) OK_1MK_2O, single peak in the linear core. (b) $OK_1M_1K_2M_2K_1M_1K_2O$, double peaks in the bounding media.

the composite trajectory may be of the type $OK_1M_1K_2M_2K_1M_1K_2O$ in fig.2.11(b). Asymmetric modes correspond to some other ways of constructing a trajectory but since the complexity of this method is now quite significant, the direct method using exact solutions is much more preferred.

2.5 Numerical Solutions

When analytical answers are not available, numerical solutions seem to be the only means that one has to resort to. In waveguide theory, this is especially true when index profiles or the nonlinearity distributions are arbitrary.

There are two classes of numerical solutions that one often encounters in waveguide optics. The first class is concerned with calculating *stationary waves* (or modes) of a translationally invariant waveguide with arbitrary cross-section. In this class, the equation to be solved involves only one independent variable, namely X, in planar geometry. Available methods for this type of problem can be found in many textbooks. Among them, the *iterative finite element method*, which is used in chapter 5, receives some discussion below. The second class involves simulation

techniques, often called 'beam propagation methods' (BPM's) [62,63,64], with the assumption that the wave solution is slowly varying in the propagating direction.

2.5.1 Iterative Finite Element Method (IFEM)

A brief description of this method may be presented as follows. To use the IFEM, the wave equation could be written in the form

$$D\psi = W^2\psi, \tag{2.38}$$

where D is a second order differential operator. This form is then converted into an iterative scheme

$$D_n\psi_{n+1} = W^2\psi_{n+1}, \tag{2.39}$$

where the second-order differential operator D_n is defined in terms of ψ_n and the arbitrary linear index profile of the waveguide. With a standard one-dimensional finite element scheme [65], equation (2.39) is discretized into an eigenvalue-eigenvector form. Suppose (ϱ_n, v_n) is the approximate solution at the nth iteration step, the the solution at the next step, $n+1$, is calculated using an inverse iteration method [66, p.193] with v_n being normalized in certain ways. Two possible normalizations are: (a) $\sum_m v_n^2(X_m)$ is set equal to a fixed power; or (b) $v_n(X_m)$ is set to some fixed value.

It is not guaranteed that this iteration scheme always converges, especially when the transverse distribution of nonlinearity is highly non-uniform. Further discussion will be presented, along with a specific example, later in chapter 5.

2.5.2 Slowly-Varying Waves

Solutions of the form (2.2) presuppose that the transverse distribution $\mathbf{e}(x,y)$ of the field is independent of z, i.e. they are stationary waves, or modes. More general solutions have $\mathbf{e}(x,y,z)$ replacing $\mathbf{e}(x,y)$ in (2.2). However, when the rapidly varying behaviour is factored out in the phase term $e^{i\beta z}$, the distribution $\mathbf{e}(x,y,z)$ can be only slowly-varying in the z-direction, such that $\partial^2\mathbf{e}/\partial z^2$ can be ignored.

In planar structures, and with the standard notation of the thesis, the wave equation in the slowly varying approximation is

$$\frac{\partial^2\psi}{\partial X^2} + iN\frac{\partial\psi}{\partial Z} - B\psi + h|\psi|^2\psi = 0, \tag{2.40}$$

where $N = 2\rho\beta$. This differs from Eqn.(2.18) only in the appearance of the $\partial/\partial Z$ term. The solution to (2.40), with some initial condition $\psi(X, Z=0) = \psi_o(X)$ can be obtained by numerical simulation along the direction of propagation.

The main advantage of numerical beam propagation techniques is their flexibility, in the sense that they can be used to study any nonlinearity law, and the effects of other important material properties such as loss, saturation, etc. can be included in a straightforward manner. They can also be used in stability tests to complement existing analytical conclusions and provide results where analytical answers are not available. However, numerical simulation techniques have their limitations which will be discussed further in the next chapter.

Two of the most popular methods are perhaps the fast Fourier transform beam propagation method [62,63], or (FFT) BPM, and the Finite Difference (FD) BPM [64]. Since computational techniques are not the main subject of this study, only the FD method, which is actually employed in later chapters, is described briefly in the following.

FD Beam Propagation

During the last few years, the FD method seems to have become more useful than the FFT method, due to the fact that the matrix resulting from discretization turns out to be tridiagonal, or quasi-tridiagonal, which takes less time to work with than a FFT method. To be more precise, suppose $N+1$ is the size of the transverse grid, then a propagation step in the FD method takes $O(N)$ operations, whereas the FFT method would take $O(N\log N)$ operations. Furthermore, the FD method does not require periodic boundary conditions, and the step size can be much larger.

In implementing the FD method, the transverse grid is $[X_s = X_0 + s\Delta X;\ s = 0,1,\ldots,N;\ \Delta X = (X_N - X_0)/N]$, and the longitudinal grid is $[Z_r = r\Delta Z;\ r = 0,1,2,\cdots]$. In discretizing $\psi(X,Z)$, the notation $\psi_s^r = \psi(X_s, Z_r)$ is used. The discretization of Eqn.(2.40), with $h = 1$ for example, is

$$\begin{aligned}\left\{\psi_{s+1}^r - 2\psi_s^r + \psi_{s-1}^r + \psi_{s+1}^{r+1} - 2\psi_s^{r+1} + \psi_{s-1}^{r+1}\right\} + 2i\frac{\psi_s^{r+1} - \psi_s^r}{\Delta Z} \\ -B(\psi_s^r + \psi_s^{r+1}) + (|\psi|_{s-1}^r)^2\psi_{s-1}^r + (|\psi|_{s+1}^r)^2\psi_{s+1}^r = 0, \quad (2.41)\end{aligned}$$

This scheme has been shown to be stable according to linear analysis [67]. Eqn.(2.41) is then converted into the matrix form

$$\begin{bmatrix} a_0 & a_1 & . & . & . & . & . \\ . & . & . & . & . & . & . \\ . & . & a_{s-1} & a_s & a_{s+1} & . & . \\ . & . & . & . & . & . & . \\ . & . & . & . & . & a_{N-1} & a_N \end{bmatrix} \begin{pmatrix} \vdots \\ \psi_{s-1}^{r+1} \\ \psi_s^{r+1} \\ \psi_{s+1}^{r+1} \\ \vdots \end{pmatrix} = \begin{pmatrix} \vdots \\ b_{s-1} \\ b_s \\ b_{s+1} \\ \vdots \end{pmatrix} \quad (2.42)$$

where

$$
\begin{aligned}
a_o &= a_N = a_s = i\frac{N}{\Delta Z} - \frac{1}{(\Delta X)^2} - \frac{B}{2} \\
a_1 &= a_{N-1} = \frac{1}{(\Delta X)^2} \\
a_{s-1} &= a_{s+1} = \frac{1}{2(\Delta X)^2} \\
b_{s-1} &= -\frac{1}{2(\Delta X)^2}\psi_{s-1}^r - (|\psi|_{s-1}^r)^2\,\psi_{s-1}^r \\
b_s &= (i\frac{N}{\Delta Z} + \frac{B}{2})\psi_s^r + \frac{1}{(\Delta X)^2}\psi_s^r + b_{s-1} + b_{s+1} \\
b_{s+1} &= -\frac{1}{2(\Delta X)^2}\psi_{s-1}^r - (|\psi|_{s+1}^r)^2\,\psi_{s+1}^r
\end{aligned}
$$

Since the equation (2.42) for ψ_s^{r+1} involves a tridiagonal matrix, it can be solved in $O(N)$ operations [68].

2.6 Conversion of Parameters

This section, which should be of interest to experimentalists, describes the relationships between the dimensionless, scaled quantities used in this thesis and the actual physical parameters. In reality, the parameters describing a layered waveguide structure, which may involve only Kerr nonlinearities, include:

linear indices	n_i	(no units),
Kerr coefficients [2]	$\bar{n}_{2i}$	(m^2/Watt),
propagation constant	β	(m^{-1}),
free-space wave number	k	(m^{-1}),
a typical length	ρ	(m),
actual field strength	E	(Volt/m),
actual power/unit length	P_a	(Watt/m).

In the present analyses, these 7 parameters are converted into the following 5 dimensionless parameters:

structural parameters	$V_i = \rho k(n_i^2 - n_{min}^2)^{1/2}$,
modal parameters	$B_i = \rho^2(\beta^2 - k^2 n_i^2)$,
asymmetry parameter	$\eta_i = \alpha_r/\alpha_i$,
scaled field	$\psi = \alpha_r^{1/2}\,E$,
scaled modal power	$P = \int_{-\infty}^{\infty} \psi^2\,dX$.

where n_{min} is the minimum among the refractive indices n_i's, $\alpha_i = 2n_i n_{2i}\rho^2 k^2$, and α_r (scaled nonlinear coefficient of the rightmost layer) is assumed positive and finite.

Conversion of Power

In practice, the total power propagating along a waveguide is given by [49]

$$P_{actual} = \frac{1}{2}\,\mathrm{Re}\int_{A_\infty} \mathbf{E}\times\mathbf{H}^*\cdot\hat{\mathbf{z}}\,dA, \tag{2.43}$$

where $\mathbf{E}$ and $\mathbf{H}$ are the electric and magnetic field vectors respectively, $\hat{\mathbf{z}}$ is a unit vector along the propagation direction, and A_∞ is the infinite cross-section. Since

$$\mathbf{E} = (0,\, E,\, 0), \quad \mathbf{H} = (h_x,\, 0,\, h_z)$$

we have

$$\mathbf{E}\times\mathbf{H}^*\cdot\hat{\mathbf{z}} = -h_x^* E = \left(\frac{\epsilon_0}{\mu_0}\right)^{1/2}\frac{\beta}{k}E^2$$

The actual power per ρ in the y-direction can therefore be expressed as

$$\boxed{P_a = \left(\frac{\epsilon_0}{\mu_0}\right)^{1/2}\frac{\beta}{k}\frac{1}{4n_r n_{2r}k^2}P,} \tag{2.44}$$

where $P = \int_{-\infty}^{\infty}\psi^2\,dX$ is the dimensionless power, and $(\epsilon_0/\mu_0)^{1/2} \approx 2.65\times10^{-3}\Omega^{-1}$.

Other Conversions

(a) - *Between Kerr coefficient $\bar{n}_{2i}$ and the nonlinear coefficient n_{2i} :*

Since actual power per unit length is

$$\int_{-\infty}^{\infty} I\,dx = \frac{1}{2}\left(\frac{\epsilon_0}{\mu_0}\right)^{1/2}\frac{\beta}{k}\int_{-\infty}^{\infty}|E|^2\,dx,$$

we have

$$I = \frac{1}{2}\left(\frac{\epsilon_0}{\mu_0}\right)^{1/2}\frac{\beta}{k}|E|^2. \tag{2.45}$$

Now,

$$n = n_0 + \bar{n}_{2i}\,I = n_0 + n_{2i}\,|E|^2,$$

therefore,

$$\boxed{n_{2i} = \frac{1}{2}\left(\frac{\epsilon_0}{\mu_0}\right)^{1/2}\frac{\beta}{k}\bar{n}_{2i}.} \tag{2.46}$$

With this, (2.44) simplifies to

$$\boxed{P_a = (2n_r\bar{n}_{2r}k^2)^{-1}\,P}. \tag{2.47}$$

in which the proportionality constant does not depend on β (and hence power). This is one of the advantages of the notation and scaling rules used here. Another

important indication in Eqn.2.47 is that real power is inversely proportional to nonlinearity, namely the Kerr coefficient.

(b) - *Between actual light intensity I and* $|\psi|^2$ *:*

By using $\psi = \alpha_r^{1/2} E$ and $\alpha_r = 2n_r n_{2r} \rho^2 k^2$, (2.45) leads to

$$\boxed{I = \frac{1}{2n_r \bar{n}_{2r} \rho^2 k^2} \psi^2,} \tag{2.48}$$

in which, if the structure is a surface, then $\rho^2 k^2 = S^2/|n_r^2 - n_l^2|$. On the other hand, if it is a waveguide, then $\rho^2 k^2 = V_r^2/|n_r^2 - n_{co}^2|$.

(c) - *Between effective index* n_{eff} *and* B_i *:*

Using the definitions of B_i and V_i, one gets

$$\boxed{n_{eff} = \beta/k = \left[n_i^2 + B_i(n_i^2 - n_{min}^2)/V_i^2\right]^{1/2}} \tag{2.49}$$

It is noted that n_{eff}, instead of B_i, has been used quite widely in the literature.

Chapter 3

Stability Analysis

In almost every mathematical model of a physical problem, a number of effects are neglected. It is therefore important to study how sensitive a particular model is to small perturbations or changes of initial conditions and of various parameters. This is the essence of stability studies in which the pioneering works of Lyapunov and Poincare are significant contributions.

One may ask the question: why not simply calculate the solutions and propagate them numerically on a high speed computer and use whatever information that can be obtained from the numerical solution? This is precisely what we can do if we desire information about one specific solution and one particular set of perturbations. However, in many problems, we want certain information about all solutions and stability properties independent of any particular type of perturbation. Another major difficulty with numerical solutions is that the methods used to generate these solutions may or may not introduce purely mathematical-numerical errors which lead to a wrong behaviour of a propagating field. (For an example, the reader is referred to Refs.[69] (numerical) and [70] (analytical) which report conflicting results in a narrow range of dispersion near a branching point.)

In the context of optical nonlinear guided waves, the stability investigation of a stationary solution is extremely important if any practical application is to made of these waves. For example, if a mode is unstable to perturbations, i.e. if it cannot propagate for a practically useful distance, it can never be practically used in an optical waveguide.

The first section of this chapter, section 3.1, describes a method for determining the stability charateristics of a mode, namely *linear analysis* [71]. The contribution that this part of the thesis has made to the field is that new exact solutions of some linearized perturbation equations which arise in the analysis have been found;

these permit stability properties of certain classes of guided waves to be determined. More importantly, the work also demonstrates, for the first time, that growth rates in linear analysis are either real or purely imaginary for fundamental modes, but that they can be complex for non-fundamental modes of a nonlinear structure. This fact has ended the long believed assumption that growth rates in linear stability analysis can only be either real or purely imaginary for modes of all orders. Later parts of section 3.1 discuss a numerical method which can be employed when exact solutions are not available. The related works by Kolokolov [72], Jones and Moloney [59] and Mitchell and Snyder [73] are also briefly reviewed, clarified and discussed. Section 3.2 contains a discussion on Lyapunov theory, which is useful for the stability determination of certain types of guided waves. Some comments on the applicability and limitation of beam propagation methods are presented in section 3.3. Finally, section 3.4 briefly discusses problems and possible future directions about transverse stability, i.e. stability to perturbations in the second transverse (y-) dimension.

3.1 Linear Analysis

For clarity of exposition, only Kerr-law nonlinearity is discussed here. The aim is to bring out the basic steps of linear analysis.

The scalar wave equation in two dimensions is

$$\frac{\partial^2\psi}{\partial X^2} + \frac{\partial^2\psi}{\partial Z^2} - B(X)\,\psi + h\psi^3 = 0, \tag{3.1}$$

in which $B(X)$ is generally a function of X, $h = \pm 1$, or 0 (i.e. the medium is generally layered, and each layer may be self-focusing, self-defocusing, or linear), and Z is the longitudinal dimension scaled by ρ.

3.1.1 Linearization

Assume now that ψ may be expressed in the form [71]

$$\psi(X,Z) = \psi_n(X) + \gamma f(X,Z), \tag{3.2}$$

where $\psi_n(X)$ is a mode whose stability is being investigated, γ is a small parameter, and f varies slowly in Z such that $\partial^2 f/\partial Z^2$ can be ignored. In linear analysis, the perturbed solution (3.2) is then substituted into Eqn.(3.1), and we retain only first-order terms in γ. This leads to a *linear* equation for $f(X,Z)$

$$\frac{\partial^2 f}{\partial X^2} + iN\frac{\partial f}{\partial Z} - Bf + h\psi_n^2(2f + f^*) = 0, \tag{3.3}$$

where $N = 2\rho\beta$, and the asterisk denotes complex conjugate.

3.1.2 The form of perturbation functions

The perturbation function $f(X,Z)$ can be taken to have the form [71]

$$f(X,Z) = (u+v)e^{\mu Z} + (u^* - v^*)e^{\mu^* Z}, \tag{3.4}$$

where u and v are functions of X only. At a first glance at (3.4), one might reasonably ask: why is a simpler form, such as

$$f = u\, e^{\mu Z}, \tag{3.5}$$

not taken instead ? The reason lies in the fact that both f and f^* occurs in Eqn.(3.3). To show that the form (3.5) is inappropriate, one can substitute it directly into Eqn.(3.3) to obtain

$$u'' + iN\mu u - Bu + h\psi_n^2 \left(2u + u^*\, e^{[\mu^* - \mu]Z}\right) = 0.$$

Since the exponential term in this expression is the only Z-dependent term, we must have either $u(X) = 0$ or μ is real. The former consequence is ruled out because we are interested in non-zero perturbations. The latter pre-supposes that μ is real, and so Eqn.(3.5) cannot give the most general form of the perturbation function f.

Now suppose $f(X,Z)$ takes the form

$$f = g(X)\, e^{\mu Z} + l(X)\, e^{\sigma Z}. \tag{3.6}$$

Substituting (3.6) into Eqn.(3.3) and dividing by $e^{\mu Z}$ gives

$$\begin{aligned} &g'' + iN\mu g - Bg + h\psi_n^2 \left[2g + g^*\, e^{(\mu^* - \mu)Z}\right] \\ &+ \left\{l'' + iN\sigma l - Bl + h\psi_n^2 \left[2l + l^*\, e^{(\sigma^* - \sigma)Z}\right]\right\} \quad e^{(\sigma - \mu)Z} = 0 \end{aligned} \tag{3.7}$$

The term involving $\exp(\mu^* - \mu)Z$ of this equation is oscillatory in Z (unless μ is real), and therefore the term involving $e^{(\sigma-\mu)Z}$ must also be oscillatory. This means $\sigma = \mu^*$. Eqn.(3.7) then becomes

$$\begin{aligned} \{l'' + iN\mu^* l - Bl + h\psi_n^2(2l + g^*)\} e^{(\mu^* - \mu)Z} \\ + \{g'' + iN\mu g - Bg + h\psi_n^2(2g + l^*)\} \;=\; 0. \end{aligned} \tag{3.8}$$

and hence

$$\begin{aligned} l'' + iN\mu^* l - Bl + h\psi_n^2(2l + g^*) &= 0, \\ g'' + iN\mu g - Bg + h\psi_n^2(2g + l^*) &= 0. \end{aligned} \tag{3.9}$$

To simplify the presentation further, we can define $g = u + v$, $l = u^* - v^*$, and this leads to the form in (3.4). The coupled equations for u and v are then

$$L_0 v = -i\Omega u, \quad L_1 u = -i\Omega v. \tag{3.10}$$

where $L_0 = d^2/dX^2 - B + h\psi_n^2$, $L_1 = L_0 + 2h\psi_n^2$, and $\Omega = \mu N$. We also have

$$L_0 L_1 \, u = -\Omega^2 \, u, \quad L_1 L_0 \, v = -\Omega^2 \, v \tag{3.11}$$

In other words, $L_0 L_1$ and $L_1 L_0$ have the same eigenvalue spectrum but different eigenfunctions.

3.1.3 The eigenvalue Ω

The nature of the eigenvalue Ω contains the important and interesting properties of the stability of stationary solutions [74]. In the spectrum of Ω, if there exists a positive value, or a complex value with a positive real part, then the mode ψ_n is unstable. Otherwise, it is stable. Furthermore, it is seen from equations (3.10) and (3.11), that if (Ω, u, v) is a solution, then so are $(-\Omega, u, -v)$ and $(\Omega^*, -u^*, v^*)$. This means the instability of a mode requires the existence of at least one real or complex eigenvalue. It also implies that, when searching for eigenvalues, it is sufficient to restrict ourselves to the first quadrant of the complex plane.

Originally, numerical (BPM) simulations showed that a perturbation to the TE_1 mode can be a growing oscilation. This implies that complex eigenvalues exist and led to the following analytic consideration of where and why they can occur.

To show that only non-fundamental modes[1] can possess complex eigenvalues, we use the following argument. Let $\langle g_1, g_2 \rangle$ be defined as the scalar product

$$\langle g_1, g_2 \rangle = \int_{-\infty}^{\infty} g_1^* \, g_2 \, dX$$

for some continuous functions g_1 and g_2 which decay to zero at infinity. Since L_0 and L_1 are self-adjoint operators, the adjoint of $L_0 L_1$ is $L_1 L_0$, and one can write

$$(-\Omega^2)^* \langle u, v \rangle = \langle L_0 L_1 \, u, v \rangle = \langle u, L_1 L_0 \, v \rangle = -\Omega^2 \langle u, v \rangle \tag{3.12}$$

Suppose ψ_0 (which is a particular case of ψ_n with $n = 0$) denotes TE_0 stationary solutions (or fundamental modes) of the wave equation. These are also the eigenfuctions with zero eigenvalues of L_0, i.e.

$$L_0 \psi_0 = 0.$$

For ψ_0, we note that $\langle u, v \rangle$ is always non-zero. To prove this, we use the fact that $\langle L_0 v, v \rangle$ is negative-definite because all eigenvalues of L_0 (including its continuous

[1] These include 'dark' guided (or self-guided) modes of all orders, as they are not fundamental modes of the waveguide they induce. For clarity, all modes discussed in this subsection are 'bright' modes.

spectrum) are real and non-positive, and the eigen-functions of L_0 can be chosen to form a complete set. Therefore, $\langle u, v\rangle = -i(\Omega^{-1})^* \langle L_0 v, v\rangle$ is a non-zero quantity. In Eqn.(3.12), this means Ω is either real or purely imaginary.

Let us now consider the TE_1 stationary solutions (ψ_1), for which L_0 is defined by $L_0 = d^2/dX^2 - B + \psi_1^2$ with $L_0\psi_1 = 0$. In this case, L_0 has both positive (for the lowest even eigenfunction) and negative eigenvalues, including the continuous spectrum. If only odd perturbations are used, i.e. u and v are odd, then $\langle L_0 v, v\rangle$ is still negative-definite because the only positive eigenvalue of L_0 is not present in the expansion of $L_0 v$ in terms of the eigenfunctions of L_0, and so Ω is real or purely imaginary. The more interesting case is when even perturbations are also allowed, as then $\langle L_0 v, v\rangle$ may vanish, and Eqn.(3.12) means Ω can thus be complex. This discovery has opened up the full variety of stability characteristics of nonlinear guided waves. The evolution of an initial perturbation can thus show both exponential growth and oscillations, as found numerically.

In light of the above argument, some properties can also be deduced for the TE_2 stationary solutions. Here, $L_0 = d^2/dX^2 - B + \psi_2^2$ with $L_0\psi_2 = 0$ and $\langle L_0 v, v\rangle$ can be zero for both even and odd perturbation functions. This means that, for TE_2 and higher-order modes, the nature of the eigenvalues does not depend on the symmetry of the perturbations.

3.1.4 Exact forms of the perturbation functions

For convenience, Eqn.(3.10) is rewritten in a more explicit form as

$$\begin{aligned} \{d^2/dX^2 - B + h\psi_n^2\}v &= -i\Omega u, \\ \{d^2/dX^2 - B + 3h\psi_n^2\}u &= -i\Omega v. \end{aligned} \tag{3.13}$$

It should be remembered that h can only be ± 1 or 0, and that the waveguiding structure is symmetric and involves no more than one type of nonlinearity. Under these circumstances, exact solutions for u and v are available for several nonlinearity types including linear, Kerr self-focusing and Kerr self-defocusing nonlinearities. These solutions will be used in later chapters to calculate the stability of modes in a number of guiding systems. The basic idea of the method is as follows: The solutions for u and v involve an exponential factor of the form e^{-px} when $x \to \infty$, and e^{px} when $x \to -\infty$. Thus, realistic solutions for u and v for the whole structure can only be formed by matching the solutions (i.e. u and v and their derivatives) at some interface; and this matching process yields the possible eigenvalues Ω. In the case of a homogeneous medium, this interface could be a ficticious one.

The available exact solutions are presented for several particular cases in the following.

Linear medium

Linearity corresponds to $h = 0$ in (3.13). If the linear region is finite, then it is not required that f (and therefore u and v) vanish at the boundaries of the region. It is elementary to show that the solution to (3.13) is

$$\begin{aligned} u &= a_1 \cosh(p\,X) + b_1 \cosh(\bar{p}\,X) \\ v &= a_1 \cosh(p\,X) - b_1 \cosh(\bar{p}\,X) \end{aligned} \tag{3.14}$$

in the case of even symmetry, and

$$\begin{aligned} u &= a_2 \sinh(p\,X) + b_2 \sinh(\bar{p}\,X) \\ v &= a_2 \sinh(p\,X) - b_2 \sinh(\bar{p}\,X) \end{aligned} \tag{3.15}$$

in the case of odd symmetry. Here $p = \sqrt{B - i\Omega}$, $\bar{p} = \sqrt{B + i\Omega}$, and a_1, a_2, b_1, b_2 are arbitrary constants. Since Eqn.(3.13) is linear, generally asymmetric solutions of u and v are given as a sum of both types in (3.14) and (3.15).

If the linear medium is semi-infinite, say including $X \to \infty$, then

$$\begin{aligned} u &= a \exp(-p\,X) + \exp(-\bar{p}\,X), \\ v &= a \exp(-p\,X) - \exp(-\bar{p}\,X), \end{aligned} \tag{3.16}$$

For $X \to -\infty$, X is to be replaced by $-X$ in (3.16).

Kerr self-focusing medium

The self-focusing effect corresponds to $h = 1$, and ψ_n in (3.13) is given by (2.21), namely

$$\psi_n(X) = \sqrt{2}\,W \operatorname{sech}[W(X - X_0)],$$

where $B = W^2 > 0$. The solutions for u and v, which decay at infinity, in this case have been found by Vysotina *et al.* in Ref.[71]. In the present notation,

$$\begin{aligned} u &= C_1 f_1(x) + C_2 \bar{f}_1(x) \\ v &= C_1 f_2(x) - C_2 \bar{f}_2(x) \end{aligned} \tag{3.17}$$

where C_1, C_2 are constants, and, for the region including $X \to \infty$,

$$\begin{aligned} f_1 &= e^{-px}(-i\xi + 2p \tanh x + 2\tanh^2 x) \\ \bar{f}_1 &= e^{-\bar{p}x}(i\xi + 2\bar{p} \tanh x + 2\tanh^2 x) \\ f_2 &= e^{-px}(2 - i\xi + 2p \tanh x) \\ \bar{f}_2 &= e^{-\bar{p}x}(2 + i\xi + 2\bar{p} \tanh x) \end{aligned} \tag{3.18}$$

where $\xi = \Omega/W^2$, $p = \sqrt{1-i\xi}$, $\bar{p} = \sqrt{1+i\xi}$, and $x = W(X - X_0)$. For $X \to -\infty$, $x = -W(X + X_0)$.

However, in Ref.[71], it was taken for granted that ξ can only be either real or purely imaginary, without noticing that the assumption was true only for fundamental modes. This assumption was also used in some later works [70,75].

A note should be taken here about the number of constants appearing in the solutions for u and v. Suppose the structure consists of one interface between a linear medium and a Kerr-law SF one. Then the continuity of u, u', v, v' leads to four equations in 3 unknown constants a (of Eqn.3.16), C_1 and C_2 (of Eqn.3.17). This imposes a condition on ξ. If the structure is asymmetric, consists of two interfaces, and is of the type SF-L-SF, then apparently there are 8 constants to be determined, of which 4 constants arise from the core solution, 2 from the solution for the left medium, and 2 from the right. However, since (3.13) is linear, this number ican be reduced to 7. As in the one-interface case, the constraint imposed on ξ comes the continuity conditions at the 2 interfaces which lead to 8 equations for 7 unknowns.

Kerr self-defocusing medium

Here, we have $h = -1$ and ψ_n in (3.13) is given by either (2.22) or (2.23).

(a) - If ψ_n is a dark soliton given by (2.22), namely

$$\psi_n(X) = W \tanh\left[\frac{W}{\sqrt{2}}(X - X_0)\right],$$

where $B = -W^2 < 0$, then the solutions for u and v which decay at infinity are [76]

$$\begin{aligned} u &= C_1 f_1(x) + C_2 \bar{f}_1(x) \\ v &= C_1 f_2(x) + C_2 \bar{f}_2(x) \end{aligned} \tag{3.19}$$

where C_1 and C_2 are arbitrary constants, and in the region including $X \to \infty$

$$\begin{aligned} f_1 &= e^{-px}(p^2 - 2 + 2p\tanh x + 2\tanh^2 x), \\ f_2 &= -i\xi e^{-px}(1 + \tfrac{2}{p}\tanh x), \end{aligned} \tag{3.20}$$

$p = (2 + \sqrt{4-\xi^2})^{1/2}$, $x = W(X - X_0)/\sqrt{2}$, $\xi = 2\Omega/W^2$, and $\bar{f}_1$, $\bar{f}_2$ are obtained from f_1, f_2 by replacing p by $\bar{p} = (2 - \sqrt{4-\xi^2})^{1/2}$. In $X \to -\infty$, x is replaced by $-x$.

As in the self-focusing case, it has been assumed that both the real parts of p and $\bar{p}$ are positive. When $\mathrm{Re}(\bar{p})$ is zero, for example, the more general form of u and v are

$$\begin{aligned} u &= C_1 f_1 + C_2 \bar{f}_1 + C_3 \bar{g}_1 \\ v &= C_1 f_2 + C_2 \bar{f}_2 + C_3 \bar{g}_2 \end{aligned} \tag{3.21}$$

where C_3 is an additional arbitrary constant, and

$$\begin{aligned} \bar{g}_1 &= e^{\bar{p}x}(\bar{p}^2 - 2 - 2\bar{p}\tanh x + 2\tanh^2 x), \\ \bar{g}_2 &= -i\xi e^{\bar{p}x}(1 - \tfrac{2}{\bar{p}}\tanh x). \end{aligned}$$

for $X \to \infty$. Solution (3.21) indeed contains 3 unknown constants C_i. This is because each term of the expression involving a C_i is itself a solution to Eqn.(3.13), and therefore their linear combination is also a solution. The number of unknown constants is thus larger than the number of determining equations, and hence Eqn.(3.21) forms a continuous spectrum of perturbation solutions with ξ being purely imaginary.

(b) - If ψ_n is given by (2.23), namely

$$\psi_n(X) = \sqrt{2}\, W \,\mathrm{cosech}[W(X - X_0)],$$

in some half-space including $X \to \infty$, where $B = W^2 > 0$, then in that half-space u and v are again given [77] in the same form as (3.19) but with [77]

$$\begin{aligned} f_1 &= e^{-px}(-i\xi + 2p\coth x + 2\coth^2 x), \\ f_2 &= e^{-px}(2 - i\xi + 2p\coth x), \end{aligned} \tag{3.22}$$

$p = \sqrt{1 - i\xi}$, $\xi = \Omega/W^2$, $x = W(X - X_0)$, and $\bar{f}_1$, $\bar{f}_2$ are obtained from f_1, f_2 by replacing ξ by $-\xi$. In $X \to -\infty$, $x = -W(X + X_0)$. The continuous spectrum arises in the same manner as in the self-focusing case.

3.1.5 Bright Solitons

In 1973, Kolokolov [72] proved the stability of radially symmetric bright solitons in a homogeneous Kerr medium using an elegant operator argument. This is reviewed and discussed in detail in a later subsection. Here, planar bright solitons in the same type of medium are shown to be stable using the above solutions (3.17)-(3.18). This is a new approach.

Now, x in (3.17)-(3.18) may be set to $x = WX$, and a ficticious interface is chosen at $x = 0$. On the right of this interface, the solutions for u and v are given by (3.17); while on the left, they can be written as

$$\begin{aligned} u &= C_3 f_1(-x) + \bar{f}_1(-x) \\ v &= C_3 f_2(-x) - \bar{f}_2(-x) \end{aligned} \tag{3.23}$$

in which only one extra constant C_3 appears because the system of equations for u, v is linear. Now if the boundary conditions of u and v result in at least an eigenvalue ξ with a non-zero real part, then the bright soliton is unstable; otherwise, it is stable.

The matching of u and v leads to

$$\begin{aligned} C_1(-i\xi) + C_2(i\xi) &= C_3(-i\xi) + i\xi \\ C_1(2 - i\xi) - C_2(2 + i\xi) &= C_3(2 - i\xi) - (2 + i\xi) \\ C_1(p\,i\xi + 2p) + C_2(-\bar{p}\,i\xi + 2\bar{p}) &= C_3(-p\,i\xi - 2p) + (\bar{p}\,i\xi - 2\bar{p}) \\ C_1[-p(2 - i\xi) + 2p] - C_2[-\bar{p}(2 + i\xi) + 2\bar{p}] &= C_3[p(2 - i\xi) - 2p] - [\bar{p}(2 + i\xi) - 2\bar{p}] \end{aligned} \tag{3.24}$$

which may be regarded as a system of simultaneous equations for C_1, C_2 and C_3. For nonzero C_1, C_2, C_3, the requirement is

$$\begin{vmatrix} -i\xi & i\xi & -i\xi & i\xi \\ 2 - i\xi & -(2 + i\xi) & 2 - i\xi & -(2 + i\xi) \\ p\,i\xi + 2p & -\bar{p}\,i\xi + 2\bar{p} & -p\,i\xi - 2p & \bar{p}\,i\xi - 2\bar{p} \\ -p(2 - i\xi) + 2p & \bar{p}(2 + i\xi) - 2\bar{p} & p(2 - i\xi) - 2p & -\bar{p}(2 + i\xi) + 2\bar{p} \end{vmatrix} = 0 \tag{3.25}$$

Elementary (and tedious) algebra shows that this equation can be reduced to

$$\xi^3 p\bar{p} = \xi^3\sqrt{1 + \xi^2} = 0 \tag{3.26}$$

which has discrete roots $\xi = 0, \pm i$. The fact that ξ can only be either zero or purely imaginary means the bright soliton is stable.

Although the result has been known for a long time, this is the first time that this same result is obtained using this particular method.

3.1.6 Dark Solitons

In a similar fashion, the stability of Kerr-law dark solitons is proved for the first time [76] by linear analysis with exact solutions. On the right of the ficticious interface at $X = 0$, u and v are given by (3.19), with $x = WX/\sqrt{2}$; while on the left, they are given by

$$\begin{aligned} u &= C_3\, f_1(-x) + C_4\, \bar{f}_1(-x) \\ v &= C_3\, f_2(-x) + C_4\, \bar{f}_2(-x) \end{aligned} \tag{3.27}$$

The continuity of u and v at $X = 0$ leads to

$$(p^2 - 2)\,(C_1 - C_3) = (\bar{p}^2 - 2)\,(C_4 - C_2) \tag{3.28}$$

$$C_1 - C_3 = C_4 - C_2 \tag{3.29}$$

$$p\,(p^2 - 4)\,(C_1 + C_3) = -\bar{p}\,(\bar{p}^2 - 4)\,(C_2 + C_4) \tag{3.30}$$

$$(p - \frac{2}{p})\,(C_1 + C_3) = -(\bar{p} - \frac{2}{\bar{p}})\,(C_2 + C_4) \tag{3.31}$$

Using (3.29) in (3.28) leads to

$$(C_1 - C_3)(p^2 - \bar{p}^2) = 0 \tag{3.32}$$

* *Case 1:* $C_1 = C_3$, $C_2 = C_4$. Eqns.(3.30) and (3.31) then reduce to

$$\begin{aligned} p(p^2-4)C_1 + \bar{p}(\bar{p}^2-4)C_2 &= 0 \\ (p - \tfrac{2}{p})C_1 + (\bar{p} - \tfrac{2}{\bar{p}})C_2 &= 0 \end{aligned} \tag{3.33}$$

For non-zero C_1 and C_2, we must have

$$\begin{vmatrix} p(p^2-4) & \bar{p}(\bar{p}^2-4) \\ (p - \frac{2}{p}) & (\bar{p} - \frac{2}{\bar{p}}) \end{vmatrix} = 0. \tag{3.34}$$

This can be reduced to

$$\xi^2\sqrt{4-\xi^2} = 0,$$

which gives either $\xi = 0$, or $\sqrt{4-\xi^2} = 0$. The case $\xi = 0$ (i.e. there is neither growth nor decay) is excluded because, for this to be consistent, f must be zero, otherwise $\psi_0(X) + f(X)$ would be another stationary solution. The case $\sqrt{4-\xi^2} = 0$ implies $\xi = \pm 2$. But then $p = \bar{p} = \sqrt{2}$, and (3.29) and (3.30) become

$$\begin{aligned} C_1 + C_2 &= C_3 + C_4, \\ C_1 + C_2 &= -C_3 - C_4, \end{aligned}$$

and hence $C_1 = -C_2$, $C_3 = -C_4$. This implies $u = v = 0$, i.e. f must again vanish.

* *Case 2:* $p^2 = \bar{p}^2$, or $\sqrt{4-\xi^2} = 0$ which has been discussed above.

The non-existence of non-zero bound solutions to the perturbation equation (3.13) means that the linearized system has only the continuous spectrum. This corresponds to $\bar{p}$ being purely imaginary, as discussed earlier. Hence the dark soliton is stable. This is slightly different from the situation for a bright soliton in a self-focusing medium where bound solutions exist and are sufficient to determine stability (subsection 3.1.5 and [71,74]).

The conclusion here is: by linear stability analysis, dark solitons in a Kerr-law self-defocusing homogeneous medium are stable. The result basically comes from the fact that in linear analysis, only the continuous spectrum of eigen-solutions, which have purely imaginary eigenvalues, exist. Perhaps even more important is the method of analysis used in this work, which involves exact solutions that may be very useful in other related problems.

3.1.7 Numerical Linear Analysis

The availability of exact solutions in the preceeding subsection is largely due to two factors:

(a) - The exact form for the mode ψ_n is available;

(b) - Eqn.(3.13) for the perturbation functions u and v is solvable in terms of elementary functions.

In many cases, one or both of these are not available. An obvious example is a waveguide with arbitrary linear index profile and/or arbitrary nonlinearity distribution, where finding a mode would certainly require numerical techniques. Even when condition (a) is met, for example, in the simple case of asymmetric self-focusing Kerr-law planar waveguides, condition (b) cannot be satisfied. This is because Eqn.(3.13) for one of the bounding media of the waveguide must be replaced by

$$\begin{aligned} \left\{\frac{d^2}{dX^2} - B + \frac{1}{\eta}h\psi_n^2\right\} v &= -i\Omega u, \\ \left\{\frac{d^2}{dX^2} - B + \frac{3}{\eta}h\psi_n^2\right\} u &= -i\Omega v. \end{aligned} \tag{3.35}$$

which does not have simple analytical solutions. Here $\eta \neq 1$ is a real constant characterising the asymmetry of the nonlinear structure.

For these numerous examples, the approach using exact solutions is not applicable. A straightforward (and perhaps 'brute force') alternative is to numerically calculate the eigenvalues Ω^2 of the operator L_0L_1 (or L_1L_0). The mode ψ_n may be given by analytical functions, or calculated numerically, and the operator L_0L_1 can discretized and represented as a matrix. Ω can then be found by diagonalizing the matrix L_0L_1; this can be conveniently carried out using available software packages (such as the NAG Fortran Library). An example of this approach is shown in chapter 5.

Although this approach can give an answer, it has some major limitations:

1. The accuracy of the calculated eigenvalues depends on the number of grid points in the discretization.

2. The continuous spectrum of L_0L_1 disappears.

3. The method is not immediately applicable to dark surface and guided waves, because the calculated eigenvalues critically depend on the size of the computation window. However, this limitation can be relieved if it can be proven

that the sign of the calculated eigenvalues, which is important in determining stability, is independent of the size of the computation window.

3.1.8 Kolokolov's Work

At this point, it is appropriate to discuss an elegant stability result [72] obtained in 1973 by Kolokolov for bright spatial solitons with radial symmetry in a homogeneous self-focusing Kerr medium. The bright soliton is a fundamental mode, ψ_0, mentioned in the preceeding subsection, and so the eigenvalue Ω is either real or purely imaginary, i.e. the eigenvalue $\Lambda = -\Omega^2$ of $L_0 L_1$ is purely real. For radial symmetry,

$$L_0 = \frac{d^2}{dR^2} + \frac{1}{R}\frac{d}{dR} - B + \psi_0, \quad L_1 = L_0 + 2\psi_0^2,$$

where R is the radial direction scaled by ρ and $B = \rho^2(\beta^2 - k^2 n_0^2)$. Instability occurs if at least one value of Λ is negative. This implies that if the minimum value of Λ is positive, the mode ψ_0 is stable. Otherwise, it is unstable.

Firstly, we have $\langle u, \psi_0 \rangle = 0$. To see this, one can write

$$\begin{aligned} -\Omega^2 \langle u, \psi_0 \rangle &= \langle L_0 L_1 u, \psi_0 \rangle = \langle u, L_1 L_0 \psi_0 \rangle \\ &= \langle u, 0 \rangle = 0 \end{aligned}$$

using (3.11) and $L_0\psi_0 = 0$. Here, the brackets are defined by $\langle g_1, g_2 \rangle = \int_0^\infty g_1^* g_2 \, R\, dR$ for continuous functions g_1, g_2 with vanishing boundary conditions at $R = 0, \infty$.

From (3.11), one can write

$$\Lambda = \frac{\langle u, L_1 u \rangle}{\langle u, L_0^{-1} u \rangle} \tag{3.36}$$

Since $\langle u, L_0^{-1} u \rangle$ is negative-definite, and since only the sign of the minimum of Λ is required, it is sufficient to find the sign of the maximum value of $\langle u, L_1 u \rangle$.

Using the method of indeterminate (Lagrange) multipliers, we form a functional

$$G = \langle u, L_1 u \rangle - a \langle u, u \rangle - b(\langle u, \psi_0 \rangle + \langle \psi_0, u \rangle)$$

with the constraints

$$\langle u, u \rangle = 1 \text{ (normalized)}, \quad \text{and } \langle u, \psi_0 \rangle = 0$$

and a, b are undertermined multipliers. By the variational principle, taking the first variation of G with respect to u gives

$$L_1 u = au + b\psi_0 \tag{3.37}$$

from which $a = \langle u, L_1 u \rangle$, the maximum of which is what we wish to determine. Let

$$u = \sum_i \alpha_i \omega_i \,, \quad \psi_0 = \sum_i c_i \omega_i \,, \tag{3.38}$$

where ω_i are orthonormal eigenfunctions of L_1 with corresponding eigenvalues λ_i. Then (3.37) becomes

$$\sum_i \alpha_i \lambda_i \omega_i = a \sum_i \alpha_i \omega_i + b \sum_i c_i \omega_i$$

and therefore

$$\alpha_i = \frac{b\, c_i}{\lambda_i - a}, \quad u = \sum_i \frac{b\, c_i}{\lambda_i - a} \omega_i .$$

Thus

$$\langle \psi_0, u \rangle = 0 = \sum_i \frac{b\, |c_i|^2}{\lambda_i - a} = b\, S(a), \text{ (say)}$$

Now, differentiating $L_0 \psi_0 = 0$ with respect to B gives

$$L_1 \frac{\partial \psi_0}{\partial B} = \psi_0 \,,$$

and so

$$L_1^{-1} \psi_0 = \frac{\partial \psi_0}{\partial B} .$$

If $P_c = \int_0^\infty \psi_0^2 \, R \, dR$, then

$$\begin{aligned} \frac{1}{2} \frac{dP}{dB} &= \left\langle \psi_0, \frac{\partial \psi_0}{\partial B} \right\rangle = \langle \psi_0, L_1^{-1} \psi_0 \rangle \\ &= \sum_i \frac{|c_i|^2}{\lambda_i} = S(0) \end{aligned} \tag{3.39}$$

The behaviour of $S(a) = \sum_i |c_i|^2/(\lambda_i - a) = 0$ is schematically shown in fig 3.1, in which λ_1 and λ_2 are the first two poles of $S(a)$. If we let a_{max} be the largest root of $S(a) = 0$, then, in effect, Kolokolov obtained the following criterions:

(a) - If $0 < \lambda_2 < \lambda_1$ then $a_{max} > 0$, and ψ_0 is unstable.

(b) - If $\lambda_2 < \lambda_1 < 0$ then $a_{max} < 0$, and ψ_0 is stable, and lastly,

(c) - If $\lambda_2 < 0 < \lambda_1$, then $f(0) > 0$ (< 0) implies $a_{max} < 0$ (> 0) and therefore ψ_0 is stable (unstable). In other words, the mode ψ_0 is stable in regions where the dispersion curve is positively sloped and unstable elsewhere.

For bright solitons in a homogeneous Kerr medium, Kolokolov found, by numerically testing the eigenvalues λ_1 and λ_2 of L_1, that only criterion (c) applies.

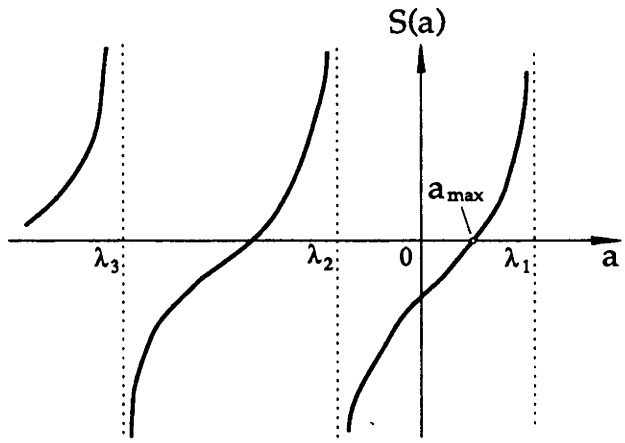

Figure 3.1: Schematic behaviour of $S(a) = \sum_i \frac{|c_i|^2}{\lambda_i - a}$.

Discussion

1. The above analysis is also applicable to planar bright solitons in the same medium, with modifications. It turns out that we then always have $dP/dB > 0$, i.e. the solitons are stable. ($P = \int_{-\infty}^{\infty} \psi_0^2 \, dX$) for a planar fundamental mode.)

2. To obtain Kolokolov's criterions for the planar case, it is not necessary to test λ_1 and λ_2 numerically to conclude that result (c) applies. Differentiating $L_0\psi_0 = 0$ with respect to X, one has

$$L_1 \frac{d\psi_0}{dX} = 0,$$

which means L_1 has a zero eigenvalue with eigenfunction $d\psi_0/dX$. Notice that $d\psi_0/dX$ is an odd function with one node. Hence zero is the second eigenvalue; the first eigenvalue must be positive with a nodeless eigenfunction, and the third and higher-order eigenvalues must be negative. The first and third eigenvalues can be identified with $\lambda_1 > 0$ and $\lambda_2 < 0$ respectively for following reason: ψ_0 is even and hence does not appear in the expansion (3.38) of ψ_0, and hence the constant c_i corresponding to λ_i also does not appear in the sum expression for $S(a)$.

3. These criterions need not be confined to bright solitons in a Kerr medium but apply also to any bright (scalar) fundamental modes of any structure. This

is because the derivation only requires the self-adjointness of the operators L_0 and L_1. However, the problem with general fundamental modes is that λ_1 and λ_2 are not amenable to analytical determination.

4. The derivation involves $\langle u, u \rangle$, and hence cannot be extended to dark waves.

Stability of Planar Surface Waves

For sometime, it was speculated that the sufficient condition $dP/dB > 0$ for stability would apply also to modes of inhomogeneous structures. Indeed, this was found to be true for a planar interface between a linear medium and a Kerr self-focussing one [78]. The slope of the dispersion curve for this case changes sign only at one point. However, when the media on both sides of the interface are self-focussing, it was found [79] this condition is not sufficient. Further investigation was needed and is discussed below.

3.1.9 Jones and Moloney's Work

This work [59] is probably the first to address the question concerning the stability of modes in a waveguide structure. Although the results obtained by these authors is expected to apply to a wider class of waveguides, the method is, to a large extent, restricted to symmetric waveguides with a linear core and Kerr self-focusing bounding media. Here, we choose to discuss only the argument for the symmetric modes.

The essence of Jones and Moloney's work[2] is the method of calculating the number n_+ of positive eigenvalues of L_1 using a topological argument. To help understanding, the following facts from Sturm-Liouville theory are noted:

1. Suppose L is a Hermitian second-order operator with eigenvalues $\ldots, \lambda_i, \ldots, \lambda_1, \lambda_0$ (in increasing order) and corresponding bound (i.e. localized) eigenfunctions $\ldots, \phi_i, \ldots, \phi_1, \phi_0$. It is well known that ϕ_0 (called the fundamental eigenfuction) has no zeros, ϕ_1 (first-order eigenfunction) has one zero, ϕ_2 has two, and so on.

2. Consider the solutions of $L\phi = \lambda\phi$ where ϕ, which is continuous and smooth everywhere, is now required to vanish at either $+\infty$ or $-\infty$ only. If $\lambda > \lambda_0$, then ϕ has no zeros. Similarly, if $\lambda_{i+1} < \lambda < \lambda_i$, then ϕ has i zeros.

[2]Which is almost incomprehensible to many people without a deep background in operator theory!

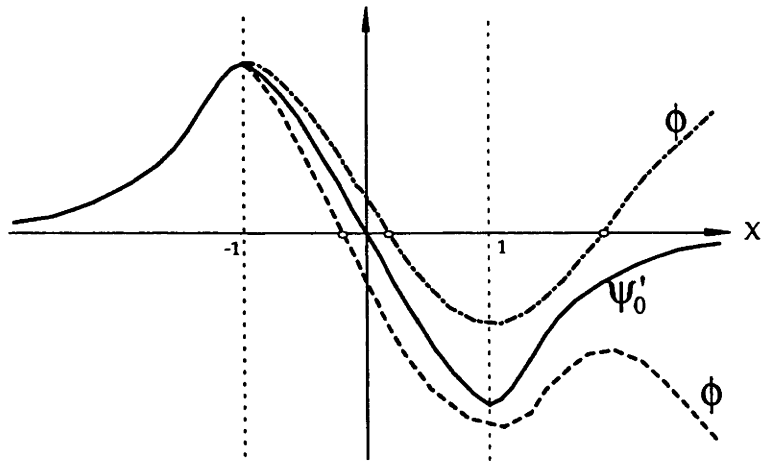

Figure 3.2: Schematic shapes of ψ_0' and ϕ.

3. To calculate n_+, it is necessary only to calculate the number of zeros of ϕ where $L_1\phi = 0$ (with the above-mentioned boundary conditions).

Differentiating $L_0\psi_0 = 0$ with respect to X, we obtain

$$L_1 \frac{\partial \psi_0}{\partial X} = a\,\delta(X+1) + b\,\delta(X-1),$$

where a and b are some constants. (The δ functions arise from the discontinuity of the structure at the waveguide interfaces.)

Since ϕ and $\partial\psi_0/\partial X$ $(= \psi_0')$ have the same vanishing boundary condition in $X \to -\infty$, they can be made identical in the left bounding medium. Across $X = -1$, the slope of ψ_0' changes abruptly according to

$$\frac{\partial \psi_0'}{\partial X} = \psi_0' \frac{\psi_0'}{\psi_0},$$

while ϕ remains smooth. In the core region, if ϕ is above ψ_0' as schematically shown by the dash-dot curve in fig.3.2, then ϕ has 2 zeros, whereas if it is below (shown by the dashed curve) then it has one zero. Which of these possibilities actually occur is dictated by the phase diagrams in fig.3.3 which show the variation of ψ_0' with ψ_0. Fig.3.3(a), (b) and (c) show the composite trajectories before, at, and beyond the bifurcation point (i.e. point N in fig.4.16) where an asymmetric mode branches off. Before bifurcation, ϕ is below ψ_0' rendering $n_+ = 1$, and Kolokolov's criterion (c) implies that the mode ψ_0 is stable. On the contrary, beyond the bifurcation point, ϕ is above ψ_0', hence $n_+ = 2$, and Kolokolov's criterion (a) implies the instability

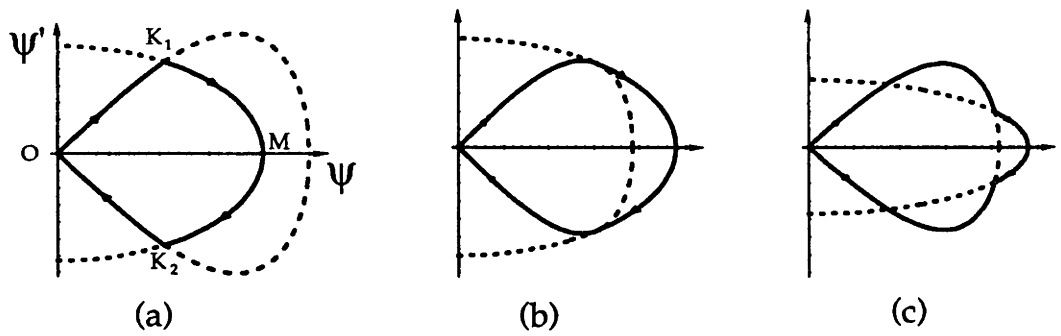

Figure 3.3: Schematic phase diagrams of the symmetric mode of a slab waveguide. (a) before, (b) at, and (c) after bifurcation (point N in fig.4.16).

of ψ_0, irrespective of the sign of dP/dB. This result agrees with that obtained by other authors using a different approach [70].

In our opinion, the main limitations of this method are as follows: (a) Phase diagrams are equation-dependent and therefore the analysis has to be repeated essentially for each point on a dispersion curve and for each particular waveguide under study; (b) Each phase diagram may correspond to more than one mode, including asymmetric modes, and it is not clear the number n_+ can be conveniently calculated using a topological argument. In fact, in Ref.[59], Jones and Moloney used a totally different approach to determine the stability of the asymmetric TE_0 branch of the symmetric waveguide.

3.1.10 Mitchell and Snyder's Work

Mitchell and Snyder have recently combined Kolokolov's and Jones-Moloney's arguments to obtain a general result for *fundamental* modes of any nonlinear waveguiding structure.

Here, the definition of a 'fundamental' mode should be given a clear definition. Since Mitchell and Snyder primarily dealt only with scalar modes of an arbitrary cylindrical structure, their (nonlinear) fundamental mode was defined (see [73]) to be the fundamental mode of the waveguide it induces, which has the largest β. In our opinion, this definition is a restricted one which provokes a confusion between mathematical and physical concepts. Indeed, the derivation of their theorem (shown below) implies that a nonlinear fundamental mode is just the fundamental eigenfunction of the *operator* L_0 (which has the largest nonzero eigenvalue). This latter definition will be used in the whole of this thesis.

For fundamental modes, it has been shown in subsection 3.1.3 that the eigen-

values of L_0L_1 can only be real. While the details of Mitchell and Snyder's work can be found elsewhere [73], the result, in the present notation, can be described as follows.

The 'degree of instability' is defined to be the number of eigenvalues of L_0L_1 which are either real and positive.

Theorem. *The degree of instability of the mode is equal to the number of positive eigenvalues of L_1 when $dP/dB < 0$ and is one less than the number of positive eigenvalues of L_1 when $dP/dB > 0$. Thus the degree of instability changes only when dP/dB changes sign or one of the eigenvalues of L_1 changes sign.*

The former case includes extrema in power dispersion (i.e. power P vs β) diagrams. The latter case happens at bifurcation points, i.e. points where two or more dispersion branches meet.

Thus, Mitchell and Snyder's theorem does not determine stability explicitly. Rather, it gives a rule of how stability changes *relatively* across special points such as extrema or points of bifurcation in the dispersion diagram. To determine stability explicitly, the stability at at least one point of a dispersion branch needs be known; such starting points may be a (stable) linear limit, or a point corresponding to a known stable mode.

An application of this theorem is discussed further in chapter 7.

3.2 Lyapunov Theory

Late in the nineteenth century, Lyapunov [80] made an important contribution in the subject of stability of a dynamical system. The theory was formulated in the language of analytical mechanics, of which a brief description is given below.

3.2.1 Background

Our system for a self-focusing medium is described by

$$iN\frac{\partial\psi}{\partial Z} = -\frac{\partial^2\psi}{\partial X^2} + B(X)\,\psi - |\psi|^2\psi, \tag{3.40}$$

in the slowly-varying approximation.

In the linear analysis approach, ψ is then assumed to be a solution with a weak dependence on Z, and which is very close to a stationary solution, as described by (3.2). The perturbed solution is then substituted into (3.40) to investigate how the perturbation behaves in an initial short distance of propagation if it is assumed to

have an exponential form (3.4). The assumption here is that the perturbation is infinitesmimal so that linear approximation for its behaviour is adequate.

In Lyapunov theory, the system (3.40) is treated as a dynamical system, with Z playing the role of time, and ψ in the role of a 'coordinate'.

Suppose the state of a general dynamical system at time t is specified by a set of coordinates x_i $(i = 1, 2, 3, ...m)$, and these coordinates satisfy the autonomous system of ordinary first-order differential equations

$$\frac{dx_i}{dt} = X_i(x_i, \cdots, x_m, t) \quad (i = 1, \cdots, m) \tag{3.41}$$

where m is the number of degrees of freedom of the system, and $X_i(x_i, \cdots, x_m, t)$ are continuous functions in some region

$$|x_i| \leq \Delta, \quad t \geq t_0 \tag{3.42}$$

(t_0 is a fixed initial instant of time).

To the equilibrium state there corresponds a zero solution $x_i \equiv 0$ of the system of equations (3.41). Such a solution pre-supposes that the right-hand sides of equations (3.41) satisfy the condition

$$X_i(0, \cdots, 0, t) \equiv 0 \quad (i = 1, \cdots, m) \tag{3.43}$$

Stability of the zero solution is defined as follows: for any $\epsilon > 0$, there exists a $\delta = \delta(\epsilon) > 0$ such that
for any $t \geq t_0$

$$|x_i(t)| < \epsilon \tag{3.44}$$

as long as

$$|x_i(t_0)| < \delta \tag{3.45}$$

$(i = 1, \cdots, m)$. Here is an important theorem:

Lyapunov's Theorem. *If there exists a function $V(x_1, \cdots, x_m, t)$ in the region (3.42) such that, for any t considered as a parameter, it has a global extremum at the point $x_1 = \cdots = x_m = 0$, whereas at the same point, and for any t, its time derivative*

$$V'(x_1, \cdots, x_m, t) = \sum_{i=1}^{n} \frac{\partial V}{\partial x_i} X_i + \frac{\partial V}{\partial t}$$

has an extremum of the opposite type, then the zero solution of the system (3.41) is stable. If the extremum of V' is also global, then the zero solution of (3.41) is asymptotically stable.

The full proof of this theorem may be found in standard texts [80]. For the present purposes, the theorem can be reduced to a simpler version, namely that the functions X_i and V are not explicitly dependent on time t. Then a special case of Lyapunov's theorem is the familiar

Lagrange's Theorem: *If in some position of a conservative system the potential energy has a minimum, then this position is a stable equilibrium of the system.*

The truth of this familiar fact may be taken as obvious, although a rigorous proof can also be found in Ref.[80]. The potential energy in Lagrange's theorem plays the role of V in Lyapunov's theorem.

A further step that makes Lyapunov's theorem closer to the present purposes is the following corollary.

COROLLARY. *If the system of differential equations (3.41) has an integral $V(x_1, \cdots, x_m, t)$ (which is not dependent on t in our case) and this integral has either a global maximum or minimum at the point $x_1 = \cdots = x_m = 0$ for any fixed t, then the zero solution of the system (3.41) is stable.*

This is because if V is an integral of the system, then by definition V is constant in time. This means $\frac{dV}{dt} = V' = 0$, and it may be taken that V' has a maximum and minimum at the point $x_1 = \cdots = x_m = 0$ for any t.

3.2.2 Application to guided waves

Lyapunov's theorem has recently been used by Hart and Wright [81] to study guided waves. To use Lyapunov's theorem, the equation describing the guided wave system firstly has to be written in a more appropriate form. The change is in the representation of the electric field $\mathbf{E}(x, y, z)$ of chapter 2. Instead of (2.2), $\mathbf{E}$ is now written as

$$\mathbf{E}(x, z) = \mathbf{e}(x, z)\, e^{i\beta_o z} \tag{3.46}$$

where β_o is the propagation constant in the linear (zero-power) limit. With the scaling rules explained in chapter 2, the equation describing the system, again in the slowly-varying approximation, is

$$iN \frac{\partial \psi}{\partial Z} = -\frac{\partial^2 \psi}{\partial X^2} + B_0(X)\, \psi - |\psi|^2 \psi, \tag{3.47}$$

where $B_0 = \rho^2(\beta_o^2 - k^2 n_0^2)$. This equation (3.47) is identical in form to Eqn.(3.40), with the following differences: (a) $B_0(X)$ is independent of power or β; (b) ψ is now

defined in a slightly different way due to the new representation (3.46) of $E(x,z)$. The reason for these changes will become clear later.

It is well known [82,78] that Eqn.(3.47) leads to two integrals of motion, namely the Hamiltonian

$$H = \int_{-\infty}^{\infty} \left(\left| \frac{\partial \psi}{\partial X} \right|^2 + B_0(X)|\psi|^2 - \frac{1}{2}|\psi|^4 \right) dX, \tag{3.48}$$

and the power

$$P = \int_{-\infty}^{\infty} |\psi|^2 \, dX. \tag{3.49}$$

For convenience, details of the derivation of H is included in the Appendix at the end of this chapter. At a fixed power P, the stationary solutions of Eqn.(3.47) correspond to the statationary points of H. To see this, one can solve the variational problem [81,82]

$$\delta(H + \sigma^2 P) = 0, \tag{3.50}$$

with σ^2 playing the role of a Lagrange multiplier. Details in the Appendix show that the result is

$$\frac{d^2\psi}{dX^2} - [\sigma^2 + B_0(X)]\,\psi + \psi^3 = 0 \tag{3.51}$$

which is a modal equation for the structure.

The stationary expression (3.50) leads to a mode, and also corresponds to either a maximum, a minimum, or a saddle point [83] of the Hamiltonian H at a fixed power P. Lyapunov's theorem requires a strong condition, namely that H is either bounded above or below. It is easy to see that, for a fixed P, H cannot be bounded above due to the presence of the $\left|\frac{\partial \psi}{\partial X}\right|^2$ term. Thus if ψ is a mode, this corresponds to a minimum (local in general) for H. Implicitly, Lyapunov theorem demands that H is a global minimum for ψ_0 as a necessary condition for stability.

It happens that, at a fixed power P, the absolute minimum for H occurs when the mode is a TE_0 mode. For this reason, modes of orders higher than the fundamental are beyond the scope of Lyapunov's theorem. Even for the fundamental TE_0 modes, H has to be tested for the minimum if more than one TE_0 mode occurs at a fixed power, as in the case of surface and guided waves.

3.2.3 Discussion

Here, we discuss the advantages and disadvantages of linear stability analysis and Lyapunov method.

1. Both methods assume the slowly-varying approximation. However, the formulation of Lyapunov method requires the rapid variation with z of the field to be factored out in the form $\exp(i\beta_o z)$ (see Eqn.3.46). At high enough powers, β may increase significantly and thus could leave a sufficiently rapid variation with z in $\mathbf{e}(x,z)$ such that the slowly-varying approximation used in 3.47 may no longer be valid.

2. Lyapunov method requires H to be a global minimum for ψ_0 to be a stable mode. However, Mitchell and Snyder [73] have shown that this is too strong a condition for a fundamental mode, and that stability of ψ_0 only requires H to be a local minimum.

3. Lyapunov method is not applicable to higher-order modes. Infact, so far in the context of guided waves, it has been used only in cases where there is only a single possible bound mode at some fixed power [77,81]. Also, since Lyapunov approach involves integrating over the whole X-axis, it is not applicable to dark waves.

4. The main limitation of linear analysis is in the determination of the first two eigenvalues λ_0, λ_1 of L_1. Even with the convenience of Mitchell and Snyder's theorem, the stability of some particular point on a dispersion branch must be known before the theorem can be applied. Sometimes, that priori knowlegde about a particular point is immediately evident from physical consideration (e.g. the branch has a linear limit) or by inferrence from some known results, but more often it still has to rely on some other methods which involve nemerical calculations. In these instances, the pro argument for it often is: "Well, but calculating it at only one point is much better than at every point!". As with lyapunov method, a common limitation of the linear analyses by Kolokolov, Jones and Moloney, and Mitchell and Snyder, is that they do not apply to nonfundamental modes - a fact that is due to the existence of complex growth rates.

5. The linear analysis approach using exact solutions as presented here works for modes of any order. It has demonstrated the full complexity of stability analysis arising from possible complex eigenvalues. The main disadvantage of this method, however, is its dependence on the availability of exact solutions.

3.3 Numerical Beam Propagation

The beam propagation method is another method that has been employed by some authors to study stability of stationary waves [14,84]. The propagation equation is Eqn.(3.40). The propagation method used in this thesis is described in chapter 2. To study stability, an exact mode plus a small perturbation is used as an initial condition for a propagation. If the field remains close to the mode during a sufficiently long distance of propagation, then the mode may be regarded as being stable. Otherwise, it is regarded as unstable. (Nevertheless, for all practical purposes, such a wave can be considered to be stable.)

Some disadvantages of this method are: (a) As is typical in numerical problems, the subsequent evolution of the solution depends on the particular initial perturbation; (b) In cases when instability is weak, it may take too long a distance for the instability before the instability can be observed; (b) There have been examples where linear analysis predicts stability [70,59] but BPM simulations indicate instability [69]. However, these contradictions occur only in very special and small ranges of parameters, and may be attributed to very sentitive dependences in the numerical simulations.

Another alternative, which can check linear stability results, is to propagate the equation (3.3) for the perturbation f; this is easier due to its linearity. Since it is linear, it is not restricted to small values, but it shows the behaviour of the perturbation only for a short initial distance of propagation.

3.4 Transverse Stability

This means stability (or instability) with respect to perturbations in the second transverse dimension, in which waveguiding structures and stationary guided waves are assumed uniform. In planar geometry, this is the y-direction; while in the circular case, this is the azimuthal ϕ-direction. Investigation of this type of stability is important because, firstly, the assumption of uniformity in this second transverse dimension is only a simplification or approximation of reality. Secondly, and more importantly, one can qualitatively predict what would happen to a mode under transverse perturbations: if the mode turns out to be transversely unstable, it would necesarily break down into beams, or filaments, as propagation proceeds, a proper description for these new formations would require two-transverse-dimenstional calculations.

For simplicity, a discussion of the situation in planar geometry is now given. The attempt here is not to present a solution of the problem but only to point out the complication that transverse stability leads to, and to suggest a direction in searching for a solution.

It is easy to see that the inclusion of the y-direction in the perturbations modifies the definition of the operators L_0, L_1 to include a $\partial^2/\partial Y^2$ term. Hence

$$L_0 = \frac{\partial^2}{\partial X^2} + \frac{\partial^2}{\partial Y^2} - B + h\psi_n^2, \quad L_1 = L_0 + 2h\psi_n^2.$$

The perturbation functions u and v are now functions of both x and y. Nevertheless, the dependence of u and v on y can allow us to make the changes

$$u \rightarrow u(X)\exp(iqy), \quad \text{and } v \rightarrow v(X)\exp(iqy),$$

where q is either real or purely imaginary. This leads to a simplification in the forms of L_0, L_1:

$$L_0 = \frac{d^2}{dX^2} - (B + q^2) + h\psi_n^2, \quad L_1 = L_0 + 2h\psi_n^2. \tag{3.52}$$

The difficulty arising from this form of L_0, L_1 is that exact solutions to the system (3.10) are no longer available.

Other possibilities are: (i) to use sophisticated analytical arguments from operator theory, which is a more preferred approach, or (ii) to apply numerical methods directly to calculate the eigenvalues of L_0L_1.

APPENDIX

(a) - Derivation the integrals of motion from Eqn.(3.47).

Eqn.(3.47) and its complex conjugate may be written as

$$\begin{aligned} iN\psi_Z + \psi_{XX} - B_0\psi + h|\psi|^2\psi &= 0 \\ -iN\psi_Z^* + \psi_{XX}^* - B_0\psi^* + h|\psi|^2\psi^* &= 0 \end{aligned} \tag{3.53}$$

Eliminating the Z-dependent terms by multiplying the first and second equations by ψ_Z^* and ψ_Z respectively, we have

$$\psi_{XX}\psi_Z^* + \psi_{XX}^*\psi_Z - B_0(|\psi|^2)_Z + h(\frac{1}{2}|\psi|^4)_Z = 0 \tag{3.54}$$

Adding and subtracting (3.54) by $\psi_X\psi_{ZX}^*$ and $\psi_X^*\psi_{ZX}$ and grouping the terms leads to

$$(\psi_X\psi_Z^*)_X + (\psi_X^*\psi_Z)_X - (\psi_X\psi_X^*)_Z - B_0(|\psi|^2)_Z + h(\frac{1}{2}|\psi|^4)_Z = 0 \tag{3.55}$$

If ψ is a bright wave (i.e. bound), then integrating over X from $-\infty$ to $+\infty$ gives

$$-\frac{d}{dZ}\left\{\int_{-\infty}^{\infty}\left(|\psi_X|^2 + B_0|\psi|^2 - \frac{1}{2}|\psi|^4\right)\,dX\right\} = 0$$

which means H as defined (3.48) is a constant.

By physical argument, the power P is necessarily a constant of motion. (It can also easily be derived analytically as well.)

(b) - Derivation of the solution of the variational problem (3.50).

$$\begin{aligned} \delta(H + \sigma^2 P) &= \delta\int_{-\infty}^{\infty}\left[|\psi_X|^2 + (B_0 + \sigma^2)|\psi|^2 - \frac{1}{2}|\psi|^4\right]\,dX \\ &= 2\,\mathrm{Re}\int_{-\infty}^{\infty}\left[\psi_X^*\,\delta\psi_X + (B_0 + \sigma^2)\,\psi^*\,\delta\psi - |\psi|^2\psi^*\,\delta\psi\right]\,dX = 0. \end{aligned}$$

Integrating the first term by part and using $\delta\psi = 0$ at $X = \pm\infty$, we get

$$\mathrm{Re}\int_{-\infty}^{\infty}\left[-\psi_{XX}^* + (B_0 + \sigma^2)\,\psi^* - |\psi|^2\psi^*\right]\,\delta\psi\,dX = 0$$

for any $\delta\psi$. Hence, (3.51) follows.

Chapter 4

Waveguides with Kerr SF Bounding Media

This chapter studies planar, or slab, waveguide structures which consist of a linear thin film and Kerr self-focusing bounding media. The waveguides are generally asymmetric, that is characterised by $V_r \neq V_l$ and/or $\eta \neq 1$, and can support asymmetric modes. The special case of symmetric waveguides is also considered.

The primary questions to be answered here are: (a) What modes can be supported by these structures; and (b) are the modes stable?

Following the usual notation, the class of modes which have m nodes in their field profiles are called TE_m modes, and only modes up to the second order, i.e. TE_0, TE_1, and TE_2, are studied in this thesis. Their stability is determined analytically using the analysis method of chapter 3.

The structure of this chapter is as follows: Section 4.1 describes the waveguide geometry, and defines the scaled quantities such as to give a succinct description with the least number of free parameters. Section 4.2 shows how the various dispersion relations are derived, while section 4.3 and 4.4 discuss the characteristics of the TE_0 and TE_1 modes respectively.

The last section (4.7) briefly reviews some related experiments on nonlinear guided waves and discusses the experimental confirmation of the present theoretical results.

4.1 Waveguide Geometry and Parameters

The linear structure and nonlinear parameters of waveguide are generally asymmetric. As illustrated in fig.4.1, the linear film of the waveguide has refractive index

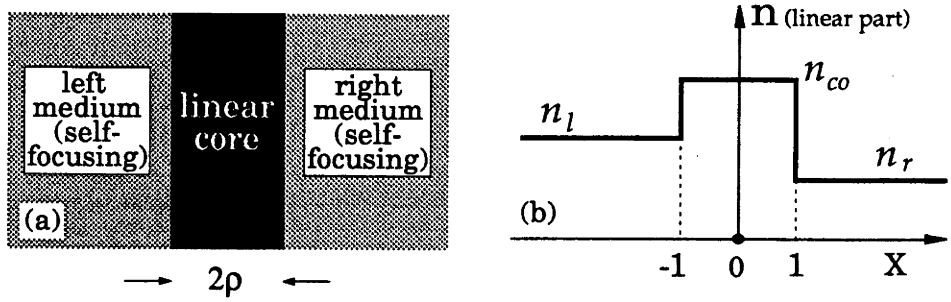

Figure 4.1: (a) Geometry of a nonlinear planar waveguide. The nonlinear bounding media are Kerr-law; (b) Asymmetric linear index profile.

n_{co}, thickness 2 units, and is located in $-1 < X < 1$ where

$$X = x/\rho.$$

Here x is the actual transverse dimension, and ρ is the half-width of the core. The left and right bounding media respectively have linear indices n_l and n_r, nonlinear coefficients n_{2l} and n_{2r}, so that the nonlinear refractive index profile is

$$n = \begin{cases} n_l + n_{2l}|E|^2, & X < -1 \\ n_{co}, & -1 < X < 1 \\ n_r + n_{2r}|E|^2, & X > 1 \end{cases} \tag{4.1}$$

where E is the electric field.

To describe the characteristics of nonlinear guided modes in this structure with the least number of parameters, it is most convenient to define the following waveguide parameters:

$$\begin{aligned} V_i^2 &= k^2\rho^2(n_{co}^2 - n_i^2), \\ \alpha_i &= 2n_i n_{2i}\rho^2 k^2, \\ \eta &= \frac{\alpha_r}{\alpha_l}, \end{aligned}$$

where $i = r, l$ and refers to the left and right media respectively. These depend only material properties. The modal parameters are W_l, W_r, B_{co}, where

$$W_i^2 = \rho^2(\beta^2 - k^2 n_i^2), \quad B_{co} = \rho^2(\beta^2 - k^2 n_{co}^2).$$

Among these, B_{co} (which may be positive or negative) is chosen to be the free parameter which depends only on V_r, V_l, and the modal power. W_r and V_l are

related to B_{co} through

$$W_i^2 = V_i^2 + B_{co}. \tag{4.2}$$

Other dimensionless parameters are the field $\psi = \alpha_r^{1/2} E$ (as in section 2.4), and the modal 'power' P

$$P = \int_{-\infty}^{\infty} \psi^2 \, dX, \tag{4.3}$$

which is directly proportional to actual modal power (see section 2.6 on the conversions of parameters). Thus, the minimal physical parameters necessary for a complete description of these guided waves are: V_r, V_l, η, and P. Given these, the propagation constant β (or B_{co}, which is regarded as a dependent variable), and the modal field $\psi(X)$ can be calculated. An alternative approach, which is mathematically more convenient and is used in this thesis, is to regard B_{co} as an independent variable, and P as a dependent one.

Recently we have also seen a published work [85] confirming these scaling rules to be the most convenient.

4.2 Dispersion Relations

Relations which describe how the modal field and modal power change with B_{co} are here called dispersion relations. We can start from the wave equation [cf.(2.18)]

$$\begin{aligned} \left\{ \frac{d^2}{dX^2} - W_l^2 + \frac{1}{\eta}\psi^2 \right\} \psi &= 0, \qquad X < -1 \\ \left\{ \frac{d^2}{dX^2} - B_{co} \right\} \psi &= 0, \qquad -1 < X < 1 \\ \left\{ \frac{d^2}{dX^2} - W_r^2 + \psi^2 \right\} \psi &= 0, \qquad X > 1. \end{aligned} \tag{4.4}$$

There are two different approaches of deriving the dispersion relations from these wave equations. The first approach is more direct, involving the explicit use of the exact form of the solutions in the different layers of the waveguide, and then applying the boundary conditions at the interfaces. The second approach does not rely on exact solutions in the bounding media, but uses only the first integrals of the wave equations, the boundary conditions, and the exact solution in the linear core only.

We note also another formalism developed by Langbein et al.[86] which is capable of dealing with arbitrary local lossless nonlinearities. Again, this formalism does not require analytical field solutions to the nonlinear wave equations in order to calculate dispersion characteristics. However, we will not go into the details here.

Before describing the two approaches, it is appropriate to discuss boundary conditions at the interfaces.

4.2.1 Boundary Conditions

In regions free of charges and currents, the boundary conditions [49] satisfied by the fields across an interface between media of differing refractive index are: (i) continuity of the magnetic field and the component of the electric field tangential to the interface; and (ii) continuity of the normal component of the displacement vector $\epsilon_0 n^2 \mathbf{E}$ (where $\mathbf{E}$ is the electric field vector).

With the TE modes supported by planar slab waveguides, the electromagnetic components are: transverse electric e_y, transverse magnetic h_x, and longitudinal magnetic h_z, where h_x and h_z are related to e_y through [49, ch.30]

$$h_x = -\left(\frac{\epsilon_0}{\mu_0}\right)^{1/2} \frac{\beta}{k} e_y, \quad h_z = -\left(\frac{\epsilon_0}{\mu_0}\right)^{1/2} \frac{i}{k} \frac{de_y}{dx}. \tag{4.5}$$

These relations (4.5) and boundary condition (i) above means that e_y *and its derivative* de_y/dx, *or equivalently* ψ *and* $d\psi/dX$, *must be continuous across the interface.* Boundary condition (ii) is not necessary for TE modes because there is no component of the electric field vector normal to the interface.

4.2.2 The First Approach

Exact solutions [87,88] to the wave equation (4.4) in the respective layers are

$$\psi = \begin{cases} W_l \sqrt{\eta}\, \mathrm{sech}[W_l(X - X_l)], & X < -1 \\ a_1 \cosh(\sqrt{B_{co}}\, X) + a_2 \sinh(\sqrt{B_{co}}\, X), & -1 < X < 1 \\ \pm W_r\, \mathrm{sech}[W_r(X - X_r)]. & X > 1 \end{cases} \tag{4.6}$$

The plus and minus signs in the last line corresponds to modes of even and odd parities respectively. When $B_{co} < 0$, the solution in the core may be written in terms of trigonometric cosine or sine functions.

In this approach, the continuity conditions [89,90] of ψ and ψ' are applied at $X = \pm 1$. While the details of derivation are exiled to the Appendix at the end of this chapter, the result is an eigenvalue equation for an unknown t:

$$\boxed{\left\{\sqrt{B_{co}}\frac{W_r}{cs}(1-t^2)^{1/2} - \sqrt{B_{co}}\, W_l \sqrt{\eta}\left(\frac{c^2+s^2}{cs}\right)\Gamma\right\}^2 = 4\eta\, W_l^4 \Gamma^2 (1-\Gamma^2)}, \tag{4.7}$$

where

$$t = \tanh G_r, \quad c = \cosh(\sqrt{B_{co}}), \quad s = \sinh(\sqrt{B_{co}}),$$

and

$$\Gamma = \pm\frac{2W_r^2\, cs}{\sqrt{B_{co}}W_l\sqrt{\eta}}(1-t^2)^{1/2}\, t \pm \frac{W_r}{W_l\sqrt{\eta}}(c^2+s^2)(1-t^2)^{1/2}.$$

For a given B_{co} (and hence W_r, W_l), Eqn.(4.7) has one or more roots for t, which corresponds one or more modes of the waveguide, provided that $|t| < 1$ and $\Gamma > 1$. The constant X_r is obtained from t through

$$X_r = 1 - \frac{1}{W_r}\tanh^{-1} t,$$

and similarly, X_l is obtained from Γ through

$$X_l = -1 - \frac{1}{W_l}\mathrm{sech}^{-1}\,\Gamma.$$

Having found X_r and X_l, the modal power, as defined by (4.3), is analytically given by

$$\begin{aligned} P &= \eta W_l\left\{\tanh\left[W_l(-1-X_l)\right]+1\right\} + W_r\left\{1-\tanh\left[W_r(1-X_r)\right]\right\} \\ &\quad + \frac{a_1}{2\sqrt{B_{co}}}\left[1+\sinh\left(2\sqrt{B_{co}}\right)\right] + \frac{a_2}{2\sqrt{B_{co}}}\left[\sinh\left(2\sqrt{B_{co}}\right)-1\right], \end{aligned} \tag{4.8}$$

where a_1 and a_2 are given by (4.33) and (4.34) respectively.

4.2.3 The Second Approach

This approach was first used apparently by Boardman and Egan in Ref.[91]. As mentioned in chapter 2, the first integrals of the wave equation [92] are

$$\begin{aligned} \left(\frac{d\psi}{dX}\right)^2 - W_l^2\,\psi^2 + \frac{1}{2\eta}\psi^4 &= 0, \\ \left(\frac{d\psi}{dX}\right)^2 - B_{co}\,\psi^2 &= C_f, \\ \left(\frac{d\psi}{dX}\right)^2 - W_r^2\,\psi^2 + \frac{1}{2}\psi^4 &= 0. \end{aligned} \tag{4.9}$$

Let ψ_l and ψ_r be the values of ψ at the left and right boundaries respectively. The continuity of ψ and ψ' at $X = \pm 1$ leads from (4.9) to

$$\begin{aligned} C_f &= W_l^2\,\psi_l^2 - B_{co}\,\psi_l^2 - \frac{1}{2\eta}\psi_l^4 \\ &= W_r^2\,\psi_r^2 - B_{co}\,\psi_r^2 - \frac{1}{2}\psi_r^4. \end{aligned}$$

Using (4.2), this leads to a relationship between ψ_l and ψ_r:

$$\frac{1}{\eta}\left(\psi_l^2 - \eta V_l^2\right)^2 - (\psi_r^2 - V_r^2)^2 = \eta V_l^4 - V_r^4, \tag{4.10}$$

which, in general, is a hyperbola between ψ_l^2 and ψ_r^2. Interestingly, the properties of this hyperbola reveal some modal characteristics:

1. When $\eta V_l^4 - V_r^4 > 0$, a typical plot of this relationship (4.10) is shown by the solid curves in fig.4.2. As the waveguide asymmetry increases, the branches become more separated. When $\eta V_l^4 - V_r^4 < 0$, the branches rotate and become the dash-dot curves. However, this case does not deserve a separate consideration because it can be reduced to the former case by interchanging the left and right bounding media.

2. When $\eta V_l^4 - V_r^4 = 0$, the hyperbolic branches reduce to two straight lines which are the asymtotes of hyperbolae with a common η but differing V_l and V_r. The straight line passing through the origin has slope $1/\eta$. This indicates that, at low (and possibly also at high) powers, $\psi_r^2/\psi_l^2 = 1/\eta$, regardless of V_l and V_r.

   In the case of symmetric waveguides, for which $V_r = V_l$ and $\eta = 1$, the hyperbolae reduce to two straight lines intersecting each other at right angles, also shown in fig.4.2. The straight line passing through the origin corresponds to symmetric or anti-symmetric modes, as $\psi_r = \pm\psi_l$, whereas the other straight line corresponds to asymmetric modes of all orders.

3. If $\eta < 0$, then Eqn.(4.10) is an ellipse. This case corresponds to waveguides with one bounding medium being self-defocusing. It can be anticipated that at low powers, the field peak in these waveguides resides in the core. As the power increases, it moves only one way to become a surface wave at the interface between the core and the self-focusing bounding medium.

The elegance of this method is that: (i) the exact form of the solutions for $|X| > 1$ is not required (see also [93,94,86]), so that other types of nonlinearity may be investigated, provided that the first integrals can be expressed in a convenient form; and (ii) the hyperbola between ψ_r^2 and ψ_l^2 indicates qualitatively the types of modes supported by the waveguides, without explicitly solving for them.

In this approach, the exact form of the modal field in the core, given by (4.6), is used. In terms of ψ_r and ψ_l, the constants a_1 and a_2 appearing in (4.6) are given by

$$\begin{aligned} a_1 &= (\psi_r + \psi_l)/2c, \\ a_2 &= (\psi_r - \psi_l)/2s, \end{aligned} \tag{4.11}$$

and

$$\psi'_{X=1} = \sqrt{B_{co}}\,(a_1\, s + a_2\, c). \tag{4.12}$$

The substitution of these expressions into the last equation of (4.9) gives

$$\boxed{B_{co}\,(a_1\, s + a_2\, c)^2 - \psi_r^2\,(W_r^2 - \tfrac{1}{2}\,\psi_r^2) = 0}\,. \tag{4.13}$$

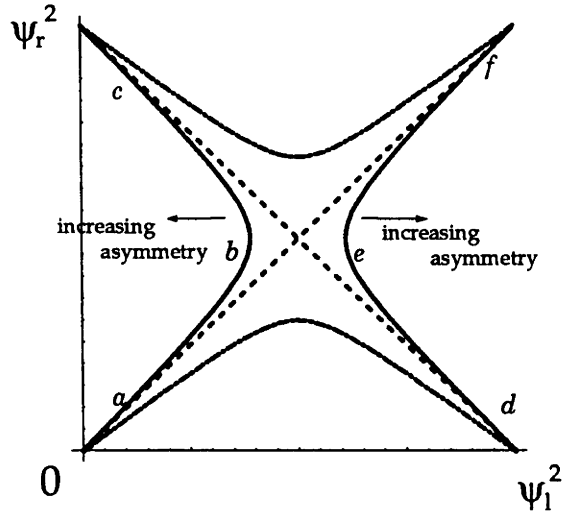

Figure 4.2: Hyperbolic relation between the fields ψ_l^2 and ψ_r^2 at the interfaces.

Together with the parabolic relation (4.10) and the expression (4.11), this equation (4.13) may be regarded as an equation for the only unknown ψ_l at a given value of B_{co}. Equation (4.13) may also be regarded as an eigenvalue equation for B_{co} with ψ_l, and hence ψ_r, given. In fact, this latter choice is more useful when one wishes to trace out the types of modes associated with each of the hyperbolic branches in fig.4.2.

Modal Power

An analytical expression can be derived for modal power in terms of the field amplitudes at the interfaces, namely ψ_r and ψ_l, and W_r, W_l, B_{co}. In deriving this expression, it is necessary to note the following relations:

$$\frac{d}{dX}\left(\frac{\psi'}{\psi}\right) = -\frac{1}{2\eta}\psi^2, \quad X < -1 \tag{4.14}$$

$$\frac{d}{dX}\left(\frac{\psi'}{\psi}\right) = -\frac{1}{2}\psi^2, \quad X > 1 \tag{4.15}$$

$$\frac{d}{dX}(\psi\psi') = C_f + 2B_{co}\psi^2, \quad |X| < 1, \tag{4.16}$$

which are obtained by using the wave equations (4.4) and the first integrals (4.9). Furthermore,

$$\lim_{X\to-\infty}\left(\frac{\psi'}{\psi}\right) = W_l, \tag{4.17}$$

$$\lim_{X\to+\infty}\left(\frac{\psi'}{\psi}\right) = -W_r. \tag{4.18}$$

The power in each region of the waveguide may thus be calculated as follows. In the region $X < -1$,

$$\begin{aligned} P_l &= \int_{-\infty}^{-1}\psi^2\,dX = -2\eta\int_{-\infty}^{-1}\frac{d}{dX}\left(\frac{\psi'}{\psi}\right)dX \\ &= 2\eta\left(W_l - \gamma_l\left|W_l^2 - \psi_l^2/2\eta\right|^{1/2}\right), \end{aligned} \tag{4.19}$$

where γ_l is the sign of ψ'/ψ at the left interface. Similarly for the region $X > 1$,

$$P_r = 2\,W_r + 2\,\gamma_r\left|W_r^2 - \frac{1}{2}\,\psi_r^2\right|^{1/2}, \tag{4.20}$$

where γ_r is the sign of ψ'/ψ at the right interface.

In the core,

$$\begin{aligned} P_{co} &= \int_{-1}^{1}\frac{1}{2B_{co}}\left[\frac{d}{dX}(\psi\,\psi') - C_f\right]dX \\ &= \frac{1}{2B_{co}}\left\{\gamma_r\left|C_f\psi_r^2 + B_{co}\,\psi_r^4\right|^{1/2} - \gamma_l\left|C_f\psi_l^2 + B_{co}\,\psi_l^4\right|^{1/2} - 2\,C_f\right\}. \end{aligned} \tag{4.21}$$

The modal power P is then the sum

$$\boxed{P = P_l + P_{co} + P_r.} \tag{4.22}$$

4.3 Fundamental (TE_0) modes

4.3.1 Modal characteristics

TE_0 modes are the lowest-order modes without any nodes in their mode profiles. Modal characteristics involve the relationships between P, B_{co}, and the mode profile. Much information about modal characteristics are contained in the so-called power-dispersion curves, which can be calculated from the solution to the wave equation for the structure.

For slab waveguides with a linear core and Kerr self-focusing bounding media, either expression (4.8) or (4.22) may be used to calculate the dispersion curves. An example is shown in fig.4.3 for the TE_0 modes of an asymmetric waveguide (with parameters shown in the caption). The calculation of these curves was carried out using the second approach described in subsection 4.2.3 above. The correspondence between the curves and the hyperbolae in fig.4.2 is as follows. For clarity, let us restrict the discussion to the solid curves in fig.4.3 which were obtained with $V_l =$

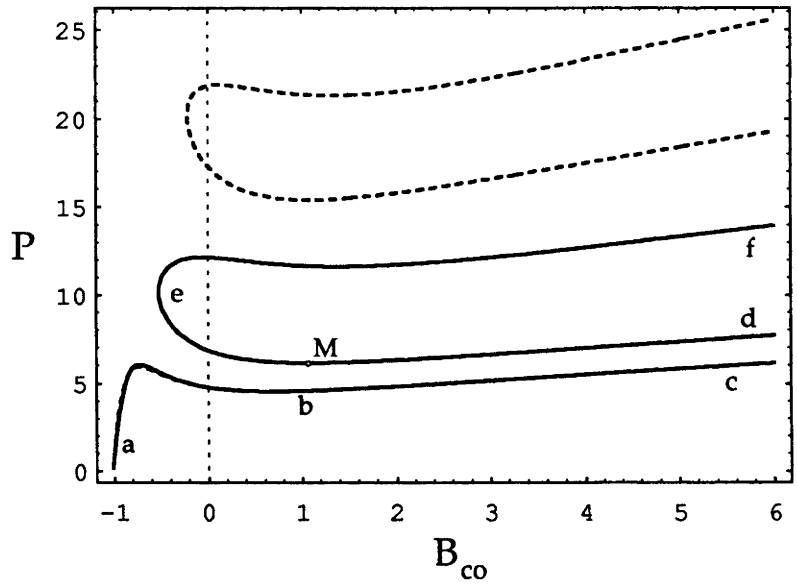

Figure 4.3: Power-dispersion curves for TE_0 modes of an asymmetric waveguide with $V_l = 1.8$, $V_r = 2.0$, and $\eta = 1.2$ (solid curves), and $\eta = 3.0$ (dashed curves). The lower branches of the two sets almost coincide. The vertical line is at $\beta/k = n_{co}$.

1.8, $V_r = 2.0$, and $\eta = 1.2$. The branch *abc* (in that order) in fig.4.3 corresponds to the hyperbolic branch *abc* (in that order) in fig.4.2. As we trace along the disperion curve from the linear (zero power) limit, the modal field evolves from a linear-like field to a field like that of a nonlinear surface mode near the left-hand interface. An illustration of this transition is shown in fig.4.4.

Similarly, the branch *def* of fig.4.3 corresponds to the hyperbolic branch *def* in fig.4.2, with field profiles shown in fig.4.5.

Linear substrate limit

As the asymmetry increases, the separation between the dispersion branches increases. For example, as the ratio η is increased from 1.2 to 3.0 in fig.4.3, the lower branch almost remains the same, but the upper branch which involves a large fraction of power residing in the left medium (or substrate), rises significantly. In the limit when one of the bounding media, taken to be the substrate for $X < -1$, is linear (i.e. $\eta \to \infty$), then only the lower dispersion branch, which has a linear limit, exists. This is illustrated by the lower dashed curve in fig.4.3. In this limit, the mode is almost linear at low powers, and this evolves into a surface mode near the right interface at high powers.

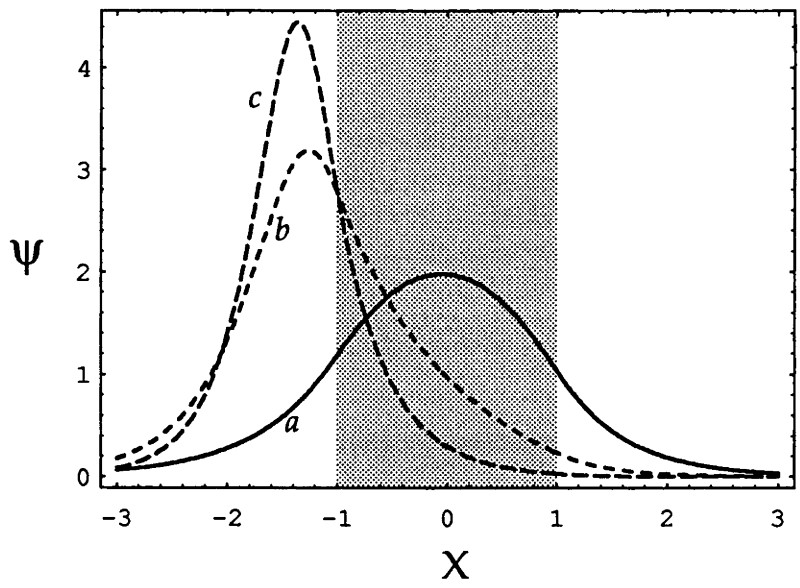

Figure 4.4: Field profiles along the dispersion curve *abc* in fig.4.3. The shaded region is the linear core.

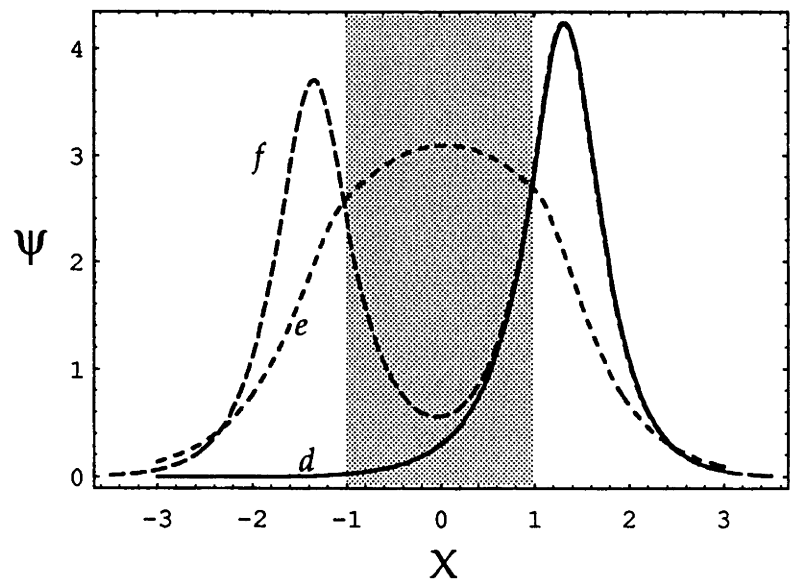

Figure 4.5: Field profiles along the dispersion curve *def* in fig.4.3.

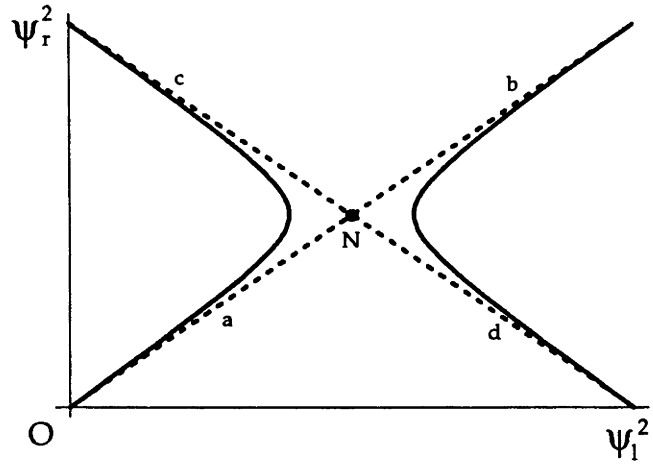

Figure 4.6: Hyperbolic relation between the fields ψ_l^2 and ψ_r^2 at the interfaces.

Skew-symmetric and symmetric waveguide limits

By 'skew-symmetric', it is meant that the relations

$$\eta V_l^4 - V_r^4 = 0, \quad \eta \neq 1 \tag{4.23}$$

are satisfied. The hyperbolae in fig.4.2, which are described by equation (4.10), then reduce to a set of straight lines which do not intersect at right angles, as shown in fig.4.6. As a consequence of skew-symmetry, there exists a bifurcation point N, i.e. a common point of three different branches, as shown in fig.4.7: one (labelled aNb) starts from the linear limit and extends to infinite B_{co}; the other two distinct branches, labelled Nc and Nd exist only beyond the bifurcation point N. A characteristic feature of the skew-symmetric mode branch aNb is that the ratio ψ_r/ψ_l of the mode along the whole branch is equal to $1/\sqrt{\eta}$, i.e. a constant independent of B_{co}. Point N of fig.4.7 corresponds to point N of fig.4.6, and the correspondence between the various dispersion branches the straight lines in fig.4.6 are indicated by the labelling letters.

When $V_l = V_r$ and $\eta = 1$, the waveguide is symmetric [61,70]. The branches Nc and Nd become identical, as shown in fig.4.8(a). The mode profiles along these branches are mirror images of each other, whereas mode profiles along the branch aNb are symmetric, single-peaked for $B_{co} < 0$, and resemble a pair of surface waves at high values of B_{co}. The peak in the symmetric-mode branch depends on the value of the waveguide parameter V: if V is less than about 1.8, the peak does not exist, and the curve is monotonically increasing. At larger values of V, the peak exists

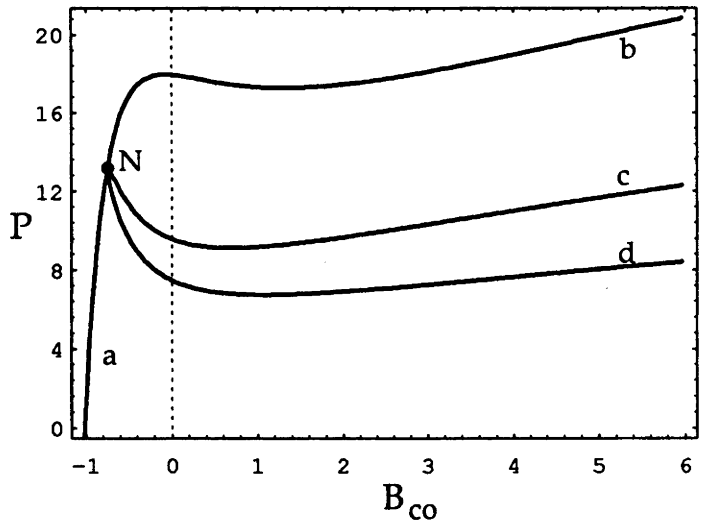

Figure 4.7: Disperion curves for a skew-symmetric waveguide, with $V_l = 1.8$, $V_r = 2.0$, and $\eta = 0.6561$ which satisfy (4.23).

at higher powers. A similar behaviour is seen for the minimum of the asymmetric mode branch: the minimum exists only for V above some minimum value. This is an interesting point, because across this minimum, stability characteristics of the asymmetric mode change from being unstable to stable. This is the subject of discussion in the following subsection.

Some realistic figures

Suppose the cladding a planar waveguide has $n_r = 1.55$, $n_{2r} = 10^{-9}\text{m}^2/\text{W}$ at wavelength 0.515 μm (e.g. those of MBBA), then the porportionality constant in the conversion formula (2.47) is about 2.17×10^{-6}.

Hence if the substrate and core are made of some appropriate materials such that the parameters of fig.4.3 are satisfied, then the scaled power range in fig.4.3 translates to real powers ranging zero to approximately 162 mW, assuming that the waveguide is 3 mm wide (in the y-direction) and the core is 2 μm thick (i.e. $\rho = 1\,\mu$m).

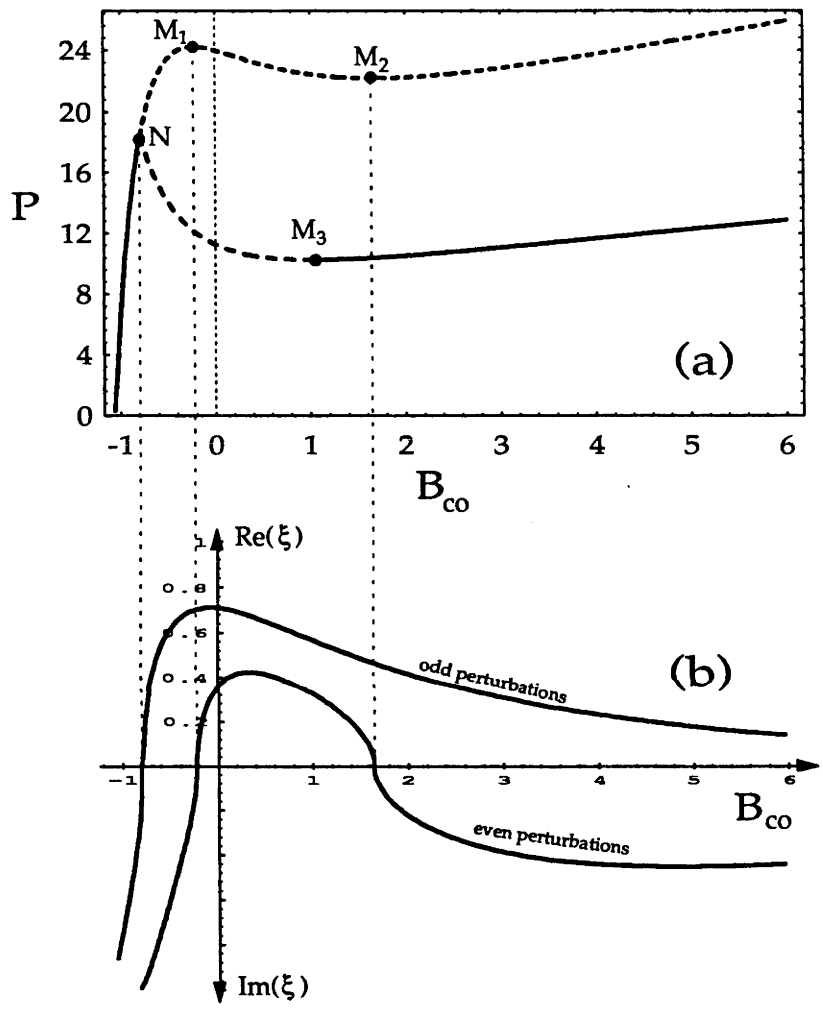

Figure 4.8: (a) Dispersion curves for a symmetric waveguide with $V_l = V_r = 2.0$. Solid curves indicate stability. (b) Stability eigenvalues for even and odd perturbations to the symmetric mode. Real (purely imaginary) values are shown in the upper (lower) half-plane. Instability is indicated by a real ξ.

4.3.2 Stability

Symmetric waveguides

The first analytical stability results for a symmetric waveguide structure were obtained by Akmediev *et al.* [70], for which the linear analysis can be simplified enormously. As has been discussed in chapter 3, stability characteristics can be determined by calculating the eigenvalue (or normalized growth rate) ξ.

For symmetric modes, this is done by matching the solutions for u and v, given by either (3.14) or (3.15) and (3.17), and their first derivatives at one of the interfaces, here chosen to be $X = 1$. With even perturbations, the matching process leads to an equation for ξ, involving a 4×4 determinant:

$$\begin{vmatrix} f_1 & \bar{f}_1 & \cosh p & \cosh \bar{p} \\ f_2 & -\bar{f}_2 & \cosh p & -\cosh \bar{p} \\ f_1' & \bar{f}_1' & p \sinh p & \bar{p} \sinh \bar{p} \\ f_2' & -\bar{f}_2' & p \sinh p & \bar{p} \sinh \bar{p} \end{vmatrix} = 0, \tag{4.24}$$

where the prime denotes d/dX, $p = \sqrt{B_{co} - i\xi}$, $\bar{p} = \sqrt{B_{co} + i\xi}$, f_1, f_2, $\bar{f}_1$, $\bar{f}_2$ are given by (3.18) with the argument x replaced by $x_c = W(1 - X_c)$.

With odd perturbations, the equation for ξ is similar to (4.24) except that the sinh and cosh functions are swapped.

The stability results for the symmetric mode are shown in fig.4.8(b). It has been shown in chapter 3 that ξ can only be real or purely imaginary for TE_0 modes, and this is confirmed in fig.4.8(b). When ξ is real, it is shown above the horizontal axis; likewise, when it is purely imaginary, it is shown below the axis. In this particular case of symmetric modes, even and odd perturbations make a difference: the symmetric mode is stable to even perturbations (which preserve the symmetry) whenever $dP/dB_{co} > 0$, i.e. in positively sloped parts of the dispersion curve, and unstable otherwise. However, to odd perturbations, the symmetric mode is unstable beyond the bifurcation point N, regardless of the slope.

For the asymmetric modes in symmetric waveguides, the matching of the boundary conditions for u and v must be carried out at both interfaces, resulting an 8×8, instead of a 4×4, determinant set to zero. It is elementary to show that this equation

is

$$\begin{vmatrix} f_1(x_1) & \bar{f}_1(x_1) & 0 & 0 & C & \bar{C} & S & \bar{S} \\ f_2(x_1) & -\bar{f}_2(x_1) & 0 & 0 & C & -\bar{C} & S & -\bar{S} \\ f_1'(x_1) & \bar{f}_1'(x_1) & 0 & 0 & pS & \bar{p}\bar{S} & pC & \bar{p}\bar{C} \\ f_2'(x_1) & -\bar{f}_2'(x_1) & 0 & 0 & pS & -\bar{p}\bar{S} & pC & -\bar{p}\bar{C} \\ 0 & 0 & f_1(x_2) & \bar{f}_1(x_2) & C & \bar{C} & -S & -\bar{S} \\ 0 & 0 & f_2(x_2) & -\bar{f}_2(x_2) & C & -\bar{C} & -S & \bar{S} \\ 0 & 0 & f_1'(x_2) & \bar{f}_1'(x_2) & -pS & -\bar{p}\bar{S} & pC & \bar{p}\bar{C} \\ 0 & 0 & f_2'(x_2) & -\bar{f}_2'(x_2) & -pS & \bar{p}\bar{S} & pC & -\bar{p}\bar{C} \end{vmatrix} = 0, \qquad (4.25)$$

where $x_1 = W(1 - X_r)$, $x_2 = -W(-1 - X_l)$, $C = \cosh p$, $\bar{C} = \cosh \bar{p}$, $S = \sinh p$, and $\bar{S} = \sinh \bar{p}$.

Solving this equation, especially when computing facilities are not adequate, can be a major problem; this justifies the preference for the study of symmetric modes by the earlier researchers [70]. It was found that the stability result for the TE_0 asymmetric mode is similar to that of the symmetric mode, with the following difference: from the bifurcation N, ξ is real, and then passes through zero at the minimum point M_3 and remains purely imaginary beyond the minimum. Hence the asymmetric mode is stable in the region with $dP/dB_{co} > 0$, and unstable elsewhere.

Asymmetric waveguides

As has been mentioned in chapter 3, the unfortunate effect of asymmetry is in the modification of the linear equations for $u(x)$ and $v(x)$ to include the asymmetry parameter η in the left bounding medium of the waveguide. Exact solutions in a convenient form for u and v are not available. However, one can always calculate the stability of stationary waves in these asymmetric waveguides by numerically calculating the eigenvalues of the operator L_0L_1. This fact is also true for higher-order modes. (See chapter 3.)

Another alternative is to use Mitchell and Snyder's theorem (see chapter 3). According to this theorem, the branch *abd* in fig.4.3 having a linear limit is stable where the slope is positive and unstable elsewhere. Regarding the upper branch, since its lower arm would coalesce with the lower branch when the waveguide becomes symmetric, it can be *inferred* that the lower arm is stable when the slope is positive. Hence tracing along the *def* branch (in that direction), stability changes from stable to unstable only at the minimum point M.

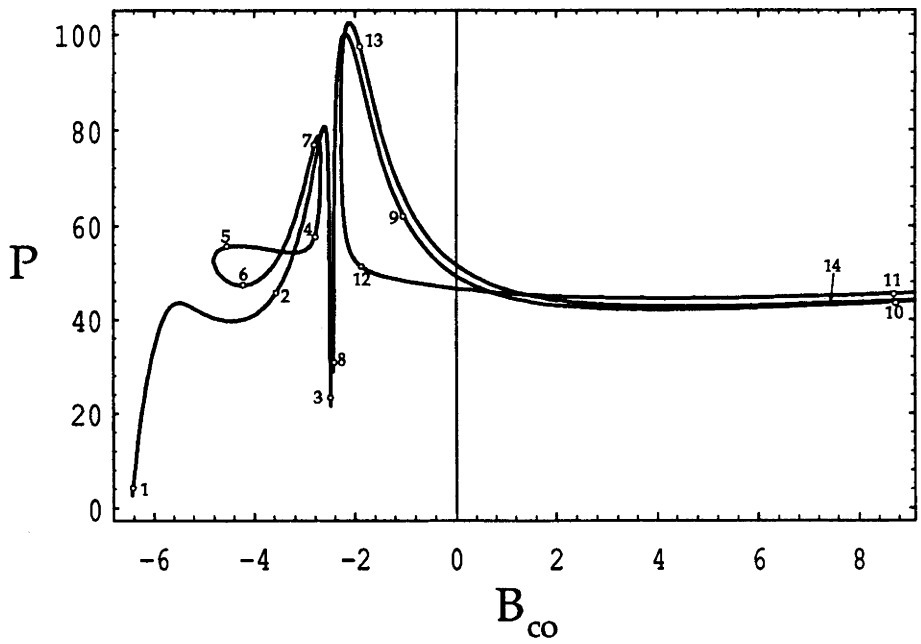

Figure 4.9: Power dispersion curves for TE_1 modes in an asymmetric waveguide with $V_l = 4.4$, $V_r = 4.6$, $\eta = 0.95$.

4.4 First-order (TE_1) modes

This section discusses the modal characteristics and stability properties of the TE_1 modes, in roughly the same sequential order as in the preceeding section. The TE_1 mode has one node in its profile, and perhaps its most remarkable feature is that complex growth rates exist, which indicate a complicated behaviour involving both oscillation and exponential growth when the mode is unstable. This happens at least in the short initial distance of propagation. However, let us first examine the modal characristics.

4.4.1 Modal characteristics

Figure 4.9 shows the dispersion curves of TE_1 modes in a slightly asymmetric waveguide with $V_l = 4.4$, $V_r = 4.6$ and $\eta = 0.95$, again by using the modal power expression (4.22). The result is a highly structured and bizarre set of dispersion curves consist of four distinct branches, two on each side of $B_{co} = -\pi^2/4$ (called the gap point). The gap around this point increases with increasing asymmetry.

On the left of the gap point, one branch starts from the linear limit and ends with a steep negative slope towards the gap point, and one closed branch having a

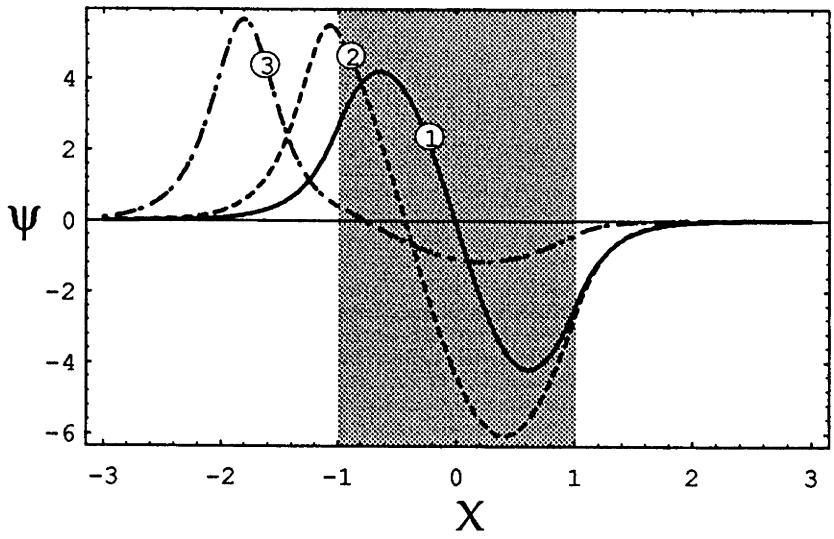

Figure 4.10: Mode shapes along the open branch to the left of the gap point. Each mode profile is associated with a point on the branch labelled by the same number.

figure-of-8 shape. Figures 4.10 and 4.11 show the variation of mode profiles along the two branches. It is observed that mode shape along the open branch varies from linear-like shape to soliton-like shape with a peak in the left medium; while that along the loop has a peak within the core and does not vary too drastically.

On the right of the gap point, again two branches exist. One of these starts with a steep positive slope near the gap point, rises to a maximum, decreases and then increases slowly to infinity. Some mode profiles along this branch are shown in figure 4.12. The other branch has its two ends at infinite B_{co}. For clarity, it is refered to as the right 'loop'. It has a local peak near that of the open branch, and one of its far arms approaches that of the open branch as B_{co} increases. Figure 4.13 shows mode profiles along this loop.

In relation to the hyperbola between ψ_l^2 and ψ_r^2 (fig.4.2), the two open branches on each side of the gap are associated with the left hyperbolic branch (labelled abc), while the two loops are associated with the def branch.

It should be mentioned that although the dispersion curves in fig.4.9 (and also in figs.4.14 and 4.15) cross one another, the modal fields are not the same at the crossing points.

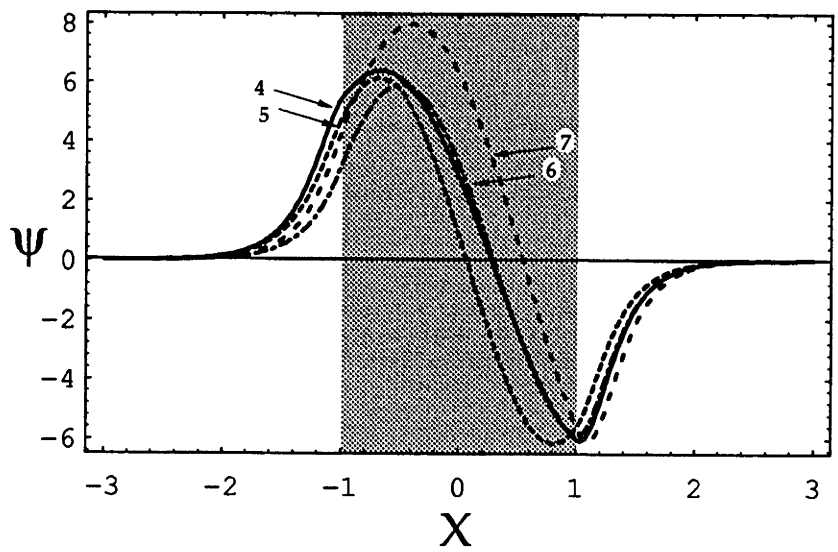

Figure 4.11: Mode shapes along the loop to the left of the gap point. Each mode profile is associated with a point on the loop labelled by the same number.

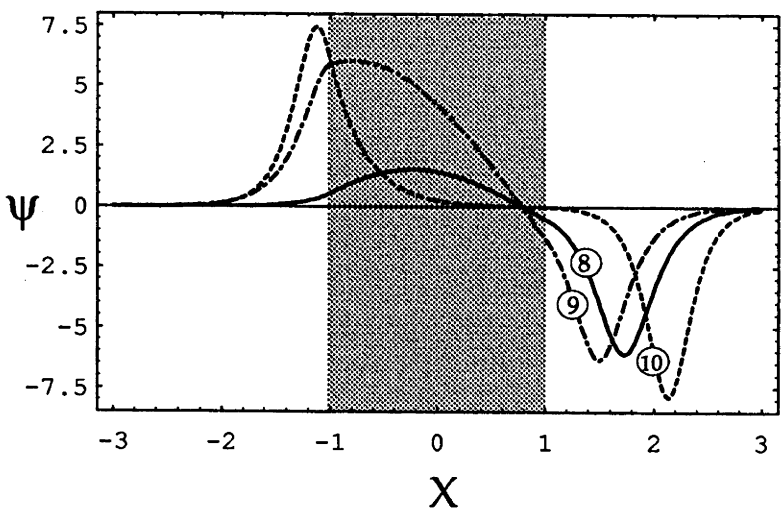

Figure 4.12: Mode shapes along the open branch to the right of the gap point. Each mode profile is associated with a point on the branch labelled by the same number.

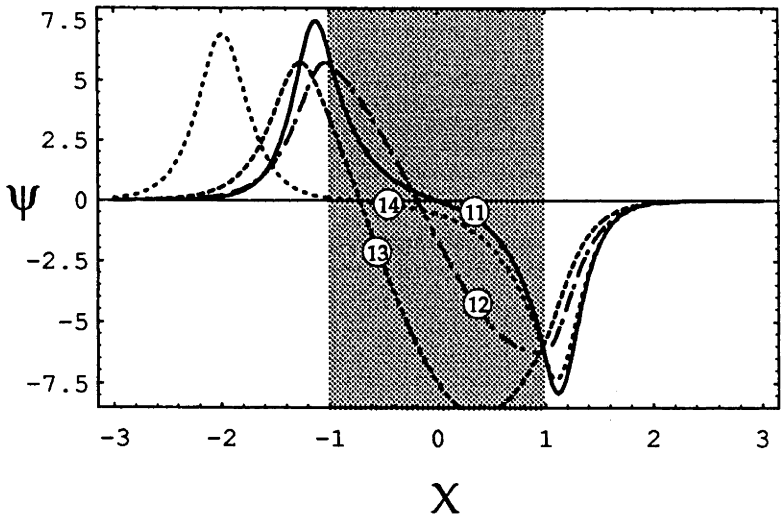

Figure 4.13: Mode shapes along the loop to the right of the gap point. Each mode profile is associated with a point on the loop labelled by the same number.

Linear substrate limit

Now, as the asymmetry increases, the first branch to shrink and disappear is the figure-of-8 loop. With $\eta = 2$ (and the same values V_r and V_l), the loop no longer exists, as shown in fig.4.14. The next to disappear are the right loop and then the right open branch. (To be exact, the right loop and right open branch do not disappear but exist at higher and higher powers as the asymmetry increases. In common sense terms, they can be regarded as gradually ceasing to exist.) The extreme case is when the left medium becomes linear, i.e. $\eta \to \infty$. In this case, the only branch remaining is the left open branch which is very similar to the left open branch in fig.4.14.

For smaller values of V_l, V_r, the dispersion curves are slightly different, but the features remains the same. An example is shown in fig.4.15. These curves are more similar to those obtained by earlier researchers [84] who overlooked the existence of the figure-of-8 loop, because of a high degree of asymmetry in their example.

The existence of the gap near $B_{co} = -\pi^2/4$ makes the dispersion curves in the case of skew-symmetry quite messy (see [95]). For clarity, they are not presented and discussed here.

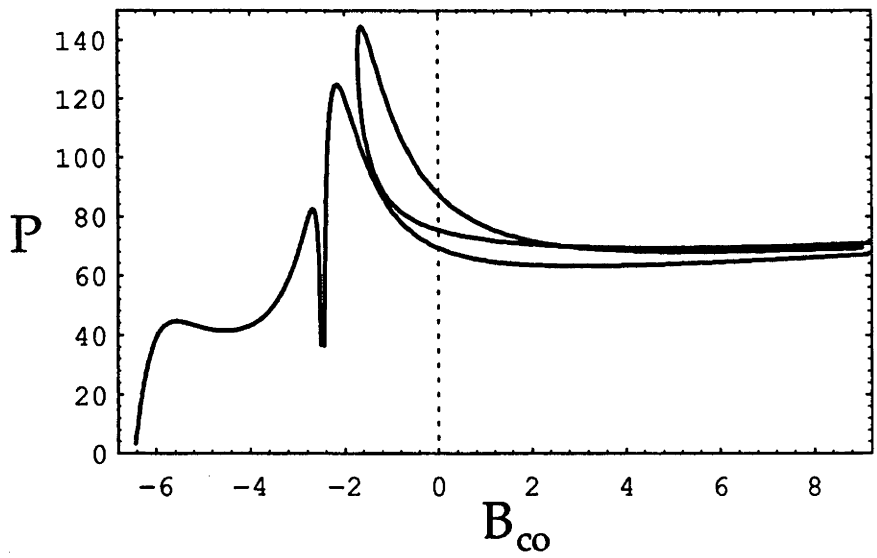

Figure 4.14: Dispersion curves for TE_1 modes as in fig.4.9 but with greater asymmetry: $\eta = 2$.

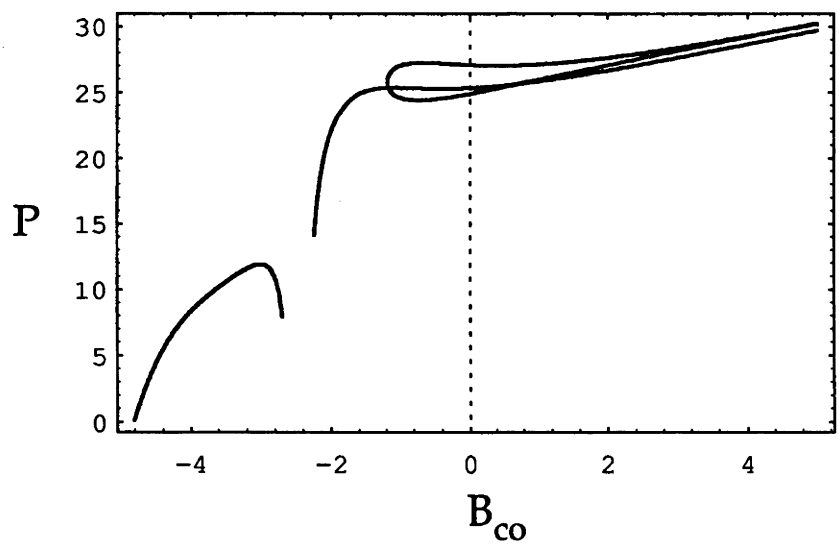

Figure 4.15: Dispersion curves for TE_1 modes in a waveguide with $V_l = 2.5$, $V_r = 3$, $\eta = 0.95$.

Some realistic figures

As in section 4.3, suppose the indices of liquid crystal MBBA are used for the cladding so that the proportionality constant in the conversion formula (2.47) is approximately equal to 2.17×10^{-6}. If the core is 3 microns thick and 3 mm wide, then the scaled power range in fig.4.9 translates to real powers ranging from zero to about 435 mW.

Of course, these figures are only representative, because the effects absorption normally present in highly nonlinear materials have been ignored. However, one certain feature is that guided power, for any nonlinear mode studied here, is inversely porportional to the Kerr coefficient, as explained by Eqn.(2.47).

Symmetric waveguides

When $V_r = V_l$ and $\eta = 1$, the waveguide becomes symmetric. The various dispersion branches typically shown fig.4.9 merge with one another to form the disperion curves shown in figure 4.16(a): an anti-symmetric mode branch, eminating from the zero-power limit; an asymmetric mode branch eminating from a bifurcation point N; and two vertical branches at $B_{co} = -\pi^2/4$ for degenerate modes. These vertical branches are the limits of the steep branches near $B_{co} = -\pi^2/4$ in fig.4.9 and has a common upper limit with $P = 4W + 2V^4/\pi^2$. One of these has a lower limit at the anti-symmetric mode branch with $P = 2W(2 + W)$; the other has a lower limit equal to $4W$. (See Ref.[95].)

For smaller values of V, for example $V = 2$ as shown in fig.4.17(a), the dispersion curves no longer have a maximum, and the degenerate branches in fig.4.16 reduce to a single point M. For even smaller values of V, such as that shown in fig.4.18(a), the anti-symmetric mode does not even have a linear limit, i.e. it exists only when the power is above some power threshold. The dispersion curve now has only one bifurcation point, N, the starting point of the asymmetric mode branch. The second bifurcation point M disappears at $V = \pi/2$ simultaneously with the loss of the linear limit .

4.4.2 Stability

For simplicity, only stability results for the anti-symmetric mode, which involves solving the relatively simple equations of the form (4.24), are presented. As shown in chapter 3, the eigenvalue ξ for TE_1 modes is either real or purely imaginary for odd perturbations but may be complex for even perturbations. In the former case

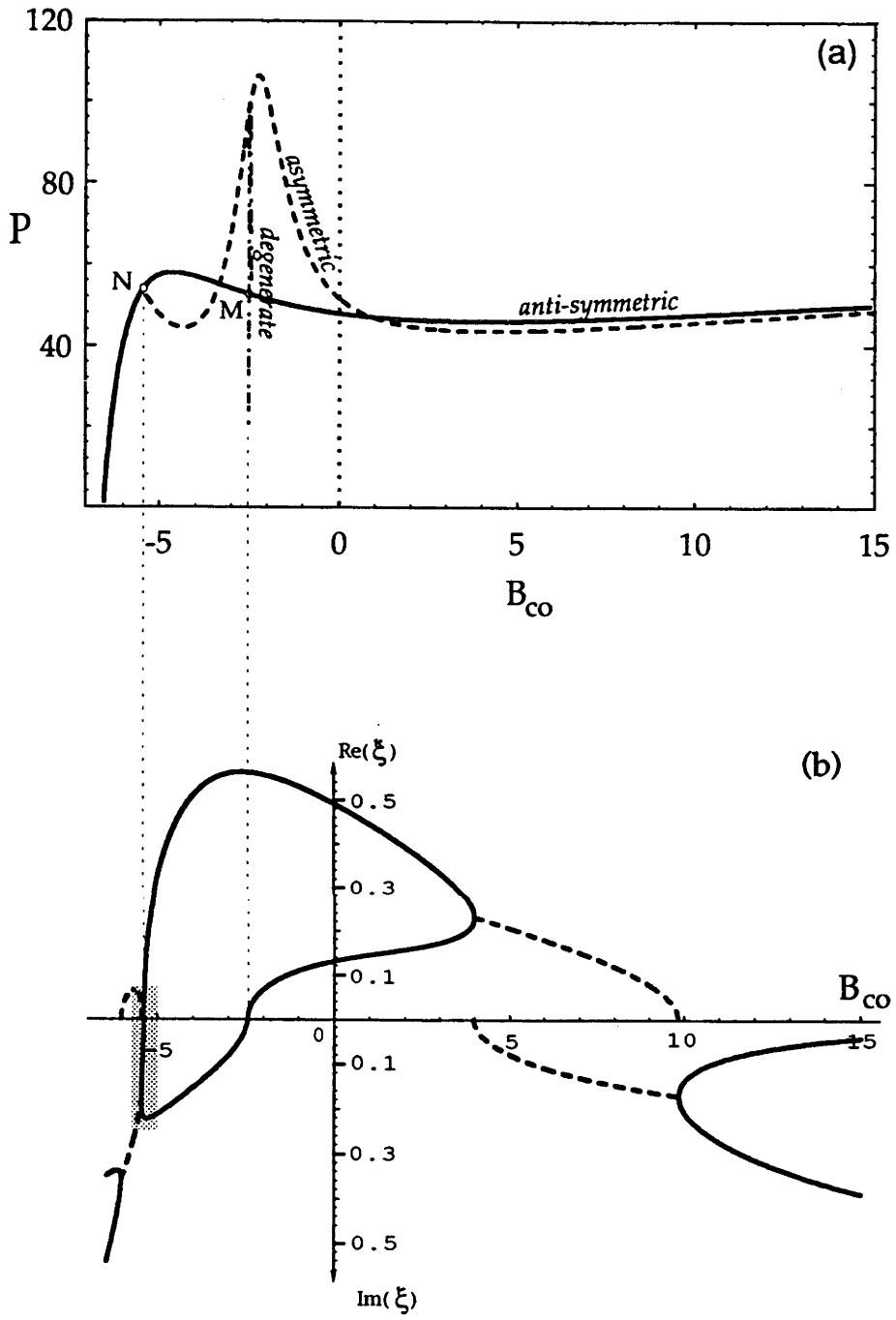

Figure 4.16: (a) Dispersion curves for symmetric waveguides with $V = V_l = V_r = 4.5$. Solid curves indicate stability. (b) Stability eigenvalues ξ for the anti-symmetric mode. Solid lines indicate ξ being either real (above the B_{co}-axis) or purely imaginary (below the B_{co}-axis), whereas dashed lines indicate ξ being complex. In the latter case, dashed lines above and below the B_{co}-axis display the real and imaginary parts respectively of ξ.

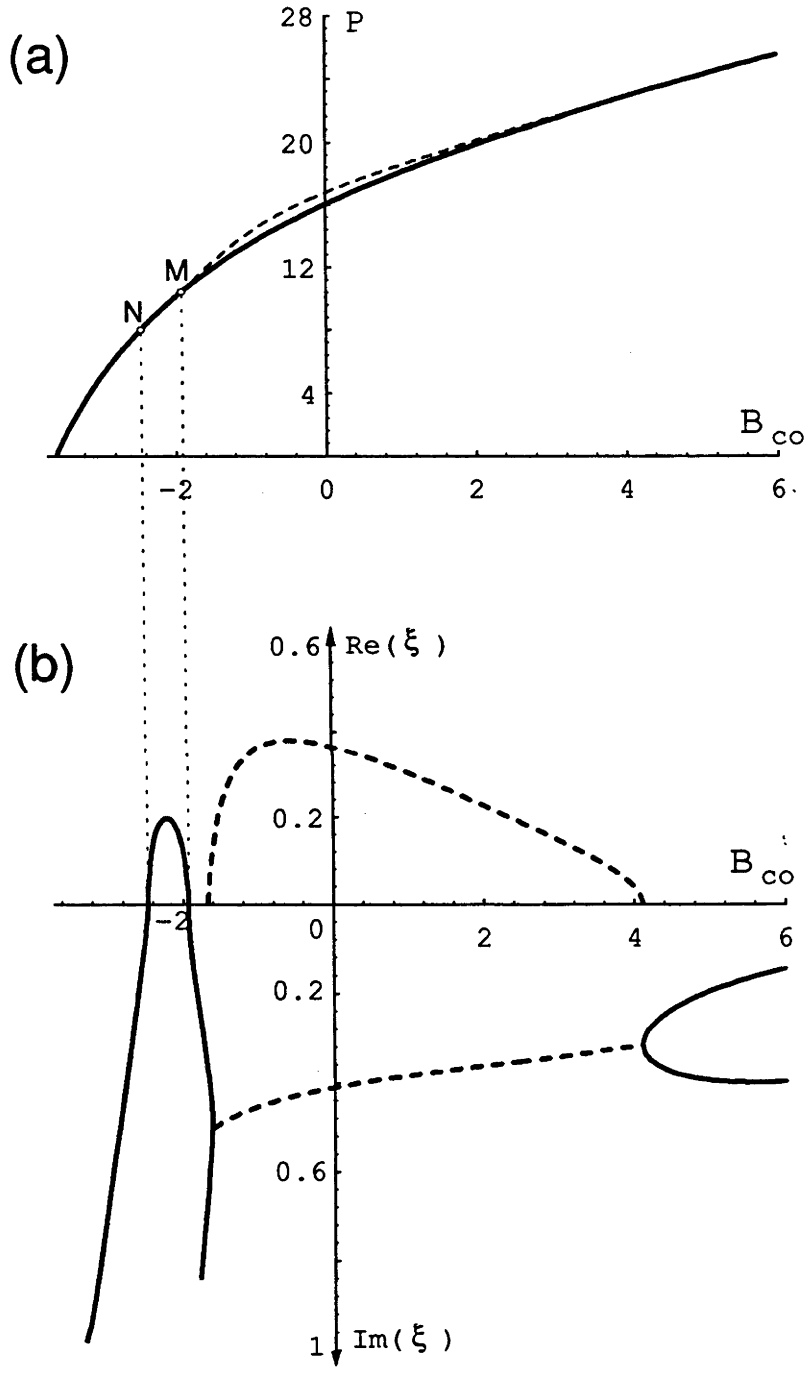

Figure 4.17: As in fig.4.16 but with $V = 2$.

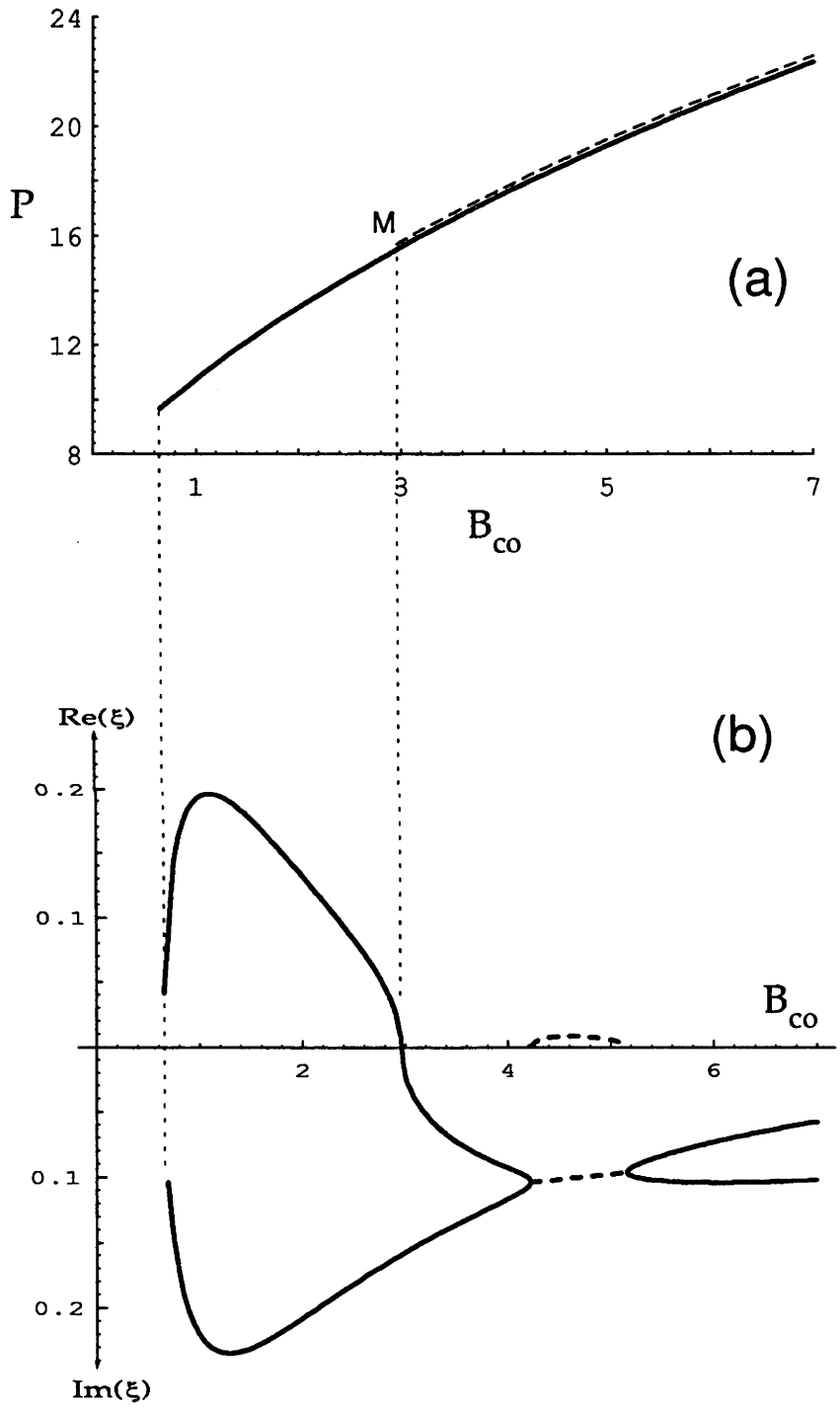

Figure 4.18: As in fig.4.16 but with $V = 0.9$.

the determinant in Eqn.(4.24) (modified for odd perturbations) can be shown to be real, while in the latter, it is complex in general. Solving this equation is therefore equivalent to solving a set of two equations separately for the real and imaginary parts of the equation.

It should also be remarked that, for both TE_0 and TE_1 stationary solutions, the perturbation functions u and v can be made real and purely imaginary, by a proper choice of phase factor, only in cases where ξ is real. This is possible because, in these cases, $\bar{f}_1$ and $\bar{f}_2$ are just complex conjugates of f_1 and f_2 respectively, and so C_1 and C_2 of Eqn.(3.17) can also be chosen to be complex conjugates. In other cases, both u and v are generally complex functions.

Since odd perturbations still have ξ being real or purely imaginary, the anti-symmetric TE_1 mode is stable where $dP/dB_{co} > 0$ and unstable otherwise. For even perturbations, fig.4.16(b) shows the results for a range of B_{co} and for $V = 4.5$. In the (stable) linear limit, corresponding to $B_{co} \approx -6.5$, at which point the waveguide can support the TE_0, TE_1 and TE_2 modes, ξ is purely imaginary, as would be expected. It can take on two different values, ξ_1 and ξ_2, which correspond to the beating frequencies with the TE_0 and TE_2 modes of the linear waveguide. At or near the linear limit, an arbitrary even perturbation can be decomposed into TE_0 and TE_2 (and radiation) components and hence the part of the perturbation which is not radiated away can only oscillate at spatial frequencies given by the difference of the TE_1 propagation constant and those of the TE_0 and TE_2 modes. As B_{co} is increased, ξ_1 and ξ_2 gradually approach each other and then become complex conjugates, causing the TE_1 mode to become unstable. As B_{co} is increased further, ξ_1 and ξ_2 both become purely imaginary again, as shown in more detail in the fig.4.19. Then, one of them becomes real at the first bifurcation point N. The other eigenvalue remains purely imaginary for a fair range of B_{co} and then becomes real at the second bifurcation point M, where the splitting of degenerate solutions occurs [61,95]. At $B_{co} \approx 4$, they merge together and become complex, and then become purely imaginary again above $B_{co} \approx 10$. Along the whole B_{co}-axis, the number of (non-degenerate) eigenvalues always remains equal to two. In general, the existence of a non-zero real part of ξ means that the stationary solution is unstable. Hence, for this particular value of $V = 4.5$, there are two finite and distinct regions of instability. One is approximately $-6.1 < B_{co} < -5.46$, well within the range from the linear limit to the first bifurcation point N. The second is from N (where $B_{co} \approx -5.4$) to some point corresponding to $B_{co} \approx 10$. In the first unstable region, the eigenvalues are everywhere complex, whereas in the second unstable region, they are complex

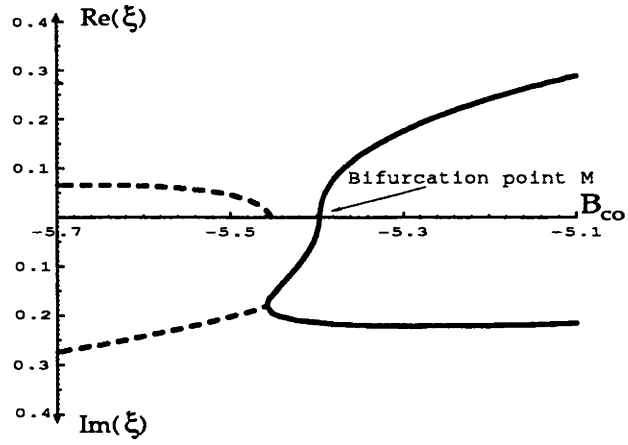

Figure 4.19: A magnification of the shaded region near $B_{co} = -5.4$ in fig.4.16(b).

only in the upper part of the region.

In fig.4.20, we show the form of the functions u and v corresponding to $B_{co} \approx -5.7$, i.e. approximately in the middle of the first instability region. Since the phases of both u and v are clearly not constant functions of X, they can not be made real or purely imaginary by a choice of the phase factor.

Figure 4.17(b) shows similar results for the case $V = 2.0$. In the linear limit, the waveguide supports only one even mode, namely the TE_0 mode. This explains why only one (purely imaginary) eigenvalue (say ξ_1) exists at low values of B_{co} in fig.4.17(b). The second eigenvalue ξ_2 appears at higher values of B_{co}. The eigenvalue ξ_1 passes through zero and becomes real at M (which is a degenerate bifurcation point), then becomes purely imaginary again at N where the asymmetric solution starts to exist. It should be noted that the positions of bifurcation points N and M are reversed compared to the $V = 4.5$ case. As B_{co} is increased further, ξ_1 approaches and merges with the second eigenvalue ξ_2 to form complex conjugates. Above $B_{co} \approx 4$, the eigenvalues become purely imaginary. Thus we have a somewhat similar pattern for the regions of instability as in the previous case, consisting of two separate regions of instability, but only one of them has complex eigenvalues for this value of V. When V is decreased from $V = 4.5$, the lower region of instability gradually disappears, whereas the upper region splits into two new regions when point M passes through point N.

Results for the last example are shown in fig.4.18(b), for $V = 0.9$. Again, the mode is unstable in two regions. One is from the power threshold to point N (where $B_{co} \approx 3.0$). The other is from $B_{co} \approx 4.2$ to $B_{co} \approx 5.2$. Unlike the previous two

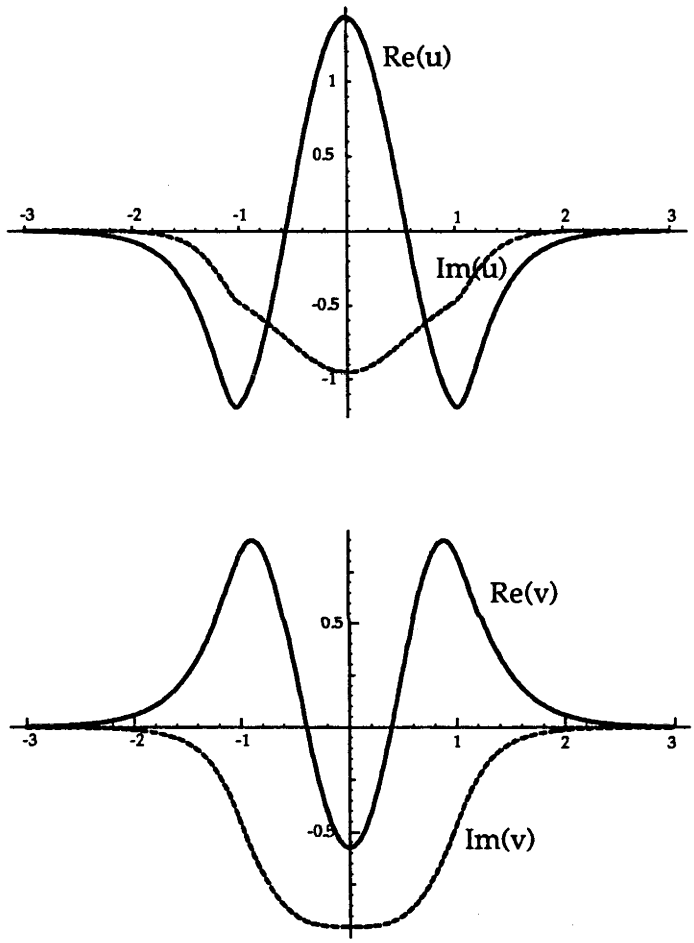

Figure 4.20: Form of the u and v functions at $B_{co} \approx -5.7$ in fig.4.16.

cases, here there is no stable region at low B_{co}. This occurs for $V < \pi/2$. It is also observed that, as V is decreased from $V = 2.0$, the first unstable region increases in size and contains only real eigenvalues, while the second region decreases and contains only complex eigenvalues.

To confirm the above results, a numerical simulation was also done for the perturbation $f(X, Z)$ which is governed by the linear perturbation equation (3.3), using the split-step Fourier transform beam propagation method. A very good agreement was obtained.

Although the stability patterns are quite complicated, and the structure of stability regions varies with different values of the waveguide parameter V, one can still observe the following general and important stability properties:

1. There are always two finite regions of instability, separated by a small region of stability.

2. The TE_1 mode is stable when B_{co} is above some minimum, in contrast to the case of TE_0 symmetric modes.

3. The region between the bifurcation points N and M is always unstable.

4. If a linear limit exists (i.e. $V > \pi/2$), the mode is stable at low powers, whereas if there is no linear limit, the mode is unstable near the lower threshold power.

From the investigation of odd perturbations, we know that the region where $dP/dB_{co} < 0$ is unstable but physical explanations for other points where the stability changes are not at all obvious. These are points where complex eigenvalues appear or disappear.

4.5 In Terms of Surface Wave Stability

The previous two chapters have shown that, above some minimum B_{co} the anti-symmetric mode is stable, whereas the symmetric mode is unstable. This might seem unexpected because in that region, both modes resemble a pair of surface modes with the same (symmetric) or opposite (anti-symmetric) parity.

Fortunately, a close examination of the relationship between these modes and surface modes reveal a plausible explanation [96]. It does not only indicate why the anti-symmetric mode is stable in the region of large B_{co} whereas the symmetric one is not, but also how complex eigenvalues arise. But first, let us briefly review the stability characteristics of a surface mode at a linear-SF interface.

4.5.1 Stability of a Surface Mode

It is well-known that a single interface between a linear medium and a Kerr self-focusing medium can support a nonlinear surface wave [97]-[99]. In the present notation, the modal field in the nonlinear medium is given by (2.21) of chapter 2, namely

$$\psi(X) = \sqrt{2}\, W_r \,\mathrm{sech}[W_r(X - X_r)], \tag{4.26}$$

while in the left (linear) medium, it is given by

$$\psi(X) = a \exp(W_l X), \tag{4.27}$$

where a is a real constant. A typical power-dispersion curve is shown in fig.4.21(a) which features a lower power threshold. It is also well-known [78][1] that the surface mode is unstable when $dP/dB_{co} < 0$ and stable when $dP/dB_{co} > 0$, as indicated by the eigenvalue ξ (solid curve in fig.4.21(b)). The ξ-curve passes through zero right at the minimum of modal power. It should also be implicitly understood that there is always a zero eigenvalue ξ at any value of B_{co}, which plays an essential role in the following discussion.

4.5.2 Lateral Field Shift in Nonlinear Medium

For convenience, the even TE_0 and odd TE_1 modes of the symmetric slab waveguide are denoted by ψ_+ and ψ_- respectively, and are assumed to have two peaks near the interfaces. The modal fields for $X > 1$, and at a fixed B_{co}, can be written as

$$\psi(X) = \sqrt{2}\, W \,\mathrm{sech}\{W[X - (X_r \mp \Delta X)]\}, \tag{4.28}$$

where ΔX is positive; the minus (plus) sign is associated with ψ_+ (ψ_-); $X_r > 1$ is the position of the peak of a surface mode at the same W if the left interface existed at an infinite distance from the coordinate origin. Thus, at some B_{co}, the peaks of ψ_+ are closer to the interfaces, while those of ψ_- are further from the interfaces, compared with the peak of the single surface mode. These differences may be regarded as arising from perturbations to the right interface by the presence of the left interface. In the limit of large B_{co}, ΔX decreases exponentially with W_r [96].

If we take the surface mode (4.26) and shift it laterally by ΔX to the left or right and solve the eigenvalue equation for ξ, then we get typical results shown in fig.4.21(b) and fig.4.22. Shifting (mathematically) the surface mode to the left causes

[1] However, Ref.[78] only calculates real eigenvalues. Here, both real and purely imaginary eigenvalues are calculated.

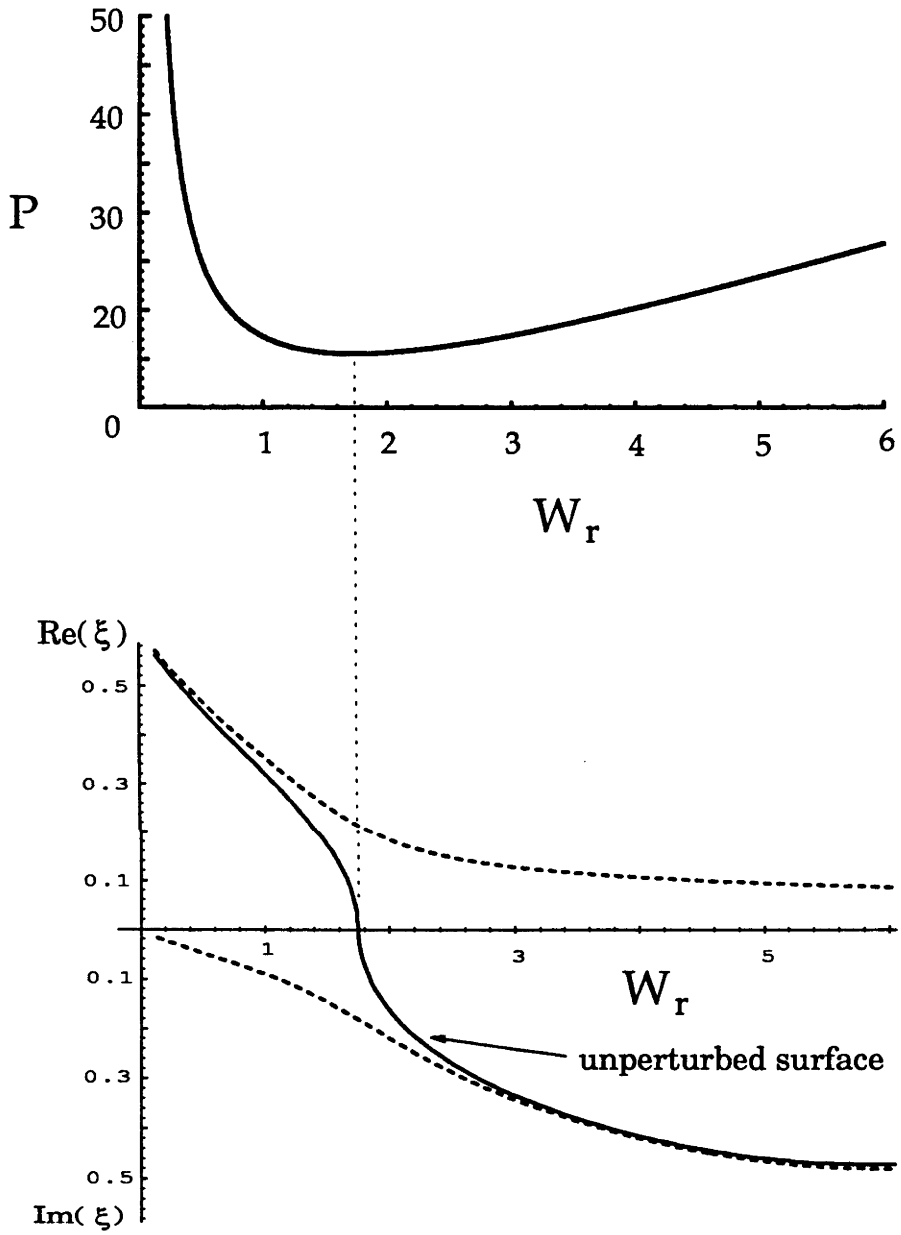

Figure 4.21: (a) A typical dispersion curve of a surface mode. (b) Stability eigenvalues. Solid curve: of an unperturbed surface mode. Dashed curve: mode displaced slightly toward the linear medium.

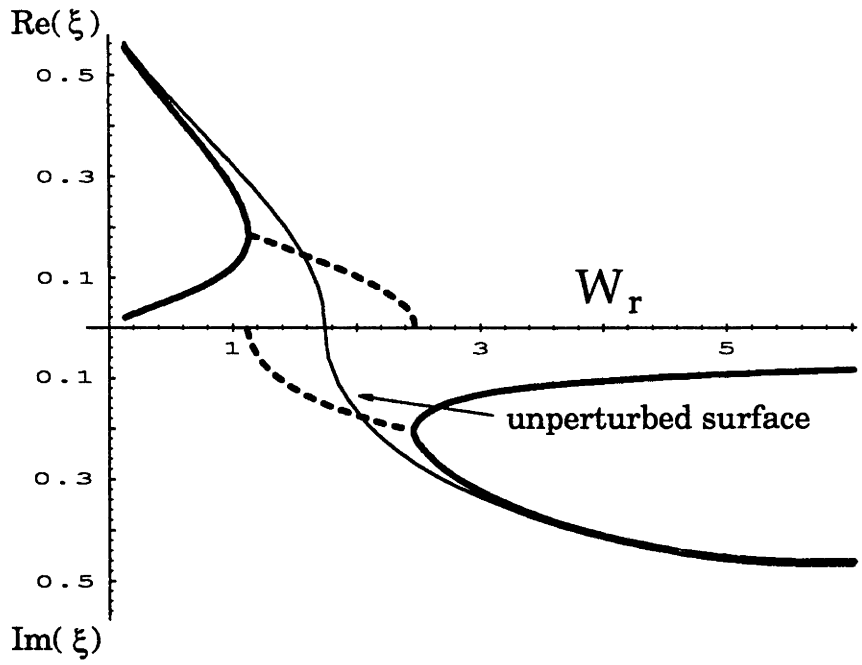

Figure 4.22: Stability eigenvalues. Solid curve: of an unperturbed surface mode. Dashed curve: mode displaced slightly away from the linear medium.

the solid line and the zero-ξ curve in fig.4.21(b) to split into two (dashed) curves which spread over the whole B_{co} of the mode: one for purely imaginary and one for real eigenvalues. On the other hand, shifting the surface mode to the right causes the formation of two (thick solid) curves as shown in fig.4.22. More importantly, there arises a gap between them, which is filled up by complex eigenvalues (dashed curves). (Strictly speaking, ΔX should be a function of B_{co}, but for illustrative purposes, a single $\Delta X = 0.005$ has been used for the whole range in these figures.) These results are reminiscent of those seen in the previous sections of this chapter.

4.5.3 Particle Analogy

The problem can also be looked at from a different viewpoint. In the high B_{co} range, the even and odd states can be considered as combinations of two surface modes which are combined in-phase or out-of-phase. Due to a field interaction term [100], the total energy in the states ψ_+ and ψ_-, at some fixed B_{co}, is not exactly twice that in the component asymmetric mode (which can be regarded as a nonlinear surface wave when B_{co} is sufficiently high). Let P_+, P_-, P_0 be the power of ψ_+, ψ_-, and the asymmetric mode ψ_a respectively. Then the dispersion diagram (fig.4.23) clearly

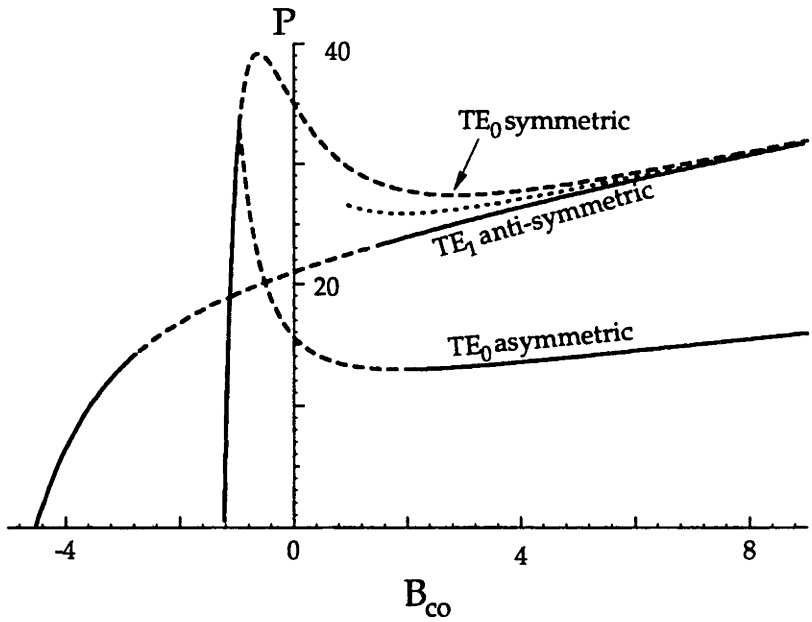

Figure 4.23: Power dispersion curves for a slab waveguide with $V = 2.5$. Dashed (solid) lines indicate stability (instability). The dotted curve indicates twice the power level of the asymmtric mode ψ_a.

shows that $P_+ > P_-$, and P_0 is between P_+ and P_-, at a fixed B_{co}. It is easy to show [96] that, in the region of high B_{co} values, the energy difference

$$\Delta P = P_+ - 2P_0 \sim 2P_0 - P_-$$

decreases exponentially with $\sqrt{B_{co}}$.

It is a general principle of physics that when two particles coalesce to form a new bound state, then the new state will be stable if the combined energy is less than that of the two components, and unstable if the combined energy is greater than the sum of the two components [101]. In our case the single nonlinear surface wave is stable. For the ψ_+ state, the energy integral is greater than the sum of the component surface waves, thus indicating probable instability, while the ψ_- state has a lower energy integral than the sum of the individual surface waves, thus implying stability. So, if we consider the TE_0 and TE_1 solutions as bound states of two surface modes, which in turn can be considered as particles [60], our example then verifies the general principle.

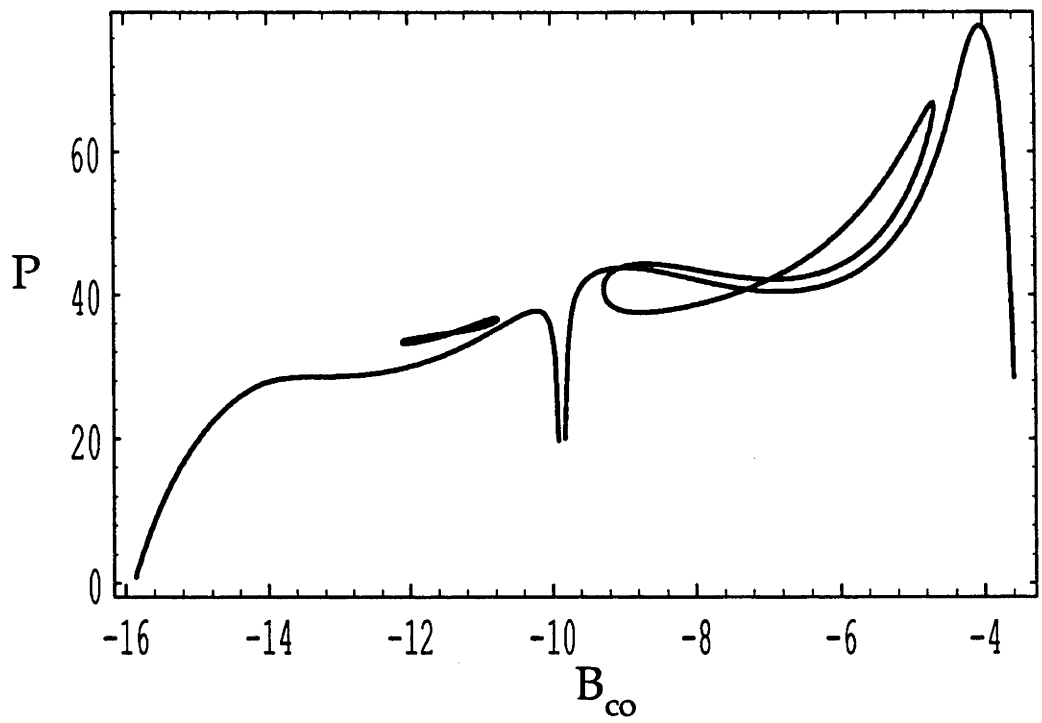

Figure 4.24: Power dispersion curves for TE_2 modes in an asymmetric waveguide with $V_l = 5.95$, $V_r = 6.05$, $\eta = 0.95$.

4.6 Second-order (TE_2) modes

Now a similar investigation of TE_2 modes is done. Previously, these modes were studied in part by Seaton *et al.* [56]. Recently, exhaustive modal calculations were reported in Ref.[95]. Their stability in the case when the growth rate ξ of the linear stability analysis is restricted to either real or purely imaginary was first in Ref.[75]. However, as has been pointed out in chapter 3, ξ may be complex for all types of perturbation, and this will be verified in this section.

4.6.1 Modal Characteristics

Figure 4.24 shows the dispersion curves of TE_2 modes in a slightly asymmetric waveguide with $V_l = 5.95$, $V_r = 6.05$ and $\eta = 0.95$, again by using power expression (4.22). For these parameters, the whole dispersion diagram consists of two figure-of-8 loops and two open branches on both sides of a gap point at $B_{co} = -\pi^2$. As in the TE_1 case, the gap width increases with increasing asymmetry. It was noticed that the disappearance of the loops is very sensitive to the asymmetry. In particular, the left

loop in fig.4.24 almost disappears even with these slightly asymmetric parameters, and does not exist at $V_l = 5.9$, $V_r = 6.1$, $\eta = 0.95$. The other loop is the next curve to disappear when the asymmetry is slightly larger. In the linear substrate limit, only the open branch with a linear limit exists.

It is interesting to note that the TE_2 modes do not exist at positive values of B_{co}. This may be explained using a contradiction argument as follows: TE_2 modes necessarily have two nodes which must be inside the linear core, because the solution in the nonlinear bounding media are in terms of a sech function. If $B_{co} > 0$, the solution in the core must be given in terms of cosh and sinh functions, or by (4.6) to be precise. This is a contradiction as a linear combination of cosh and sinh functions does not have two nodes.

As the waveguide approaches symmetry, the dispersion curves merge with one another to become four different branches (see fig.4.25): one branch for symmetric modes, one for asymmetric modes, and two vertical branches for degenerate modes at $B_{co} = -\pi^2$, similar to the situation for TE_1 modes considered in the preceeding section. The vertical branches have a common upper limit at the asymmetric mode branch with $P = 4W + V^4/2\pi^2$ (see [95]) and lower limits given by the same expressions as in the TE_1 case. A major difference is that the asymmetric mode branch now has both starting and ending points on the symmetric mode branch. The number of bifurcation points is now three, namely N, M, and N' as indicated in fig.4.25. For $V < 3\pi/2$, TE_2 modes may exist without a linear limit. These properties may be used for producing standardized optical pulses [56].

4.6.2 Stability

The procedure of calculating stability properties here is exactly the same as for TE_1 modes. Figures (4.26) and (4.27) show the results for symmetric TE_2 modes in a symmetric waveguide with $V = V_l = V_r = 6.0$. The treatment is restricted to symmetric modes only.

The important point to note is that complex eigenvalues occur, as shown in fig.4.27, for even perturbations which preserve the symmetry of the mode. This is in agreement with the prediction in chapter 3. For this particular value of V, there exist two purely imaginary eigenvalues near the linear limit, which then merge together and become complex conjugates for a substantial part of the range of the mode existence. The behaviour of ξ can be quite wild. For example, at $B_{co} \approx -4.4$, $\mathrm{Re}(\xi)$ vanishes, whereas $\mathrm{Im}(\xi)$ seems to shoot off to infinity, although computational difficulty prevents a clear appearance in the diagram. At $B_{co} \approx 4$, at which a

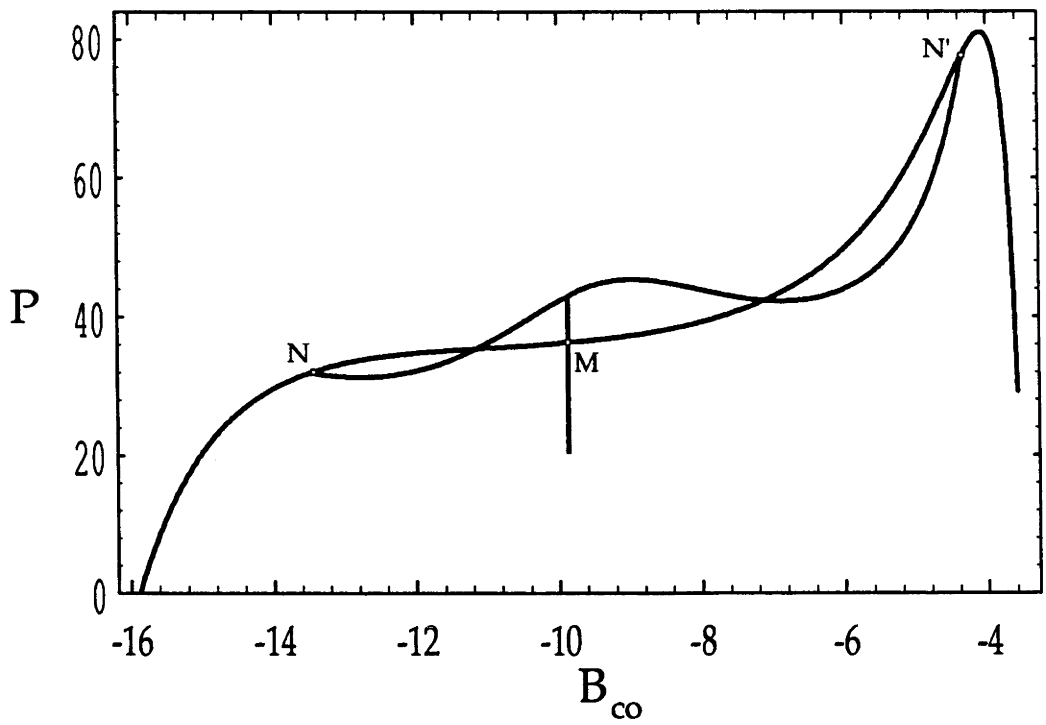

Figure 4.25: Power dispersion curves for TE_2 modes in a symmetric waveguide with $V_l = V_r = 6$.

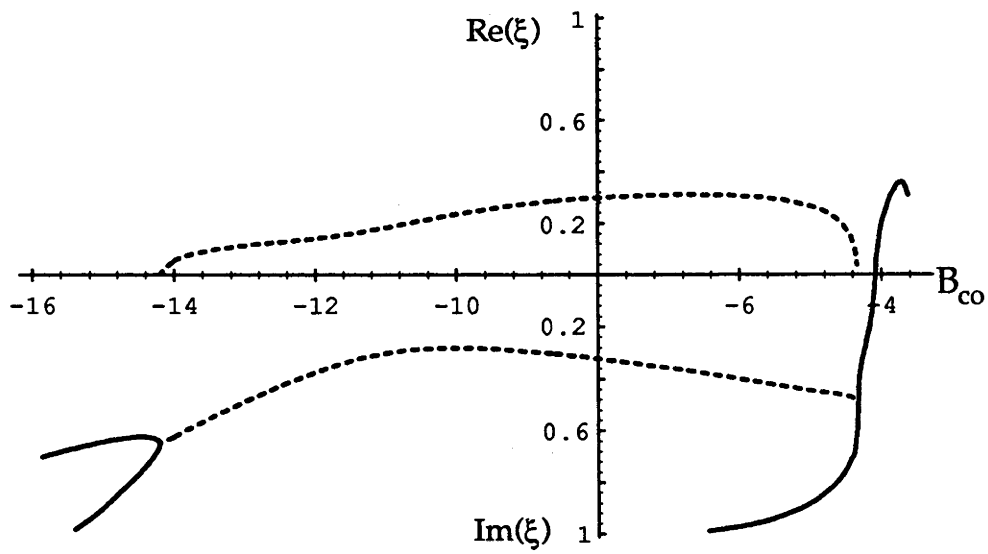

Figure 4.26: Stability eigenvalues ξ of even perturbations on symmetric TE_2 modes in a symmetric waveguide with $V = 6$. The line notation is the same as in fig.4.16(b).

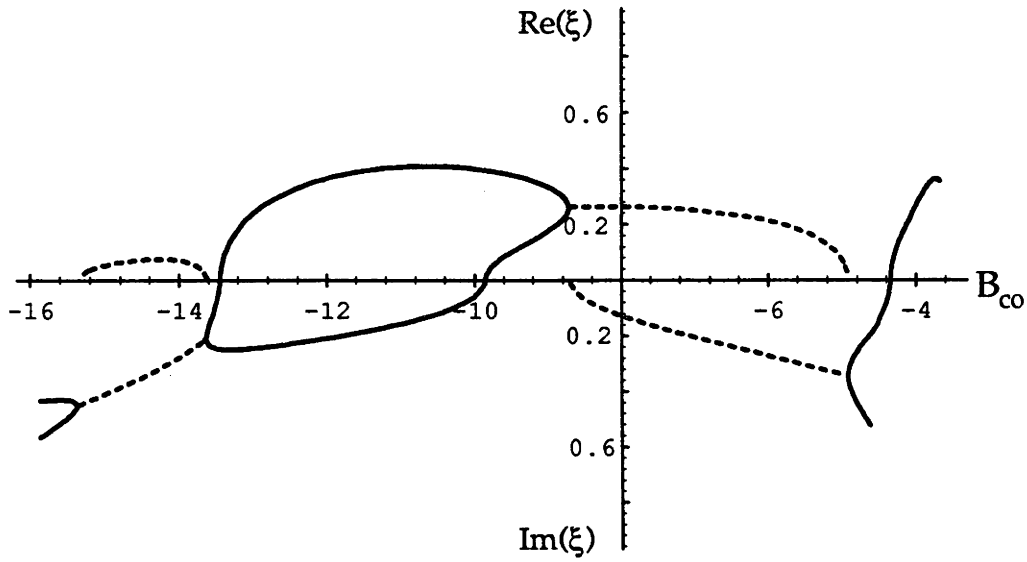

Figure 4.27: As in fig.4.26, but for odd perturbations.

maximum occurs, another eigenvalue passes from purely imaginary to real. The result is the nonlinear TE_2 symmetric mode is stable to even perturbations in an initial interval of B_{co} near the linear limit and in another small interval just before the maximum power, as indicated by solid parts in fig.4.25.

To odd perturbations, it is interesting to note that the passings of ξ from purely imaginary to real occur only at the three bifurcation points, as in the case of TE_1 modes to even perturbations. Tracing from the linear limit, the mode is stable only for a small range of B_{co}, and then unstable due to the existence of complex eigenvalues. It then becomes stable again in a short range of B_{co} just before the first bifurcation point. Another stable range exist just before the the last bifurcation point.

Putting even and odd perturbations together, the result is: the TE_2 symmetric mode is stable only for a short range of B_{co} near the linear limit. If V is such that a linear limit does not exist, it is conjectured with an analogy with the TE_1 case that the TE_2 symmetric mode is always unstable.

4.7 Experimental Relevance

In the past few years several experiments, which confirm the existence of nonlinear slab guided waves, have been performed. Most related to the present theoretical

studies are the experiments by Vach *et al.* [102] and Bennion *et al.* [103]. Unfortunately, the highly nonlinear materials (liquid crystal MBBA and liquid CS_2) used in these experiments have large losses, and therefore a critical comparison can not be made with the theoretical calculations here. However, within a generous tolerance, the theoretical results roughly agree with those of experiments. (A discussion on the effect loss is included in chapter 7.)

The experiment in [102] is a verification of both the TE_0 and TE_1 nonlinear modes. It used a linear substrate ($n_s = 1.52$), a linear thin film ($n_{co} = 1.61$, $\rho = 0.5\mu$m) and a nonlinear cladding (liquid crystal MBBA with $n_r = 1.55$, $n_{2r} = 10^{-9}$ m^2/W at $\lambda = 0.515\mu$m). These parameters correspond to $V_r = 2.66$, $V_l = 3.24$ which are close to the parameters of fig.4.15 for the TE_1 mode, which indicates dimensionless power levels approximately in the range $0 < P < 12$.

Using these values, the actual power per ρ (in the y-direction) given by (2.47) becomes

$$P_a = 2.2 \times 10^{-6} P.$$

The beam width used in [102] is 1 mm (in the y-dimension). Hence the theoretical actual power calculated here is not more than about 50 mW. This is roughly in agreement with Ref.[102], which reports input powers of a few hundred miliwatts and output powers of less than 2.5 mW. A more precise comparison is not possible due to the presence of absorption effects of the MBBA liquid crystal. A pronounced hysteresis effect was observed for the TE_1 mode due to the localization of its peak in the nonlinear medium. For the TE_0 mode, these absorption and hysteresis effects became evident only at the highest power levels used by the researchers (see [102]).

The experiment in [103] is a confirmation of the existence of the nonlinear TE_0 mode. The experimental configuration is somewhat similar to that used by Vach and co-workers. Instead of liquid crystal MBBA, it used the liquid CS_2 (carbon disulphide) as the nonlinear cladding, which has a high Kerr coefficient $n_{2r} = 3\times10^{-9}$ m^2/W. A pronounced hysteresis behaviour was also observed which could only be explained by the existence of the nonlinear TE_0 mode and the strong nonlinearity of the liquid CS_2.

APPENDIX

Equating ψ and ψ' at $X = 1$ (the right interface) gives

$$a_1\, c + a_2\, s = \pm W_r \operatorname{sech} G_r, \tag{4.29}$$

$$b\,(a_1\, s + a_2\, c) = \mp W_r^2 \operatorname{sech} G_r \tanh G_r, \tag{4.30}$$

where $G_r = W_r(1 - X_r)$, $c = \cosh(\sqrt{B_{co}})$, $s = \sinh(\sqrt{B_{co}})$, and $b = \sqrt{B_{co}}$.

At the left interface, we have

$$a_1\, c - a_2\, s = W_l \sqrt{\eta} \operatorname{sech} G_l, \tag{4.31}$$

$$b\,(-a_1\, s + a_2\, c) = -W_l^2 \sqrt{\eta} \operatorname{sech} G_l \tanh G_l, \tag{4.32}$$

where $G_l = W_l(-1 - X_l)$.

Equations (4.29) and (4.31) give

$$2a_1 c = \pm W_r \operatorname{sech} G_r + W_l \sqrt{\eta} \operatorname{sech} G_l, \tag{4.33}$$

$$2a_2 s = \pm W_r \operatorname{sech} G_r - W_l \sqrt{\eta} \operatorname{sech} G_l, \tag{4.34}$$

while equations (4.30) and (4.32) give

$$2b\, a_2 c = \mp W_r^2 \operatorname{sech} G_r \tanh G_r - W_l^2 \sqrt{\eta} \operatorname{sech} G_l \tanh G_l, \tag{4.35}$$

$$2b\, a_1 s = \mp W_r^2 \operatorname{sech} G_r \tanh G_r + W_l^2 \sqrt{\eta} \operatorname{sech} G_l \tanh G_l. \tag{4.36}$$

The substitution of (4.34) and (4.33) into (4.35) and (4.36) leads to

$$b\frac{c}{s}\left[\pm W_r \operatorname{sech} G_r - W_l \sqrt{\eta} \operatorname{sech} G_l\right] = \mp W_r^2 \operatorname{sech} G_r \tanh G_r - W_l^2 \sqrt{\eta} \operatorname{sech} G_l \tanh G_l, \tag{4.37}$$

$$b\frac{s}{c}\left[\pm W_r \operatorname{sech} G_r + W_l \sqrt{\eta} \operatorname{sech} G_l\right] = \mp W_r^2 \operatorname{sech} G_r \tanh G_r + W_l^2 \sqrt{\eta} \operatorname{sech} G_l \tanh G_l. \tag{4.38}$$

Adding and subtracting (4.37) and (4.38), and using the identity $c^2 - s^2 = 1$, gives

$$\pm b\, W_r \left(\frac{c^2 + s^2}{cs}\right) \operatorname{sech} G_r - b\frac{W_l \sqrt{\eta}}{cs} \operatorname{sech} G_l = \mp 2W_r^2 \operatorname{sech} G_r \tanh G_r, \tag{4.39}$$

$$\pm b\frac{W_r}{cs} \operatorname{sech} G_r - b\, W_l \sqrt{\eta} \left(\frac{s^2 + c^2}{cs}\right) \operatorname{sech} G_l = -2W_l^2 \sqrt{\eta} \operatorname{sech} G_l \tanh G_l \tag{4.40}$$

Letting $\Gamma = \operatorname{sech} G_l$, $t = \tanh G_r$, and noting that t and G_l may be positive or negative, (4.39) and (4.40) lead to the eigenvalue equation (4.7).

Chapter 5

Waveguides involving SDF Nonlinearities

Two types of symmetric waveguides, which possess interesting stability properties, are studied in this chapter. The first type involves a linear core and Kerr self-defocusing bounding media; while in the second type, Kerr self-defocusing nonlinearity is in the core and the bounding media are Kerr self-focusing. The restriction to symmetric waveguides is only due to the fact that no drastically new features, both in modal characteristics and stability properties, appear when asymmetry is included.

For the first type, Hart and Wright in Ref.[81] did similar work in which the TE_0 mode of a linear thin film, bounded by a linear substrate and a Kerr self-defocusing cladding, was shown to be stable by appealing to the Lyapunov theorem. The work in this chapter solves the stability problem of all TE modes of a symmetric waveguide by using linear stability analysis. In addition, it also discusses some interesting modal characteristics and some potential applications.

For the second type, this work, as far as we know, is probably the first to appear in the literature. The effect of a self-defocusing core is seen through a decrease of β with power near the linear limit. By using Kolokolov's criterions, it is found that the stability pattern of the TE_0 modes is similar to that in the linear-core case.

In the last decade, several authors have also studied planar waveguides involving self-defocussing nonlinearities. For example, Akhmediev [104] and Seaton et al.[105] studied a simple structure where a linear film is bounded by a self-defocussing cladding and a linear substrate. Akhmediev [106] also considered waveguides of the L-SDF-air type. The main conclusion from the these investigations is that the effect of the SDF nonlinearity is to drive the effective index β/k backwards to a linear

cut-off value, and that the field at cut-off is a plane wave in one of the semi-infinite bounding medium. Boardman and co-workers [107] had some discussion about the competition of confining the wave field between the two bounding media when they have opposite noninearities.

The results presented here in this chapter not only agree with these works but also extends to include the important issue of stability, in a concise and convenient formulation.

The waveguide geometry is similar to that of fig.4.1 of chapter 4, only simpler, in that all the parameters, including linear index profile and nonlinear coefficients, are symmetric, and the bounding media may be Kerr self-defocusing or self-focusing. As has been stated in the introductory chapter, we consider idealized cases where instantaneous response is assumed, nonlocal and thermal effects are ignored, in a nonlinear medium.

This chapter consists of two sections: section 5.1 studies waveguides of the first type mentioned above; while section 5.2 is devoted to the second type.

5.1 Waveguides with SDF bounding media

5.1.1 Modal Characteristics

The scalar TE wave equation takes the simple form

$$\begin{aligned} \psi'' - W^2\psi - \psi^3 &= 0, \quad |X| > 1 \\ \psi'' - B_{co}\psi &= 0, \quad |X| < 1 \end{aligned} \tag{5.1}$$

where $W^2 = \rho^2(\beta^2 - k^2 n_l^2) = \rho^2(\beta^2 - k^2 n_r^2)$, and $B_{co} = \rho^2(\beta^2 - k^2 n_{co}^2)$.

Modal field

The eigenmode solution for the bounding media is given by (2.23) of chapter 2 in terms of the cosech function, namely

$$\psi(X) = \pm\sqrt{2}\, W \,\mathrm{cosech}[W(X \pm X_0)].$$

Since the cosech function has a singularity at $X = \mp X_0$, this solution is physically appropriate only if $|X_0| < 1$. More broadly speaking, it is only possible in a structure with one or more interfaces.

A general solution in the linear core is given by (2.15) of chapter 2. However, in the case of even symmetry, the solution is simply

$$\psi(X) = a_2 \cosh(\sqrt{B_{co}}\, X), \tag{5.2}$$

while in the case of odd symmetry, it becomes

$$\psi(X) = a_1 \sinh(\sqrt{B_{co}}\, X), \tag{5.3}$$

where B_{co} may be negative or positive. Dispersion relations are obtained by applying the continuity condition of ψ and ψ' at only one of the interfaces, e.g. at $X = 1$, because we confine ourselves to even or odd symmetry. For even symmetry, this leads to

$$\begin{aligned} a_2 \cosh(\sqrt{B_{co}}) &= \sqrt{2}\, W \operatorname{cosech}[W(1 - X_0)] \\ a_2 \sqrt{B_{co}} \sinh(\sqrt{B_{co}}) &= -\sqrt{2}\, W^2 \operatorname{cosech}[W(1 - X_0)] \operatorname{cotanh}[W(1 - X_0)]. \end{aligned}$$

Hence,

$$\sqrt{B_{co}} \tanh \sqrt{B_{co}} = -W \operatorname{cotanh}[W(1 - X_0)], \tag{5.4}$$

or

$$X_0 = 1 - \frac{1}{W} \tanh^{-1} \left[-\frac{W}{\sqrt{B_{co}} \tanh \sqrt{B_{co}}} \right], \tag{5.5}$$

Once X_0 is known, it is straightforward to solve for a_2 via

$$a_2 = \sqrt{2}\, W \operatorname{cosech}[W(1 - X_0)] / \cosh \sqrt{B_{co}}.$$

In a similar fashion, one can show that the analogous expressions for the case of odd symmetry are

$$X_0 = 1 + \frac{1}{W} \tanh^{-1} \left[-\frac{W \tanh \sqrt{B_{co}}}{\sqrt{B_{co}}} \right], \tag{5.6}$$

and

$$a_1 = \sqrt{2}\, W \operatorname{cosech}[W(1 - X_0)] / \sinh \sqrt{B_{co}}.$$

Some typical mode shapes are shown in fig.5.1 and fig.5.2. As can be seen, the mode shapes always have peaks within the film. Heuristically, this is because the self-focusing effect of the nonlinear media only makes the contrast between the film and the bounding medium even sharper, and hence guidance by the core is increased. Furthermore, the induced index profile of the whole waveguide has a W-shape, as shown in fig.5.3. This is a potentially useful and interesting feature as it explains the occurence of the abrupt cut-off in the $V = 2$ dispersion curve of fig.5.4. Since the peak must reside within the film, the solution within the core must be a trigonometric function. This leads to an existence condition:

$$-V^2 < B_{co} < 0. \tag{5.7}$$

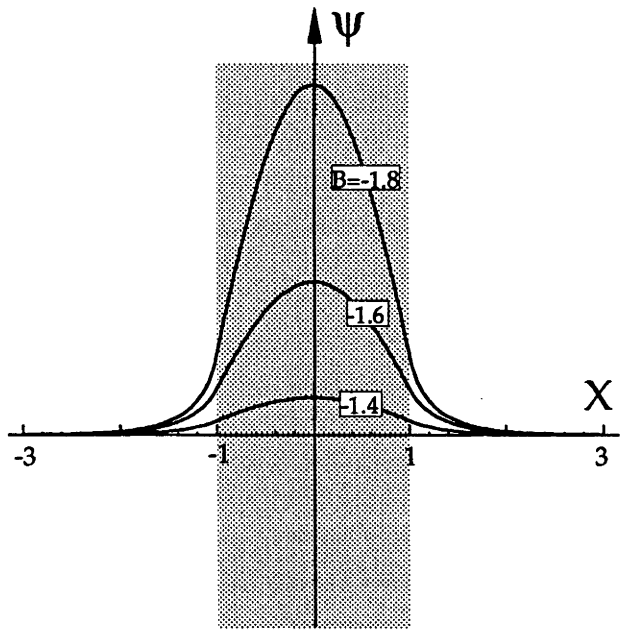

Figure 5.1: Some shapes of the TE_0 symmetric mode.

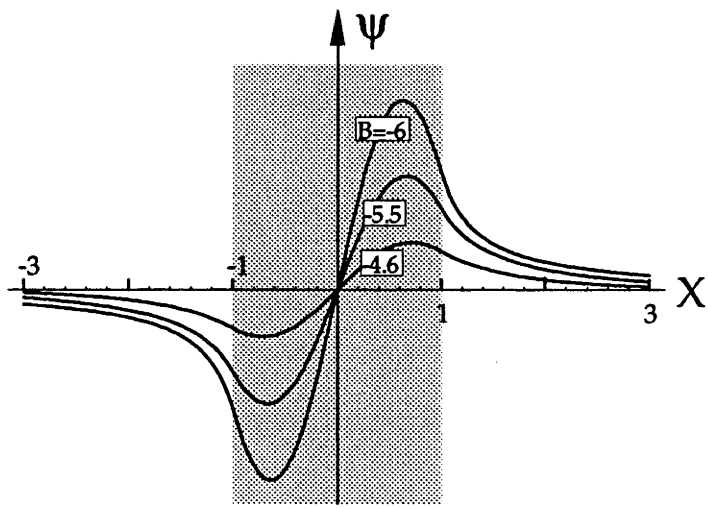

Figure 5.2: Some shapes of the TE_1 anti-symmetric mode.

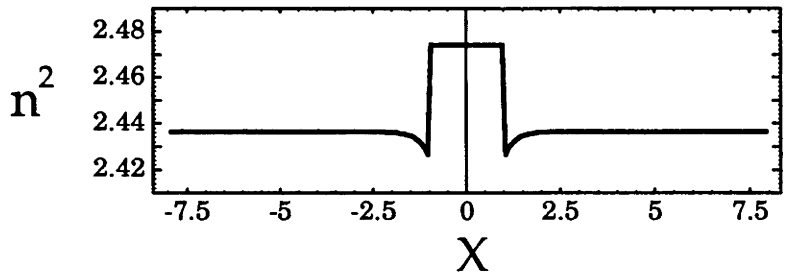

Figure 5.3: A typical induced index profile of a waveguide with a SDF bounding media.

Modal power

Having obtained X_0 using (5.5) or (5.6), the modal power P, defined by (4.3) of chapter 4, can be shown to be

$$P = a_2^2 \left[-\frac{\sinh(2\sqrt{B_{co}})}{2\sqrt{B_{co}}} + 1 \right] + 4W \left\{ \text{cotanh}[W(1 - X_0)] - 1 \right\}, \tag{5.8}$$

for even modes, and

$$P = a_1^2 \left[\frac{\sinh(2\sqrt{B_{co}})}{2\sqrt{B_{co}}} + 1 \right] + 4W \left\{ \text{cotanh}[W(1 - X_0)] - 1 \right\}, \tag{5.9}$$

for odd modes.

Some examples are shown in fig.5.4. All dispersion curves in this system have a negative slope, i.e. $dP/dB_{co} < 0$. An important point to note is that this feature is not restricted to our particular system but is present in all systems involving only linear or self-defocussing nonlinearities.

The power expressions (5.8) and (5.9) both contain a term involving $\text{cotanh}[W(1-X_0)]$. With reference to (5.4) this means that the modal power of even modes is infinite at $B_{co} = -k^2\pi^2/4$, $k = 1, 3, 5, \cdots$. This is because the term $\sqrt{B_{co}} \tanh \sqrt{B_{co}}$ becomes $-u \tan u$, $(u = \sqrt{|B_{co}|})$ when $B_{co} < 0$ which, in turn, has singularities at $u = k\pi/2$. For the same reason, the modal power of the odd modes becomes infinite at points corresponding to $k = 2, 4, 6, \cdots$

Combining this fact with the existence condition (5.7) leads to an interesting conclusion: to have an upper threshold, the TE_0 mode requires $V < \pi/2$ (i.e. the waveguide is single-moded in the zero-power limit) and the TE_1 mode requires $V < \pi$ (i.e. the waveguide is two-moded in the linear limit). In physical terms, these threshold phenomena can be explained heuristically by realizing that when the (linear) waveguide parameter V is small, the modal field spreads out further

into the cladding and hence sees more of the effect of the induced index dips. The higher the modal power, the deeper and wider these dips become. If the confinement of the waveguide does not increase fast enough with the decrease of B_{co}, it becomes cut off, i.e. it does not support modes at any wavelength.

5.1.2 Stability

There are two analytical methods available for determining the stability of guided waves in this waveguide. The first is a linear analysis method which involves the exact solution discussed in chapter 3. The second method uses the Lyapunov theorem whose applicability is more limited compared with the first method because it can only be applied to the TE_0 modes.

Linear Analysis

As for guided waves in self-focusing waveguides discussed in chapter 4, stability characteristics can be determined by calculating the eigenvalue ξ.

For symmetric modes, the matching of u and v given by (3.14) and (3.19) of chapter 3, and their derivatives at $X = 1$, leads to

$$\begin{vmatrix} f_1 & \bar{f}_1 & C & \bar{C} \\ f_2 & \bar{f}_2 & C & -\bar{C} \\ f_1' & \bar{f}_1' & p_u S & \bar{p}_u \bar{S} \\ f_2' & \bar{f}_2' & p_u S & -\bar{p}_u \bar{S} \end{vmatrix} = 0, \tag{5.10}$$

for symmetric perturbations. Here, f_1, $\bar{f}_1$, f_2, $\bar{f}_2$ are given by (3.22) of chapter 3, the prime denotes d/dX, $p_u = \sqrt{B_{co} - i\xi}$, $\bar{p}_u = \sqrt{B_{co} + i\xi}$, $C = \cosh p_u$, $\bar{C} = \cosh \bar{p}_u$, $S = \sinh p_u$, and $\bar{S} = \sinh \bar{p}_u$.

The analogous equation for odd perturbations can be obtained simply by swapping C and S in (5.10). Solving these equations gives the allowed discrete eigenvalues ξ, if they exist. The results are shown in fig.5.5, which displays existing eigenvalues ξ for TE_0 (a) and TE_1 (b) modes over certain ranges of B_{co}. A general feature is that, for both types of waves, ξ is purely imaginary, meaning the guided waves are all stable.

For the TE_0 mode, there exists only one discrete eigenvalue corresponding to an odd eigenfunction f (i.e. u and v are odd), as shown by the dashed curve in fig.5.5(a). Only one discrete eigenvalue is possible here because, for this curve, $V = 2 < \pi$ and the waveguide is two-moded. The unique ξ obtained corresponds to beating with

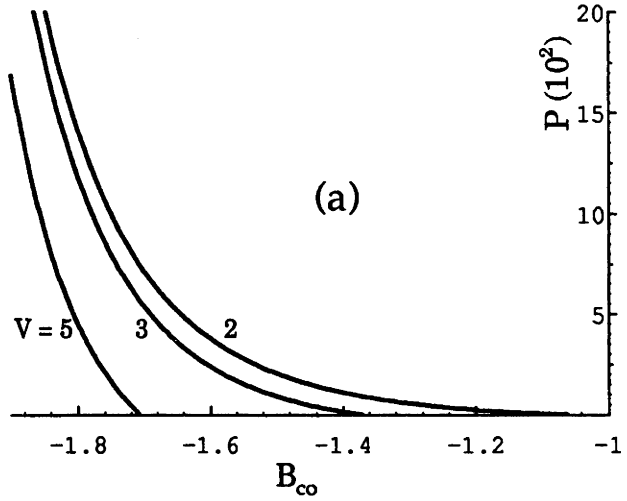

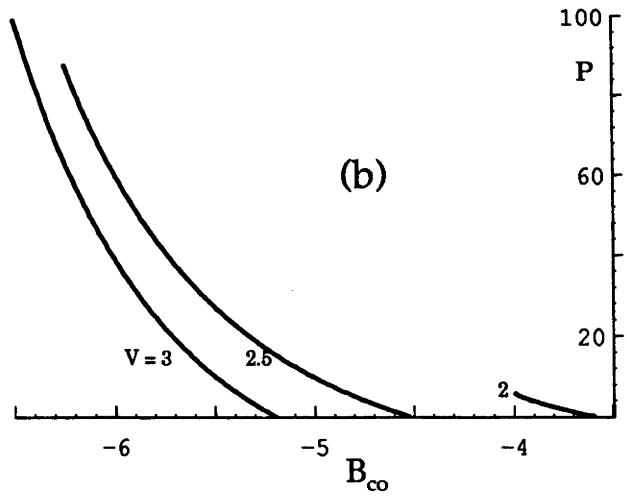

Figure 5.4: (a) Power-dispersion curves for TE_0 modes for several values of V. The curves have a singularity at $B_{co} = -\pi^2/4$. (b) Dispersion curves for TE_1 modes.

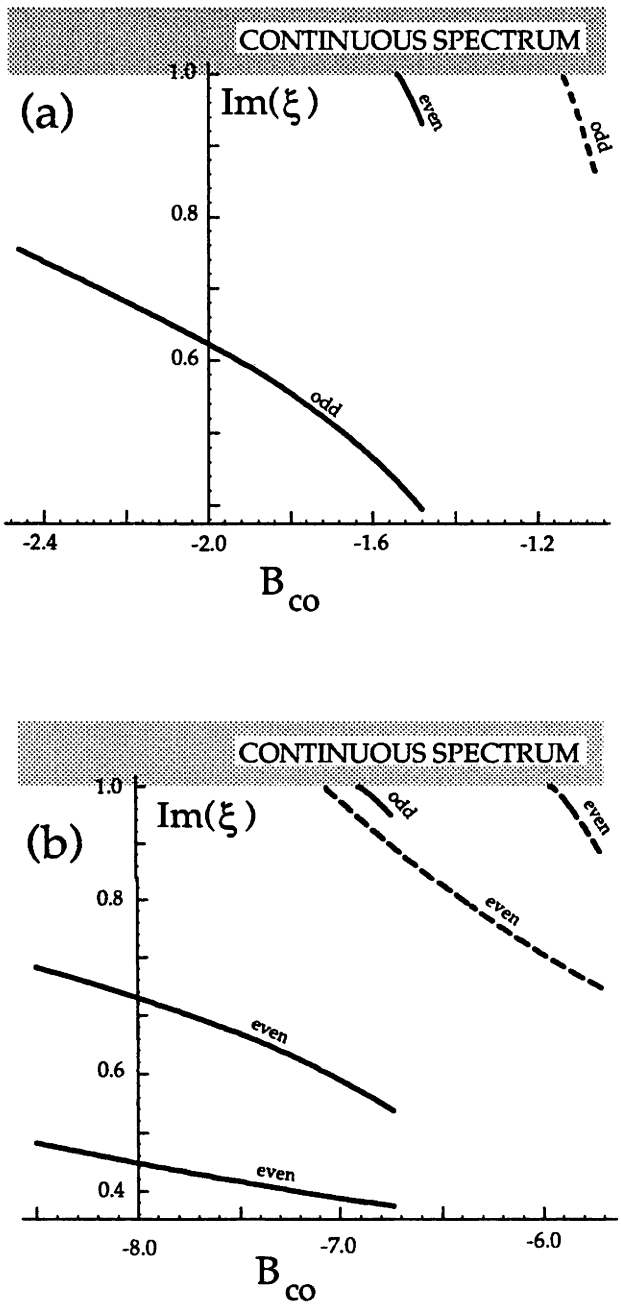

Figure 5.5: Purely imaginary eigenvalues ξ of linear analysis. (a) TE_0 modes. The dashed curve is for odd perturbations, calculated with $V = 2$. Solid curves are for even and odd perturbations as indicated, with $V = 3.5$. (b) A similar diagram for the TE_1 mode. Dashed curves have $V = 3.5$; solid curves have $V = 5$.

the second mode. As can be observed, the eigenvalue remains discrete for a short range of B_{co} (or guided power P) and then merges with the continuous spectrum.

The solid lines in fig.5.5(a) are obtained with $V = 3.5 > \pi$. This value of V allows for two eigenfunctions, one odd and one even. The eigenvalue of the even eigenfunction exists for a short range of B_{co} and also merges into the continuous spectrum. Higher values of V would allow for higher-order eigenvalues, but the general behaviour is the same: higher-order eigenvalues exist for some range and then merge with the continuous spectrum, while lower-order eigenvalues increase slowly (with power P) but always remain discrete.

For the TE_1 mode, the behaviour of eigenvalues is similar. The dashed lines in fig.5.5(b) are calculated with $V = 3.5$, which allows for two discrete eigenvalues with even eigenfunctions. Both of them merge with the continuous spectrum at certain powers. It should be remembered that this is in contrast to the behaviour of its self-focusing counterpart in which two discrete, purely imaginary eigenvalues merge with each other at certain points and then become real or purely imaginary again, leading to a complex picture of stability regimes [74]. The solid curves in fig.5.5(b) are for $V = 5$, which allows for an odd eigenfunction in addition to the even ones, but no new features appear.

So, these results have established that at least the first two guided modes (i.e. TE_0 and TE_1) of the nonlinear waveguide with a thin linear film bounded by self-defocusing medium are stable because the eigenvalues involved in the linear analysis are all purely imaginary. Although the same approach can be applied to higher-order guided waves with equal ease, it is not carried out here because of their apparently poor prospect of potential applications. However, it is conjectured that guided modes of all orders in this type of waveguide, if they exist, are stable.

Lyapunov Method

As has been mentioned at the begining of this chapter, that the stability of the TE_0 mode is studied in Ref.[81], using the Lyapunov theorem. Although the structure investigated in Ref.[81] is different from the one studied here, the method of Lyapunov stability is equally applicable. The reason for this applicability is explained simply as follows.

In chapter 3, it has been shown that the necessary condition for Lyapunov stability is that the Hamiltonian H be bounded below. This is immediately satisfied by the fact that the mode being investigated is a TE_0 (i.e. fundamental) mode, and is unique at a fixed power.

Lyapunov's theorem does not apply to higher order modes because for these modes, the Hamiltonian assumes a local minimum, not necessarily a global minimum as implicitly demanded by the theorem.

5.1.3 Potential Applications

As has been mentioned in Ref.[81], the existence of cut-offs in modal power, such as those shown in fig.5.4 corresponds to upper threshold devices proposed by Seaton *et al.* [3], and Stegeman *et al.* [108]. The advantage, in idealized cases, of having both bounding media self-defocussing is that the threshold power can be made smaller. In practice, it is often the case that having more nonlinear media means more loss.

Another potential switching application proposed here relies on the fact that modes of this SDF-L-SDF structure induce W-shape waveguides, as mentioned earlier. Without going into details, the operating principle of the switch may be described as follows. In the theory of linear waveguides, it is well-known that W waveguides have non-zero cut-off, i.e. a W waveguide can have non-zero waveguide parameter V but still not support guided modes. Thus, if a mode of this nonlinear structure is used as a pump wave, the W waveguide induced by the pump can be regarded as a linear waveguide for another weak signal at a different wavelength. The weak signal is 'on' or 'off' depending on whether the induced waveguide is above or below cut-off, which can be controlled by varying the pump power.

Some realistic figures

Supposing the PTS (crystal), which has a negative Kerr coefficient $n_2 = -4 \times 10^{-16}$ m^2/W, is used for the core, and the other parameters of fig.5.4 are satisfied, then the power ranges of fig.5.4(a) and (b) translate to approximately (0, 140 W) and (0, 710 W) respectively, by using Eqn.(2.47). These conversions are based on the assumption the core is 2 microns thick and 3 mm wide (in the y-direction), and that problems usually associated with real materials such as loss, saturation, etc. are not present.

5.2 Waveguides with a Self-defocusing Core

The presence of nonlinearity in the finite core complicates the problem considerably. This is because, although exact solutions for Kerr nonlinearity exist in terms of elliptic functions, these are often very inconvenient to work with, e.g. in calculating

mode shapes and power-dispersion curves. In addition, the method of linear stability in chapter is not directly applicable because exact solutions for the linearized perturbations are not available.

Here, TE_0 modes are calculated numerically using the iterative finite element method (IFEM) described briefly in chapter 2. The stability of the modes is determined numerically in the framework of Kolokolov's approach which was presented in chapter 3. The results are compared with the familiar case of a linear-core waveguide.

5.2.1 Calculation of Modes

To calculate modes numerically using the IFEM, the scalar wave equation for this system is written in the form

$$D\psi = W^2\psi \tag{5.11}$$

where

$$D = \begin{cases} \dfrac{d^2}{dX^2} + \psi^2, & |X| > 1 \\ \dfrac{d^2}{dX^2} - \dfrac{1}{\eta}\psi^2 + V^2, & |X| \leq 1 \end{cases} \tag{5.12}$$

$\eta = \alpha_r/|\alpha_{co}|$, $\alpha_{co} < 0$ is the scaled nonlinear coefficient of the core, and other quantities are defined in chapter 4.

The method used here to calculate the TE_0 fields and the corresponding power-dispersion curves is basically similar to the finite element method proposed earlier in Ref.[109]. Although the method can be applied to any nonlinearity, we use the Kerr nonlinearity for simplicity. With the standard one-dimensional finite element scheme [65], Eqn.(5.12) is discretized into an eigenvalue-eigenvector form and can be solved numerically using the iteration scheme $D_n\psi_{n+1} = W^2\psi_{n+1}$, where

$$D_n = \begin{cases} \dfrac{d^2}{dX^2} + \psi_n^2, & |X| > 1 \\ \dfrac{d^2}{dX^2} - \dfrac{1}{\eta}\psi_n^2 + V^2, & |X| \leq 1 \end{cases}$$

In calculating each point of a dispersion curve, $\psi_n(X)$ is normalized such that $\psi(X_m)$ is equal to some fixed parameter d, where X_m is the position of the peak intensity when the field is at high B_{co}. For Kerr bounding media, $X_m \approx \pm 1.6$. ψ_{n+1} is then determined using the inverse iteration method [66]. Iteration stops when ψ_{n+1} is sufficiently close to ψ_n. This condition may be quantified by a criterion such as $\sum_j |\psi_{n+1}(X_j) - \psi_n(X_j)| < \Delta$, where X_j are some equally spaced points and Δ is some small tolerance. Dimensionless power $P = \int_{-\infty}^{\infty} \psi^2\, dX$ may be approximated

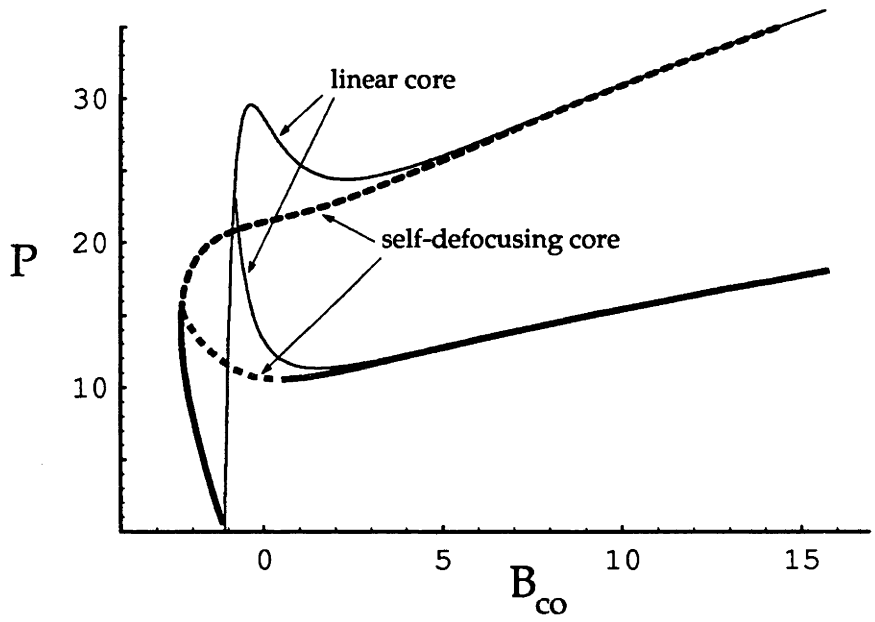

Figure 5.6: Dispersion curves (thick lines) for $V = 2.2$, $\eta = 3.3$. Solid (dashed) curves indicate stability (instability). Thin solid curves are the dispersion curves for the same V and $\eta = \infty$ (i.e. linear core).

by $\sum_{i=1}^{M} \psi^2(X_i)\delta X$ where $M+1$ is the dimension of the eigen-vector ψ and $\delta X = X_{i+1} - X_i$ is the discretization interval. By varying the parameter d over some chosen range, a smooth power-dispersion curve, together with the field ψ at points along the curve, can be calculated. For the symmetric mode, iterations can start from the zero-power limit using the linear mode shape as a first approximation, and d is varied from zero to some maximum value. Iterations for the asymmetric mode can start by using a surface mode (or simply one half of the symmetric mode calculated in the final step above) and decreasing d. In these calculations, we use 119 points (i.e. $M = 119$) for the computation window $X \in (-3, 3)$. It is noted that convergence would not be obtained above some B_{co} if power P is varied as a parameter. We also cannot pretend that convergence for this iterative scheme is guaranteed for all possible cases, e.g. when the core is significantly more nonlinear than the bounding media, leading to lower values of η. However, this scheme presents one possible method to compute stationary modes, and is quite efficient when the nonlinear coefficients of the respective layers are not too dissimilar.

Power dispersion curves using this iterative scheme for $V = 2.2$, $\eta = 3.3$ are shown in fig.5.6. For comparison purposes, the dispersion curves (thin solid lines) for the linear-core case (with the same V) are also shown. The difference introduced

by the self-defocusing core is that dP/dB_{co} is negative from the linear limit to the bifurcation point. This is quite sensible physically because below the bifurcation point, a significant fraction of the total power of the mode is in the core and this lowers the refractive index of the core. This in turn leads to a reduction in the effective index of the waveguide. The N-shape of the dispersion curve for the symmetric mode also disappears and the curve becomes monotonically increasing when the core is self-defocusing. This is even more pronounced for lower values of η, and can be attributed to the fact that the self-defocusing effect of the core weakens its guiding property when it contains a significant fraction of total modal power. At high values of B_{co}, the linear- and self defocusing-core cases do not differ much, because in this region, the guided modes are virtually surface modes and so the nonlinear effect of the core is negligible. Some mode shapes are shown in fig.5.7(a) for the symmetric mode. At low powers, the peak of the symmetric mode is within the core. As the power is increased, two peaks near the interfaces form in the mode shapes; this occurs at lower powers than in the linear-core case. Fig.5.7(b) shows some mode shapes for the asymmetric mode.

5.2.2 Modal Stability

We use a semi-numerical method based on Kolokolov's criterions in chapter 3 for calculating stability. In this method, instead of calculating the eigenvalues of the product operator L_0L_1, it is necessary to calculate only the first two eigenvalues λ_1 and λ_2 of L_1. This is a problem which is much easier and is less prone to numerical errors. As has been mentioned in chapter 3,

$$L_1 = d^2/dX^2 - B(X) + 3h\psi_0^2,$$

where

$$B = \begin{cases} W^2, & |X| > 1 \\ B_{co} = W^2 - V^2, & |X| \leq 1 \end{cases}, \qquad h = \begin{cases} 1, & |X| > 1 \\ -1/\eta = \alpha_r/\alpha_{co}, & |X| \leq 1 \end{cases}$$

For a homogeneous Kerr medium [72], only criterion (c) of Kolokolov (chapter 3) applies. In the present problem, all three conditions apply.

The operator L_1 is represented by a square matrix, and the eigenvalues λ_1, λ_2 are calculated using the inverse iteration method [66]. It is more convenient to define another operator $S_1 = L_1 + W^2$, and then λ_1 and λ_2 are accordingly shifted by W^2 in the positive direction.

Fig.5.8(a) indicates the stability properties of the symmetric mode. The solid

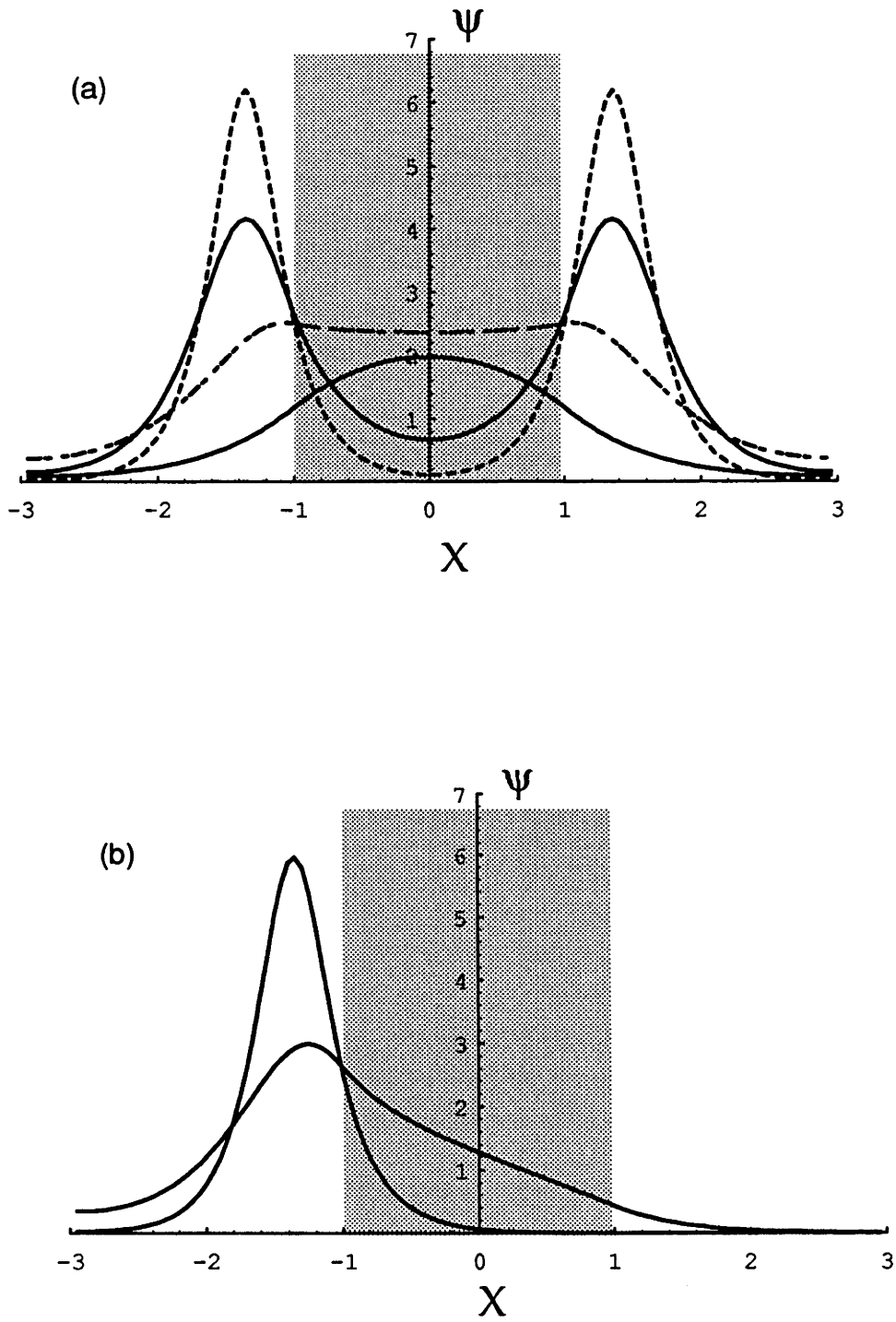

Figure 5.7: Some mode shapes for symmetric (a) and asymmetric (b) modes in a waveguide with a self-defocusing core.

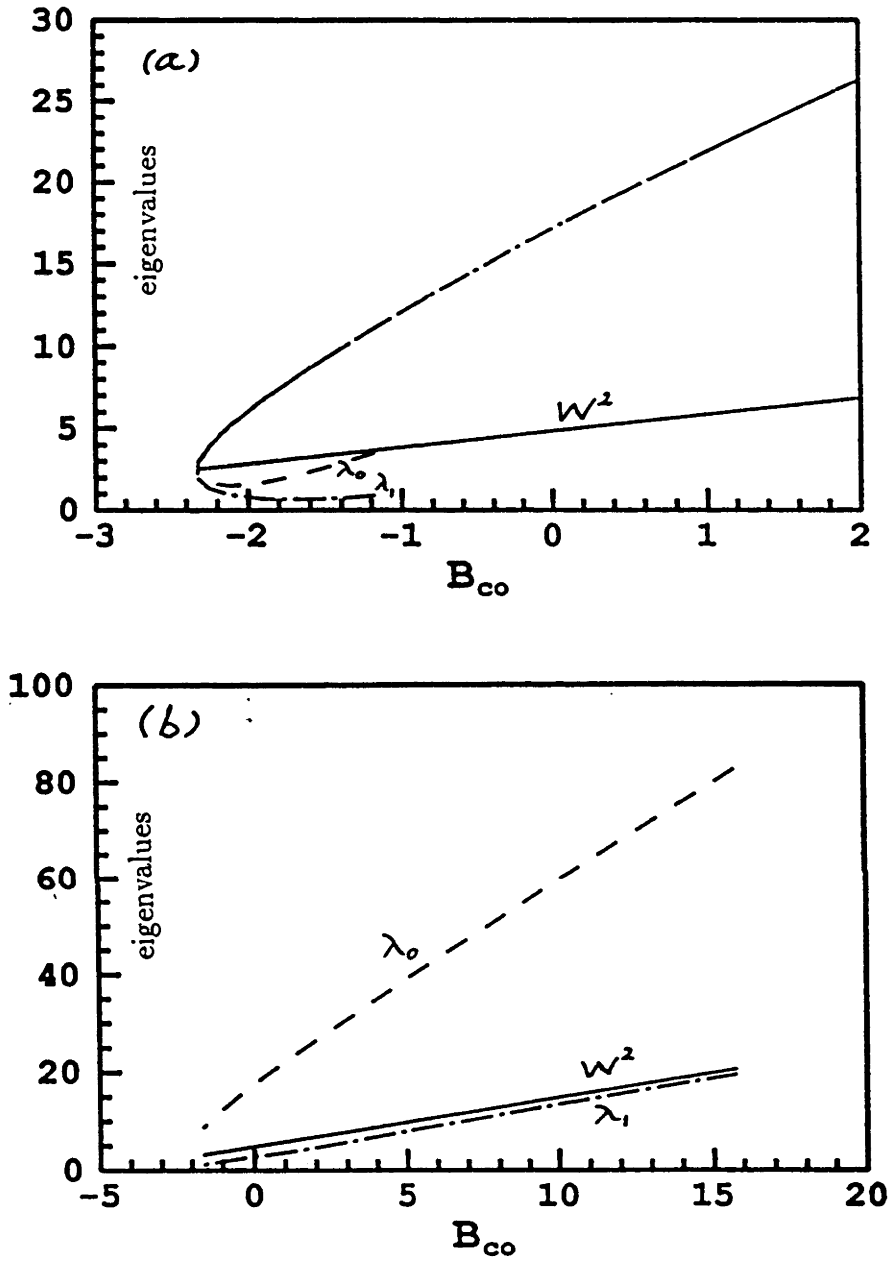

Figure 5.8: Curves for W^2 (solid) and the eigenvalues λ_1 (dash), λ_2 (dash-dot) of S_1. (a) symmetric modes; (b) asymmetric modes.

line is simply W^2 as a function of B_{co}; this is a straight line because $W^2 = V^2 + B_{co}$. The dash and dash-dot curves are for λ_1 and λ_2 respectively. As we trace from the linear limit (fig.5.6) to the bifurcation point, we have $\lambda_2 < \lambda_1 < W^2$ which is equivalent to criterion (b) of Kolokolov. Therefore the mode is stable in this range (as shown by the thick solid line in fig.5.6), although dP/dB_{co} is negative. In fact, this is the only different feature of stability compared to the linear-core case [59,61]. This is also consistent with the obvious fact that the symmetric mode is stable in the linear limit. As we continue beyond the bifurcation point, λ_1 and λ_2 become almost identical and satisfy $W^2 < \lambda_2 < \lambda_1$ (criterion (a)), and so the mode is unstable (indicated by the dash line in fig.5.6). A closer examination reveals that as we go past the bifurcation point, λ_1 and λ_2 do not become greater than W^2 simultaneously, and so there exists a small but finite region near the bifurcation point where criterion (c) applies.

For the asymmetric mode, fig.5.8(b) indicates $\lambda_2 < W^2 < \lambda_1$, and so the mode is stable in the region with positive dP/dB_{co}, and unstable otherwise. This result is the same as in the linear-core case.

Thus, the general stability result is similar to the well-known case of a linear core, except that the symmetric mode is stable from the linear limit to the bifurcation, although the dispersion curve is negatively sloped in this range.

Chapter 6

Dark Guided Waves

The preceeding chapters have examined nonlinear guided waves which are localized or bound in one transverse dimension. In practice, all structures are necesasarily three dimensional, which means that if modal power is sufficiently high, modes (in self-focusing media) will become unstable and might collapse to a singularity [16,17], a well-known phenomenon in bulk media. Another possible problem with self-focusing waveguides is that their modes might contain peak intensities that are substantially above the average intensity of the waveguide; and this can cause multiphoton absorption processes [40].

Dark waves [110] are free from the problems mentioned above, although they may not appear very attractive with respect to device implications because of their high modal powers (infinite in principle!). Nevertheless, they have been observed in several different experiments [111,112,113]. The work presented here has received greatest motivation from a recent experimental work which reported dark solitons being observed with moderately low powers [37], and which used chinese tea as the self-defocusing bulk medium! This work also demonstrated other interesting phenomena such as the formation of stable waveguides and structures equivalent to Y-junction splitters and other devices. At the present time the trade-off is that response time is very long in such high-nonlinearity materials.

Dark waves arise from the study of a class of unbound modes existing in both linear and nonlinear structures. In linear structures these modes are the periodic radiation modes which are the basis of transient propagation phenomena in linear waveguides [49]. In nonlinear structures these are periodic modes expressed in terms of elliptic functions [54], whose limiting forms are often called solitons. In a self-focusing medium, they are the (bound) bright solitons or guided waves studied in previous chapters. In a self-defocusing medium, they are the unbound, dark solitons

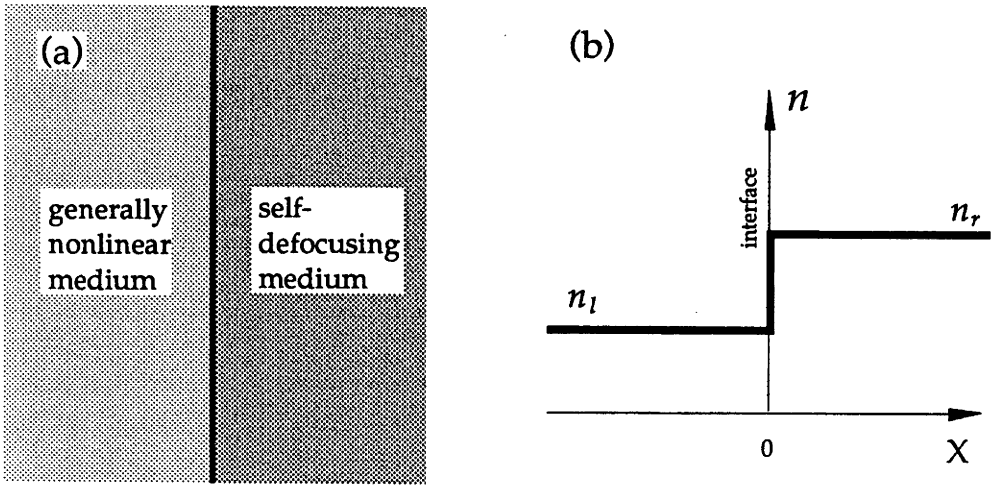

Figure 6.1: (a) Geometry of a 'dark' surface. (b) linear index profile.

or dark guided waves, and are the subject of study in this chapter.

Again, the work here focuses on two points: what types of dark modes can exist, and whether or not they are stable. For dark guided waves, one can proceed and study structures which invove as many nonlinear interfaces as one likes. However the single and double interface problems chosen for investigation in this chapter are the simplest structures that can be investigated analytically, and which contain most of the characteristic features of dark guided waves. Since the power of a dark mode is infinite, some authors have defined a non-physical 'dark power' P_D [114]. Here we choose not to use it because in a given medium a dark mode can be specified by its propagation constant β (or its equivalent).

The chapter is divided into two sections: the first (section 6.1) is on dark and bright-dark surface waves; and the second (section 6.2) is on dark and grey guided waves in slab waveguides.

6.1 Surface Waves

Throughout this chapter, the term 'surface waves' means modes which are supported by a planar interface between two media, at least one of which is self-defocusing. For convenience, Kerr nonlinearity is assumed on both sides of the interface. The interface geometry is shown in fig.6.1. The left medium may be self-defocusing, linear, or self-focusing, while the right medium is allowed to be self-defocusing only.

The notation here is similar to that of chapter 4, except that W_l^2 $(= \rho^2(\beta^2 - k^2 n_l^2))$ is now replaced by B_l which may be negative or positive. $B_r = -W_r^2$ is always negative. We also define a surface parameter $S = \rho k(n_r^2 - n_l^2)^{1/2}$ and an asymmetry parameter $\eta = \alpha_r/|\alpha_l| > 0$. Here ρ is a conveniently chosen scaling length.

The wave equation thus has the form [cf.(2.18)]

$$\begin{aligned} \psi'' - B_l\psi + \frac{h}{\eta}\psi^3 &= 0, \qquad X < 0 \\ \psi'' - W_r^2\psi - \psi^3 &= 0, \qquad X > 0 \end{aligned} \tag{6.1}$$

where, as in chapter 4, $\psi = \alpha_r E$, $h = -1, 0$, or 1 depending on whether the left medium is self-defocusing, linear or self-focusing respectively.

By using the eigenmodes of the respective media (chapter 2), guided wave solutions can be found for various types of interface, as shown in the subsections below. With regards to stability however, the present analytical method is applicable only to the linear-SDF interface type. This is because whenever two different types of nonlinearity are involved, exact forms for the perturbation functions are not available.

6.1.1 Linear-SDF Interface

This type of interface was first studied in Ref.[115] but in a rather restricted parameter space using quite involved analysis. The analysis presented here uses the smallest number of scaled parameters to describe the problem and thus is more general.

Modal field

In this type of interface, $\eta = \infty$, and guided waves solutions exist only for $B_l > 0$ (or $0 < B_l < S^2$). In terms of the effective refractive index, $n_{eff} = \beta/k$, this condition is equivalent to $n_l < n_{eff} < n_r$. The modal solution is

$$\psi = \begin{cases} a\, e^{\sqrt{B_l}X}, & X < 0 \\ W_r \tanh\left[\dfrac{W_r}{\sqrt{2}}(X - X_r)\right], & X > 0 \end{cases} \tag{6.2}$$

where a and X_0 are constants to be determined, and continuity of ψ and ψ' at $X = 0$ leads to

$$\begin{aligned} a &= \left(-\sqrt{B_l} + \sqrt{S^2 + W_r^2}\right)/\sqrt{2} \\ X_0 &= -\frac{\sqrt{2}}{W_r}\tanh^{-1}\left[\frac{a}{W_r}\right] \end{aligned} \tag{6.3}$$

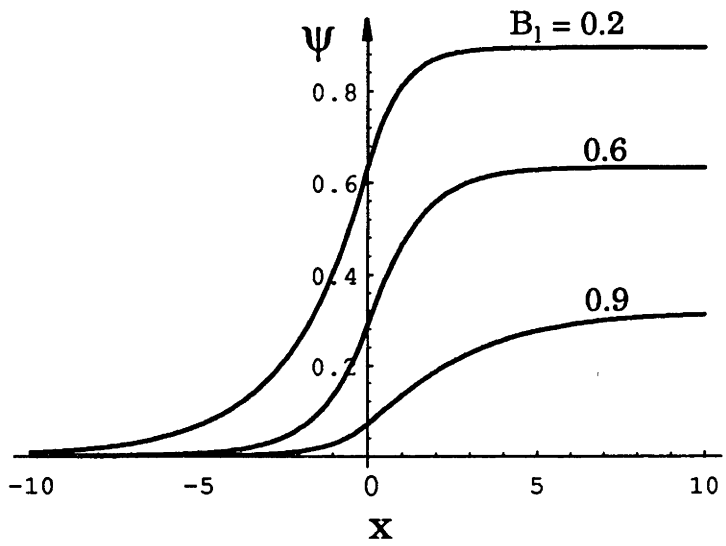

Figure 6.2: Some mode profiles of a linear-SF interface.

Some mode shapes given by these solutions are shown in fig.6.2. As B_l approaches zero, the field in both media approaches a plane wave with maximum amplitude S.

Unlike their bright counterparts, the dark surface modes do not have a fixed field amplitude at the interface.

Stability and propagation

The stability property for these surface modes is now determined using the linear analysis method described in chapter 3. In the left medium, the perturbation functions u and v are given by (3.16) with x replaced by $\sqrt{B_l}X$; while on the right, they are given by (3.19) and are assumed to be localized. Applying boundary conditions u and v then leads to the following equation

$$\begin{vmatrix} 1 & 1 & f_1 & \bar{f}_1 \\ 1 & -1 & f_2 & \bar{f}_2 \\ p_l W_l & \bar{p}_l W_l & f_1' & \bar{f}_1' \\ p_l W_l & -\bar{p}_l W_l & f_2' & \bar{f}_2' \end{vmatrix} = 0, \tag{6.4}$$

where $p_l = \sqrt{B_l - i\xi}$, $\bar{p}_l = \sqrt{B_l + i\xi}$, and f_1, $\bar{f}_1$, f_2, $\bar{f}_2$ are given by (3.20) with $x = W_r\,(X - X_0)/\sqrt{2}$, and the prime denotes d/dX.

It turns out that Eqn.(6.4) does not have any root ξ with a non-zero real part, implying that the surface mode is stable. This result is in agreement with a numerical

simulation using the beam propagation method shown in fig.6.3. This simulation was obtained by using a surface mode at $B_l = 0.2$ (with mode profile shown in fig.6.2), displaced laterally to the left by $\Delta X \approx 1.0$, as an initial condition. (Other parameters are shown in caption of fig.6.3.) The propagation along a surface was done for a distance of 75 units. $\Delta X \approx 1.0$ is a significantly large perturbation. Nevertheless, it can be observed that the wave asymptotically adjusts itself to an exact surface mode plus some radiation dispersing into the self-defocusing medium. In other words, a surface mode has been excited. A similar behaviour was observed when the mode was displaced to the right. This result is not only in agreement with Ref.[114] on the ground that the surface mode is stable to small perturbations (i.e. within the framework of linear analysis) but it also indicates that the mode is stable to relatively large perturbations.

It should be stressed that all numerical simulations in this chapter are not proofs of stability but only confirmations of analytical stability results.

6.1.2 SDF-SDF Interface

This type of interface, for which $h = -1$, can support two different classes of surface modes. The first type is a *'half-dark'* type, similar to the modes of a linear-SDF interface considered above, and is reported here for the first time. The second type may be called a *'full dark'* type, which was also studied earlier in Ref.[115] with a minor limitation discussed in the preceeding subsection.

Half-dark Surface Mode

The mode is called 'half-dark' because it is dark on the left, and has a bright uniform background on the right of the interface. The modal solution on the left is given by a decaying cosech function:

$$\psi = \sqrt{2\eta B_l}\,\mathrm{cosech}\left[\sqrt{B_l}(X - X_l)\right], X < 0, \tag{6.5}$$

while on the right, it is given again by (6.2). The existence condition is the same as for linear-SDF interface.

Letting

$$x = \mathrm{cotanh}[\sqrt{B_l}(-X_l)], \quad y = \tanh[\frac{W_r}{\sqrt{2}}(-X_r)],$$

it follows that the boundary conditions at $X = 0$ lead to an eigenvalue equation given by

$$\sqrt{x^2-1}\left[x - \sqrt{x^2-1}\right] = \frac{W_r^2}{2B_l\sqrt{\eta}}, \quad x < -1 \tag{6.6}$$

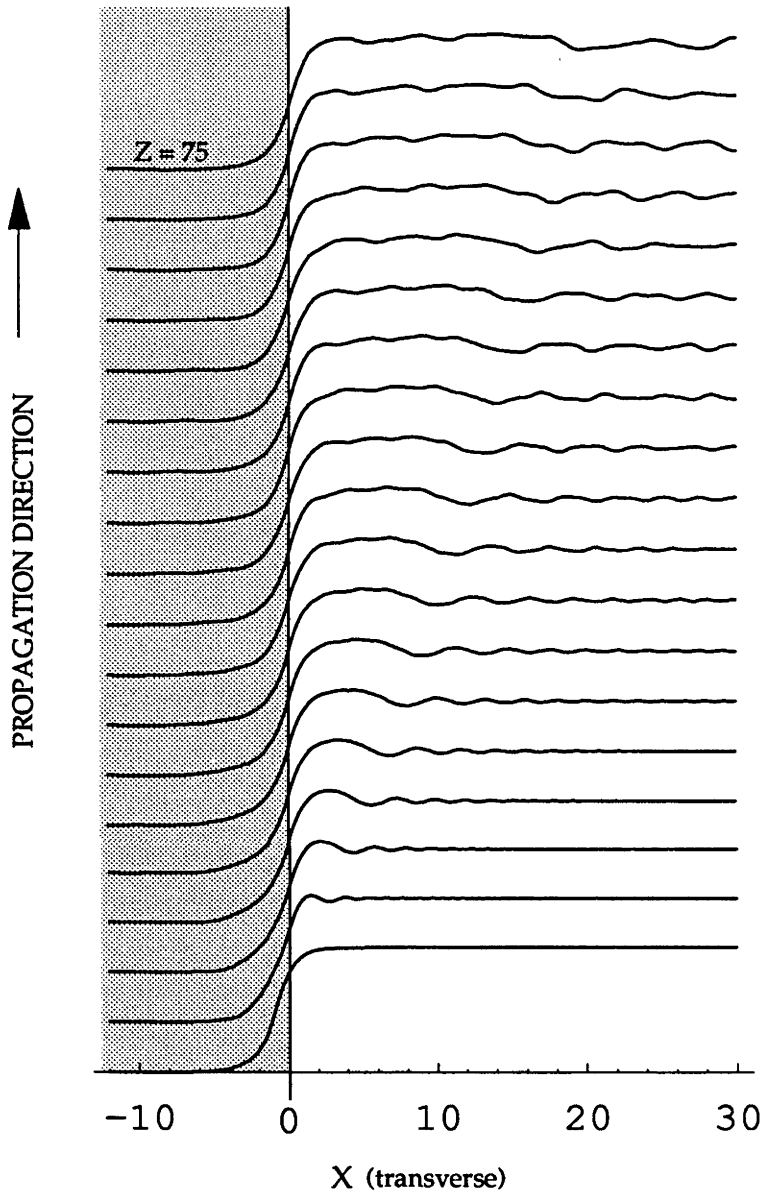

Figure 6.3: Propagation, for a distance of $Z = 75$, of the intensity profile of a surface wave which has the exact shape of a surface mode at $B_l = 0.2$ but displaced to the left by $\Delta X \approx 1$. $S = 1$, $n_l = 1.5$, $n_r = 1.57$. The wave quickly adjusts itself to a surface mode plus some radiation emitted into the self-defocusing medium.

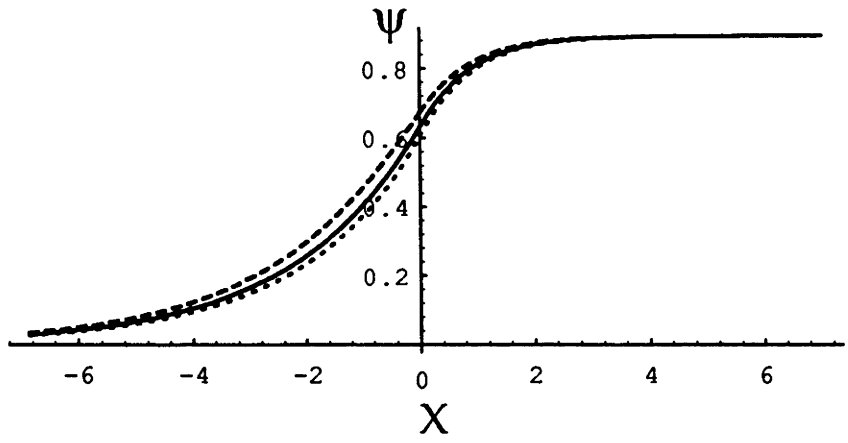

Figure 6.4: Comparison between half-dark surface modes of linear-SDF (solid curve), SDF-SDF (dotted), and SF-SDF (dashed) interfaces all of which have $S = 1$, $\eta = 3.3$, $W_r^2 = 0.8$.

from which it follows that

$$y = -\sqrt{2\eta}\,\frac{\sqrt{B_l}}{W_r}\sqrt{x^2 - 1}, \tag{6.7}$$

and

$$\begin{aligned} X_l &= -(\text{cotanh}^{-1}x)/\sqrt{B_l} \\ X_r &= -(\sqrt{2}\tanh^{-1}y)/W_r. \end{aligned} \tag{6.8}$$

A comparison between a mode of this type and a mode of the linear-SDF interface, both having the same right medium, the same S, and at the same B_l, is made in fig.6.4. It can be observed that when the left medium is self-focusing, the mode is shifted slightly into the left medium, while a self-defocusing left medium has the opposite effect. When there is little power in the left medium, i.e. when W_r is close to zero, the modes are almost identical, as one would expect.

Full-dark surface mode

Here the modal solutions on both sides of the interfaces are given by tanh functions:

$$\psi = \begin{cases} \sqrt{-\eta B_l}\tanh\left[\sqrt{\dfrac{-B_l}{2}}(X - X_l)\right], & X < 0 \\ W_r \tanh\left[\dfrac{W_r}{\sqrt{2}}(X - X_r)\right], & X > 0 \end{cases} \tag{6.9}$$

whose existence requires $B_l < 0$, or equivalently, n_{eff} is less than both n_r and n_l. Using boundary conditions at the interface, we get

$$\begin{aligned} X_r &= \frac{\sqrt{2}}{W_r}\tanh^{-1}\left(\frac{\Gamma}{W_r}\right) \\ X_l &= \sqrt{\frac{2}{-B_l}}\tanh^{-1}\left(\frac{\Gamma}{\sqrt{-\eta B_l}}\right) \end{aligned} \tag{6.10}$$

where

$$\Gamma = \pm\sqrt{(-W_r^2 - B_l\sqrt{\eta})/(1 - 1/\sqrt{\eta})} \tag{6.11}$$

The $\pm$ sign indicates that, for a given W_r, the zero intensity of the mode may be on either side of the interface, as shown by some examples in fig.6.5.

However, these dark surface waves do not exist for all $B_r < 0$, because, for X_r, X_l to exist and be given by (6.10), the conditions

$$-1 < \Gamma^2/B_r < 0, \; -1 < \Gamma^2/\eta B_l < 0, \quad \text{and}\, \Gamma^2 > 0$$

must be satisfied. These conditions lead to two cases:

(1) - if $\eta > 1$, then $B_r/B_l > \sqrt{\eta}$.

(2) - if $\eta < 1$, then, among other conditions, $B_r/B_l < \sqrt{\eta} < 1$.

Case (2) is ruled out, because $n_l < n_r$ and therefore $B_r/B_l > 1$. Case (1) has an interesting consequence: the dark surface waves exist only below a certain maximum value of W_r. At this maximum, the zero-intensity dips of the two dark modes coincide at the interface.

Finally, expressions (6.10) and (6.11) allow us to see that, for some fixed W_r, as S increases, the intensity minima move away from the interface, and the field amplitude for the left medium also decreases.

6.1.3 SF-SDF Interface

In Eqn.(6.1), h is now positive, and the necessary conditions for guided waves solutions to exist are the same as in the linear-SDF case, namely $n_l < n_{eff} < n_r$, or $B_l > 0$. Letting $W_l = \sqrt{B_l}$, the solution in this case is then

$$\psi = \begin{cases} -W_l\sqrt{2\eta}\,\mathrm{sech}[W_l(X - X_l)], & X < 0 \\ \pm W_r \tanh\left[\dfrac{W_r}{\sqrt{2}}(X - X_r)\right], & X > 0 \end{cases} \tag{6.12}$$

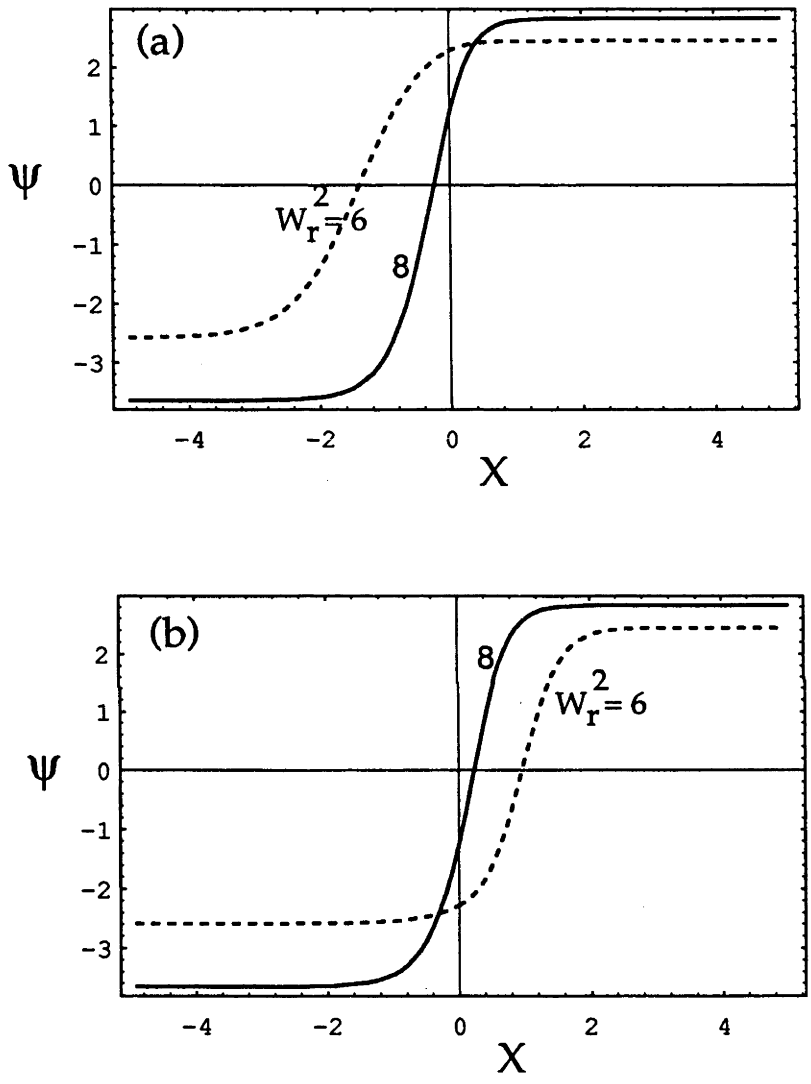

Figure 6.5: Some mode profiles of a SDF-SDF interface with $S = 2$, $\eta = 3.3$. (a) node on the left of the interface; (b) node on the right.

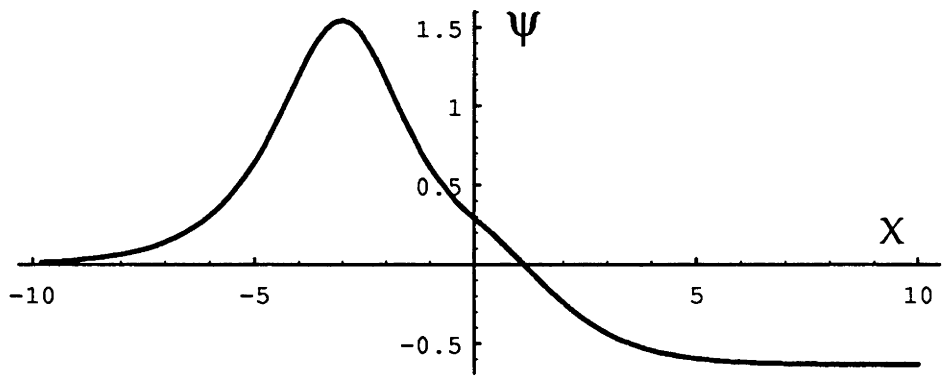

Figure 6.6: Mode profile of a bright-dark mode at a SF-SDF interface with $S = 1$, $\eta = 2.0$, $W_r^2 = 0.4$.

The derivation of modal characteritics is axactly analogous to the half-dark mode of the SDF-SDF interface. Defining

$$x = \tanh\left[W_l(-X_l)\right], \quad y = \tanh\left[\frac{W_r}{\sqrt{2}}(-X_r)\right],$$

the eigenvalue equation is then

$$\sqrt{1-x^2}\left[x - \sqrt{1-x^2}\right] = \frac{W_r^2}{2W_l^2\sqrt{\eta'}}, \quad |x| < 1. \tag{6.13}$$

From which we find that

$$y = -\sqrt{2\eta}\,\frac{W_l}{W_r}\sqrt{1-x^2}, \tag{6.14}$$

and

$$\begin{aligned} X_l &= -(\tanh^{-1}x)/W_l \\ X_r &= -(\sqrt{2}\tanh^{-1}y)/W_r. \end{aligned} \tag{6.15}$$

which may be positive or negative.

The solution with the plus sign has a peak in the left self-focusing medium, as shown in fig.6.6. This is the case where a bright soliton coexists with a dark soliton (in the right self-defocusing medium), and therefore may be called a *bright-dark* surface mode. The solution with the minus sign corresponds to a *half-dark* mode. The similarity of this mode to half-dark mode of the other two types of interface is shown in fig.6.4. The self-focusing left medium shifts the mode to the left slightly, compared with that of linear-SDF interface. This shift is very small at larger values of W_r. So, it is interesting to realize that half-dark solutions exist in all types of interface involving a self-defocusing medium.

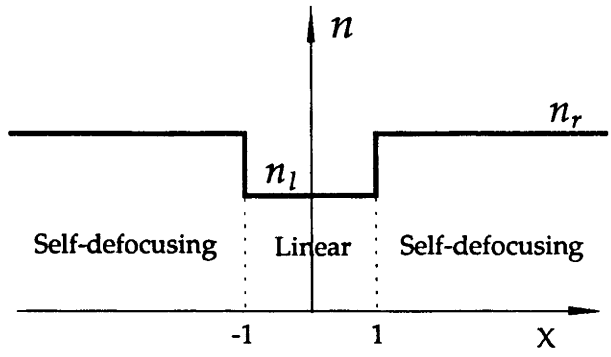

Figure 6.7: Geometry of a 'dark' waveguide.

Conditions for the existence of roots x to Eqn.(6.13) lead to an interesting constraint on modal parameters W_r and W_l. It can be shown that the ratio W_r/W_l must be less than a certain positive constant which depends only on η. In other words, the bright-dark soliton solution to this interface exists only in some part of the whole range $0 < W_l^2 < S^2$. For the half-dark solution, this cut-off is the major difference compared to the case of a linear-SDF interface, although the field shapes are very similar.

6.2 Guided Waves

On this topic, namely guided waves in self-defocusing slab waveguides, Ref.[116] is probably the first report on the calculation of symmetric and anti-symmetric modes in symmetric geometries. Here asymmetric modes in symmetric waveguides, and a discussion on asymmetric waveguides are also given.

The term 'guided waves' here refers to stationary waves supported by a symmetric 3-layer planar structure with the geometry shown in fig.6.7. This structure is similar to that of the self-focusing waveguide in chapter 4, except that the bounding media are now self-defocusing and identical, and the refractive index n_{co} may be lower (hollow waveguide) or higher (normal waveguide) than the index $n_r = n_l$ of the bounding media. For hollow waveguides, the parameter V is now defined as $V = -\rho k|n_{co}^2 - n_r^2|^{1/2}$, a negative number. B_{co} and $B_r = -W_r^2$ are the modal parameters for the core and the bounding media respectively. The wave equation now has solutions in the form [116]

$$\psi = \begin{cases} \pm W_r \tanh\left[\frac{W_r}{\sqrt{2}}(X - X_j)\right], & |X| > 1 \\ a\,\sinh(\sqrt{B_{co}}X) + b\,\cosh(\sqrt{B_{co}}X), & |X| < 1 \end{cases} \tag{6.16}$$

in which X_j ($j = l, r$ for the left and right bounding media respectively), and a, b are constants (real or purely imaginary). A necessary restriction on these solutions is that ψ must be real in $|X| < 1$, because it is always real in $|X| > 1$. By matching ψ and ψ' at $X = \pm 1$, and after some simple manipulations, we obtain

$$\begin{aligned} -W_r^2 + (-as + bc)^2 &= \pm\sqrt{2\,B_{co}}(ac - bs) \\ -W_r^2 + (as + bc)^2 &= -\sqrt{2\,B_{co}}(ac + bs) \end{aligned} \tag{6.17}$$

where $c = \cosh(\sqrt{B_{co}})$ and $s = \sinh(\sqrt{B_{co}})$. Hence two possible cases arise: either

$$abcs = -ac\sqrt{B_{co}/2}, \quad \text{using the plus sign in (6.17), or} \tag{6.18}$$

$$abcs = -bs\sqrt{B_{co}/2}, \text{using the minus sign.} \tag{6.19}$$

These cases lead to symmetric, anti-symmetric and asymmetric modes considered separately below.

6.2.1 Symmetric Modes

This class of solutions is obtained by putting $a = 0$ in (6.18). Then (6.17) gives

$$b = \frac{1}{2c^2}\left(\sqrt{2B_{co}}\,s \pm \sqrt{2s^2B_{co} + 4c^2W_r^2}\right) \tag{6.20}$$

This is the dark counterpart of the symmetric TE class of bright guided waves in self-focusing planar waveguides [61]. Either the plus sign or minus sign in (6.20) (and also in (6.22-6.23) below) has to be appropriately chosen such that X_l, X_r exist and are real, i.e.

$$|bc/W_r| < 1.$$

Let us consider the example of a hollow waveguide (i.e. $n_{co} < n_r$). In the region $0 < B_{co} < V^2$ (or the effective index $n_{eff} = k/\beta$ satisfies $n_{eff} > n_{co}$), the field in the linear film has a cosh shape with no zero intensity points, as typically shown in fig.6.8 by the solid curves. It resembles a 'grey' soliton and may be called a TE_0 symmetric mode. (It is easy to see that for normal waveguides, these grey modes do not exist because the solution in the core cannot have a cosh form.) As B_{co} decreases and become less than zero (or $n_{eff} < n_{co}$), the mode abruptly changes to a TE_2 mode having a cos shape in the core and two nodes, or zero intensity points, (fig.6.8, dash-dot curves). Near $B_{co} = 0$, the two nodes within the self-defocusing media can have a large separation from one another, and they move closer to the interfaces as B_{co} becomes lower. As B_{co} decreases even further, the TE_2 mode would cease to exist

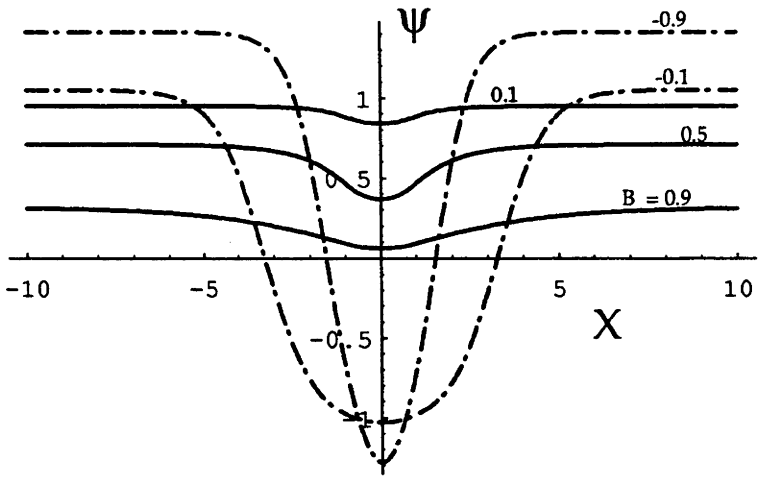

Figure 6.8: Some profiles of the TE_0 (solid) and TE_2 (dash-dot) symmetric modes in a slab waveguide.

and the TE_4 modes (with 4 zeros) would appear, and so on. However, any realistic self-defocusing nonlinearity must necessarily be saturable at high enough powers, and so only a finite number of these dark modes can actually exist. Nevertheless, the Kerr model used here should give a good approximate description, at least for modes of the lowest orders.

In normal waveguides which have $n_{co} > n_r$, solutions in the core can only be trigonometric, and so 'grey' modes do not exist. A similar pattern of other modes exists.

Stability and propagation

The process of determining stability is similar to that used for the bright guided modes of chapter 4, except that u and v in the bounding medium is given by (3.19).

For the TE_0 (grey) mode, the result is the same as for dark surface modes shown in the previous section, namely no eigenvalue ξ with a non-zero real part exists, and therefore it is stable to all perturbations. As before, a BPM simulation, shown in fig.6.9, confirms this result. In this simulation, an exact grey mode at $B_{co} = 0.5$ (with mode profile shown in fig.6.8) is displaced laterally to the right by $\Delta X \approx 0.5$ and then allowed to propagate for a distance of 60 units. Again, the wave quickly adjusts itself to a grey mode, plus some radiation dispersed evenly into the bounding self-defocusing medium. The grey mode is indeed very stable, and the numerical simulation in fig.6.9 indicates that it could be excited by end-fire coupling.

In theory, the power of any guided mode involving dark waves is infinite. In

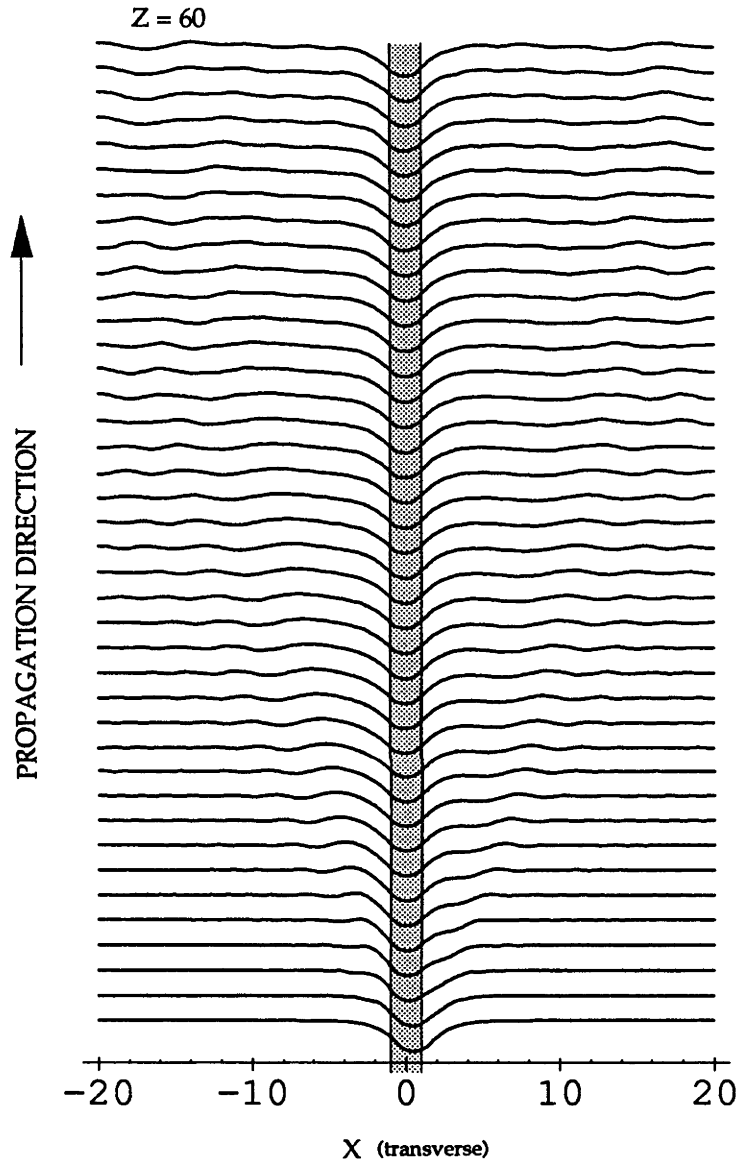

Figure 6.9: As in fig.6.3 but for the TE_0 grey wave (displaced to the right by $\Delta X \approx 0.5$), with: $Z = 60$, $B_{co} = 0.5$, and $V = -1$.

practice, however, truncated but stable dark spatial solitons with necessarily have finite powers have been experimentally observed [37]. We can thus expect similar behaviours for truncated dark guided waves in interface and waveguide structures. This feature of high stability in a finite background has its analogue in the temporal domain, where it has been found [117] that a dark pulse on the background of a relatively short bright pulse exhibits characteristics of a dark temporal soliton. In other words, the effect of truncation is only very slight.

The result for the TE_2 mode is that it is unstable to any perturbation. The existing complex eigenvalues ξ for $V = -1$ are shown in fig.6.10 in which the solid and dashed curves indicate real and imaginary parts of ξ respectively. The mode exists in the range $-9.8 < B_{co} < 0$ approximately. In case (a) of fig.6.10 at low values of B_{co}, the 'growth rates' are a pair of complex conjugates, then they become two distinct real values for some range, and then merge with each other to become complex again. The situation in case (b) of fig.6.10 is similar to case (a) except that when the pair of complex roots becomes real, one of them vanishes and become purely imaginary (not shown here) at $B_{co} \approx -4.35$, then becomes real again at $B_{co} \approx -2.1$ before merging with the other eigenvalue to become complex. Since either real or complex growth rates exist in the whole range of the TE_2 mode, the mode is unstable.

These TE_2 results are confirmed numerically in fig.6.11, using the beam propagation method, in which an exact TE_2 (symmetric) mode at $B_{co} = -0.9$ (with mode profile shown in fig.6.8) is displaced laterally to the right by $\Delta X \approx 0.3$ and let to propagate for a distance of $Z = 200$. At this value of B_{co}, the growth rates (fig.6) are real for even perturbations and complex for odd perturbations. It is observed that the field distribution near the core undergoes wide lateral oscillations. After some distance, the intensity peak within the core starts to have pulsating behaviour, and the field far in the bounding medium also starts to become non-uniform. These are indications of instability.

Similarly, the TE_2 mode in a normal waveguide ($V > 0$) was found to be unstable to all perturbations.

6.2.2 Anti-symmetric Modes

Similarly, by putting $b = 0$ in (6.19), we get the class of antisymmetric modes characterized by

$$a = \frac{1}{2s^2}\left(-c\sqrt{2B_{co}} \pm \sqrt{2c^2B_{co} + 4s^2W_r^2}\right) \tag{6.21}$$

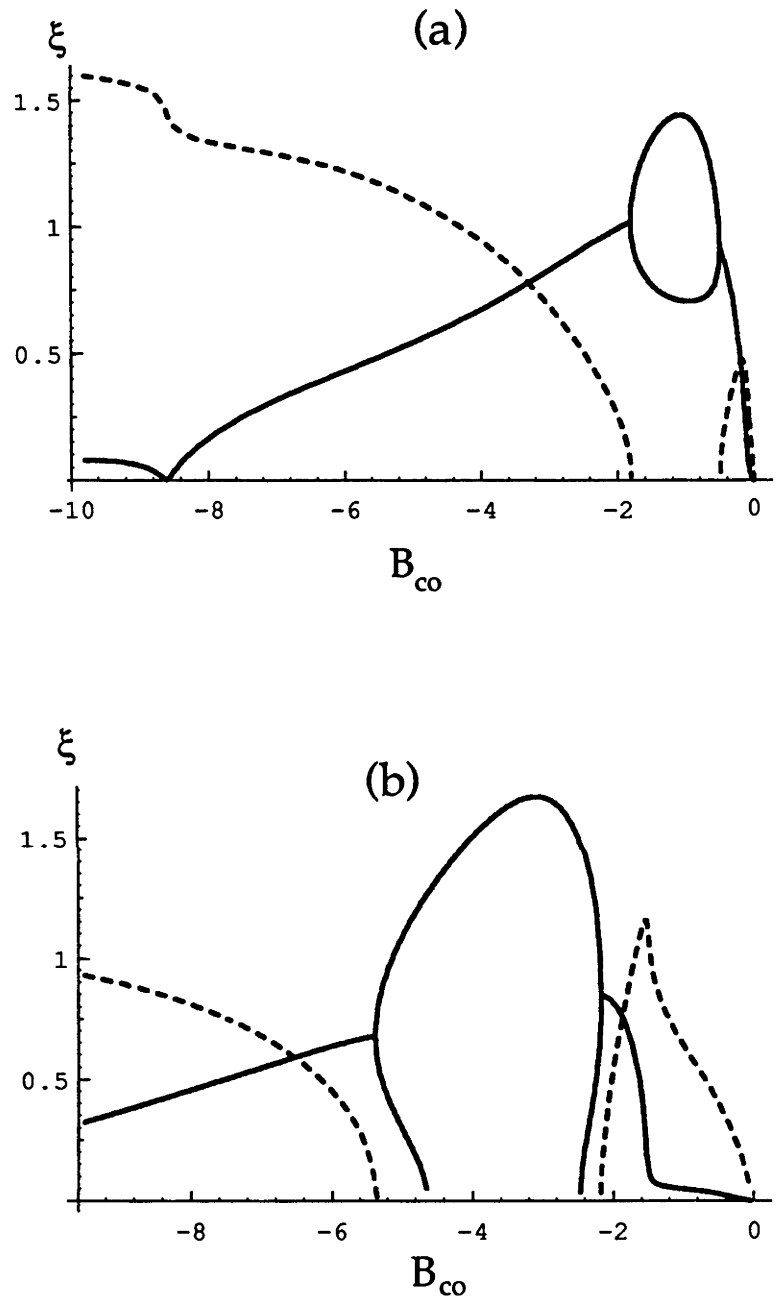

Figure 6.10: Curves of eigenvalue ξ for the TE_2 mode with respect to (a) even and (b) odd perturbations in the whole range of existence of the mode. $V = -1$. The solid (dashed) curves displays the real (imaginary) part of ξ.

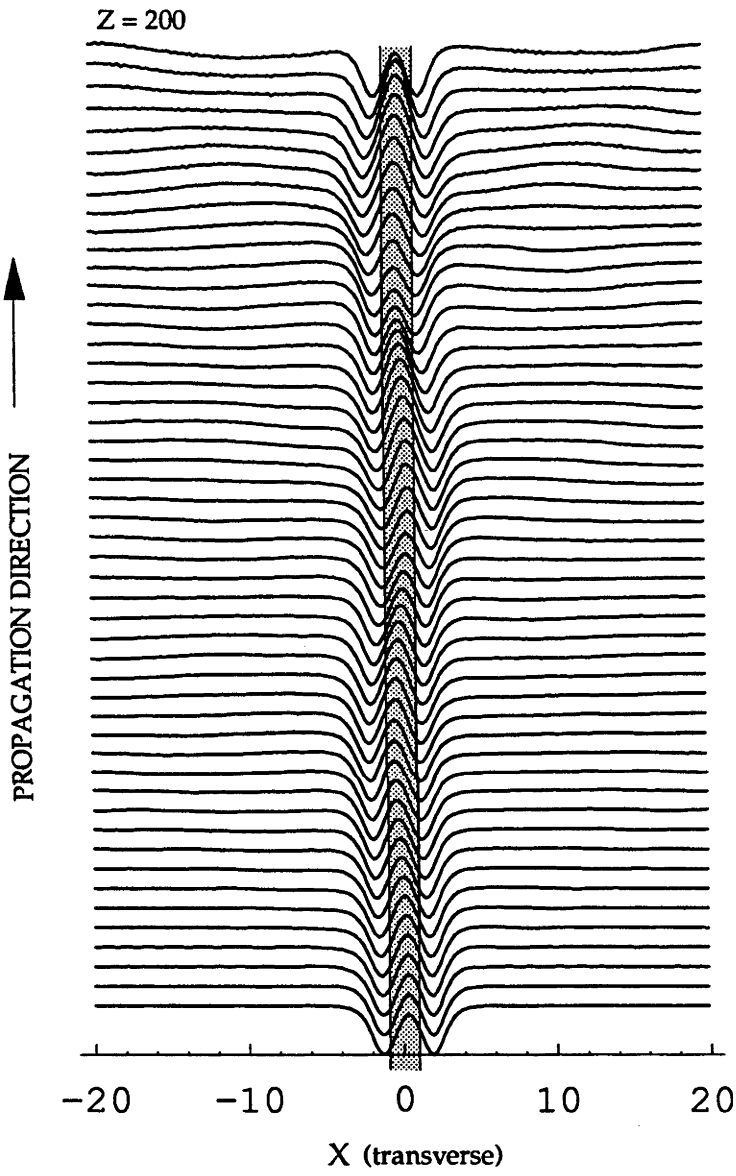

Figure 6.11: As in fig.6.3 but for the TE_2 symmetric wave (displaced to the right by $\Delta X = 0.3$), with: $Z = 200$, $B_{co} = -0.9$, and $V = -1$.

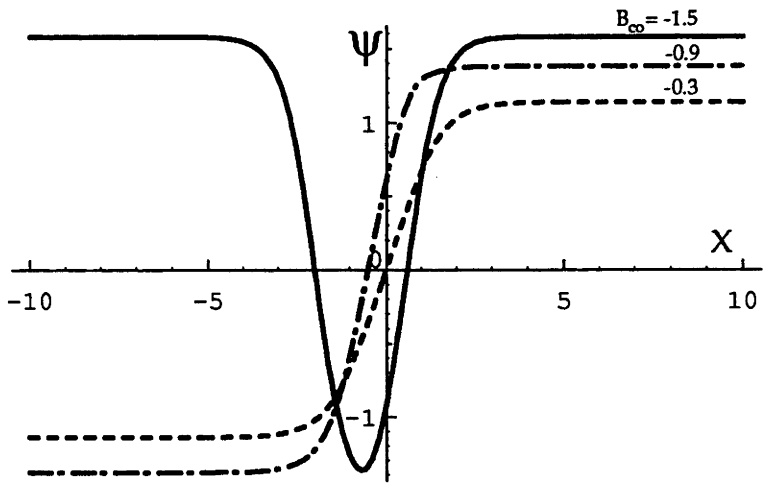

Figure 6.12: Typical profiles of the TE_2 asymmetric modes (solid), TE_1 anti-symmetric (dashed), and TE_1 asymmetric (dash-dot) modes.

The profile of a typical TE_1 anti-symmeric mode which has one node in the centre of the film is shown in fig.6.12 (dashed curve), which resembles a dark soliton in a homogeneous medium. As for the TE_0 symmetric mode, the TE_1 mode exists only in a finite interval of B_{co}. In constrast to the TE_0 mode however, the TE_1 mode can exist in both hollow and normal waveguides. The mode pattern arised as B_{co} decreases is similar to the symmetric counterparts.

Stability and propagation

For brevity, stability properties of only the TE_1 anti-symmetric mode are discussed here. The interesting results are: in hollow waveguides, the TE_1 mode is stable to odd perturbations, but unstable to even perturbations, and therefore generally unstable; in normal waveguides, the mode is stable to any small perturbations. It is not obvious how this interesting difference can be explained in physical terms.

Fig.6.13 shows the growth rate of instability to even perturbations of the (anti-symmetric) TE_1 mode, for $V = -1$. The mode exists in the range $-2.5 < B_{co} < 1$ approximately. At low values of B_{co}, the growth rates are complex. They vanish at $B_{co} \approx -1$ and then become real for the rest of the range, implying that the mode is unstable to even perturbations in the whole range of its existence. However, to odd perturbations, only purely imaginary eigenvalues exist, and therefore the mode

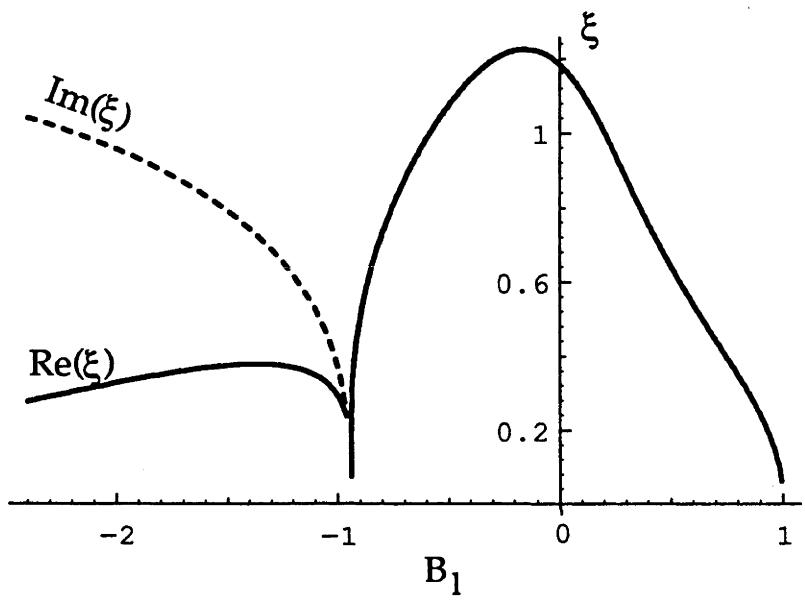

Figure 6.13: Eigenvalue ξ (or growth rate) curves for the TE_1 anti-symmetric mode in the whole range of its existence, (with respect to even perturbations). Solid curves indicate the real part of ξ, while the dash curve shows its imaginary part. ξ is real for $B_{co} > -1$ approx. Here, $V = -1$ (hollow waveguide).

is stable. These different effects of symmetry of a perturbation on the stability of a mode is reminiscent of similar effects seen in some other systems. For example, the bright symmetric TE_0 mode of a linear slab bounded by a self-focusing medium [70], in the regime of high B_{co}, is stable to even perturbations but unstable to odd perturbations. A similar effect has also been reported [118] concerning dark solitary waves trapped in media with gain and loss.

To numerically demonstrate that the TE_1 mode in a hollow waveguide is unstable to generally asymmetric perturbations, an exact TE_1 mode at $B_{co} = -0.3$ (which has profile shown in fig.6.12) is displaced to the right by $\Delta X \approx 0.24$ and allowed to propagate for a distance of 250 units, as shown in fig.6.14. At this value of B_{co}, fig.6.13 indicates that the associated growth rate of instability is real and close to the maximum. It can be seen that a dark soliton is emitted into the bounding medium. A transient bright peak is also formed within the core and seems to decay away. This behaviour supports the instability result.

To demonstrate that this same TE_1 mode is stable to odd perturbations, the simulation shown in fig.6.15 was done. Here, the initial condition at $Z = 0$ is an exact TE_1 mode at the same value of B_{co} as in fig.6.14, except that the field in the interval $-3 < X < 3$ is now replaced by a linear function of the form $\psi = aX$ (a is a real constant, such that ψ is continuous at $X = \pm 3$). This is the reason for the parabolic shape of the initial intensity profile in fig.6.15. The propagation was done for a distance of $Z = 120$, and one can see that a TE_1 mode is excited with some radiation dispersed evenly into the bounding medium. This result not only supports the linear analysis results stated earlier but also indicates the possibility of end-firing excitation of the TE_1 mode.

The stability of a TE_1 mode in normal waveguides is demonstrated in fig.6.16. Here $V = 1$, and a displacement perturbation of $\Delta X = 0.25$ to the same exact mode as used in fig.6.14 is used. It is observed that the perturbed wave only oscillates slightly about its equillibrium as it propagates, whereas the perturbed wave in fig.6.14 (which has a smaller displacement perturbation of $\Delta X = 0.24$) emits a dark soliton shortly after launching.

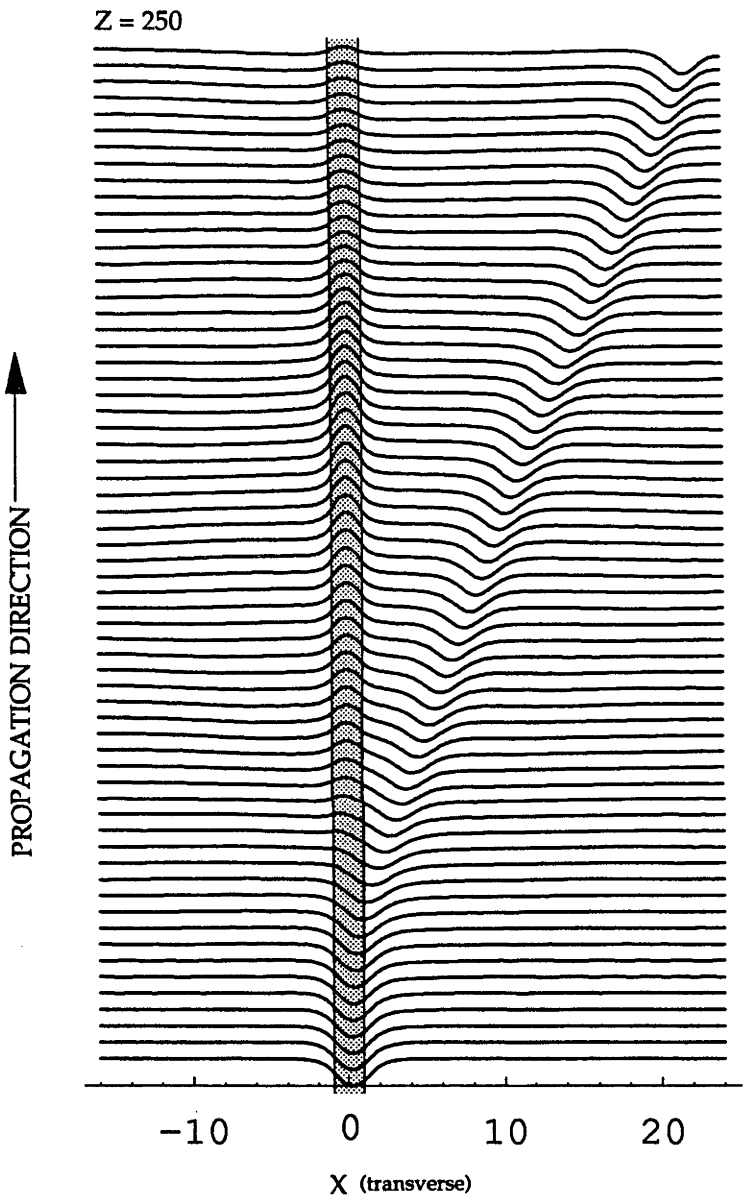

Figure 6.14: As in fig.6.3 but for the TE_1 anti-symmetric wave (displaced to the right by $\Delta X \approx 0.24$), with: $Z = 250$, $B_{co} = -0.3$, and $V = -1$.

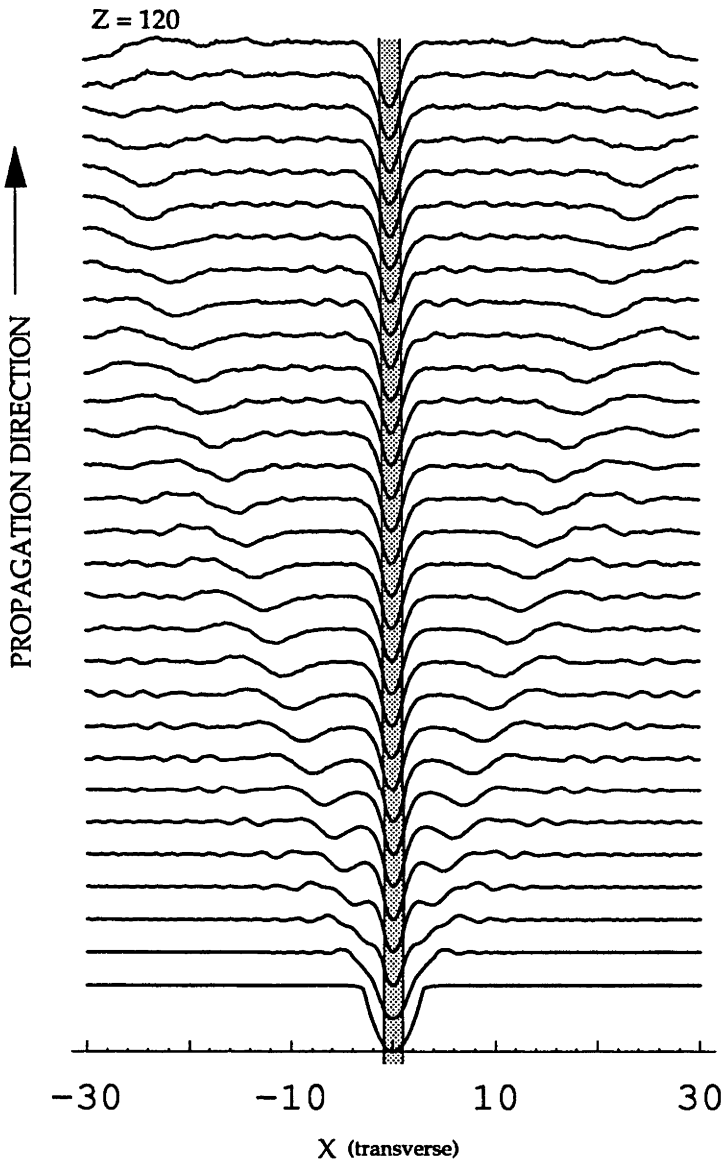

Figure 6.15: Simulation of a TE_1 wave with an anti-symmetrically perturbation. The initial field within $-3 < X < 3$ has the form $\psi = aX$ but is identical with an exact mode at $B_{co} = -0.3$ elsewhere. Here $V = -1$.

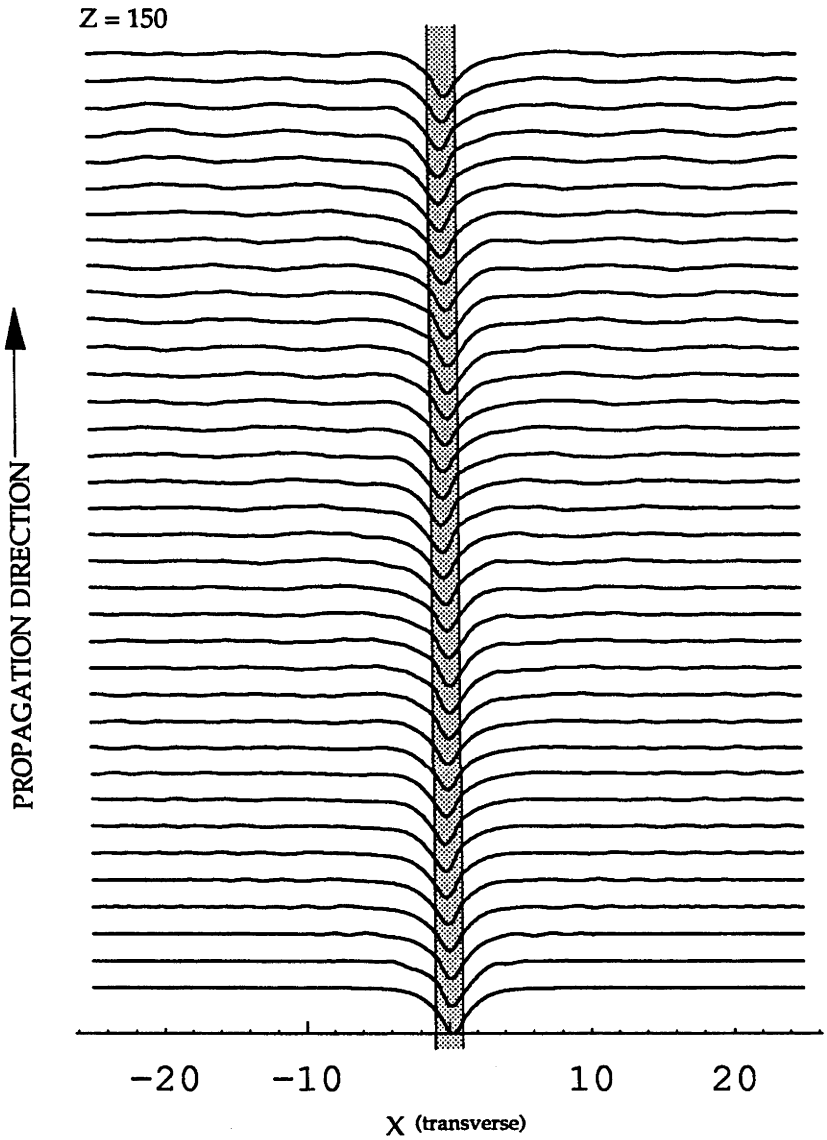

Figure 6.16: Demonstration of the stability of a TE_1 anti-symmetric mode in a normal waveguide with $V = 1$, $n_l = 1.57$, $n_r = 1.5$. The initial condition is the same exact mode as used in fig.6.14 displaced to the right by $\Delta X = 2.5$.

6.2.3 Asymmetric Modes

One class of asymmetric modes, with ψ having the same sign at $X = \pm\infty$, (i.e. even parity), is obtained by taking $a \neq 0$ in (6.18). By using (6.17), we arrive at

$$\begin{aligned} b &= \frac{1}{s}\sqrt{\frac{B_{co}}{2}} \\ a &= \pm\frac{1}{s}\sqrt{\pm V^2 - c^2 B_{co}/2s^2} \end{aligned} \tag{6.22}$$

The first $\pm$ sign simply corresponds to solutions which are mirror images of each other. The second $\pm$ sign corresponds to normal or hollow waveguides respectively. This class of solutions is the dark counterpart of the TE asymmetric classes of bright guided waves [61]. However, in constrast to self-focusing waveguides, the asymmetric TE_0 mode does not exist in self-defocusing waveguides because boundary conditions can not be satisfied. Fig.6.12 (solid curve) shows the profile of a typical TE_2 asymmetric mode which exists only in a certain finite range of B_{co}.

Another class of asymmetric modes with odd parity can be obtained by putting $b \neq 0$ in (6.19). These modes are characterised by

$$\begin{aligned} a &= -\frac{1}{c}\sqrt{\frac{B_{co}}{2}} \\ b &= \pm\frac{1}{c}\sqrt{\pm V^2 - s^2 B_{co}/2c^2} \end{aligned} \tag{6.23}$$

The $\pm$ signs correspond to modes which are reflection images of each other through the origin. For the particular value of $V = -1$, the asymmetric mode of the TE_1 (antisymmetric) mode exist only in a small range of B_{co}, approximately $-0.94 < B_{co} < -0.86$. A typical mode profile of this mode is shown in fig.6.12 (dash-dot curve).

6.2.4 Asymmetric Waveguides

If the symmetric waveguide examined so far in this section becomes only slightly asymmetric, then the mirror image degeneracy of these symmetric, anti-symmetric and asymmetric modes is lifted, and we can expect a splitting of modes similar to the case of bright guided waves studied in chapter 4. Moreover, when the waveguide asymmetry becomes large enough, a totally new class of modes can be guided in the waveguide. Figure 6.17 schematically shows a waveguide geometry in which this is possible. The linear indices n_l, n_r may be chosen such that $n_l < n_r$, and n_{co} may be lower than n_l or higher than n_r.

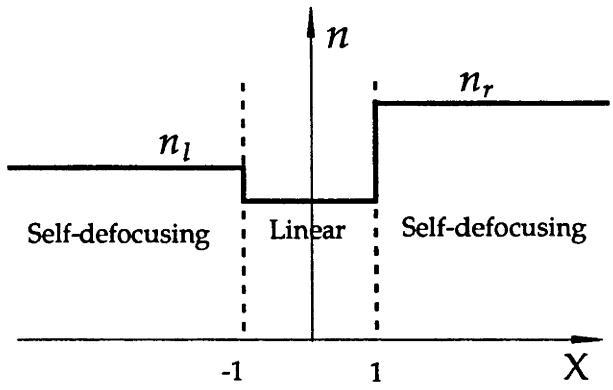

Figure 6.17: Geometry of an asymmetric waveguide with self-defocusing bounding media.

The characteristically new feature of this class of asymmmetric modes is that the modal solution is given by a cosech function in the left medium, instead of a tanh function as in previous cases. The right medium again has a solution in the form of a tanh function as before. For this reason, this class of solutions may be called the asymmetric class of a 'half-dark' type. In terms of the effective index n_{eff}, a necessary condition for this type of solutions to exist is $n_l < n_{eff} < n_r$.

In fact, simple exact modal solutions of the 'half-dark' type also exist in terms of the cosech function (see chapter 2) when the left medium is generally power-law self-defocusing.

6.3 Experimental Relevance

One of the main advantages of dark waves is their very high degree of stability compared with their bright counterparts [37]. The numerical simulations in this section have also shown that if a dark mode is stable according to linear analysis, then it is very stable (i.e. to relatively large perturbations). In fact, Ref.[37] has reported the formation of dark solitons from plane waves with a π phase jump as an initial perturbation.

So far, no experiments on dark modes guided by interfaces or waveguides have been reported. However, the results of the reported experiments with homogeneous media can be used to verify, to some extent, the validity of the theoretical calculations presented here in this chapter.

For example, the experiment in Ref.[37] used a self-defocusing medium (chlorophyll in an ethanol solvent) with $n_{2r} = -5 \times 10^{-7}$ cm^2/W at wavelength $\lambda = 514$

nm and intensities around 20-30 W/cm^2. If we use this value of n_{2r} for the right medium of a SDF-SDF interface, which has $S = 2$ (see fig.6.5) and dimensionless intensities $|\psi|^2$ of around 4, then the expression (2.48) shows that the index-squared jump $n_r^2 - n_l^2$ between the left and right media must be of the order of $3 - 4 \times 10^{-5}$. This is consistent to the index change, of the order of 10^{-6}, due to nonlinearity reported in [37].

Chapter 7

Generalization, Discussions, and Conclusion

This is the last chapter of the thesis.

The first section of the chapter extends some of the works in the preceeding chapters to deal with power-law nonlinearities which include Kerr nonlinearities as special cases. The extension was motivated primarily by a quest to understand theoretically how the characteristics of guided waves depend on the nonlinear exponent q (which is equal to 1 in the Kerr-law case). In reality, it has been shown that power-law nonlinearities where $q < 1$ may be possible in semiconductors [45]-[48].

The second section is some general discussions about nonlinear films, an extension that could have been studied in a similar manner, and on other important aspects of nonlinear guided-wave optics, such as the effects of material absorption, nonlinear saturation, diffusion, and the question of mode excitation. These issues are of course crucially important in the practical realization of nonlinear guided waves, such as those investigated in this thesis.

The final section is a few words of conclusion, re-encapsulating the main contributions of this thesis to our base of knowlegde of nonlinear guided-wave optics, and suggesting some directions for future research efforts.

7.1 Guided Waves in Power-law Media

This is not the first time that power-law nonlinearities are studied. For example, Ankiewicz and Peng [119] recently investigated power-law nonlinear optical fibers; Stegeman et al. [120,51], Langbein et al. [58], also studied briefly their effect on the dispersion of planar surface and guided waves.

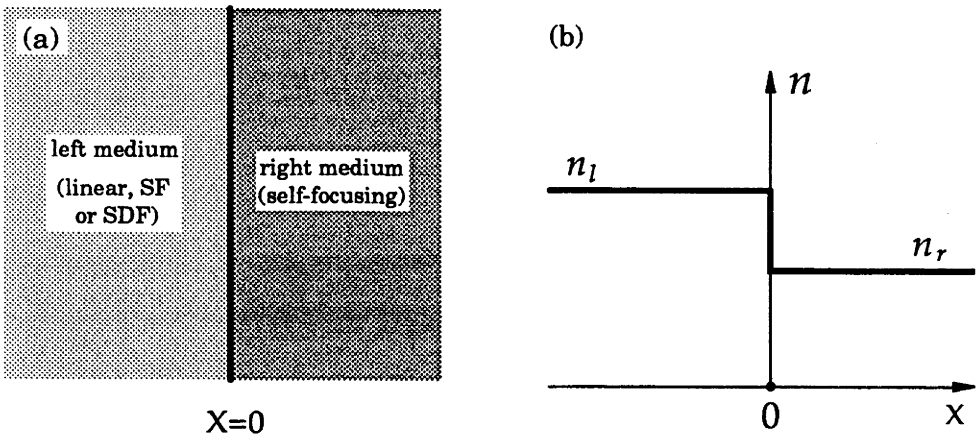

Figure 7.1: (a) Geometry of a power-law nonlinear planar interface. (b) linear index profile.

The structures studied here are nonlinear interfaces and slab waveguides similar to those considered in chapters 4, 5 and 6. In terms of refractive index n, the power-law nonlinearity can be expressed as

$$n = n_0 + n_2|E|^{2q},$$

where n_0 is the linear index, and n_2 is the nonlinear coefficient (which is not necessarily in units of m^2/W). It is found that guided waves in structures which involve a nonlinearity with $q > 4$ are all unstable.

The structure of this chapter is as follows: section 7.1.1 examines surface waves in various types of interface: SF-SF, L-SF, and SDF-SF. Section 7.1.2 studies slab waveguides with a linear core and self-focusing or self-defocusing bounding media. Lastly, section 7.1.3 discusses the stability of these surface and guided modes by using Mitchell and Snyder's theorem (chapter 3).

7.1.1 Surface Waves

The geometry of a power-law interface is depicted in fig.7.1. The interface is located at $X = 0$, between two generally dissimilar power-law media. The left medium may be linear, self-focussing, or self-defocusing, while the right medium is self-focusing. In special cases where only linear and Kerr nonlinearitiesare involved, it is well-known [97,92] that surface-guided waves can exist. Here, we show that this fact is not restricted to Kerr nonlinearities.

As has been mentioned in chapter 2, the field ψ in power-law cases is defined as

$$\psi = \alpha_r^{1/2q_r} E$$

where $\alpha_r = 2n_0 n_{2r} \rho^2 k^2$ is the scaled nonlinear coefficient of the right medium. The definition of the asymmetry parameter η is now

$$\eta = \frac{\alpha_r^{q_l/q_r}}{|\alpha_l|}.$$

The modal parameters W_r and W_l have the same definitions as before, and are all real and positive for bright modes. As for the 'dark' surfaces in chapter 6, here we define a surface parameter $S = \rho k (n_l^2 - n_r^2)^{1/2}$.

The scalar wave equation for these types of interace takes the form

$$\begin{aligned} \psi'' - W_l^2 \psi + \frac{h}{\eta} \psi^{2q_l+1} &= 0, \qquad X < 0 \\ \psi'' - W_r^2 \psi + \psi^{2q_r+1} &= 0, \qquad X > 0 \end{aligned} \tag{7.1}$$

where $h = -1, 0, \text{or } -1$ depending on whether the left medium is self-defocusing, linear, or self-focusing.

SF-SF Interface

This case has $h = 1$ in (7.1) which has solutions

$$\psi = \begin{cases} \left[\eta W_l^2 (1+q_l)\right]^{1/2q_l} \operatorname{sech}^{1/q_l} \left[q_l W_l (X - X_l)\right], & X < 0 \\ \left[W_r^2 (1+q_r)\right]^{1/2q_r} \operatorname{sech}^{1/q_r} \left[q_r W_r (X - X_r)\right], & X > 0 \end{cases} \tag{7.2}$$

where X_l, X_r are constants to be determined. When $q_l = q_r = 1$, these solutions reduce to the well-known sech solutions [87,88]. The continuity of ψ and ψ' at $X = 0$ leads to

$$\left[\eta W_l^2 (1+q_l)\right]^{1/2q_l} s_l = \left[W_r^2 (1+q_r)\right]^{1/2q_r} s_r, \tag{7.3}$$

$$\left[\eta W_l^2 (1+q_l)\right]^{1/2q_l} (-W_l)\, s_l\, t_l = \left[W_r^2 (1+q_r)\right]^{1/2q_r} (-W_r)\, s_r\, t_r, \tag{7.4}$$

where $s_i = \operatorname{sech}^{1/q_i}[q_i W_i(-X_i)]$, and $t_i = \tanh[q_i W_i(-X_i)]$. Hence

$$W_l\, t_l = W_r\, t_r. \tag{7.5}$$

From (7.3),

$$s_l^2 = \frac{[W_r^2(1+q_r)]^{q_l/q_r}}{\eta W_l^2 (1+q_l)} (1 - t_r^2)^{q_l/q_r}. \tag{7.6}$$

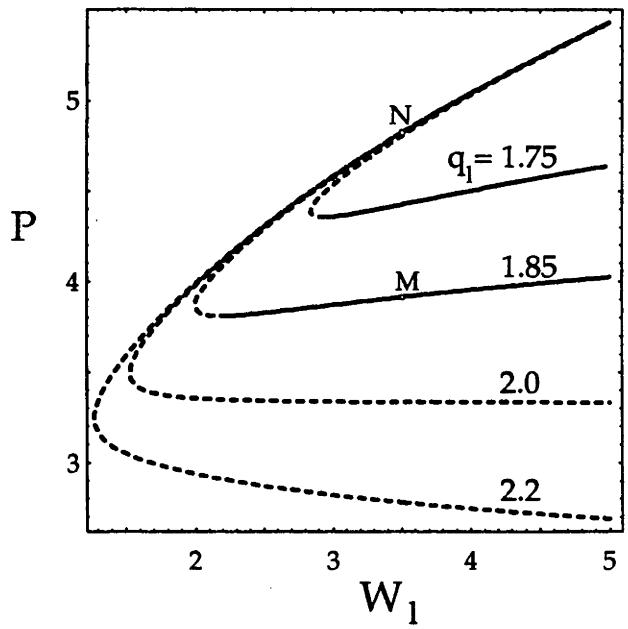

Figure 7.2: Power dispersion curves for $S = 0, q_r = 1.5$, and several values of q_l. Solid lines indicate stability.

With this, (7.5) becomes a single equation for t_r

$$\boxed{\pm W_l (1 - s_l^2)^{1/2} = W_r t_r} \tag{7.7}$$

which may be taken as a dispersion relation. Once t_r is known, other parameters X_l and X_r follow. Modal power $P = \int_{-\infty}^{\infty} \psi^2 dX$ in the general case where $q_l \neq 1$, $q_r \neq 1$ cannot be given in a closed and simple form, but it can always be calculated numerically on a computer. Some typical power dispersion curves for this type of interface are shown in fig.7.2. Along each dispersion curve (corresponding to a particular q_l), the upper (lower) branch has the peak of the field in the right (left) medium, corresponding to the plus (minus) sign in (7.7) . One can observe that the upper branches of the curves almost coincide with one another at large W_l, where the left medium has little effect. As q_l increases, less power is required to achieve the same W_l, because the left medium becomes more nonlinear. Some typical mode profiles are shown in fig.7.3

A characteristics of these bright surface modes is that the field amplitude at the interface is independent of modal power P. Indeed, only straightforward algebra, involving the dispersion relation (7.7), is needed to show that the interface field

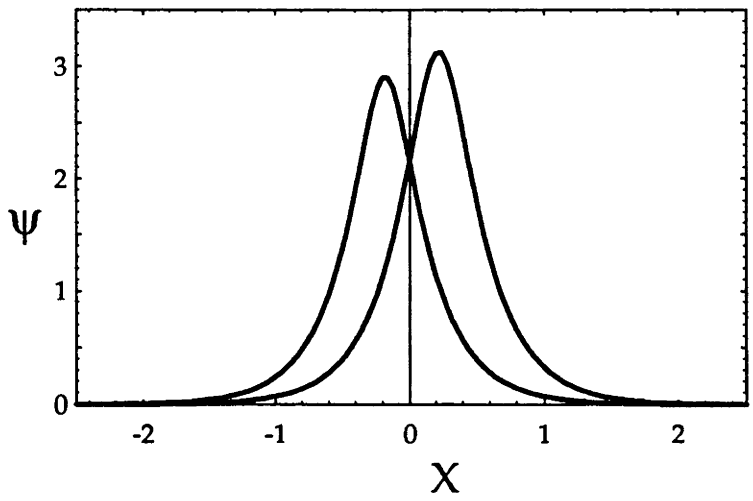

Figure 7.3: Mode profiles corresponding to points M (left peak) and N (right peak) of fig.7.2 with $W_l = 3.5$, $q_l = 1.85$.

amplitude, denoted by A, is

$$A = [W_r^2(1+q_r)]^{1/2q_r} s_r^{1/q_r}, \tag{7.8}$$

and satisfies

$$\frac{A^{2q_r}}{1+q_r} - \frac{A^{2q_l}}{\eta(1+q_l)} = S^2. \tag{7.9}$$

This equation does not involve W_r or W_l, but depends only the surface parameter S, η, and q_r, q_l. In the case when $q_l = q_r = 1$ (i.e. Kerr interface), then A is given simply by

$$A = S/\sqrt{\frac{\eta - 1}{2\eta}}$$

which agrees with the calculations in Ref.[60]. For arbitrary q_l, q_r, equation (7.9) would have to solved numerically.

Equation (7.9) can also serve as a test for the existence of these surface modes, since surface modes exist only if (7.9) has a real and positive root for A. In the case of Kerr-Kerr interface, this condition is simply: $\eta > 1$ and $S > 0$.

It should be stressed that, in Kerr-Kerr or Kerr-linear interfaces, surface modes require $n_r \neq n_l$, but in power-law interfaces, this is no longer a necessary condition.

Linear-SF Interface

This type of interface may be rgarded as a limit of the type considered in the preceeding subsection when $\alpha_l \to 0$, or $\eta \to \infty$. The nonlinear exponent q_l may be

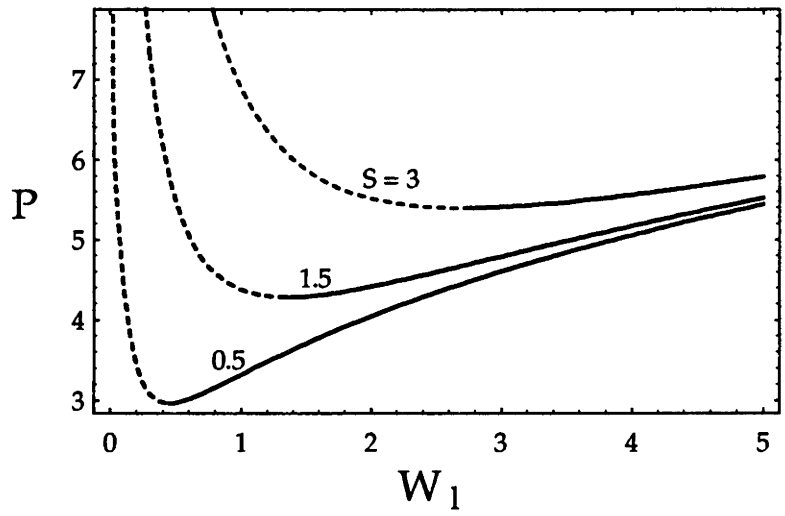

Figure 7.4: Power dispersion curves for linear-SF interfaces. here $q_r = 1.5$. Solid lines indicate stability. All curves approach infinity at $W_l \to 0$.

taken to be any positive number.

As in the linear-Kerr interface first studied by Tomlinson [97], the peak of the surface mode can only be in the nonlinear right medium. The field at the interface then becomes

$$A = S^{1/q_r}(1 + q_r)^{1/2q_r} \tag{7.10}$$

Fig.7.4 displays typical power-dispersion curves for this type of interface for $q_r = 1.5$ and several values of S. At a fixed W_l, it can be observed that an increase in S causes in an increase in power; this is partly indicated by (7.10). On the other hand, an increase in q_r would shift the dispersion curves downward, because less power is needed with larger nonlinearity to obtain the same value of W_l.

SDF-SF Interface

This type of interface (which has $h = -1$ in (7.1)) differs from the SF-SF type in the form of the modal solution in the left medium. Instead of sech function, we now have the cosech function (for the left medium only).

The derivation for the dispersion relation exactly parallels the SF-SF case. Instead of (7.5), (7.6) and (7.7), we now have

$$W_l \coth(-X_l q_l W_l) = W_r t_r, \tag{7.11}$$

$$c_l^2 = \operatorname{cosech}^2(-X_l q_l W_l) = \frac{[W_r^2(1 + q_r)]^{q_l/q_r}}{\eta W_l^2(1 + q_l)}(1 - t^2)^{q_l/q_r}, \tag{7.12}$$

$$-W_l(1+c_l^2)^{1/2} = W_r\, t_r \tag{7.13}$$

respectively. Here, the peak of the surface mode can reside only in the right medium.

The field A at the interface, again given by (7.8), is also independent of power, and satisfies almost the same expression as (7.9):

$$\frac{A^{2q_r}}{1+q_r} + \frac{A^{2q_l}}{\eta(1+q_l)} = S^2 \tag{7.14}$$

This is interesting and unexpected because one would expect that, at higher powers, the field would shift into the right medium due to the self-defocusing effect, and hence that A would decrease. Expression (7.14) implies this is not the case, because at higher modal powers, there is actually less power in the left medium, and hence the self-defocusing effect becomes less and less dominant.

From (7.14), the existence requirement for bright surface waves along this type of interface is simply: $S > 0$ (or $n_l > n_r$), and any (positive) value of η.

Another interesting feature of this type of interface is that dispersion curves terminate at finite powers when $W_l = 0$, as can be seen in fig.7.5 and fig.7.6. This is because the waveguides induced by the modes themselves become cut off at $W_l = 0$. Fig.7.5 shows the variation of modal power with q_l while keeping S, q_r, and η fixed. It is observed that, at low values of W_l, P increases with q_l. This is because the field is shifted more into the right medium and becomes larger to compensate for the self-defocusing effect of the left medium. Fig.7.6 shows a similar variation with S while keeping q_r, q_l and η constant. An explanation for the behaviour in this case is similar to that for the linear-SF interface.

Finally, we'd like to comment that one could go on and study cases in which the linear index profiles are step-like but graded, such as those carried out by Varshney et al.[121] and Wachter et al.[122] who studied an interface between a linear exponential-like graded-index medium and a Kerr self-focussing one.

7.1.2 Guided Waves

The investigation here is analogous to that of chapter 4. However, for simplicity, only TE_0 modes are investigated in these structures. Qualitative properties of higher-order modes can then be inferred from these TE_0 modes and the TE_1 modes of the Kerr-law case.

The waveguide structure examined here is similar to that described in fig.4.1 of chapter 4, except that the bounding media are now power-law. The definitions of modal parameters W_r, W_l, and B_{co} are also the same. There are now two waveguides

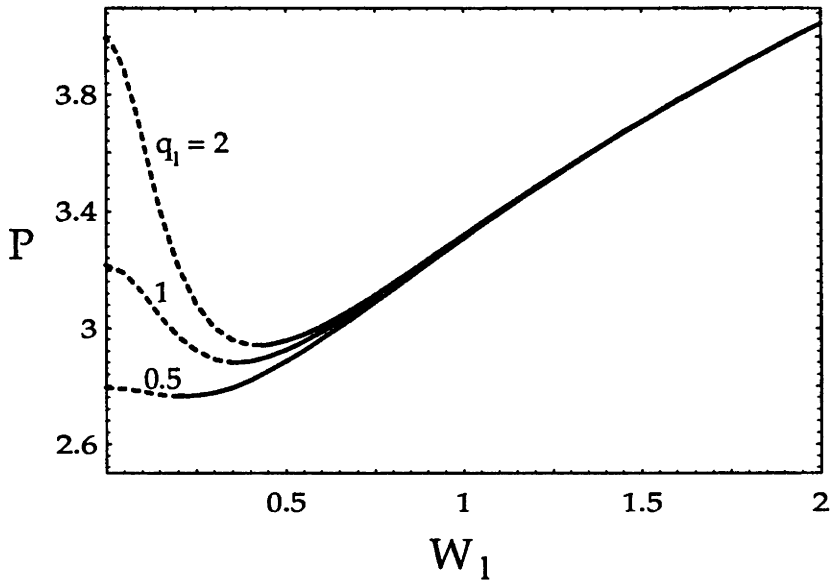

Figure 7.5: Power dispersion curves for SDF-SDF interfaces. $S = 0.5$, $q_r = 1.5$ and $\eta = 3.5$. Solid lines indicate stability. All curves terminate at finite powers when $W_l = 0$.

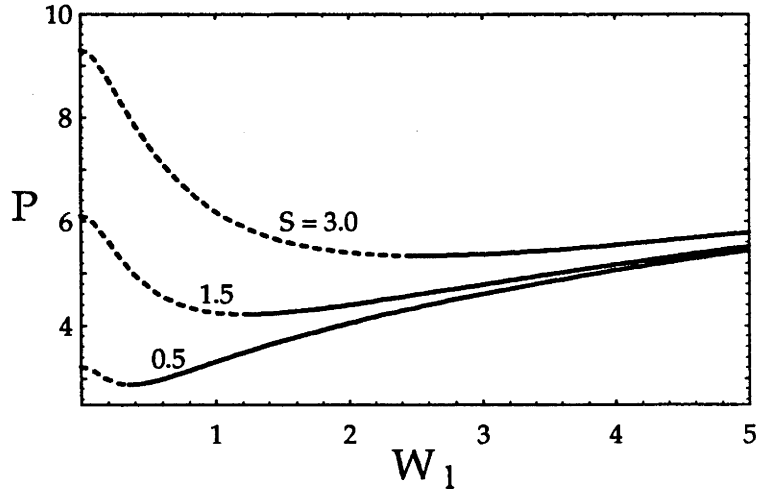

Figure 7.6: Power dispersion curves for SDF-SF interfaces. $q_l = 2$, $q_r = 3$ and $\eta = 3.5$. Solid lines indicate stability. All curves terminate with finite powers at $W_l = 0$.

parameters V_r and V_l defined by $V_i = \rho k(n_{co}^2 - n_i^2)^{1/2}$ for the left and right media respectively. We consider all possible nonlinear-linear-nonlinear combinations: both bounding media being self-focusing (subsection 7.1.2); both being self-defocusing (subsection 7.1.2); and one self-focusing, one defocussing (subsection 7.1.2).

Self-focusing bounding media

The derivation of dispersion characteristics is completely analogous to the case studied in section 4.2 of chapter 4. The modal solutions in the bounding media are again given by (7.2); the solution in the linear core is the familiar hyperbolic (or trigonometric) form (2.15). Without going into details, the dispersion relation for this case is

$$\boxed{\left\{\psi_r\sqrt{B_{co}}\,\frac{1}{cs}\,(1-t^2)^{1/2q_r} - \psi_l\sqrt{B_{co}}\,\frac{s^2+c^2}{cs}\Gamma\right\}^2 = 4W_l^2\psi_l^2\,\Gamma^2\,(1-\Gamma^{2q_l})} \qquad (7.15)$$

where

$$\begin{aligned}
\psi_r &= [(1+q_r)W_r^2]^{1/2q_r} \\
\psi_l &= [\eta(1+q_l)W_l^2]^{1/2q_l} \\
t &= \tanh\left[W_r q_r(1-X_r)\right] \\
\Gamma &= \mathrm{sech}^{1/q_l}\left[W_l q_l(-1-X_l)\right] \\
&= \pm\frac{2W_r\psi_r cs}{\psi_l\sqrt{B_{co}}}(1-t^2)^{1/2q_r}\,t \pm \frac{\psi_r(s^2+c^2)}{\psi_l}(1-t^2)^{1/2q_r}
\end{aligned}$$

and $c = \cosh(\sqrt{B_{co}})$, $s = \sinh(\sqrt{B_{co}})$. Once t is determined from (7.15), other parameters X_l, X_r follow. As for power-law surface waves, guided power P is calculated numerically on a computer.

Fig.7.7 displays dispersion curves for TE_0 modes in an asymmetric waveguide having symmetric linear index profile. Mode shapes along the various branches are very similar to the case of chapter 4. The crossing of the two branches in fig.(7.7) does not entail a 'crossing' of the field profiles. For high values of B_{co}, we observe that the lower arm of the upper branch is below the lower branch (which has a linear limit), although the fields corresponding to both arms are surface-like and stable. This would become immediately self-evident when it is recalled that the mode with a peak in the more nonlinear medium must have a lower power.

Regarding the index profiles induced by these modes in the waveguide, an example which resembles a coupler at high powers is shown in fig.7.8(a). This could be the basis of the switching operation of a weak signal launched at a different wavelength into one of the channels of the induced coupler.

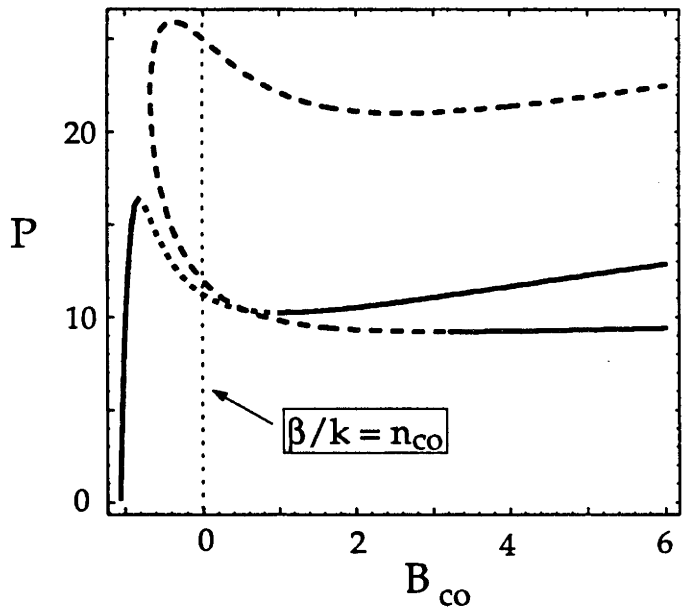

Figure 7.7: Power dispersion curves for a slab waveguide with $V_r = V_l = 2$, $q_r = 1$ (Kerr right medium), $q_l = 1.5$ and $\eta = 1.4$. Solid lines indicate stability.

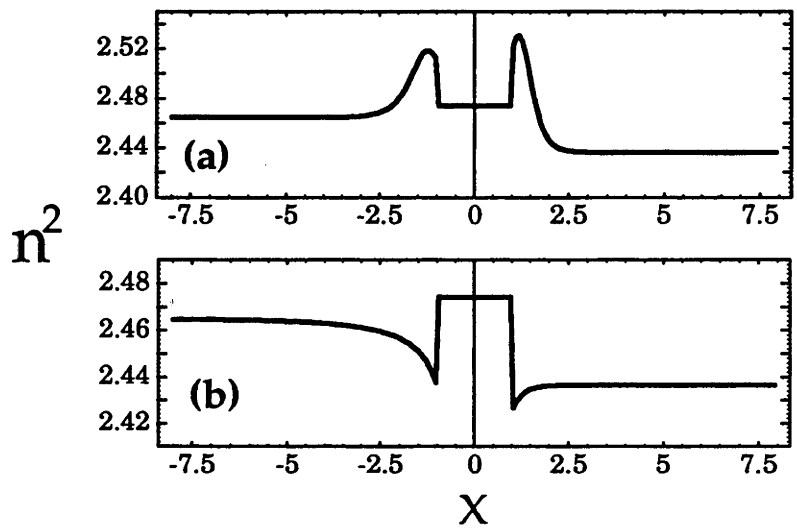

Figure 7.8: Refractive index profiles induced by guided modes. (a) in a SF-L-SF waveguide; (b) in a SDF-L-SDF waveguide.

In the symmetric limit, the branches merge with one another, as in chapter 4, to form a symmetric-mode branch and an asymmetric-mode branch, as shown in fig.7.9. The curves for Kerr-law case are also shown for comparison purposes. However, it should be borne in mind that the power scale in fig.7.9 does not directly reveal the relative real powers of the Kerr-law and power-law cases. This is because in each case, the nonlinear exponent α_r is involved in the scaling (or definition) of power P. However, fig.7.9 contains useful information about the characteristics of each individual type of nonlinearity.

Self-defocusing bounding media

The waveguide geometry discussed here has both bounding media self-defocusing; in them the modal solutions are given in terms of cosech functions. In an analogous manner, it is easy to show that the dispersion relation is now

$$\boxed{\left\{\psi_r\sqrt{B_{co}}\,\frac{1}{cs}\,(t^2-1)^{1/2q_r}-\psi_l\sqrt{B_{co}}\,\frac{s^2+c^2}{cs}\,\Gamma\right\}^2=4W_l^2\psi_l^2\,\Gamma^2\,(1-\Gamma^{2q_l})} \qquad (7.16)$$

where

$$\begin{aligned} t &= \text{cotanh}\,[W_r q_r(1-X_r)] \\ \Gamma &= \text{cosech}^{1/q_l}\,[W_l q_l(-1-X_l)] \\ &= \frac{2W_r\psi_r cs}{\psi_l\sqrt{B_{co}}}(t^2-1)^{1/2q_r}\,t+\frac{\psi_r(s^2+c^2)}{\psi_l}(t^2-1)^{1/2q_r}, \end{aligned}$$

and $B_{co}<0$. Other quantities are as previously defined.

The features of the dispersion curves in the present case are similar to those of the the Kerr-law case studied in chapter 5, namely that dispersion curves always eminate from the linear limit and have a negative slope (i.e. $dP/dB_{co}<0$) throughout. An example is shown by the thin solid curve in fig.7.9. Although this example is for a symmetric waveguide, asymmetry only modifies or distorts the curve slightly; it does not add any new features. As in chapter 5, the dispersion curve may extend to infinite power at some value of B_{co}, or it may terminate abruptly with finite power, depending on the value of V.

Also as in chapter 5, the induced index profiles, like those shown in fig.7.8(b), have a W-shape. At the point where the curve terminates (if it does), the guided mode is a mode at cut-off of this induced W-shape waveguide.

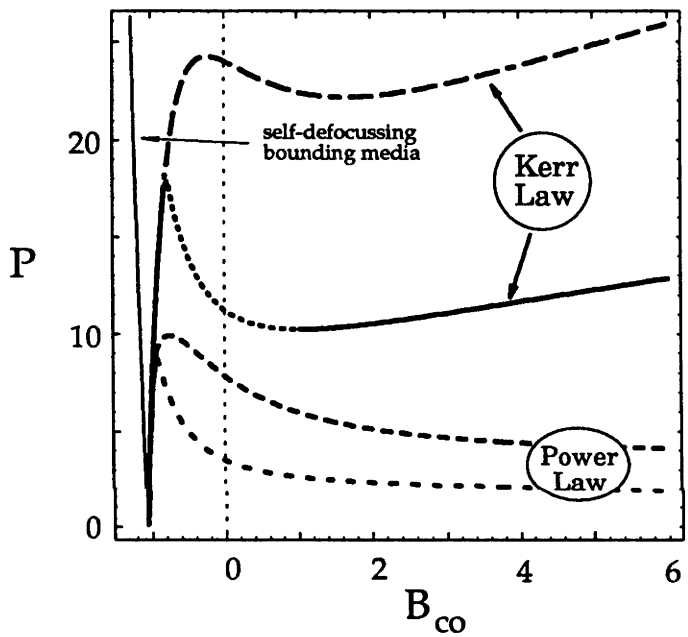

Figure 7.9: Power dispersion curves for symmetric slab waveguides with $V = 2$. The power-law curves have $q_l = q_r = 1.5$. The thin solid line is for a symmetric waveguide with self-defocusing bounding media, with $q_l = q_r = 1.5$. Solid lines indicate stability.

Mixed bounding media

This is the last possible nonlinear-linear-nonlinear combination. Without loss of generality, the left medium is taken to be self-defocusing, the right medium be self-focusing. The waveguide is a really asymmetric one, and hence one would expect to find only one branch in its dispersion diagram. This is indeed true, as seen in fig.7.10. The curve is calculated using the same dispersion relation (7.15) of case where both media are self-focusing, except that now Γ is defined as

$$\Gamma = \text{cosech}^{1/q_l}\left[W_l q_l(-1 - X_l)\right]$$

As is typical of systems involving self-defocusing nonlinearity, the dispersion curve in fig.7.10 eminates from the linear limit with a negative slope before looping into a N shape as W_l increases. The modal field at large values of W_l approaches that of a surface mode at an interface between a linear medium and a self-focusing one.

Because the left medium is self-defocusing and the right medium is self-focusing, the induced index profile has a dip and a spike near the left and right interfaces respectively, as shown by in the inset of fig.7.10. At larger W_l, at which the mode becomes similar to a surface mode at the right interface, the dip would decreases in depth, while the spike would increase in height.

7.1.3 Stability

In all dispersion diagrams of this chapter, solid (non-solid) lines indicate stability (instability). These results are obtained by using Mitchell and Snyder's theorem presented in chapter 3. In some cases, this has to be used in conjunction with an inference about a starting point.

Let us first examine the dispersion curves of surface modes in fig.7.2, which do not feature a linear limit. From Mitchell and Snyder's theorem, it can be definitely concluded that the upper branch is always unstable. The lower branch is stable when the exponent q_l is less than 2, as it then has a positive slope. This result is inferred from the known result [60] of a Kerr-Kerr interface, and from the fact that solitons in a homogeneous power-law medium with nonlinear exponent $q > 2$ are unstable [5]. An interesting fact is noted here: *If a soliton is unstable in a homogeneous medium, it cannot be stabilized by using an interface with another nonlinear medium.* The results indicated in fig.7.4, fig.7.5 and fig.7.6 were obtained, also with similar arguments.

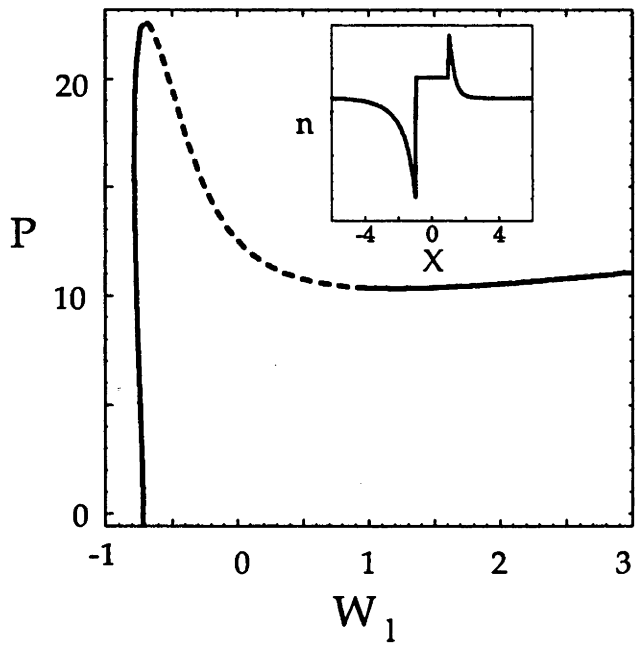

Figure 7.10: Power dispersion curve a slab waveguide with mixed nonlinearities. $V_l = 1$, $V_r = 2$, $q_l = 1.5$, $q_r = 1$, and $\eta = 2$. Solid lines indicate stability.

The case of waveguides is even simpler, because often one of their dispersion curves has a linear limit. For example, in fig.7.7, which shows the dispersion curves of an asymmetric power-law waveguide, the mode is stable from the linear limit to the maximum point, and from the (local) minimum point onwards to higher values of B_{co}, according to Mitchell and Snyder's theorem. The positively sloped part of lower branch of the other (upper) dispersion curve is inferred to be stable because, in the symmetric waveguide limit, it coalesces with the stable part of the lower curve. The remaining part of the upper curve can easily be deduced to be unstable.

Again by Mitchell and Snyder's theorem, it is an easy task to deduce the stability results indicated in fig.7.9 and fig.7.10.

7.2 Discussions

Up to this point, all what we originally have to share in the reservoir of knowledge about this particular field of science, namely nonlinear guided-wave optics, have been presented. Now is some space reserved for some general discussions.

7.2.1 Nonlinear films

We have considered both SF and SDF nonlinearities but only in infinite or semi-infinite media. When they confined in a finite medium, such as a planar film, the field solutions are given in terms of elliptic functions which can be computed using existing numerical algorithms [68]. In the literature, we have seen Akhmediev et al.[123], and Fedyanin et al.[124] investigated a Kerr thin film bounded on both sides by linear dielectric media. Their computational approaches differ but the general result is that TE modes of several orders can be supported, and when the linear part of the film is lower than that of the bounding media, there is a lower power threshold which may potentially be exploited in lower-power threshold devices.

In our point of view, these results could have been anticipated from what we already know about the surface face supported by a single planar interface between a linear and a Kerr SF medium. Further more, based on the elliptic forms of the field solution, one would realize that the nonlinear film can support TE_0 modes which have more than one peak within the film; this has in fact been confirmed by Ogusu [125] who also found that these modes are unfortunately unstable. We anticipate that if the bounding media are allowed to be SDF, instead of linear, then the surface-like TE_0 waves studied by Ogusu may be stable. In general, allowing the bounding media to be nonlinear (either SF or SDF, or mixed) would leading to a much richer modal structure which is mostly, if not all, unstable.

7.2.2 Nonlinear saturation

In a real material the nonlinear index change Δn_{NL} cannot grow without limit due to various mechanisms. In fact, an upper limit for Δn_{NL} in materials available at the present time is about 0.1. The question here is: how does this affect the dispersion characteristics of the nonlinear guided waves ?

The answer is quite simple because the when β/k is close $n_L + \Delta n_{NL}$ (n_L is the zero-power effective index), the system behaves like a linear system. This means all dispersion curves in this thesis, which would extends to infinite β and P, would go asymtotically vertical near this value of β/k. The works by Stegeman et al. [51] for example has confirmed this.

However, it should be self-evident that, in order for saturation not to destroy the interesting nonlinear behaviours discussed so far, an essential requirement is that the linear index mismatch of a waveguide must be less than Δn_{NL}. Regarding stability, Mitchell and Snyder's result allows the stability of TE_0 modes to be determined in

the same way as for Kerr nonlinearities; while for higher-order modes, there are no off-hand answers.

7.2.3 Lossy media

The presence of absorption in real materials, especially in the more nonlinear materials, mathematically destroys the idealized stationary propagation phenomena, because the power carried by a wave must necessarily decrease as it propagates. It is therefore important to know under what circumstances the guided-wave characteristics given by the lossless theory can still be useful, and how the lossless theory has to be modified to include the effects of loss.

In attempts to solve this problem, Ariyasu et al.[126,127] and Boardman et al.[107] have derived analytically the attenuation coefficient of a propagating wave. This coefficient corresponds to the effective refractive index $n_{eff} = n_R + in_I$ being complex, where n_I accounts for absorption. However, it should be noted that the strong assumption used by these authors is that the fields used in the evaluations of n_{eff} is approximately that of the lossless fields. This means that these results only apply to the initial short distance of propagation of an initially stationary state. In their particular example of a linear film bounded by a linear substrate and a very lossy nonlinear cladding (liquid crystal MBBA), the main conclusion is that, while the variation of n_R with power is the same as in the lossless case, n_I (of the order of 10^{-4}) is also dependent on power, and the variation is quite strong.

For the waves studied here, similar derivations are expected to be possible. Furthermore, when loss is small enough, propagation can be adiabatic, and stability characteristics of the lossless case should still hold. The field profile is expected to vary smoothly along a disperion branch while power decreases [128]. If the wave encounters a power miminum in its dispersion branch, it may 'jump' to a lower-power branch with a part of its power radiated into the bounding media. On the other hand, if loss is not small and is distributed non-uniformly across the waveguide structure, then the propagation behaviour is likely to be well beyond the prediction of the lossless theory. For example, a peak initially in one layer might be attracted to another layer as propagation proceeds.

7.2.4 Mode excitation

Just as stability is an important consideration in understanding the propagation of a nonlinear mode, the question of mode launching is also very important from a

practical point of view. How can one excite the mode corresponding to some point on one of the dispersion curves shown in this and the preceeding chapters ? While a rigorous answer to this question is outside the scope of the thesis, some comments can be made as follows.

Firstly, the wanted mode must be stable. In most cases, this condition can be checked using linear stability analysis as described in chapter 3, but in some special cases, nonlinear waves have been experimentally excited although they are unstable according to linear analysis. Examples include one-transverse-dimensional dark solitons in chlorophyl solution [37]. (In our point of view, this is because the solitons are unstable only to long wavelength transverse perturbations which are not available in a bulk medium with a finite (or truncated) transverse dimension.)

Secondly, there must be an appropriate launching technique. Since the advent of integrated optics, there have been suggested at least two methods of guided-wave excitation, namely distributed coupling and end-fire coupling. In distributed coupling, an incident wave is launched into a waveguide through some appropriately prepared structure such as a prism or a grating. These techniques have proved to be useful in linear waveguide optics (see e.g. [31]). However, when nonlinearity is present, it is not clear how coupling can be achieved because of the complicated interaction between transversal and longitudinal nonstationary effects driven by the nonlinear properties of the whole configuration.

In end-fire coupling, appropriately tailored wavefields are launched into the end-face of a nonlinear waveguide. In a practical situation, such launched field can presumably be made possible by mounting a linear waveguide structure at one of the end faces. However, no experiments using this technique have been reported, as far as we are concerned. Numerically, Wright et al. [129] have used an initial wavefield in the form of a gaussian beam with variable width, height and peak position. They found that a mode, which is found to be stable analytically, can be excited only if the initial wavefield is sufficiently close to the exact mode at that input power level. This requirement seems quite hard to be achieved experimentally. If initial mismatch is large, the excited wave may decay via the emission of a soliton into the bounding nonlinear media, or just by diffraction.

We can expect that similar behaviours would also be observed with the TE_0 and TE_1 bright modes studied in this thesis. For dark guided waves, their high stability (in cases they are stable) should make it relatively easy to excite. The technique of end-firing combined with phase masking has been used by many experimentalists, such as Luther-Davies et al.[37] and Swartzlander et al.[111], for dark solitons in

homogeneous medium. And we can expect that these techniques also have some relevance to the cases of dark waves guided by planar interfaces and waveguides.

There has been another launching technique proposed by Lederer et al.[130] which takes the advantage of the phenomena of Bragg reflection. With this technique, it seems possible that linear planar guided modes can be excited by plane waves incident directly from the air. However, it is not clear how it can be applied to nonlinear strutures. Suppose this structure is properly mounted to an end-face of our nonlinear waveguide. How can the excited linear field in the Bragg waveguide can be monitored to closely match an exact mode of our nonlinear waveguide ?

In summary, the question of excitation of nonlinear guided modes is far from satisfactorily answered, except in the restricted framework of numerical simulations.

7.3 Conclusion

In conclusion, the main problems that have been treated in this thesis are:

1. Firstly, modal characteristics of various new modes of light propagation in nonlinear planar interfaces and waveguides, which can be self-focussing, self-defocussing, or mixed, have been analytically calculated. These also include asymmetric and slightly asymmetric waveguide structures. A distinctive feature is that the power dispersion curves for asymmetric waveguides can be very 'dense', or highly structured, especially for the TE_1 modes. For self-defocussing waveguides, dispersion curves are simpler, the propagation constant generaly decareases with increasing modal power, and in which an upper threshold power can exist; this makes it potentially useful for upper threshold devices. Similar characteristics have also been found for power-law nonlinear interfaces and waveguides.

2. Secondly and more importantly, we have found analytical answers to the question of stability for some types of stationary waves (modes), on the basis of linear stability analysis. These waves include 1-transverse-dimensional dark solitons, TE_0, TE_1 and TE_2 waves in symmeric waveguides with Kerr (focussing or defocussing) and power-law bounding media, and surface waves at an interface between a linear medium and a Kerr nonlinear one. Crucial to these findings are simple analytical solutions for the perturbations in linear analysis which also allow the growth rates of instability to be calculated directly. Another important fact arising from these results is that these growth rates are real

for TE_0 modes but can be complex for higher-ordered modes, contrary to the long believed assumption.

We have also reviewed, clarified some of the current analytical stability studies.

3. Finally, we have briefly discussed related problems and practical issues such as materials, material absorption, nonlinear saturation, and mode excitation.

After all, the works presented here, although certainly contributing our base of knowledge of nonlinear guided-wave optics, seems to be only the start of a more fruitful and profitable intellectual adventure.

Among the topics that have been left out, and will probably be touched on in the near future, is the case of TE propagation in fibers with circular cross-sections. This geometry is convenient as it allows the exact calculation of the TE waves, whose characteristics should have some similarities to their planar counterparts.

The stability to perturbations in polarizations other than that of a mode is another important question, from both practical and theoretical perspectives.

And, for example, what happens if we have not cw light but pulses propagating down a nonlinear waveguide ? These are some of the seemingly endless questions that the author of this thesis will humbly try to answer, in the course of his time ...

That was me (second from right) in 1978, with my classmates.

Bibliography

[1] J. Tyndall, *Proc. Roy. Inst.*, **1**, p446, (1854)

[2] G.I. Stegeman and C.T. Seaton, 'Nonlinear integrated optics', *Appl. Phys. Rev.*, **58**, p.R57-78, (1985)

[3] C.T. Seaton, Xu Mai, G.I. Stegeman and H.G. Winful, 'Nonlinear guided waves applications', *Opt. Eng.*, **24**, pp593-99, (1985)

[4] A.W. Snyder, D.J. Mitchell, L. Poladian, and F. Ladouceur, 'Self-induced optical fibers - spatial solitary waves', *Opt. Lett.* , **16**, 21-23 (1991)

[5] A.W. Snyder and D.J. Mitchell, 'Spatial solitons of the power law nonlinearity', *Opt. Lett.* , (to be published)

[6] A.W. Snyder and H.T. Tran, 'Surface modes of power-law nonlinearities', *Opt. Commun.*, (submitted)

[7] H.T. Tran and A.W. Snyder, 'Power-law nonlinear waveguides', *IEEE J. Quantum Electron.*, (submitted)

[8] D. Marcuse, *Theory of Dielectric Optical Waveguides* , Academic Press, New York (1974)

[9] H. Kogelnik, *Integrated Optics*, Vol.**7**, Topics in Applied Physics, ed. T. Tamir (Springer, Berlin).

[10] J.E. Sipe and G.I. Stegeman, *J. Opt. Soc. Am* , **69**, 1676-93 (1979)

[11] U. Langbein, F. Lederer and H.E. Ponath , *Opt. Quantum Electron.* , **16**, 251-9 (1984)

[12] U. Langbein, F. Lederer and H.E. Ponath , *Opt. Acta* , **31**, 1141-9 (1984)

[13] S.M. Jensen, 'The nonlinear coherent coupler', *IEEE J. Quantum Electron.* , **QE-18**, 1580-83 (1982)

[14] D.Mihalache, M. Bertolotti and C. Sibilia, 'Nonlinear wave propagation in planar structures', in *Progress in Optics* E. Wolf Ed., Vol.**27**, pp229-309, (1989).

[15] A. Hasegawa and F. Tappert, 'Transmission of stationary nonlinear optical pulses in dispersive dielectric fibers, II. Normal dispersion', *Appl. Phys. Lett.* , **23**, 171-2 (1973)

[16] P. L. Kelly, 'Self-focusing of optical beams', *Phys. Rev. Lett.*, **15**, 1005-07, (1964)

[17] R. Y. Chiao, E. Garmire, and C. H. Townes, 'Self-trapping of optical beams', *Phys. Rev. Lett.*, **15**, 479-82, (1964)

[18] Y.R. Shen, *The principles of Nonlinear Optics*,John Wiley & Sons, (1990).

[19] N. Bloembergen, *The principles of Nonlinear Optics*,John Wiley & Sons, (1990).

[20] P N Butcher and D Cotter, *Nonlinear Optics*, Benjamin, New York, (1965).

[21] P.L. Chu and B. Wu, 'Optical switching in twin-core erbium-doped fibers', *Opt. Lett.*, **17**, 255, (1992)

[22] W. Sohler and H. Suche, *Appl. Phys. Lett.*, **33**, p.518, (1978)

[23] R.G. Smith, 'Optical power handling capacity of low loss optical fibers as determined by stimulated Raman and Brillouin', *Sov.Phys.Tech.Phys.* **33**, pp1333-1337, (1988)

[24] R.H. Stolen, E.P. Ippen, and A.R. Tynes, 'Raman oscillation in glass optical waveguide', *Appl. Phys. Lett.* **20**, 62-4, (1972)

[25] W. Kaiser and C.G.B. Garrett, *Phys. Rev. Lett.* **8**, pp404-6, (1961)

[26] E.P Ippen and R.H. Stolen, *Appl. Phys. Lett.* **21**, pp539-40, (1972)

[27] B.E. Briley, *An Introduction to Fiber Optics System Designs*, North-Holland, (1988)

[28] S.E. Miller, 'Overview of telecommunications via optical fibers', *Proc. IEEE* **68**, pp1173-74, (1980)

[29] M.J. Howes, and D.V. Morgan, *Optical Fibre Communications*, John Wiley & Sons, (1980)

[30] Y. Suematsu, and Ken-Ichi Iga, *Introduction to Optical Fiber Communications*, John Wiley & Sons, (1982)

[31] R.G. Hunsperger, *Integrated optics: theory and technology*, 2nd edition, Springer-Verlag, Heidelberg, (1985)

[32] H.P. Nolting Ed., *Integrated Optics*, Springer-Verlag, Heidelberg, (1985)

[33] C. Vassallo, *Optical Waveguide Concepts*, Elsevier Science Publishers, (1991)

[34] A.A. Maier, 'Optical transitors and bistable devices utilizing nonlinear transmission of light in systems with unidirectional coupled waves', *Sov. J. Quantum Electron.* , **12**, 1490-94 (1982)

[35] A.A. Ankiewicz, ' Novel effects in nonlinear coupling', *Opt. Quantum Electron.* , **20**, 329 (1988)

[36] A.W. Snyder, D.J. Mitchell, L. Poladian, D.R. Rowland, and Y. Chen, 'Physics of nonlinear fiber couplers', *J. Opt. Soc. Am. B* , **8**, 2102-2118 (1991)

[37] Barry Luther-Davies, Y. Xiaoping, 'Waveguides and Y-junctions formed in bulk media using dark spatial solitons', *Opt. Lett.* , **17**, 496-8 (1992); 'Steerable optical waveguides formed in self-defocusing media by using dark spatial solitons', *Opt. Lett.* , **17**, 1755-7 (1992)

[38] G.I. Stegeman, 'Material requirements for nonlinear third order phenomena in waveguides', in: Nonlinear Optics: fundamentals, materials and devices, S. Miyata Ed., 337-53 (North-Holland, 1992)

[39] G.I. Stegeman, 'Current status of nonlinear materials and their application to waveguide devices', in: Integrated Photonics Research, Topical Meeting, Palm Springs, (1993)

[40] J.S.Aitchison, A.M.Wiener, Y. Silberberg, M. K. Oliver, J. L. Jackel, D. E. Leaird, E. M. Vogel, and P. W. E .Smith, 'Observation of spatial optical solitons in a nonlinear glass waveguide', *Opt. Lett.*, **15**, 471-3 (1990)

[41] C. Sauteret, J.P. Hermann, R. Frey, F. Pradere, and J. ducuing, *Phys. Rev. Lett.*, **36**, p.956, (1976)

[42] R.W. Munn and C.N. Ironside, *Principles and Applications of Nonlinear Optical Materials*, Blackie Academic & Professional, CRC Press, (1993)

[43] V. E. Zakharov and A. B. Shabat, 'Interaction between solitons in a stable medium', *Sov. Phys. JETP*, **37**, 823-28 (1973)

[44] V. E. Zakharov and A. B. Shabat, 'Exact theory of two-dimensional self-focusing and one-dimensional self-modulation of waves in nonlinear media', *Sov. Phys. JETP*, **34**, 62-9, (1972)

[45] R.K. Jain, and R.C. Lind, *J. Opt. Soc. Am.*, **73**, 647 (1983)

[46] D.S. Chemla, D.A.B. Miller, P.W. Smith, *Opt. Eng.*, **24**, 556 (1985)

[47] J.G.H. Mathew, A.K. Kar, N.R. Heckenberg, and I. Galbraith, *IEEE J. Quantum Electron.*, **QE-21**, 774 (1985)

[48] S.S. Yao, C.Karaguleff, A. Gabel, R. Fortenberry, C.T.Seaton, and G.I. Stegeman, 'Ultrafast carrier and grating lifetimes in semoconductor-doped glasses', *Appl. Phys. Lett.* , **46**, 801 (1985)

[49] A. W. Snyder, J. D. Love, *Optical waveguide theory*, Chapman & Hall, (1983)

[50] S.J. Al-Bader and H.A. Jamid, 'Guided waves in nonlinear saturable self-focusing thin films', *IEEE J Quantum Electron.* **23**, p1947, (1987)

[51] G.I. Stegeman, E.M. Wright, C.T. Seaton, J.V. Moloney, T-P Shen, A.A. Maradudin and R.F. Wallis, 'Nonlinear slab-guided waves in non-Kerr-like media', *IEEE J. Quantum Electron.*, **QE-22**, 977-983 (1986)

[52] D.Mihalache, D.Mazilu, M. Bertolotti and C. Sibilia, 'Exact solutions for transverse electric polarized nonlinear guided waves in saturable media', *J. Mod. Opt.* **35**, pp1017-1027, (1988).

[53] V.E. Wood, E.D. Evans, and R.P. Kenan, 'Soluble saturable refractive-index nonlinearity model', *Opt. Commun.* **69**, pp156-60, (1988).

[54] See for example, Tyn Myint-U and L. Debnath, *Partial Differential Equations for Scientists and Engineers, 3rd Ed.*, North-Holland, (1987), p.436

[55] A.W. Snyder, D.J. Mitchell, and B. Luther-Davies, 'Black and gray spatial solitons', *J. Opt. Soc. Am. B*, (submitted)

[56] C.T. Seaton, J.D. Valera, R.L. Shoemaker, G.I. Stegeman, J.T. Chilwell, and S.D. Smith, 'Calculations of nonlinear TE waves guided by thin dielectric films

bounded by nonlinear media', *IEEE J. Quantum Electron.*, **QE-21**, 774-82 (1985)

[57] K.M. Leung, *Phys. Rev. A* **31**, p1189, (1985); *Phys. Rev. B*, **32** pp.5093-101, (1985).

[58] , U. Langbein, F. Lederer and H.E. Ponath , *Opt. Commun.*. , **53**, 417-20 (1985)

[59] C. K. R. T. Jones and J. V. Moloney, 'Instability of standing waves in nonlinear optical waveguides', *Phys. Lett. A*, **117**, pp175-80, (1986)

[60] A. B. Aceves, J. V. Moloney, and A. C. Newell, 'Theory of light beam propagation at nonlinear interfaces. I. Equivalent-particle theory for a single interface', *Phys. Rev. A*, **39**, pp.1809-1827, (1989)

[61] N. N. Akhmediev, 'Novel class of nonlinear surface waves: asymmetric modes in a symmetric layered structure', *Sov. Phys. JETP*,**56** 299-303, (1982)

[62] M.D. Feit and J.A. Fleck,Jr., 'Light propagation in graded-index optical fibers', *Appl. Opt.*,**24** 3990–98, (1978)

[63] J. Van Roey, J.van der Donk, and P.E. Lagasse, 'Beam-propagation method: analysis and assessment', *J. Opt. Soc. Am.*,**71** 803-1-, (1981)

[64] R. Scarmozzino and R.M. Osgood,Jr., 'Comparison of finite-difference and Fourier-transform solutions of the parabolic wave equation with emphasis on integrated-optics applications', *J. Opt. Soc. Am. A*,**8** 724-31, (1991)

[65] O.C. Zienkiewicz, *The Finite Element Method*, McGraw-Hill, 3rd ed. (1977)

[66] S.D. Conte and C. de Boor, *Elementary Numerical Analysis - An Algorithmic Approach, 3rd Ed.*, McGraw-Hill, (1980).

[67] T.R. Taha and M.J. Ablowitz, 'Analytical and Numerical Aspects of Certain Nonlinear Evolution Equaion', *J. Computional Phys.*, **55**, 203-30 (1984).

[68] W.H. Press, B.P. Flannery, S.A. Teukolsky, and W.T. Vetterling, *Numerical Recipes: The art of scientific computing*, Cambridge University Press (1986)

[69] L. Leine, Ch. Wachter, U. Langbein, and F. Lederer, 'Propagation phenomena of nonlinear film-guided waves: a numerical analysis', *Sov.Phys.Tech.Phys.* **32**, pp104-5, (1987)

[70] N.N. Akhmediev and N.V. Ostrovskaya, 'Stability of nonlinear waves in a symmetric planar waveguide', *Sov.Phys.Tech.Phys.* **33**, pp1333-1337, (1988)

[71] N. V. Vysotina, N. N. Rozanov, and V. A. Smirnov, 'Small-scale self-focusing of nonlinear surface waves', *Sov.Phys.Tech.Phys.* **32**, pp104-5, (1987)

[72] A. A. Kolokolov, 'Stability of the lowest-order mode of a nonlinear wave equation in a cubic medium', *Lettere al Nuovo Cimento*, **8**, 197-200, (1973)

[73] D.J. Mitchell and A.W. Snyder, 'Stabiltiy of fundamental modes on nonlinear optical guides', *J. Opt. Soc. Am. B*, (submitted)

[74] H. T. Tran, J. D. Mitchell, N. N. Akhmediev, and A. Ankiewicz, 'Complex eigenvalues in stability analysis of nonlinear planar guided waves', *Opt. Commun.* **93**, 227, (1992).

[75] H.T. Tran and A.Ankiewicz, 'Instability regions of nonlinear planar guided waves', *IEEE J. Quantum Electron.*, **QE-28**, 488-92 (1992).

[76] H. T. Tran, 'Stability of dark solitons: linear analysis', *Phys. Rev. A*, **46**, 7319-21 (1992)

[77] H. T. Tran, 'Stability of bright TE waves in slab waveguides with a self-defocusing bounding medium', *Opt. Lett.*, **17**, 1767-9 (1992)

[78] N.N. Akhmediev, V.I. Korneev, and Y.V. Kuz'menko, 'Excitation of nonlinear surface waves by Gaussian light beams', *Sov Phys. JETP*, **61**, 62 (1985)

[79] J.V. Moloney, 'Transverse effects in nonlinear optics', in: *Proc. NATO ASI School*, Lucca, Italy (1987)

[80] F.R. Gantmakher, 'Lectures in Analytical Mechanics', Mir Publisher, Moscow, 1966.

[81] D. Hart and E. M. Wright, *Opt. Lett.*, 'Stability of the TE_0 guided wave of a nonlinear waveguide with a self-focusing bounding medium', **17**, 121, (1992).

[82] E.A. Kuznetsov, A.M. Rubenchik, and V.E. Zakharov, 'Soliton stability in plasma and hydrodynamics', *Phys. Rep.* **142**, 104, (1986)

[83] R.A. Sammut, Q.Y. Li, and C. Pask, 'Variational approximations and mode stability in planar nonlinear waveguides', *J. Opt. Soc. Am. B*, **9**, 884 (1992)

[84] J. Ariyasu, C. T. Seaton, G. I. Stegeman, and J. V. Moloney, 'New theoretical developments in nonlinear guided waves: Stability of TE_1 branches', *IEEE J. Quantum Electron.* **QE-22**, pp984-6, 1986

[85] L. Torner and J.P Torres, 'Similarity rules for nonlinear Kerr-like slab optical waveguides', *IEEE J. Quantum Electron.*, **28**, pp1571-85 (1992)

[86] U. Langbein, F. Lederer, T. Peschel, and H.E. Ponath, *Opt. Lett.* **10**, 571, (1985)

[87] M. Miyagi and S. Nishida, *Sci. Rep. Tohoku Univ. B* **24**, 53, (1972)

[88] A.E. Kaplan, *Sov. Phys. JETP* **24**, 114, (1976); *Sov. Phys. JETP* **45**, 896, (1977);

[89] G.I. Stegeman, C.T. Seaton, J.T. Chilwell and S.D. Smith, *Appl. Phys. Lett.* **44**, 830, (1984)

[90] D. Mihalache, D. Mazilu, and H. Totia, *Phys. Scr.* **30**, 335, (1984)

[91] A. Boardman and P. Egan, 'Theory of optical hysteresis for TE guided modes', *Phil. Trans. R. Soc. Lond. A* **313**, pp363-9, (1984)

[92] A.A. Maradudin, in: *Optical and acoustic waves in solids: modern topics*, ed. M. Borissov, p.72, World Scientfic Publishing, Singapore, (1983)

[93] A.D. Boardman and P.Egan *J. Phys. Colloq.* (France) **45**, C5-291-303, (1984)

[94] A.D. Boardman and P.Egan, *IEEE J. Quantum Electron.* **QE-21**, 1701-13, (1985); *IEEE J. Quantum Electron.* **QE-22**, 319-24, (1986)

[95] A.Ankiewicz and H.T.Tran, 'A new class of nonlinear guided waves', *J. Mod. Opt.*, **38**, pp1093-1106, (1991)

[96] N.N. Akhmediev, A. Ankiewicz, and H.T. Tran, 'Stability analysis of even and odd waves of symmetric nonlinear planar optical waveguides', *J. Opt. Soc. B*, **10**, 230-6, (1993)

[97] W. J. Tomlinson, 'Surface waves at a nonlinear interface', *Opt. Lett.*, **5**, 323-5, (1980)

[98] V.M.Agranovich, V.S.Babichenko, V.Ya.Chernyak, *JETP Lett.*, **32**, p.512, (1980).

[99] A. A. Maradudin, 's-polarized nonlinear surface polaritons', *Z. Phys. B*, **41**, pp.341-344, (1981)

[100] A.Ankiewicz, 'Novel effects in nonlinear coupling', *Opt.Quant.Electron*, **20**, pp.329-337 (1988).

[101] R.J.Black and A.Ankiewicz, *Am.J.Phys.*, **53**, pp.554-563, (1985).

[102] H. Vach, C.T. Seaton, G.I. Stegeman and I.C. Khoo, 'Observation of intensity-dependent guided waves', *Opt. Lett.*, **9**, 238-40 (1984)

[103] I. Bennion, M.J. Goodwin, and W.J. Stewart, 'Experimental nonlinear optical devices', *Electron. Lett.*, **21**, 41 (1985)

[104] N.N. Akhmediev, *Sov. Phys. JETP*, **56**, 299-303, (1982)

[105] C.T. Seaton, J.D. Valera, R.L. Shoemaker, G.I. Stegeman, J.T. Chilwell, and S.D. Smith, *Appl. Phys. Lett.*, **45**, 1162-63, (1985)

[106] N.N. Akhmediev, *Sov. Tech. Phys. Lett.*, **198**, 249-50, (1982)

[107] A.D. Boardman, P. Egan, F. Lederer, U. Langbein, and D. Mihalache, 'Third-order nonlinear electromagnetic TE and TM guided waves', in: Nonlinear Surface Electromagnetic Phenomena, ed. H.E. Ponath and G.I. Stegeman, North-Holland, chap.2, (1991)

[108] G.I. Stegeman, C.T. Seaton, W.M. Hetherington III, A.D. Boardman and P. Egan, in: Nonlinear Optics: Materials and Devices, eds. C. Flytzanis and J.L. Oudar (Springer, Berlin) (1986)

[109] K. Hayata, M. Koshiba, and M. Suzuki, 'Finite-Element solution of arbitrarily nonlinear, graded-index slab waveguides', *Electron. Lett.*, **23**, 429-31, (1987)

[110] H.T. Tran, 'Stability of stationary dark waves guided by nonliner surfaces and waveguides', *J. Opt. Soc. Am. B*, (to be published)

[111] G.A. Swartzlander, D.R. Andersen, J.J. Regan, and A.E. Kaplan, 'Observation of spatial dark waves and solitons, *OSA Annual Meeting*, Vol. 18 of 1989 OSA Technical Digest Series, p.272

[112] D.R. Andersen, D.E. Hooton, G.A. Swartzlander, A.E. Kaplan, 'Direct measurement of the transverse velocity of dark spatial solitons', *Opt. Lett.*, **15**, 783-5, (1990)

[113] G.R. Allan, S.R. Skinner, D.R. Andersen, A.L. Smirl, 'Observations of fundamental dark spatial solitons in semiconductors using picosecond pulses', *Opt. Lett.*, **16**, 156-8, (1991)

[114] D. R. Andersen and S. R. Skinner, 'Stabiltiy Analysis of the fundamental dark surface wave', *J. Opt. Soc. Am. B*, **8**, 2265-8 (1991)

[115] S.R.Skinner, D. R. , 'Stationary fundamental dark surface waves', *J. Opt. Soc. Am. B*, **8**, pp759-64 (1991)

[116] Y. Chen and H. T. Tran, 'Gray and dark spatial solitary waves', *Opt. Lett.*, **17**, 530-32 (1992)

[117] Yuri Kivshar, 'Dark solitons in nonlinear optics', *IEEE J. Quantum Eletron.*, **29** , 250-64 (1993)

[118] Y. Chen, 'Stability of dark solitary waves trapped in media with gain and loss', *Phys. Rev. A*, **45** 6922-24 (1992)

[119] A. Ankiewicz, and G.D. Peng, 'Generalized Gaussian analysis of fibers with non-Kerr-law nonlinearities', *Opt. Quantum Electron.*, **25** (1993)

[120] G.I. Stegeman, C.T. Seaton, J. , T.P. Shen, and J.V. Moloney, *Opt. Commun.*, **56**, 365 (1986)

[121] R.K. Varshney, M.A. Nehme, R. Srivastava, and R.V. Ramaswamy, *Appl. Opt.*, **25** 3899 (1986)

[122] Ch. Wachter, U. Langbein, and F. Lederer, *Appl. Phys. B*, **42** 161 (1987)

[123] N.N. Akhmediev, K.O. Boltar, and V.M. Eleonskii, *Opt. Spectrosk.*, **53** 906 (1982); *Opt. Spectrosk.*, **53**, 1007, (1982).

[124] V.K. Fedyanin and D. Mihalache, *Z. Phys. B*, **47** 167 (1982)

[125] K. Ogusu, 'Stability of a new type of stationary waves guided by a nonlinear hollow waveguide', *Opt. Commun.* , **83**, 260 (1991)

[126] J. Ariyasu, C.T. Seaton, and G.I. Stegeman, *Appl. Phys. Lett.*, **47** 355-7 (1985)

[127] J. Ariyasu, C.T. Seaton, G.I. Stegeman, A.A. Maradudin, and R.F. Wallis, *J. Apll. Phys.*, **58** 2460-6 (1985)

[128] L. Leine, C. Wachter, U. Langbein, and F. Lederer, *Opt. Lett.*, **12** 747 (1987)

[129] E.M. Wright, G.I. Stegeman, C.T. Seaton, and J.M. Moloney, *Appl. Phys. Lett.*, **49** 435 (1986)

[130] F. Lederer, U. Trutschel, and C. Wachter, *J. Opt. Soc. Am. A*, **8** 1536 (1991)